EPRI

Topics:
Spent-fuel storage
Thermal-hydraulic models
Heat transfer
Radiation shielding

EPRI NP-5128
Project 2406-4
PNL-6054
UC-85
Interim Report
April 1987

The TN-24P PWR Spent-Fuel Storage Cask: Testing and Analyses

Prepared by
Pacific Northwest Laboratory
Virginia Power Company
and
EG&G, Idaho National Engineering Laboratory

The TN-24P PWR Spent-Fuel Storage Cask: Testing and Analyses

NP-5128

Research Project 2406-4
PNL-6054
UC-85

Interim Report, April 1987

Prepared by

PACIFIC NORTHWEST LABORATORY
Battelle Boulevard
Richland, Washington 99352

Principal Investigators
J. M. Creer
T. E. Michener
M. A. McKinnon
J. E. Tanner
E. R. Gilbert
R. L. Goodman

VIRGINIA POWER COMPANY
Post Office Box 26666
Richmond, Virginia 23261

Principal Investigators
D. A. Dziadosz
E. V. Moore
H. S. McKay
D. P. Batalo

EG&G, IDAHO NATIONAL ENGINEERING LABORATORY
550 Second Street
Idaho Falls, Idaho 83415

Principal Investigators
D. H. Schoonen
M. F. Jensen
C. K. Mullen

Prepared for

Virginia Power Company
U. S. Department of Energy
and
Electric Power Research Institute
3412 Hillview Avenue
Palo Alto, California 94304

EPRI Project Manager
R. W. Lambert

LWR Fuel and Spent-Fuel Storage Program
Nuclear Power Division

ORDERING INFORMATION

Requests for copies of this report should be directed to Research Reports Center (RRC), Box 50490, Palo Alto, CA 94303, (415) 965-4081. There is no charge for reports requested by EPRI member utilities and affiliates, U.S. utility associations, U.S. government agencies (federal, state, and local), media, and foreign organizations with which EPRI has an information exchange agreement. On request, RRC will send a catalog of EPRI reports.

NOTICE

Prepared by
Pacific Northwest Laboratory
Virginia Power Company
and
EG&G, Idaho National Engineering Laboratory

REPORT SUMMARY

SUBJECTS: Analysis and testing / Waste management / Fuel and core management and development

TOPICS: Spent-fuel storage; Heat transfer; Thermal-hydraulic models; Radiation shielding

AUDIENCE: Fuels engineers / R&D scientists

The TN-24P PWR Spent-Fuel Storage Cask: Testing and Analyses

This test program represents a major milestone in qualifying large metal casks as an alternative for on-site storage of spent nuclear fuel. Successful testing of the TN-24P spent-fuel storage cask has confirmed that it offers a technically sound and practical method for meeting the utility industry's increasing storage needs.

BACKGROUND

Under a cooperative program sponsored by DOE, Virginia Power Company, and EPRI, engineers at the Idaho National Engineering Laboratory (INEL) are testing three types of metal dry spent-fuel storage casks. The cask described in this report is the TN-24P—a forged steel body cask. EPRI report NP-4887 presents findings for one of the other casks—the CASTOR-V/21; test results for the third cask, the MC-10, will be published later in 1987. In addition to the INEL tests and as part of the cooperative program, Virginia Power applied for and received a license to store fuel in metal casks at its Surry nuclear power station.

OBJECTIVES

To determine the thermal, shielding, and operational performance of the TN-24P storage cask and to demonstrate the ability of computer codes to model the cask system and predict its thermal performance.

APPROACH

The test program included cask testing and pre- and posttest analyses. Actual testing, at INEL's Test Area North, required shipping of 24 PWR spent-fuel assemblies from Virginia Power's Surry nuclear power station, instrumenting the cask and loading it with fuel assemblies, and testing it in horizontal and vertical positions with three different internal storage environments (nitrogen, helium, and vacuum). The project team, using the COBRA-SFS computer code being developed by Pacific Northwest Laboratory, predicted the cask's thermal performance and compared their predictions with actual test data. They then predicted the cask's posttest performance, taking into account differences between actual test conditions and pretest prediction assumptions.

RESULTS

The tests demonstrated that the TN-24P cask is well suited to store spent fuel. The cask showed exceptionally good heat transfer performance, with peak cladding temperatures remaining under the allowable 380°C for helium and nitrogen environments with a cask heat load of 20.6 kW. Shielding

performance met design expectations, with the exceptions of the cask bottom and minor peaks at the sidewalls near the top and bottom of the cask.

At conditions near the cask's thermal design limits, the COBRA-SFS code predicted well both the shapes of the temperature profiles and the actual temperatures. Pretest predictions agreed within 20°C of actual test data; differences were reduced to about 16°C in a posttest analysis that corrected for heat conduction in the fuel basket and for assumptions of heat transfer between the cask and the railcar test fixture.

EPRI PERSPECTIVE

This testing program quantified the thermal and shielding performances of the TN-24P cask. It also demonstrated that handling and loading these 100-t containers are relatively straightforward processes, introducing no unusual demands on personnel or facilities. The program achieved remarkably smooth testing despite the number of contractors and sites, the complicated instrumentation, the shipping of major quantities of spent nuclear fuel, and the use of complex new computer codes.

PROJECT

RP2406-4
EPRI Project Manager: Ray W. Lambert
Nuclear Power Division
Contractors: Pacific Northwest Laboratory; Virginia Power Company; EG&G, Idaho National Engineering Laboratory

For further information on EPRI research programs, call EPRI Technical Information Specialists (415) 855-2411.

ABSTRACT

A performance test of a Transnuclear, Inc. TN-24P storage cask configured for pressurized water reactor (PWR) spent fuel was performed. The test was the second of a series of cask performance tests planned under a cooperative agreement between Virginia Power and the U.S. Department of Energy. The performance test consisted of loading the TN-24P cask with 24 PWR spent fuel assemblies from Virginia Power's Surry reactor. Cask surface and fuel assembly guide tube temperatures were measured, as were cask surface gamma and neutron dose rates. Testing was performed with vacuum, nitrogen, and helium backfill environment in both vertical and horizontal cask orientations. Limited spent fuel integrity data were also obtained.

Results of the performance test indicate that the TN-24P cask exhibited exceptionally good heat transfer performance when dissipating about 21 kW. Maximum measured assembly guide tube temperatures in vacuum, nitrogen, and helium backfills in a vertical/horizontal cask orientation were 278/268°C, 232/247°C, and 214/208°C, respectively. These are significantly less than the 380°C allowable for a total heat load of 24 kW. Significant convection heat transfer was present in vertical nitrogen and helium test runs, as indicated by peak temperatures occurring in the upper regions of the fuel assemblies. Pretest temperature predictions of the COBRA-SFS heat transfer computer code were in good agreement (within 25°C) with test data, and post-test predictions agreed exceptionally well (within 20°C) with data.

Measured cask surface gamma and neutron dose rates were generally less than the design goal of 60 mrem/h. Localized peaks as high as 90 mrem/h were measured on the side of the cask. The maximum measured dose rate coincided with an empty bolt hole under the test lid (316 mrem/h) and would be less if the standard lid and protective cover were in place. The maximum dose rate on the bottom of the cask was 135 mrem/h gamma plus 64 mrem/h neutron (199 mrem/h). This indicates the need for additional shielding on the bottom if the cask is stored horizontally. With minor refinements to the shielding design, dose rates can be limited to less than 60 mrem/h.

ACKNOWLEDGMENTS

The authors acknowledge the support of Virginia Power, the U.S. Department of Energy, the Electric Power Research Institute, EG&G Idaho Inc., the Pacific Northwest Laboratory, Lawrence Livermore National Laboratory, and Transnuclear, Inc. The TN-24P cask performance test and its documentation were truly a team effort, and the contributions of the following persons are greatly appreciated.

Technical Management Committee

M. L. Smith, Chairman (VP)
H. S. McKay (VP)
C. T. Snow (VP)
R. W. Lambert (EPRI)
G. H. Beeman (PNL)
J. P. Collins (DOE-RL)

Virginia Power

B. Wakeman
S. M. Bowman
W. A. Peterson
J. Miller
N. Wolfhope
J. G. Fisher

DOE Headquarters

D. Shelor

DOE Richland

R. D. Izatt

EPRI

R. F. Williams

DOE Idaho

C. P. Gertz
M. W. Fisher

PNL

C. M. Heeb
D. F. Newman
A. J. Currie

EG&G Idaho, Inc.

G. R. Rodman
L. R. McKay
N. Wilde

TN

B. R. Teer
M. E. Mason
K. Goldmann

LLNL

H. W. Culham
C. F. Smith
V. M. Oversby

From both heat transfer and shielding perspectives, the TN-24P cask with minor refinements can be effectively implemented at reactor sites and central storage facilities for safe storage of spent fuel.

CONTENTS

ILLUSTRATIONS

TABLES

NOMENCLATURE

ABBREVIATIONS AND ACRONYMS

CFA	INEL Central Facilities Area
DAS	data acquisition system
DOE	U.S. Department of Energy
DOE-RL	DOE Richland Operations Office
DOP	Detailed Operating Procedure
EOC	end of cycle
EPRI	Electric Power Research Institute
FRDS	failed fuel rod detection system
H/U	hydrogen-to-uranium (ratio)
INEL	Idaho National Engineering Laboratory
LLNL	Lawrence Livermore National Laboratory
M/S	multisphere spectrometer
MTU	metric ton uranium
NBS	National Bureau of Standards
NOD	VP Nuclear Operations Department
NRC	U.S. Nuclear Regulatory Commission
NWPA	Nuclear Waste Policy Act
OSRD	Operation Safety Requirements Document
PNL	Pacific Northwest Laboratory
PWR	pressurized water reactor
R&D	research and development
RPD	relative power density
SAR	Safety Analysis Report
SCAP	Solicitation for Cooperative Agreement Proposal
SWR	Site Work Release
TAN	Test Area North
TC	thermocouple
TED	track etch dosimeter
TEPC	tissue equivalent proportional counter
TLD	thermoluminescent dosimeter
TN	Transnuclear, Inc.

UBC	Uniform Building Code
UT	ultrasonic techniques
VP	Virginia Power

SYMBOLS AND NOTATIONS

α_i	set of wall numbers with a thermal conduction connnection to wall node i
β_i	set of wall numbers with a thermal radiation connection to rod i
γ_i	set of subchannel numbers with a thermal connection to rod i
Δt	time step
Δx	axial step
ε	surface emittance or a member of a set
ζ_i	set of rod numbers with a thermal radiation connection to rod i
θ	problem orientation, angle from vertical
κ_i	set of rod numbers with a thermal radiation connection to wall i
λ_i	set of rod numbers with a thermal connection to subchannel i
ξ_i	set of subchannel numbers with a thermal connection to wall i
ρ	density
σ	Stephan-Boltzmann constant
σ_i	set of wall numbers with a thermal radiation connection to wall i
τ_i	set of wall numbers for walls that connect to subchannel i
ψ_i	set of transverse gap connections to subchannel i
ℓ	length of tranverse momentum control volume
A	area
C,c	drag, axial loss coefficient, empirical coefficient, or specific heat
D_h	hydraulic diameter
e_{ik}	multiplier (±1) that gives the correct sign to the transverse connection terms
f	friction factor
F_{ij}	radiation exchange factor, surface i to j
g	acceleration due to gravity
Gr	Grashoff number
h,H	fluid enthalpy, average film coefficient, or heat transfer coefficient
H_g	fuel-cladding gap conductance
K	thermal conductivity
L	length
Nu	Nusselt number
P,p	pressure
Pr	Prandtl number
q''_{rad}	thermal radiation transport

q'''	volumetric heat generation in wall
R	radius
R_c	outer radius of the cladding
Re	Reynolds number
R_f	outer radius of the fuel material
S	transverse gap width
T	temperature
T_c	cladding temperature
T_{fs}	temperature of the fuel surface
T_s	local surface temperature
T_w	wall temperature
t	time
U	effective wall conductance
u	transverse velocity
v	axial velocity
w_T	crossflow due to turbulent exchange
y_c	cladding thickness
Z	factor for effective fluid radial conduction length

SUPERSCRIPTS

n	time step level or Nusselt number exponent
*	donor cell quantity
$\overline{\quad}$	average value

SUBSCRIPTS

c	cladding
D	diameter
f	friction or fuel
i	subchannel number or generalized subscript for matrix notation
HTR	heat transfer from a rod
HTW	heat transfer from a wall
j	axial level or generalized subscript for matrix notation
II JJ	refer to channel numbers on either side of a transverse gap
k	transverse gap number
m	mixed convection or wall number
n	rod number
r	radiation

R	rod
fs	fuel surface
T	transverse
W	wall

EXECUTIVE SUMMARY

This report documents a heat transfer and shielding performance test conducted on a Transnuclear, Inc. TN-24P pressurized water reactor (PWR) spent fuel storage cask. Under a cooperative agreement program between Virginia Power (VP) and the U.S. Department of Energy (DOE), performance testing was conducted by the Pacific Northwest Laboratory (PNL) operated for DOE by Battelle Memorial Institute, the Idaho National Engineering Laboratory (INEL) operated for DOE by EG&G Idaho, Inc., and VP. The Electric Power Research Institute (EPRI) participated in the cooperative cask testing program via a separate agreement with VP. Testing was conducted at INEL's Test Area North (TAN) cask testing facility and consisted of pretest preparations, performance testing, and post-test activities. Pretest preparations included conducting cask-handling dry (cold) runs and characterizing PWR spent fuel assemblies from VP's Surry Nuclear Power Plant. The performance test matrix included six runs consisting of two cask orientations and three backfill environments. Post-test activities included crud collection.

The TN-24P spent fuel storage cask consists of a forged steel body for structural integrity and gamma shielding, surrounded by a resin layer for neutron shielding. The resin layer is enclosed in a smooth steel outer shell. The cask cross section is shown in Figure S-1. The cask is 5.0 m (16 ft) long and 2.3 m (7.5 ft) in diameter and weighs approximately 100 tons when loaded with unconsolidated PWR spent fuel. The fuel basket within the cask is configured to hold 24 PWR spent fuel assemblies and is composed of stacked, interlocking plates constructed of aluminum and boron. The Surry spent fuel assemblies used during testing are of a standard Westinghouse 15 x 15 rod design. The cask is closed with a lid having two concentric metallic O-ring seals plus a protective cover sealed with one rubber O-ring gasket to seal the cask cavity from the environment.

Dry (cold) runs of cask handling and fuel loading with a nonirradiated dummy fuel assembly were performed before the Surry spent fuel was loaded in the cask. The objectives of the dry runs were to gain operational experience and to finalize handling and test procedures. Each dry run was conducted successfully without unusual problems or significant modifications to the cask or handling equipment.

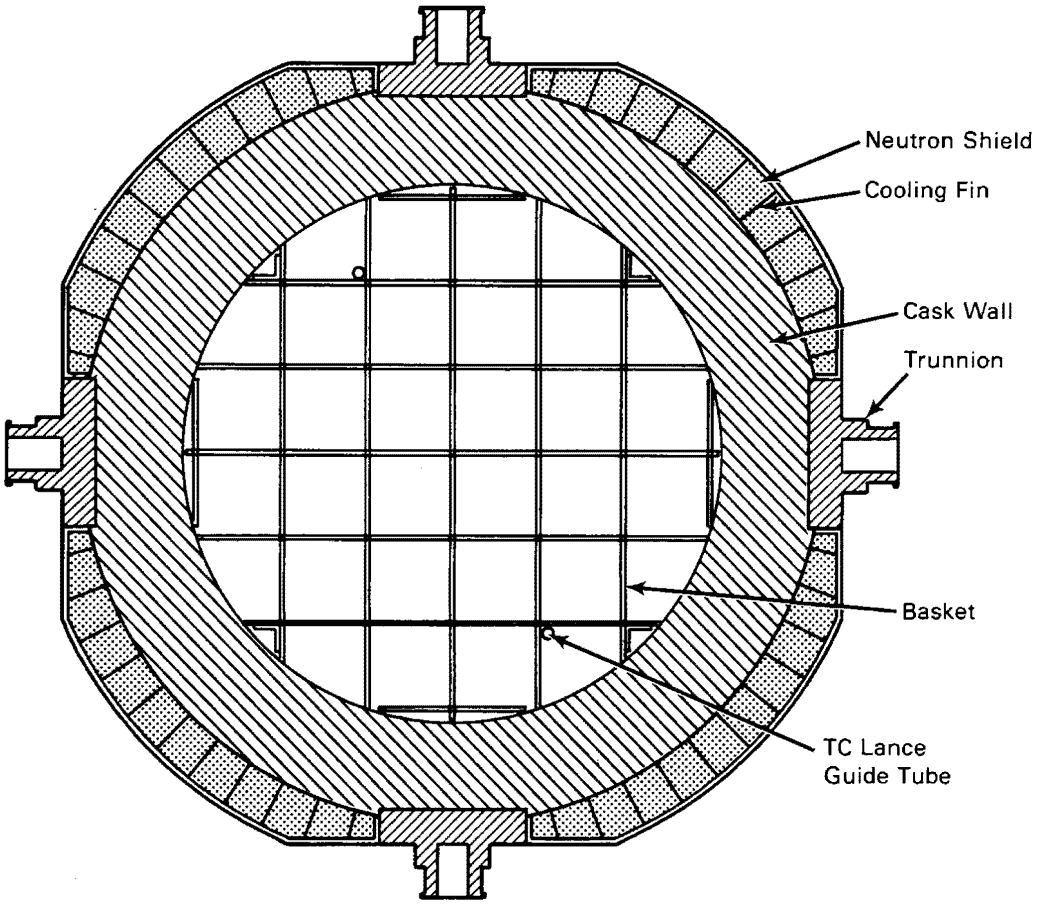

Figure S-1. TN-24P Cask Cross Section

The Surry PWR spent fuel assemblies were characterized using in-basin ultrasonic examinations, video recordings, and photography. Smear samples were also collected. The results of these examinations revealed no indication of any failed fuel before the TN-24P cask performance test. However, gas samples taken during the actual testing indicated the presence of one or more leaking fuel rods.

Based on pretest ORIGEN2 predictions, fuel assembly decay heat generation rates totaled approximately 20.6 kW at the start of testing and 20.3 kW at the end of testing (Table S-1). The decay heat output of the assemblies ranged from 845 to 919 watts, with an average output per assembly of 860 watts at the start of testing. The fuel assemblies had cooling times of 50 months at the start of testing. The load pattern placed the hot assemblies in the center of the basket and the cooler assemblies around the outside. The fuel loading pattern was expected to create a relatively flat radial temperature profile across the basket during

Table S-1

SURRY PWR SPENT FUEL CHARACTERISTICS

Assembly	Burnup, GWd/MTU	Initial Enrichment, wt%	Decay Heat Pred., W Start 1/14/86	Decay Heat Pred., W End 2/06/86
W02, W10, W16, W19 W23, W45, W49	29.8	3.2	845	832
W01, W17, W28, W38 W44, W46, W52	30.0	3.2	852	839
W06, W13, W27, W34	30.5	3.2	859	846
V03, V10, V16, V26	30.6	2.91	870	857
V18, V22	31.5	2.91	919	905
		Total	20,636	20,315
		Average	860	846

testing. Pretest heat transfer predictions using the COBRA-SFS computer code indicated that peak cladding temperatures in nitrogen and helium would be below or near 259 and 230°C, respectively.

Figure S-2 shows the predicted axial decay heat profile assumed for each of the Surry assemblies. Measured axial power profiles for the Surry assemblies were not available for predicting axial decay heat profiles of the assemblies used in the TN-24P cask performance test. Axial gamma radiation scans previously obtained on Turkey Point reactor fuel assemblies were used to predict an assembly axial burnup distribution. The Turkey Point reactor and spent fuel are Westinghouse PWR designs and are essentially the same as those for the Surry plant. ORIGEN2 was used with the assembly axial burnup distribution and the Surry operating history to determine the predicted axial decay heat profile shown in Figure S-2. The dips in the decay heat profile are due to grid spacers. Axial decay heat profiles are important in the placement of fuel rod temperature instrumentation and as input to heat transfer computer codes because they strongly affect the shape of measured axial fuel temperature profiles.

The outer surface of the cask was instrumented with 35 thermocouples (TCs), 95 gamma dose rate sensors, and 95 neutron dose rate sensors. Fifty-four TCs contained in

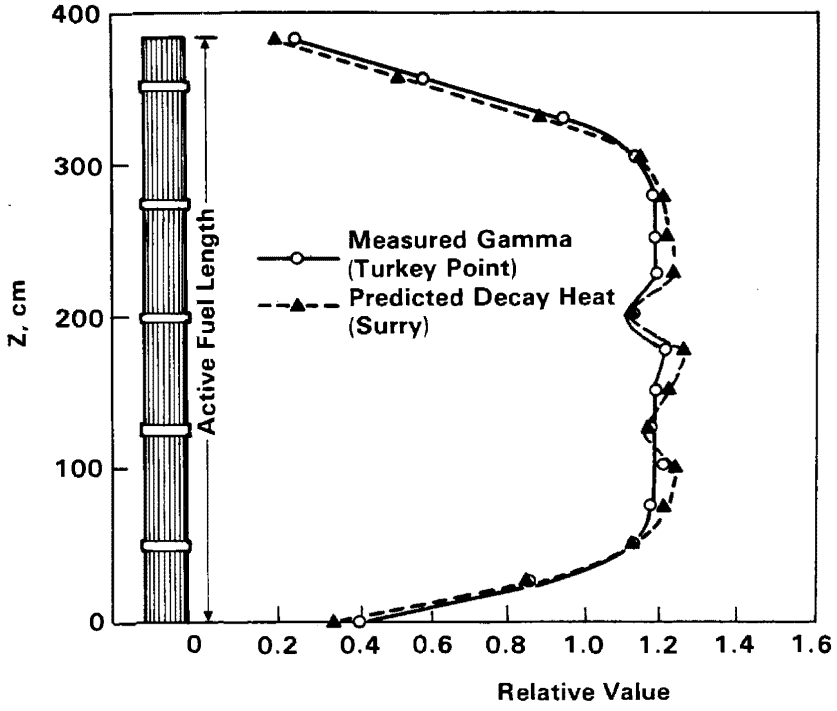

Figure S-2. Measured Gamma and Predicted Decay Heat Axial Profiles

nine lances (six per lance) were inserted through the cask lid into fuel assembly or basket guide tubes. Of the nine TC lances, seven were inserted into fuel assembly guide tubes and two were positioned in simulated guide tubes attached to the basket as shown in Figure S-3. An additional 14 TCs were attached to the basket as shown in Figure S-4.

The cask test matrix included assessments of performance with a full load of fuel (24 assemblies), vertical and horizontal cask orientations, and vacuum, nitrogen, and helium backfill environments. The test matrix and corresponding measured peak guide tube temperatures and estimated peak cladding temperatures are presented in Table S-2. Peak cladding temperatures were estimated by using calculated guide tube-to-hot rod temperature differences from the COBRA-SFS computer code.

Table S-2 indicates that peak cladding temperatures were less than the 380°C allowable for all fill gases and cask orientations tested. In general, the cask heat transfer performance was concluded to be exceptionally good because the difference between the ambient and the peak cladding temperature in helium and nitrogen, when the cask was dissipating approximately 21 kW, was 100°C less than specified for the cask operating limit of 24 kW in the cask topical safety analysis report.

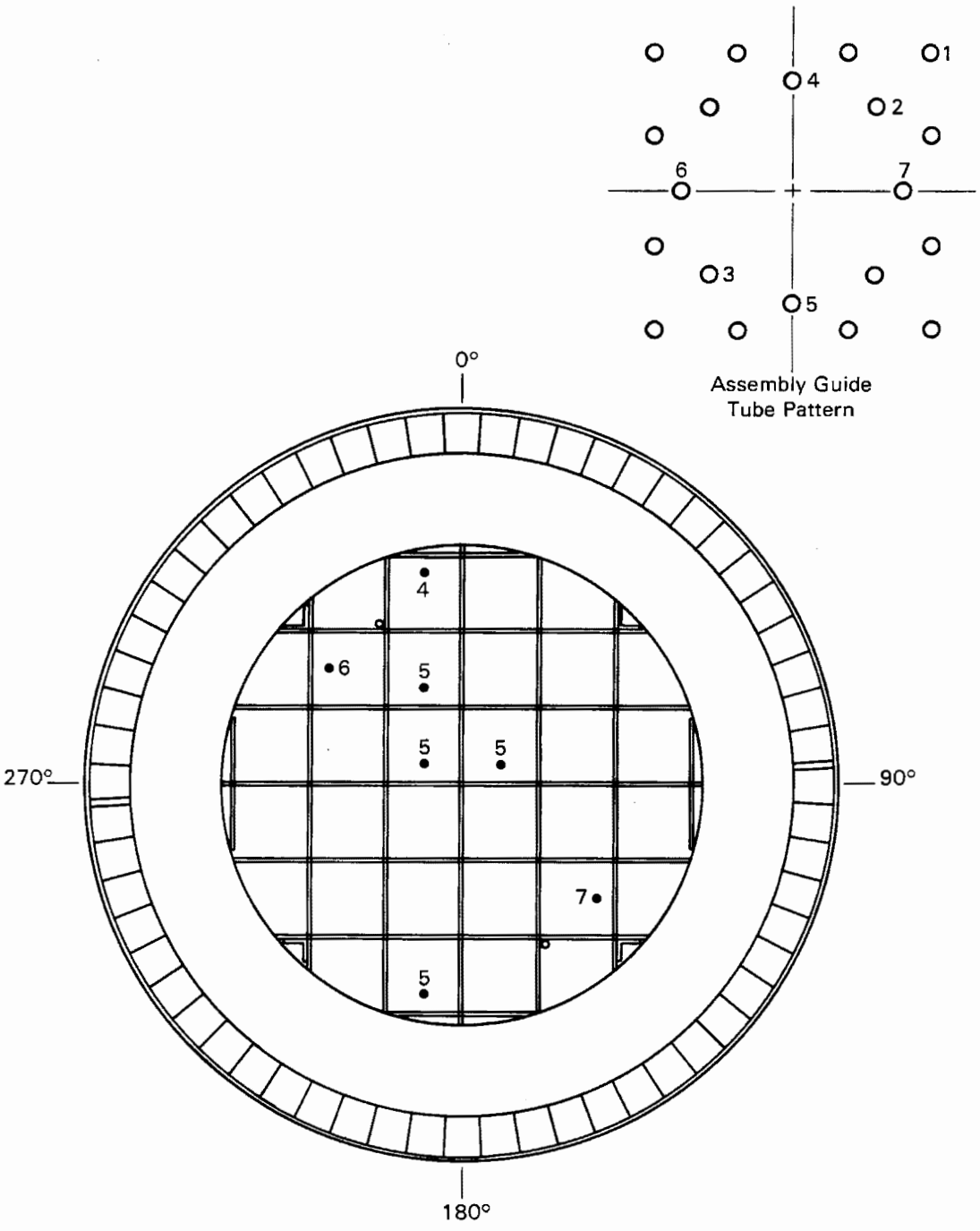

Figure S-3. Thermocouple Lance Locations

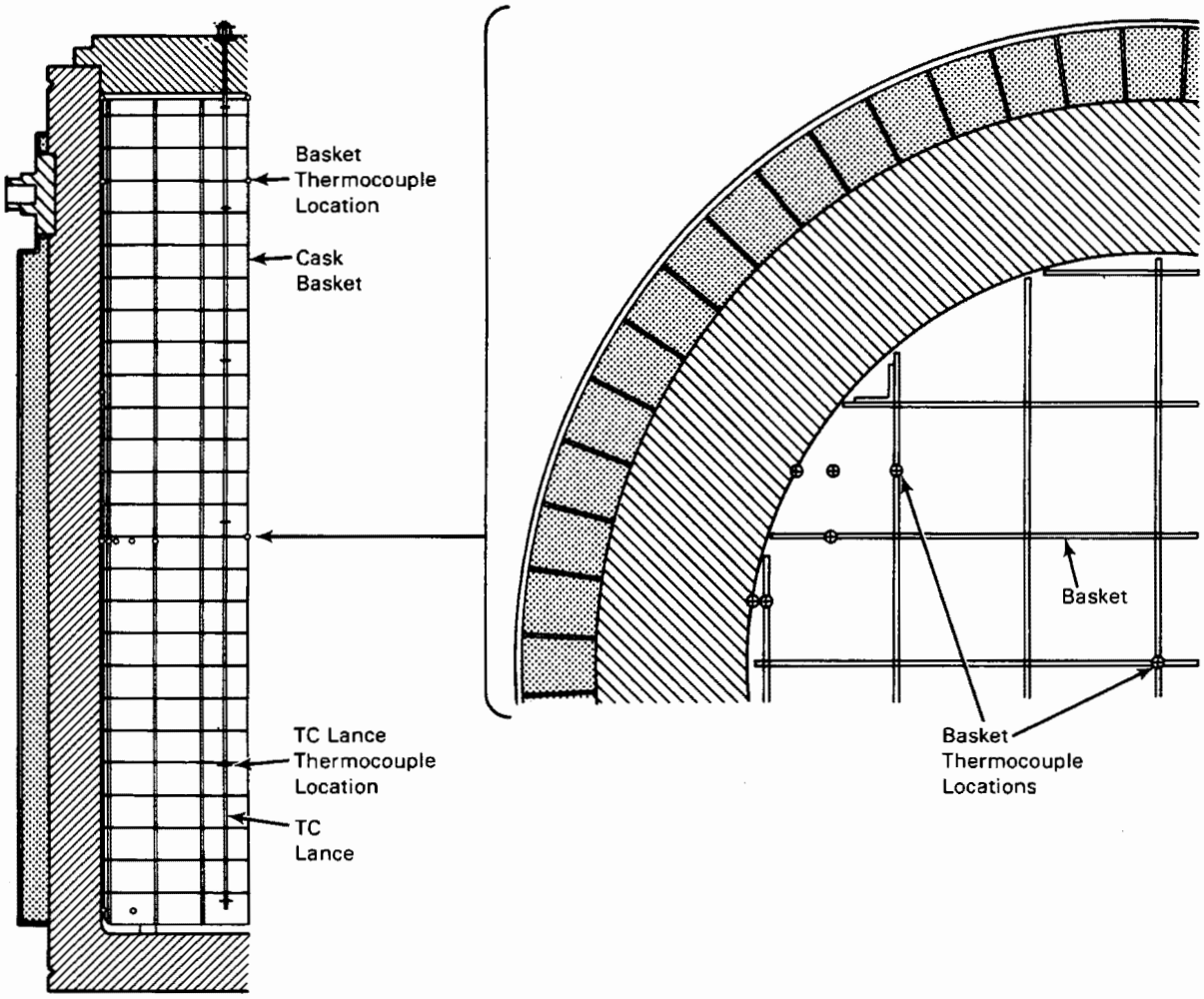

Figure S-4. Basket Thermocouple Locations

Table S-2

TN-24P CASK TEST MATRIX AND PEAK TEMPERATURES

Run No.	Orientation	Backfill	Cask Heat Load, kW	Ambient Temp, °C	Measured Guide Tube Temp, °C	Estimated Peak Clad. Temp, °C
1	Vertical	Helium	20.6	18	214	221
2	Vertical	Nitrogen	20.6	20	232	241
3	Vertical	Vacuum	20.6	20	278	290
4	Horizontal	Helium	20.5	18	208	215
5	Horizontal	Nitrogen	20.4	21	247	256
6	Horizontal	Vacuum	20.3	19	268	280

Axial and radial guide tube temperature profiles for the six test runs are shown in Figures S-5 and S-6. Attention should be given to data points only. The corresponding lines are provided for clarity and do not necessarily represent actual profiles. The axial profiles are for the hot center assembly, and the radial profiles are for the axial location of the peak temperature for each of the respective runs. The axial profiles vividly show the effects of convection in nitrogen in a vertical orientation where peak temperatures are skewed toward the top of the cask. The vertical helium run also shows the effect of convection, although the effect is not as pronounced as for nitrogen. This is not surprising, because the density and viscosity of helium are not conducive to convection; i.e., buoyancy forces in helium

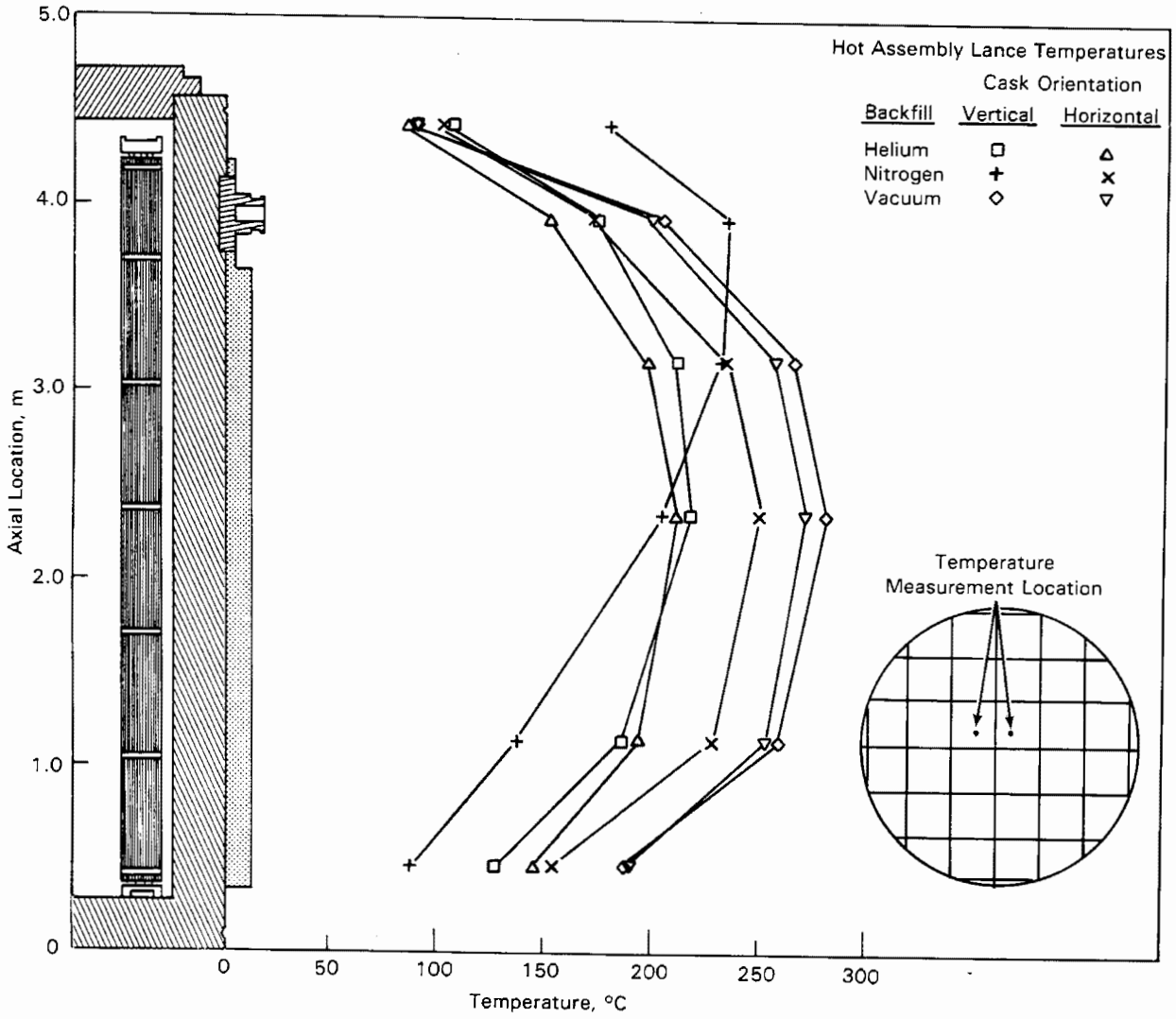

Figure S-5. Effect of Gas Environment and Cask Orientation on Axial Temperature Profiles

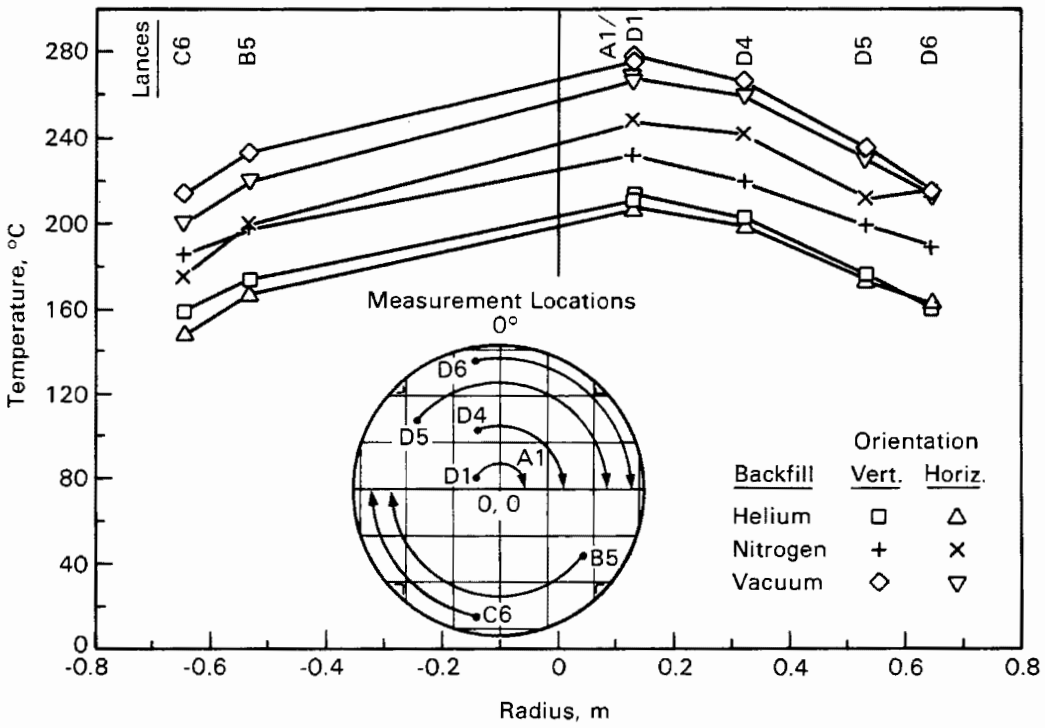

Figure S-6. Radial Temperature Profiles Measured Near Peak Axial Temperatures

are about one-fourth those in nitrogen. Note that the peak temperature in the vertical nitrogen run is less than the peak temperature in the horizontal nitrogen run. This indicates that convection in vertical nitrogen compensates for the increased conduction between the fuel and basket in the horizontal run. In the helium runs, the horizontal run is a little cooler than the vertical run, indicating that conduction is more dominant than convection. This is not surprising, because the conductivity of helium is five times that of nitrogen.

Symmetry with respect to the predicted axial decay heat profile over the active length of the fuel assemblies in the vertical vacuum and all horizontal axial temperature profiles indicates that axial convection in these runs was negligible (Figure S-5). These profiles are similar to the axial gamma and decay heat profiles previously presented in Figure S-2. The lack of axial convection in vacuum and horizontal runs is reasonable, because significant density gradients cannot develop in a vacuum or in an orientation with low axial gravitational forces.

Radial temperature profiles at the hot elevation for the fuel assemblies of six test runs are shown in Figure S-6. The data indicate relatively flat profiles across the

fuel assemblies. Most of the temperature drop in the cask occurs between the basket and the inner wall of the cask. Steep gradients across the basket-to-inner wall gap indicate that the gap is important to the heat transfer design of the cask.

The COBRA-SFS heat transfer code was used to select spent fuel assemblies for the test, determine the loading pattern, and identify optimal TC locations. Selected COBRA-SFS pre- and post-test predictions are shown in Figures S-7 and S-8 for vertical test runs. In general, the COBRA-SFS predictions of peak guide tube temperature agree well with experimental data. The largest variation occurred for the vertical nitrogen case where the predicted temperature was 20°C higher than the measured peak guide tube temperature. The mean difference between calculated and measured temperatures of the peak guide tube for the six runs was 9°C with a standard deviation of ±8°C, with only the horizontal vacuum simulation underpredicting the peak guide tube temperature by 4°C. The temperature profiles are reasonably good for all three backfill environments.

After the test was completed, it was observed that axial conduction in the aluminum basket could not be neglected and that calculated heat transfer near the bottom of the cask did not adequately represent the flow of heat from the basket and cask bottom to the rail car. These two post-test model changes affected the predicted axial profiles but did little to change the predicted peak guide tube temperatures. Again, as in the pretest predictions, the greatest discrepancy occurred for vertical nitrogen where a 16°C overprediction occurred. The mean temperature difference between the measured peak temperature and the post-test prediction was 6 ± 7°C.

Gamma and neutron dose rates on the top, side, and bottom of the cask are shown in Figures S-9, S-10, and S-11. The radiation source strength was higher for the test fuel than fuel considered in the cask topical safety analysis report. A peak gamma dose rate of 58 mrem/h was measured on the top of the primary lid (Figure S-9) at 45 degrees (the outer lid was not used during testing). The total dose rate (gamma plus neutrons) was approximately 90 mrem/h near the center of the primary lid. When the neutron shield and protective cover are used on the cask during normal operation, these dose rates should be reduced significantly.

The total dose rates along most of the cask side are less than 20 mrem/h (Figure S-10). There were localized peaks in the gamma and neutron dose rates of up to 54 mrem/h and 37 mrem/h, respectively. The neutron dose rate peaks were relatively low, but the gamma peaks were substantial. The localized peaks occur at locations above and below the neutron shield, and adjacent to fuel assembly upper and lower

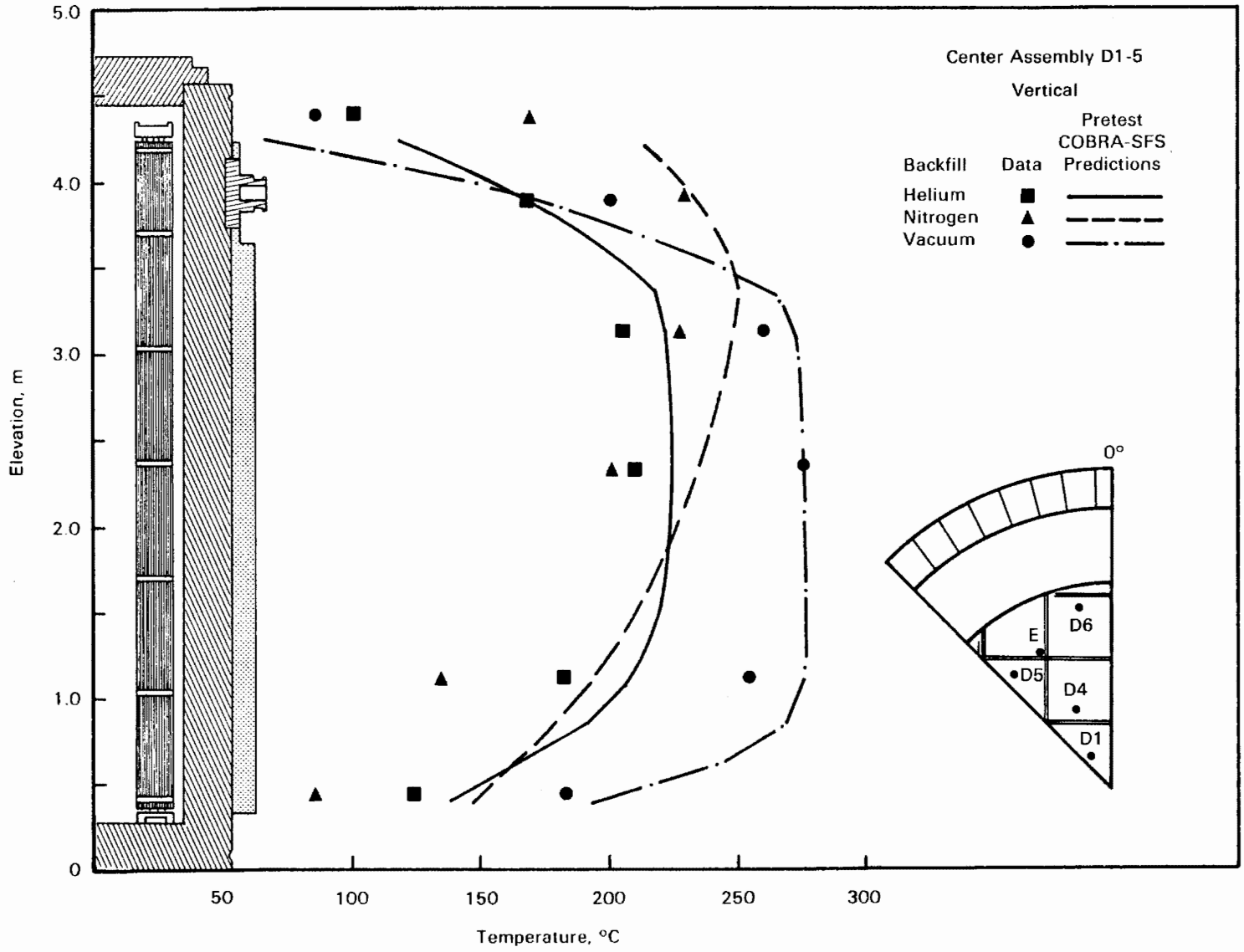

Figure S-7. Pretest Axial Temperature Profile Predictions Compared to Vertical, Vacuum, Nitrogen, and Helium Data

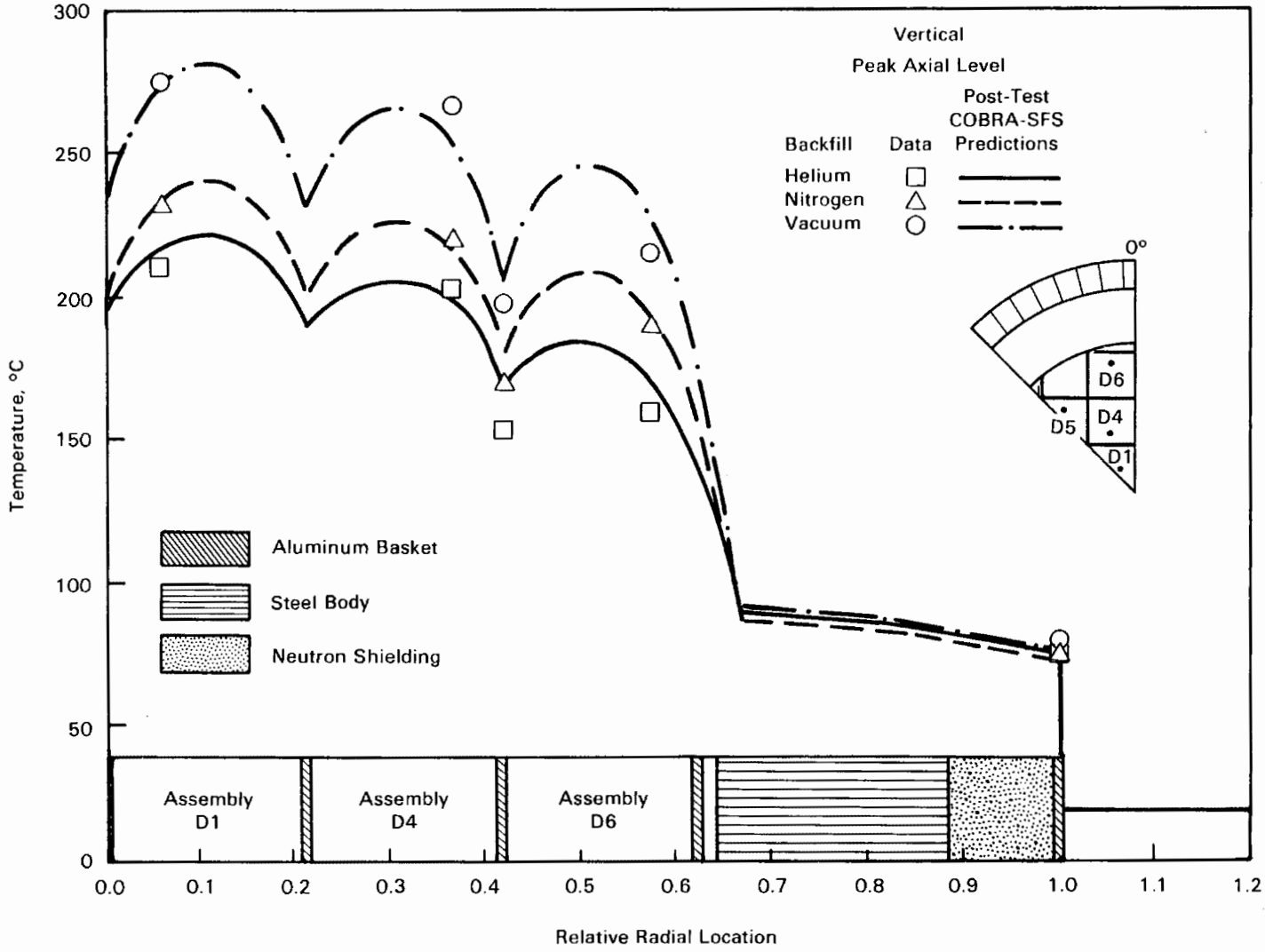

Figure S-8. Post-Test Radial Temperature Profile Predictions Compared to Vertical, Vacuum, Nitrogen, and Helium Data

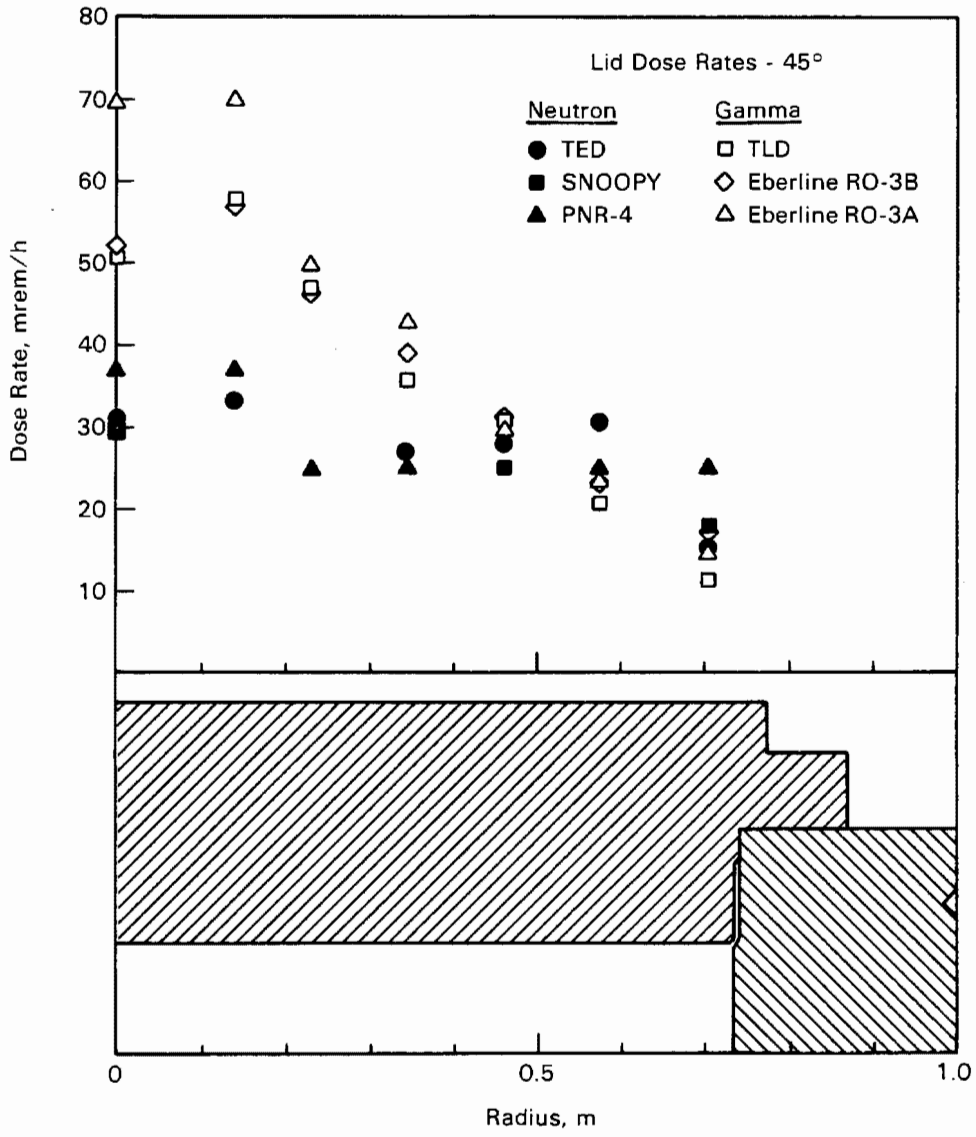

Figure S-9. Gamma and Neutron Dose Rate Profiles Measured on Cask Primary Lid

end fittings. However, minor refinements in the gamma and neutron shielding design at locations corresponding to the dose rate peaks could reduce the gamma peaks significantly. The maximum dose rate measured was 316 mrem/h on the edge of the lid near the drain/fill flange. This dose rate is not shown in Figure S-10 and appears to be caused by an empty bolt hole under the test lid. When the standard lid and protective cover are placed on the cask, this dose rate will be reduced.

Dose rates on the bottom of the cask (Figure S-11) peak at or near the center (200-mrem/h total from TEDs and TLDs), and are uniform on the remainder of the

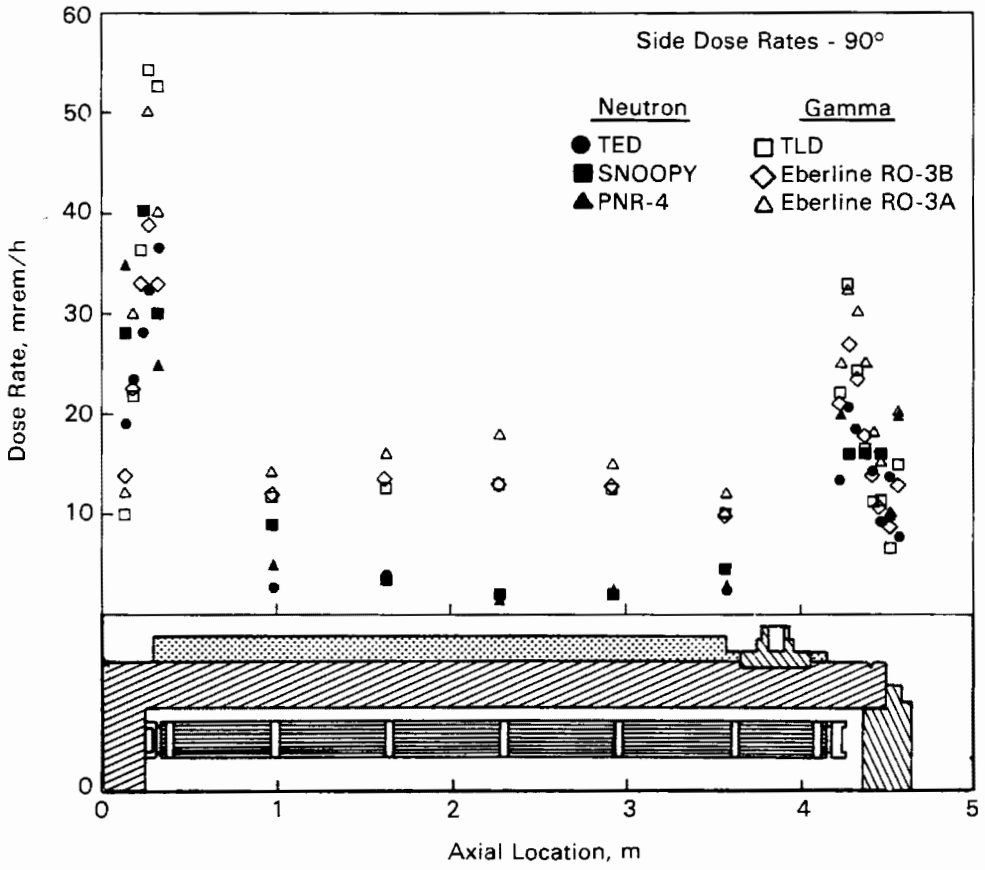

Figure S-10. Gamma and Neutron Dose Rate Profiles Measured on Cask Side

surface. These relatively low dose rates are not of concern if the cask is oriented vertically and is sitting on a concrete pad. They could be of concern if the cask were oriented horizontally.

The overall shielding performance of the TN-24P cask was good and met the intended design goal of ≤60 mrem/h except on the bottom and as noted for the peaks on the side. With a very minor refinement in the gamma and neutron shielding design, total dose rates can easily be reduced to less than 60 mrem/h.

The cask performance test demonstrated that the TN-24P cask could be satisfactorily handled and loaded dry. It was concluded that the heat transfer performance of the cask was exceptionally good. Peak cladding temperatures with helium and nitrogen backfills in a vertical cask orientation were less than 380°C with a total cask heat load of 21 kW. The shielding performance of the cask met design expectations (≤60 mrem/h), except on the cask bottom and in areas of the peaks on the cask

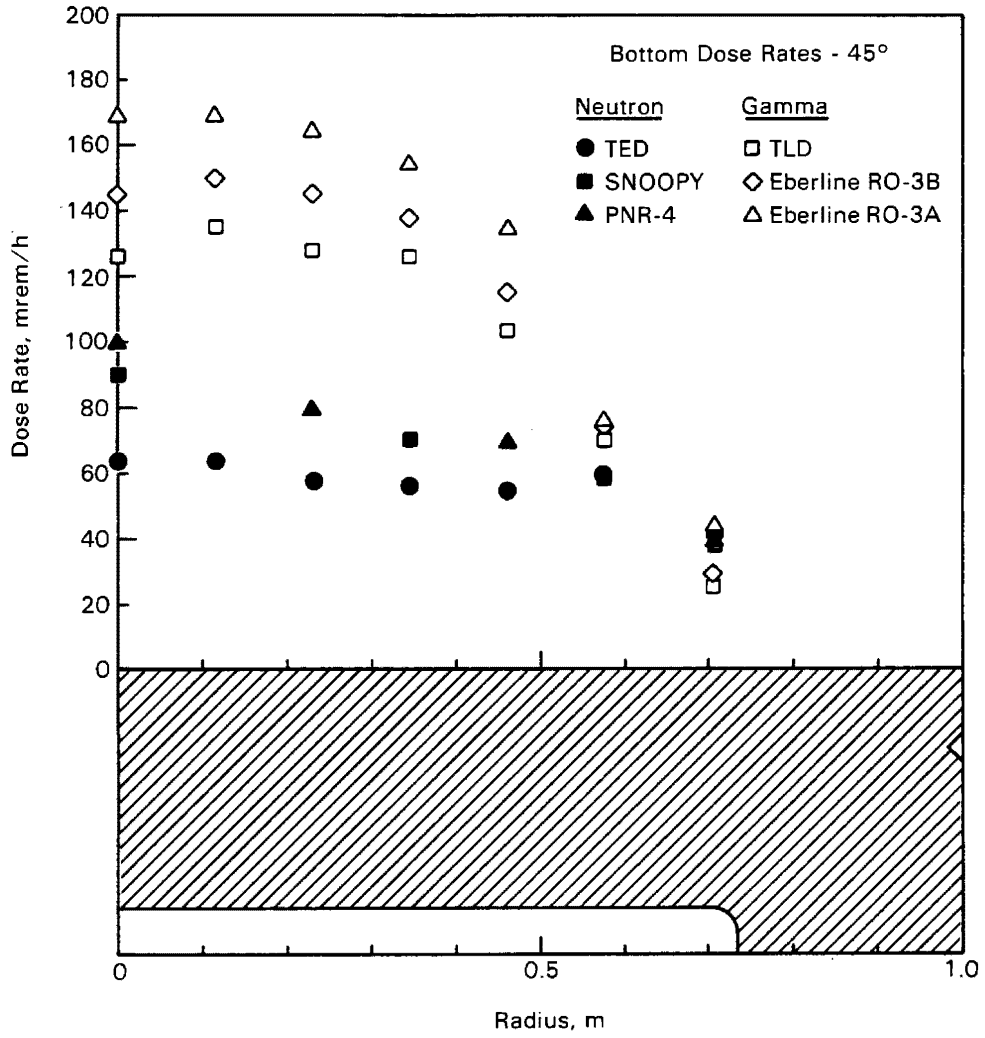

Figure S-11. Gamma and Neutron Dose Rate Profiles Measured on Cask Bottom

side. Cask surface dose rates of <60 mrem/h can easily be achieved with minor refinements in the gamma and neutron shielding design. From both heat transfer and shielding perspectives, the TN-24P cask can, with minor refinements, be effectively implemented at reactor sites and central storage facilities for safe storage of spent fuel.

Section 1

INTRODUCTION

Implementation of spent fuel dry storage systems may be required in the late 1980s when several at-reactor storage basins attain maximum capacity (1). The Nuclear Waste Policy Act of 1982 (NWPA) assigns the U.S. Department of Energy (DOE) the responsibility for assisting utilities with their spent fuel storage problems. An additional provision of the NWPA is that DOE, in cooperation with the private sector, enter into demonstration programs of spent fuel dry storage systems at nuclear power reactor sites. The objective of the cooperative demonstrations is to establish one or more storage technologies that the U.S. Nuclear Regulatory Commission (NRC) may, by rule, approve for use at civilian reactor sites without the need for additional site-specific approvals by the NRC. In addition, the NWPA authorizes DOE to establish a research and development (R&D) program at federally-owned facilities as part of the cooperative demonstrations, to collect data necessary to assist utilities in their licensing activities.

In May 1983, a Solicitation for Cooperative Agreement Proposal (SCAP) was issued to the private sector by the DOE Richland Operations Office (DOE-RL), and proposals were received in August 1983. Virginia Power (VP) proposed that pressurized water reactor (PWR) spent fuel storage cask performance testing be conducted at a federal site in support of its at-reactor license demonstration. Virginia Power and DOE signed a Cooperative Agreement in March 1984, and VP signed a separate agreement with the Electric Power Research Institute (EPRI), essentially establishing a three-party cooperative agreement.

A preliminary assessment of candidate federal sites capable of performing dry storage system tests was undertaken by the Pacific Northwest Laboratory (PNL) in parallel with the issuance and response to the SCAP. The three sites evaluated were Idaho, Nevada, and Hanford. In July 1984, DOE selected the Test Area North (TAN) facility located at the Idaho National Engineering Laboratory (INEL) operated by EG&G Idaho, Inc., as the federal cask testing facility, and the VP/DOE cask performance testing effort was initiated.

The technical baseline of the cooperative agreement for cask performance testing at TAN is to test three different cask designs with unconsolidated spent fuel and two cask designs with consolidated fuel. Unconsolidated fuel cask testing was planned in 1985 and 1986, and consolidated fuel testing is planned in 1987 and 1988. The second unconsolidated fuel cask test, using a TN-24P cask designed and manufactured by Transnuclear, Inc., is documented in this report. The results of the first unconsolidated fuel cask test using a CASTOR-V/21 cask were reported previously (2).

The work began with a revision to TAN's safety analysis documents to permit dry loading of unconsolidated PWR fuel in the TN-24P cask. Dry (cold) runs with a nonirradiated dummy fuel assembly were performed to gain operating experience and finalize handling and test procedures. The PWR spent fuel assemblies were ultrasonically examined and videotaped in the Surry spent fuel pool to ensure their integrity. The TN-24P cask was delivered to TAN, and 24 PWR assemblies were shipped from Surry to TAN using Transnuclear TN-8L shipping casks. The exterior cask surface was instrumented with thermocouples (TCs) and radiation dose rate sensors. The interior of the cask and basket came with 14 TCs attached. Additional thermocouples were inserted into selected fuel assembly guide tubes and basket locations after the cask was loaded with 24 fuel assemblies. A test station was prepared, comprising a rail car and a data acquisition system. Prior to testing, selected fuel assemblies were videotaped and photographed, and smear samples were collected and analyzed. Six runs involving a combination of cover gases and cask orientations were performed during the test. The backfill environments used were vacuum, nitrogen, and helium; these gases were sampled and analyzed to detect leaking fuel assemblies. Both vertical and horizontal orientations were investigated, and test runs were performed inside under controlled conditions.

This report documents the performance test using a TN-24P cask. The conclusions and recommendations are presented in Section 2. In Section 3, the TN-24P cask, the Surry PWR fuel assemblies, cask and fuel instrumentation, the TAN cask testing facility, the test plan, and the cask-handling procedures and experience are presented. Heat transfer and shielding data are presented and discussed in Section 4. Pre- and post-test heat transfer predictions obtained with the COBRA-SFS computer program are compared to test data in Section 5.

Section 2

CONCLUSIONS AND RECOMMENDATIONS

Performance testing of a TN-24P PWR spent fuel storage cask was successfully completed at TAN. The test demonstrated that the cask could be satisfactorily handled and loaded dry, and demonstrated the heat transfer and shielding performance of the cask when loaded with 24 PWR spent fuel assemblies generating approximately 21 kW. The heat transfer performance of the cask was exceptionally good, as indicated by acceptable peak cladding temperatures (3) (<380°C) with vacuum, nitrogen, and helium backfill gases with the cask in a vertical and horizontal orientation. The shielding performance did not meet design expectations (≤60 mrem/h), but dose rates of <60 mrem/h could be easily established with minor gamma and neutron shielding design refinements. From both heat transfer and shielding perspectives, the TN-24P cask can, with minor refinements, be used effectively to safely store spent fuel at reactor sites and central storage facilities.

The following sections present specific conclusions and recommendations noted during the testing and analyses effort.

CONCLUSIONS

The results of the cask performance test permit the following conclusions:

Cask Handling and Loading

- The TN-24P cask can be satisfactorily handled in many reactor facilities with only minor modifications to the supplied handling equipment and procedures.
- Dry (cold) runs with a nonirradiated dummy assembly of all steps required to handle and test the cask were valuable in familiarizing personnel with cask handling characteristics and in finalizing test procedures.
- Approximately 1 hour was required to pump the cask down to 1 mbar and backfill with gas to 850 mbar. During a double pumpdown/ backfill operation, measured guide tube temperatures increased by <15°C during a 2-hour period. It is anticipated that evacuating and backfilling the cask after loading in a water basin will require a longer period and result in higher temperature increases.

- Contamination was not a major problem during fuel assembly air transfers between the shipping and storage casks. About 4 hours of decontamination were required to remove localized contamination on the personnel work platform between the storage and shipping cask.

- When loading dry, sealing surface protectors are required to ensure that crud or particles do not lodge on these surfaces and result in blemishes or scratches that could compromise the finish of sealing surfaces.

- The total personnel radiation exposures during the 3 months in which the TN-24P cask was handled, loaded, and tested were relatively low (approximately 1.2 man-rem). The exposure at a reactor or storage facility will be even lower because casks will not be loaded incrementally or worked around continuously.

Heat Transfer Performance

- The heat transfer performance of the cask was exceptionally good. Peak temperatures were 100°C less than the allowable (<380°C) for all backfill conditions and orientations tested when dissipating 21 kW. The design heat load was 24 kW for a 46°C ambient and a maximum cladding temperature of 375°C.

- The design of the TN-24P fuel basket resulted in significant convection for vertical nitrogen and noticeable convection for vertical helium backfill gases. Peak temperatures with both backfills in the vertical orientation occurred in the upper one half of the instrumented guide tubes.

- The peak temperature with nitrogen (232°C) in a vertical cask was only slightly higher than with helium (214°C), indicating that convection with nitrogen almost compensated for the higher (five times) thermal conductivity of helium.

- In a horizontal orientation, the added contact conductance between fuel assemblies and basket fuel tubes did not compensate for convection with nitrogen; i.e., peak temperatures in a horizontal orientation were higher than in a vertical orientation for a nitrogen backfill.

- Backfill gas affects the temperature drop between the basket and the cask wall. This temperature drop accounts for most of the change in magnitude of the radial temperature profile due to different backfill gases.

- Relatively large temperature differences (20 to 100°C) between the basket and the cask wall indicate that the basket-to-inner cask wall interface is important to the heat transfer performance of the cask.

- Temperature transients in the cask were not excessive. They were less than 12°C/h on heatup (helium to vacuum) and 30°C/h on cooldown (vacuum to helium) for a 20.6-kW heat load in the cask.

- For a given heat load, temperatures in a standard TN-24 cask will be higher than for the TN-24P test cask because of the use of aluminum in the TN-24P and stainless steel in the TN-24 basket and the

COBRA Heat Transfer Analysis

- Comparison of pretest predictions of peak temperatures with data showed excellent agreement. The maximum disagreement was less than 20°C and occurred for the vertical nitrogen run.

- Comparisons of pretest predictions with data showed the need to model axial conduction through the segmented aluminum basket and to model the rail car as a fin attached to the bottom of the cask during the vertical runs.

- Post-test predictions of peak temperatures were in excellent agreement with data. The mean temperature difference between predicted peak temperature and measured value was 6°C, with a standard deviation of 7°C. The greatest difference (16°C) was for the vertical nitrogen run.

- Including axial conduction in the basket gave a clear improvement in the shape of the predicted axial profiles.

- The COBRA-SFS best-estimate prediction of the maximum heat that can be dissipated by a vertical TN-24P cask exposed to 54°C ambient was 1.03 kW per assembly for helium backfill and 0.50 kW per assembly for the nitrogen case. The helium case was limited by the basket material (250°C), whereas the convection in the nitrogen case makes the neutron shield on the lid (140°C) the limiting condition. If the neutron shield were removed or insulated from the primary lid, then the heat load could be increased to 0.85 kW per assembly before the basket temperature limit is reached for vertical nitrogen.

Shielding Performance

- Most total dose rates on the cask surface were less than 100 mrem/h.

- Total dose rates (gamma and neutron) on the TN-24P cask side were generally less than the 60 mrem/h design goal. Peaks near the ends exceeded the goal.

- The peak dose rate of 310 mrem/h occurred on the cask lid. This peak will be reduced when the neutron shield and protective cover are present.

- Additional gamma and neutron shielding would be required on the bottom of the cask to reduce dose rates below the measured value of 199 mrem/h.

- Dose rates from standard TN-24 casks will be higher than those measured on the TN-24P test cask due to a thinner cask wall, lid, and bottom in the TN-24 cask.

Fuel Characterization and Integrity

- Results of pretest and in-test fuel integrity activities resulted in the conclusion that no failed fuel rods were loaded in the TN-24P cask.
- One or more fuel rods began to leak during the first horizontal test run. The size of the leak was concluded to be small from gas sampling results.
- Fuel inspection showed that the elevations of the upper ends of some fuel rods in an assembly were different (misaligned) by up to approximately 2.5 cm (1 in.), which could affect future rod consolidation activities.
- Video scans and photography indicated the presence of an intermittent crud layer on the fuel assemblies.
- Smear samples from selected fuel assemblies indicated that large quantities of ^{60}Co were present, but no fission product species were detected.

RECOMMENDATIONS

The results and conclusions of this work led to the following recommendations:

Cask Handling and Loading

- The cask information required prior to handling a cask should include cask design drawings and specifications, operating and maintenance manuals, procedures, and spare parts.
- Dry (cold) runs of the cask and associated equipment should be performed for all phases of cask handling and loading, including backfilling the cask with a cover gas and gas sampling. Cask vendor representatives should be present onsite for operational and functional checkouts of the cask.
- Cask-handling procedures are site-specific, and procedures should be developed for each site. The experience gained during this performance test will be helpful in developing such procedures.
- The cover gas system used to evacuate, backfill, monitor, and obtain gas samples should be carefully designed. The difficulty associated with backfilling the cask with a pure (>99%) cover gas and obtaining gas samples without introducing air should not be underestimated. The cask should be pumped down and backfilled a minimum of two times to ensure purity (>99%) of the final cover gas.

Heat Transfer Performance

- Critical basket gaps should be controlled. Basket designs should maximize thermal conductance between the basket and cask wall.

COBRA-SFS Heat Transfer Analysis

- COBRA-SFS is an effective code that can be used to accurately predict temperatures in spent fuel dry storage systems and, once successfully evaluated and documented, it will be available for design and licensing safety analyses.

- COBRA-SFS predictions of peak dry storage system temperatures within 25°C can be obtained. Further, if it is desirable to improve this agreement, the following, in order of importance, should be pursued:

  - System geometries, especially gap widths and characteristics of contacting surfaces, must be better known.

  - Emissivities of important basket/cask components should be measured.

  - The accuracy of the correlation used to represent heat transfer to and from the cask exterior wall should be improved.

- The heat transfer data contained in this report can be used to evaluate other heat transfer codes.

Shielding Performance

- Minor refinements to the gamma shield adjacent to fuel assembly end fittings should be made to decrease peak dose rates to <60 mrem/h.

- Additional shielding is needed on the bottom of the cask for horizontal storage.

- Modifications to the lid design are required to reduce streaming at the lid parting plane.

Fuel Characteristics and Integrity

- It may be worthwhile to perform post-test fuel inspections in an attempt to locate the fuel assembly(s) with the leaking fuel rod(s) and to characterize the nature of the failure.

Section 3

CASK PERFORMANCE TESTING

Details of the cask performance test using a TN-24P cask are discussed in this section. Based on availability and program schedule, an existing TN-24P (prototype) was used for testing instead of a commercial TN-24. The TN-24P cask and instrumentation are described, as are the Surry PWR spent fuel assemblies and associated instrumentation. The major differences between the TN-24P and TN-24 cask are presented with a brief discussion of the impact these differences have on the performance results. The data acquisition system used to receive and process instrumentation signals is described. A description of the INEL cask-testing facility is provided. The test plan is presented, and the procedures resulting from the plan are summarized. Experiences gained during cask-handling dry runs and testing are described.

TN-24P CASK AND ASSOCIATED INSTRUMENTATION

The TN-24P cask has a forged steel body for structural integrity and gamma shielding, surrounded by a resin layer for neutron shielding, which is enclosed in a smooth steel outer shell. The loaded cask weighs approximately 100 tons on the fuel pool crane hook. The cask has a cylindrical cavity that holds a fuel basket designed to accommodate 24 intact PWR fuel assemblies. The basket is made of a neutron-absorbing material, borated aluminum, to control criticality. The cavity atmosphere is designed to be nitrogen or helium at a positive pressure.

The cask is sealed with a single lid. A protective cover, bolted to the body, provides weather protection for the lid penetrations. Two concentric metallic O-rings are provided for sealing the lid to the cask body, and an elastomer O-ring is used with the protective cover. The body is fitted with three pairs of removable trunnions for handling and transport. A polyethylene neutron shielding disk is attached to the lid when the cask is in storage. If the cask is stored in a horizontal orientation, a neutron shielding disk must also be attached to the cask bottom.

The major differences between the TN-24P test cask and standard TN-24 casks occur in cask body thickness, basket material, and neutron shield structure. These differences are listed in Table 3-1.

Table 3-1

DIFFERENCES BETWEEN TN-24 PROTOTYPE (TN-24P) AND STANDARD TN-24 CASKS[a]

Parameter	TN-24	TN-24P
Cask Body		
Cask OD, cm (in.)	225 (88.5)	228 (89.8)
Steel shell thickness, cm (in.)	24 (9.5)	27 (10.6)
Bottom thickness, cm (in.)	26.7 (10.5)	28 (11.0)
Outer shell thickness, cm (in.)	1.9 (0.75)	1 (0.39)
Bottom chamfer	yes	no
Neutron shielding annulus	Resin in aluminum cans that butt against cask body and outer shell.	Resin butts against cask body and is between copper fins that are welded to outer shell.
Shell penetrations	None	One
Lid		
Lid thickness, cm (in.)	26.7 (10.5)	28.5 (11.2)
Lid bolts (No. x dia., in.)	48 x 1.50	40 x 1.65
Neutron shielding thickness, cm (in.)	7 (2.75)	10.7 (4.2)
Penetrations	2	1
Basket		
Material	Borated stainless steel with copper cladding	Borated aluminum
Plate size (height x thickness, in.)	41 x 0.6 (16.2 x 0.22) 0.3 (0.118 in. copper)	16 x 1 (6.3 x 0.39)
Construction	Full interlocking plates	Semi-interlocking plates with connecting angles
Instrumentation	No internal thermocouples	Internal thermocouples
Protective Cover	1.9 (0.75 in. thick) bolted to cask body	0.8 (0.315 in. thick) attached by clamps to cask body
Loaded weight on storage pad (lb)	83.5 MT (184,000)	87.1 MT (192,000)

[a]Data presented were provided by M. Mason of Transnuclear, Inc., June 20, 1985.

The TN-24P basket is composed of borated aluminum plates, while the standard TN-24 basket is assemblied from copper-clad borated stainless steel plates. The TN-24P has an instrument penetration in the cask body containing thermocouples that are attached to the basket. The standard TN-24 contains no instrumentation penetration.

These differences impact the cask performance in two ways: 1) the dose rate for standard TN-24 casks will be higher than for the TN-24P test cask due to differences in wall thickness, and 2) temperatures in standard TN-24 casks will be higher due to basket materials and neutron shield structure.

The remainder of this section will describe the TN-24P cask. A detailed description of the cask can be found in References 4 and 5.

Cask Body

The cask body is a one-piece cylindrical structure composed of forged steel (4). The overall external dimensions of the cask body are 5063 mm (16.6 ft) long and 2281 mm (7.5 ft) in diameter (Figure 3-1). All surfaces except sealing surfaces are coated with a deposit of zinc-aluminum alloy. Sealing surfaces are clad with stainless steel. Internal surfaces have an aluminum titanium oxide overcoat; exterior surfaces are covered with white silicone paint.

The cask body consists of a 270-mm-thick (10.6-in.) cylindrical shell welded to a 280-mm (11-in.) bottom plate. A neutron shield containing L-shaped copper plates is welded to the cylindrical shell. The copper plates are welded to the inner surface of the neutron shield and provide enhanced heat conduction through the resin compound of the neutron shield. The cask can accommodate six bolted trunnions for handling and tie-down, four near the top and two near the bottom. Finally, the cask body has an instrumentation orifice sealed by a metallic gasket.

The diameter of the inner cavity is 1455 mm (57.3 in.), and the overall inner cavity length is 4150 mm (163.4 in.). Precision-machined surfaces are provided at the open end of the cask cavity for positive gasket sealing, and bolt holes are included at these location to secure the cask lid and protective cover.

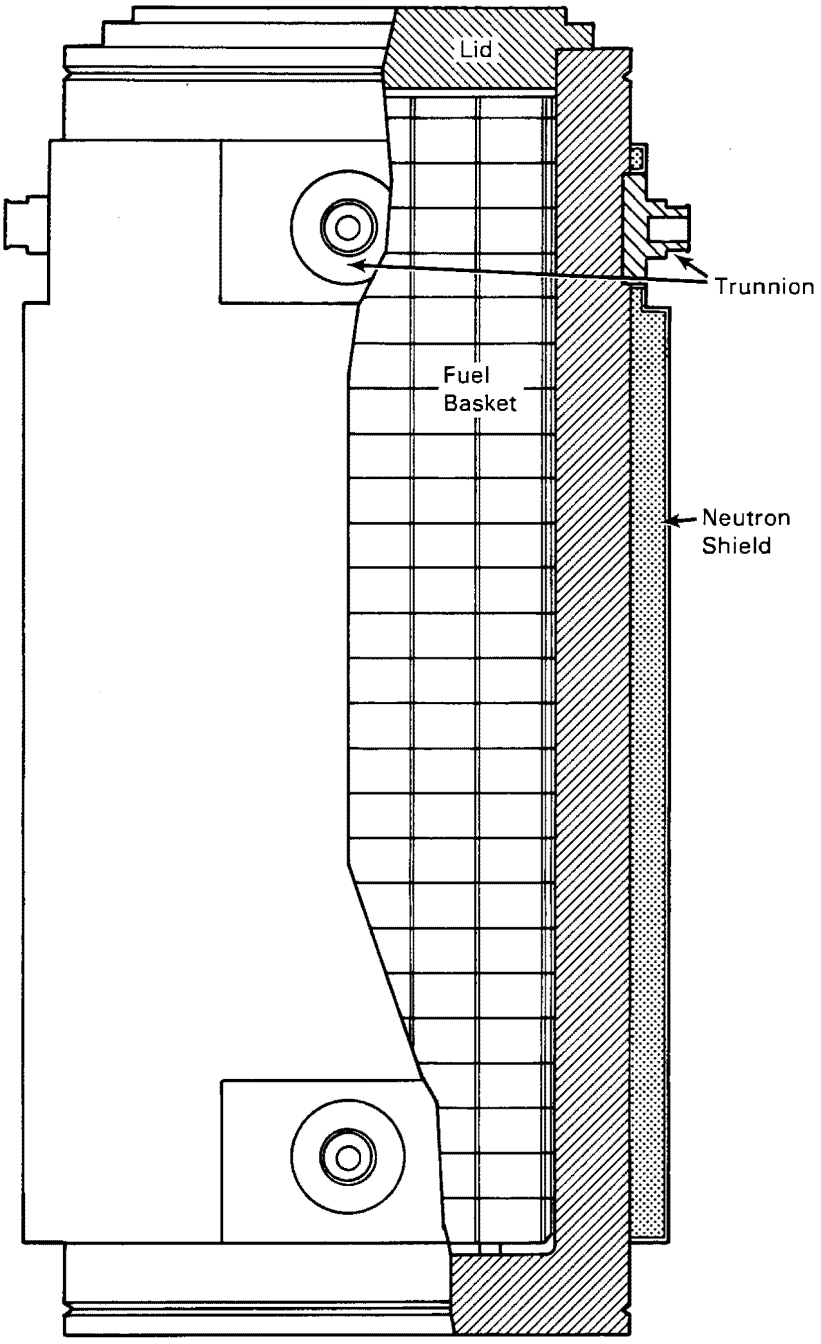

Figure 3-1. TN-24P PWR Spent Fuel Storage Cask

Spent Fuel Basket

The basket comprises an array of 24 fuel tubes/channels that provide structural support and positive positioning of the fuel assemblies. The basket (Figure 3-2) is composed of stacked interlocking plates constructed of aluminum and boron. The plates are 10 mm (0.4 in.) thick and 160 mm (6.3 in.) wide, and vary in length depending on their position in the basket. Each layer of the basket is bolted to four uprights that are used to tie the basket together in the axial direction and support the basket. The uprights provide a 45-mm (1.8-in.) gap between the bottom of the basket and the bottom of the cask. This gap plus the 29-mm (1.1-in.) gap between the top of the basket and the cask lid provide convection paths for the gas in the cask. The basket overall height is 4121 mm (162.2 in.). The position of the basket within the cask is maintained by bars welded to the interior surface of the cask. The bars act as guides for the interlocking plates.

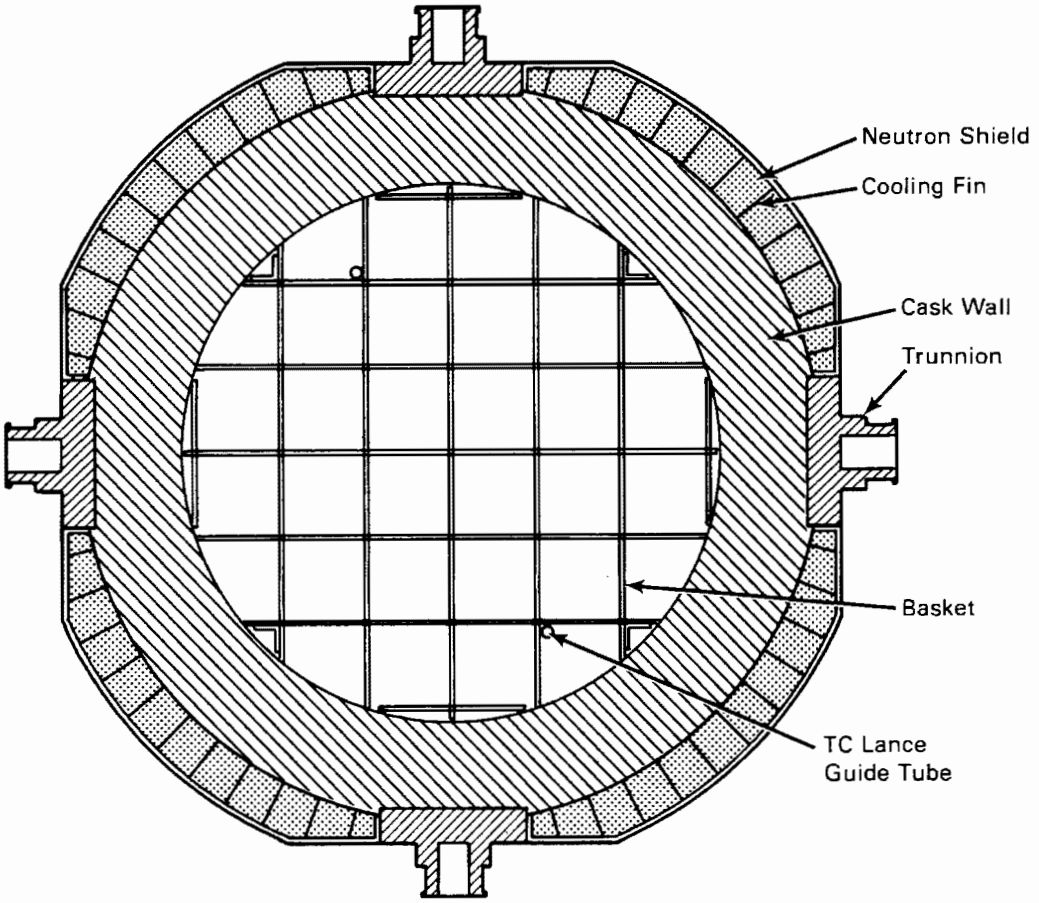

Figure 3-2. TN-24P Cask Cross Section

Two aluminum tubes are welded to the aluminum basket in two locations that did not interfere with the fuel. The tube locations match penetrations in the lid used to insert TC lances and provide temperature readings typical of the basket.

Cask Lid

A carbon steel lid, 1720 mm (5.6 ft) in diameter and 285 mm (11.2 in.) thick, is provided (Figure 3-3). The lid is fastened to the cask body with 40 bolts matching index marks on the lid and cask for proper alignment. Sealing is ensured by a double O-ring metallic gasket installed in a stainless steel-coated lid groove. A 5-mm-diameter (0.2-in.) penetration through the lid provides access to the annulus between the two seals to perform post-assembly leak testing. Additional sealing is obtained by a Viton O-ring fitted between the protective cover and a groove in the top surface of the cask wall.

An operations orifice is located in the lid for access to the internal cavity. It consists of a plug extended by a base acting as a radiation trap, a tightening ring, and an orifice plate. Sealing of this penetration is ensured by an O-ring metallic gasket fitted on the orifice plate. Sealing is monitored through a test orifice closed by a test plug.

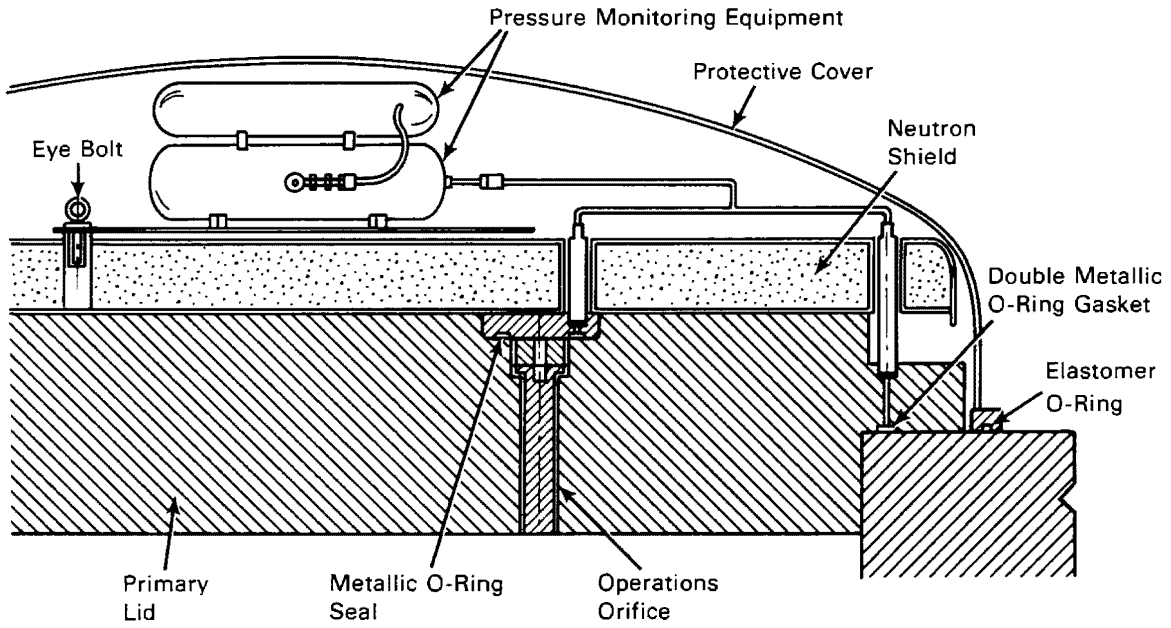

Figure 3-3. TN-24P Cask Lid

A neutron shielding drum is bolted to the lid. It consists of granular polypropylene wrapped in a carbon-steel drum. The drum is composed of a flat circular head closed with a circular welded plate. Its finished size is 105.5 mm (4.2 in.) thick by about 1700 mm (70 in.) in diameter. To facilitate operations, test plugs in the lid and operations orifice plate are easily accessible while the drum is in place.

A protective cover fits over the lid and neutron shielding drum. This cover consists of a carbon-steel ellipsoidal head and a flange equipped with one rubber O-ring gasket. The cover is 1815 mm (71.5 in.) in diameter and 498 mm (19.6 in.) deep. It is fastened to the body of the cask using eight bolts and clamps. Two penetrations are provided in the protective cover for instrumentation leads and for leak-checking the attached cover. The interspace between the lid and the protective cover contains the pressure monitoring loop. This loop pressurizes and monitors the space between the double O-ring metallic gaskets during long-term storage. It also pressurizes and monitors the operations orifice seal. The loop consists of connections to the lid and operations spaces to be monitored, a pressure monitoring tank, a reference pressure tank, a pressure sensor, and two thermocouples. The thermocouples provide data concerning whether pressures changes are due to temperature changes or leakage.

A non-standard lid with nine penetrations for thermocouple lances was used during the performance testing (Figure 3-4). The TC lances will be described in detail in the next section. Eight of the penetrations are machined with 18-mm (0.7-in.) holes through the lid and countersunk (20 mm, 0.8 in.) to accept the TC lances and 105-mm-diameter (4-in.) flanges. The ninth penetration has a hole through the lid for a TC lance and accepts a 140-mm-diameter (5.5-in.) flange. The pattern of the nine fuel assembly instrumentation penetrations was selected to measure radial temperature profiles across the basket in the spent fuel assemblies. Cask evacuation, gas backfill, pressure monitoring, and gas sampling were done using the instrumentation port through the side of the cask. The test lid used a single Viton O-ring and 20 bolts instead of the double O-ring metallic seal and 40 bolts used with the primary lid. Like the primary lid, the test lid was 1725 mm in diameter and 285 mm thick. However, the neutron shielding drum, protective cover, and pressure monitoring loop were not used during the performance test. Gas backfilling, gas sampling, and pressure monitoring were performed through the instrumentation port by means of a cross manifold when the test lid was on the cask.

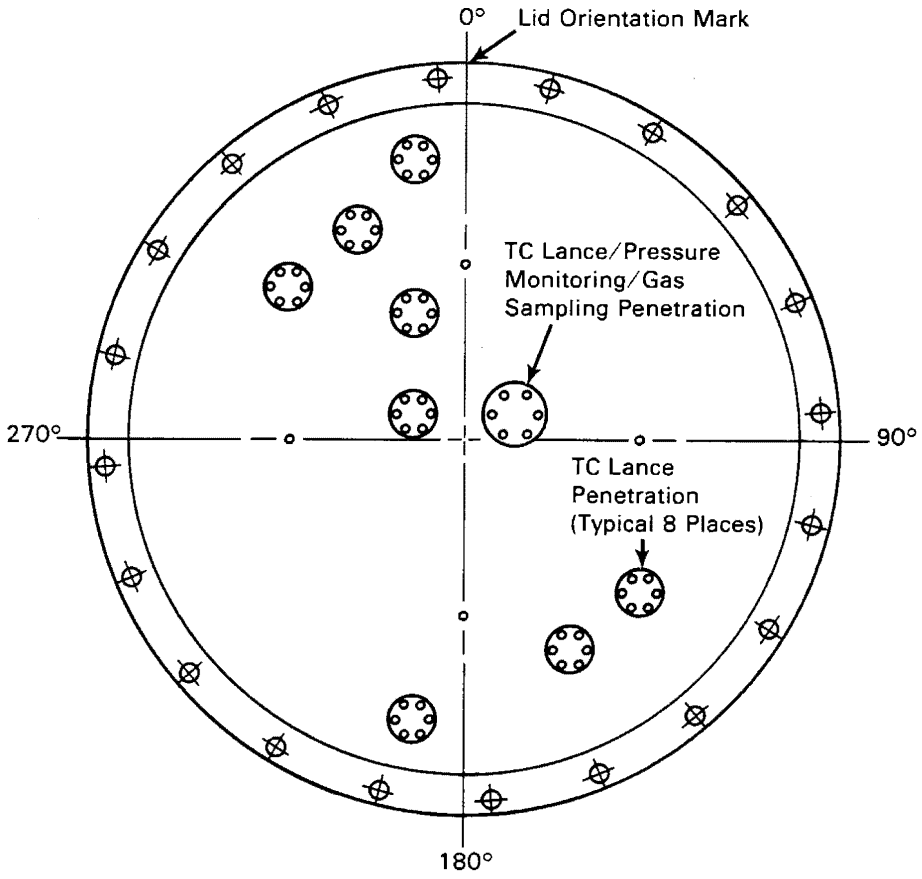

Figure 3-4. TN-24P Cask Non-Standard Test Lid

Cask Cavity Pressure Measurements

A Leybold Heraeus model MAC 2000 pressure transducer was used to measure cask cavity pressures. The transducer had a range of 0 to 2000 mbar and a stated accuracy of ±0.02% of full scale. The transducer was connected to the quick-disconnect penetration provided in the primary lid of the cask (Figure 3-4) via the valve tree shown in Figure 3-5. The signal from the transducer was conditioned and read out on the data acquisition system (DAS) described in a later section.

Internal Temperature Instrumentation

Fourteen Type K TCs were permanently attached to the inner wall and basket of the cask. Figure 3-6 identifies the locations of these thermocouples. An additional 54 TCs were placed in the fuel assemblies and basket using TC lances (Figures 3-7 and 3-8). Each TC lance had six TCs installed in an 8-mm-diameter (0.315-in.) tube as shown in Figure 3-7. Lances were inserted through instrumentation penetrations in the primary test lid (Figure 3-4) and into selected guide tubes of seven fuel

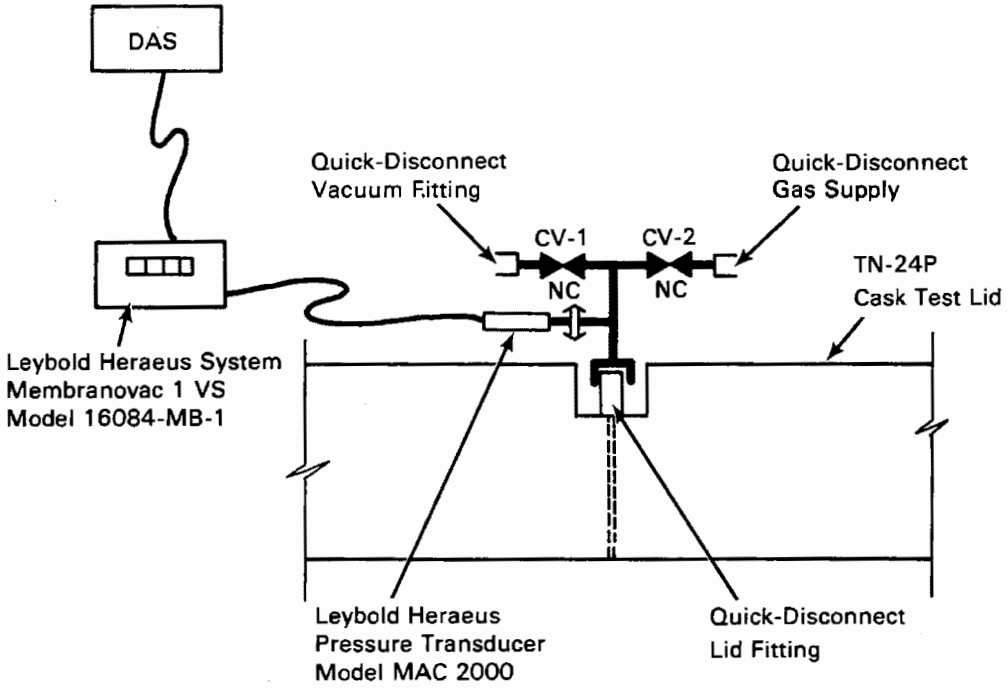

Figure 3-5. Pressure Transducer Valve Tree

assemblies and into two simulated guide tubes attached to the basket (Figure 3-8). Standard elastomer O-rings in the TC lance flanges were used to establish seals between the cask inner cavity containing spent fuel and the outside environment.

The selected axial and cross-sectional locations of the TC lance thermocouples facilitated redundancy, evaluations of temperature symmetry, and determinations of axial and radial temperature profiles in both vertical and horizontal orientations.

Exterior Surface Temperature Instrumentation

The exterior surface of the cask was instrumented with 35 iron/constantan Type J TCs. Figures 3-9 and 3-10 identify the locations of the TCs on the primary lid, barrel, and bottom of the cask. Only during horizontal testing were TCs placed on the bottom of the cask. The TC patterns on each surface were selected to provide appropriate axial, radial, and circumferential temperature profiles.

Exterior Surface Dose Rate Instrumentation

Gamma dose rates were measured on the surface of the cask with thermoluminescent dosimeters (TLDs). Neutron dose rates were measured with track etch dosimeters (TEDs). Portable hand-held survey instruments were used to measure both gamma and

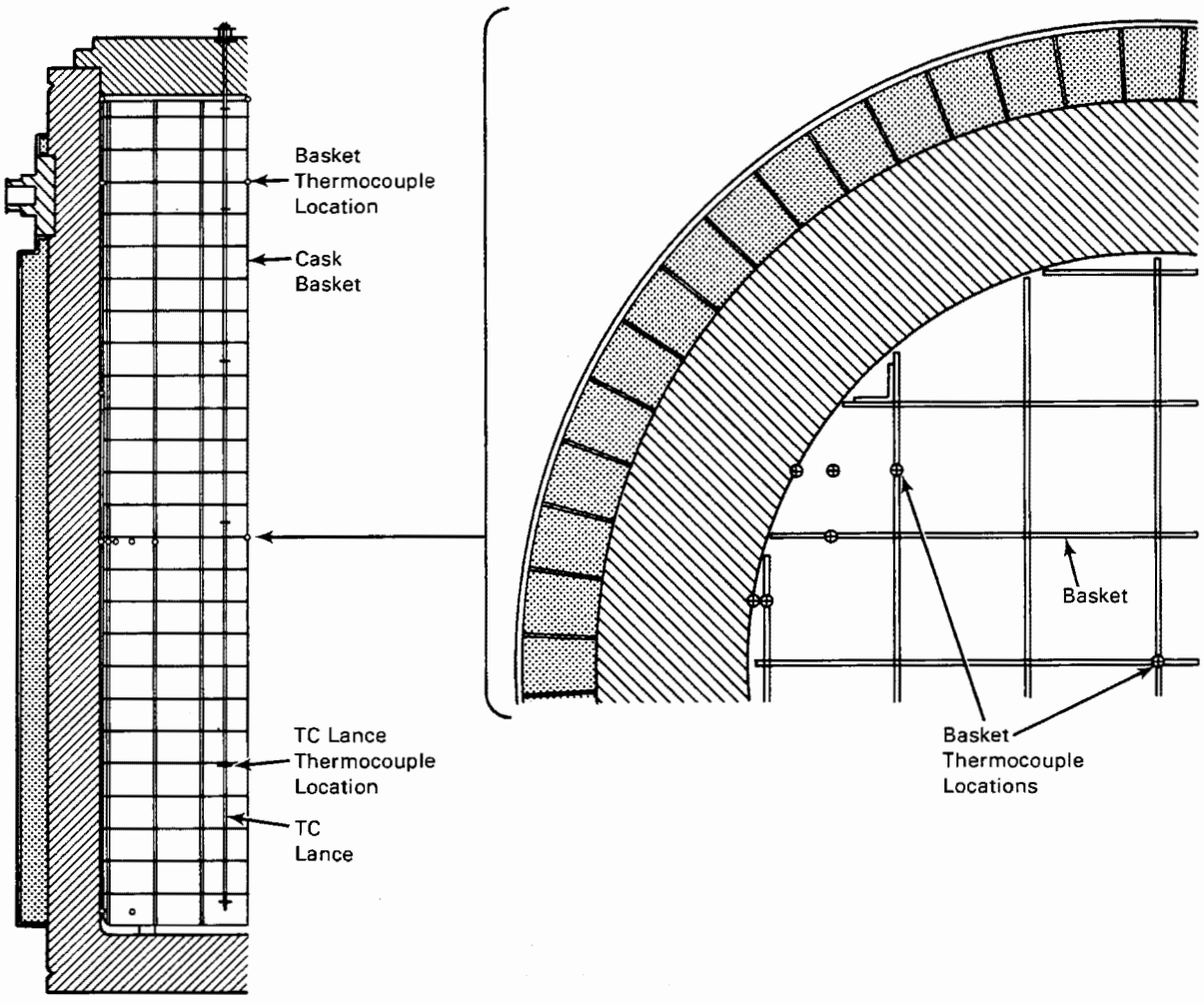

Figure 3-6. Basket Thermocouple Locations

neutron dose rates. Data obtained from these sources are presented and discussed in Section 4. The dosimeters and hand-held instruments, along with energy spectra instrumentation required to calibrate the TLDs and TEDs, are briefly discussed in the following sections.

Energy Spectrum Instruments. Energy spectra measurements were required to determine accurate gamma and neutron dose equivalents from TLD and TED measurements, i.e., to calibrate the TLDs and TEDs. Gamma energy spectra were measured with an intrinsic germanium spectrometer at a few selected locations. The spectrometer, a semiconductor-type radiation detector, consists of a germanium crystal operated as a reverse biased diode. Gamma rays that interact within the crystal cause ionization, and the resulting charged particles produce an electron current that is collected at

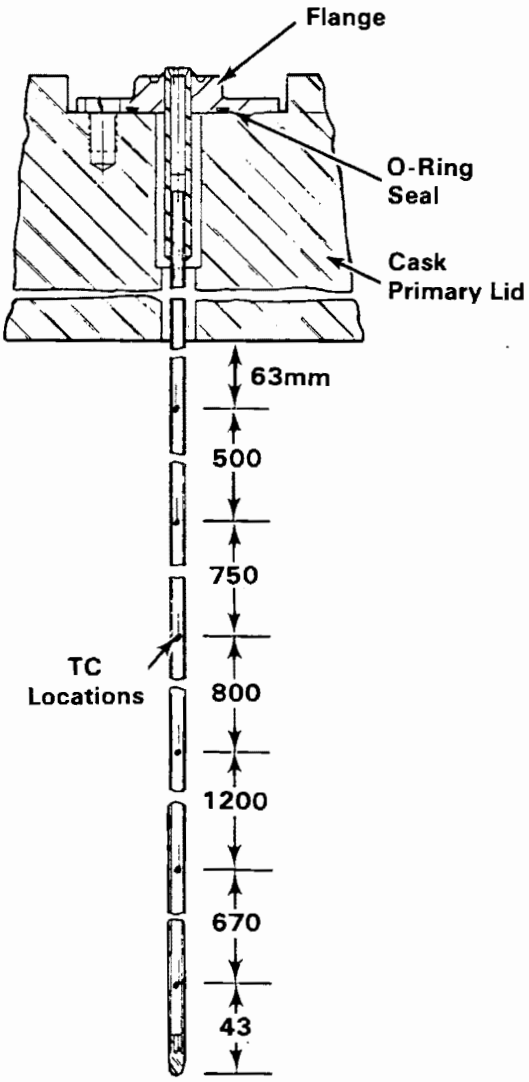

Figure 3-7. Thermocouple Lance

the electrodes. The electron current is proportional to the energy deposited within the crystal. A detailed description of the intrinsic germanium spectrometer is provided in (6).

Neutron dose equivalents and energy spectra were measured with a multisphere spectrometer on the surface and 1 m (3.3 ft) from the surface at locations previously indicated for gamma energy spectra measurements. The multisphere spectrometer consists of ^{6}Li iodide scintillation crystal optically coupled to a photomultiplier tube. The detector is used in conjunction with a cadmium cover and five high-density polyethylene spheres of varying sizes. For a single location, count rate measurements are taken with the bare detector, with a cadmium cover on the detector,

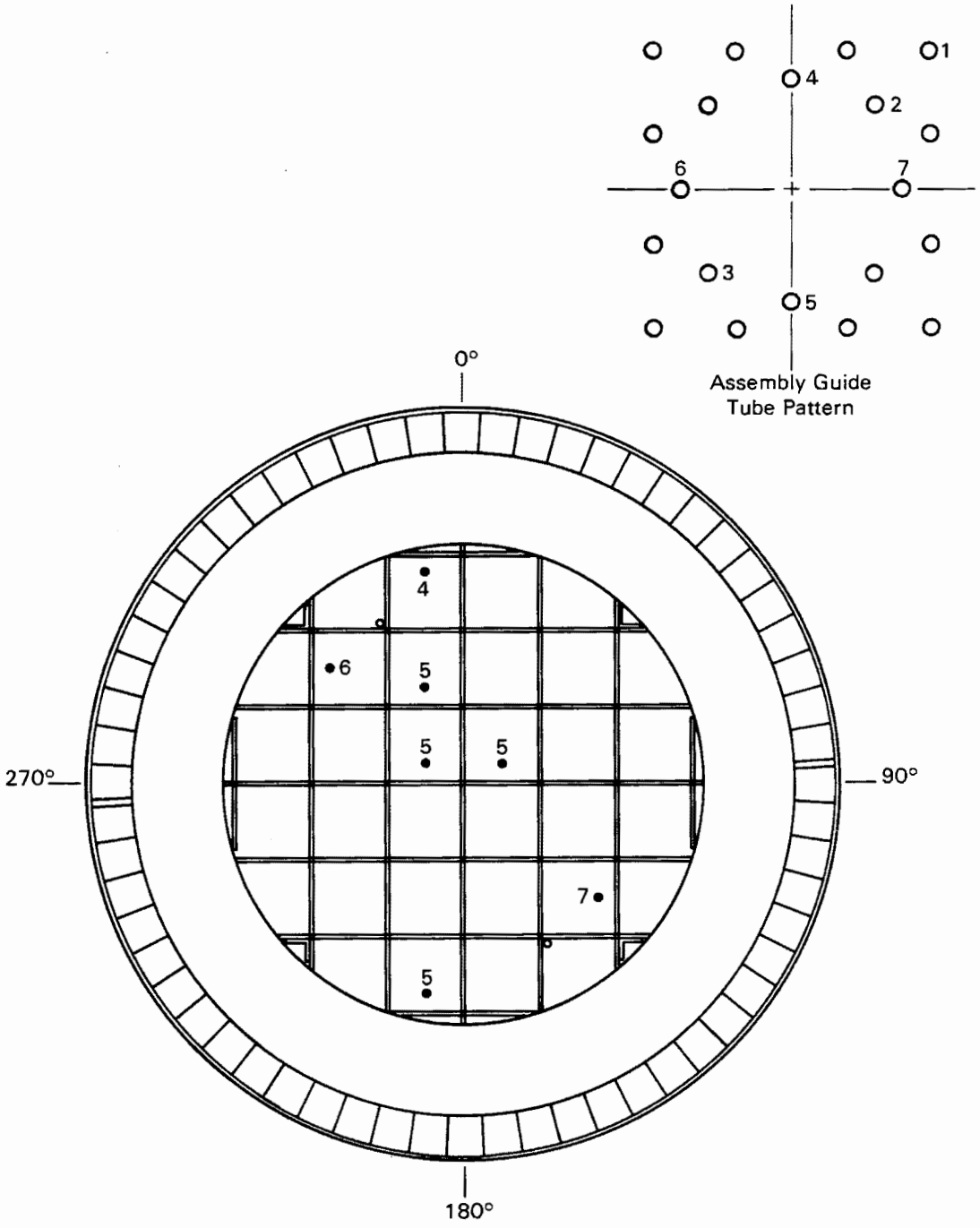

Figure 3-8. Thermocouple Lance Locations

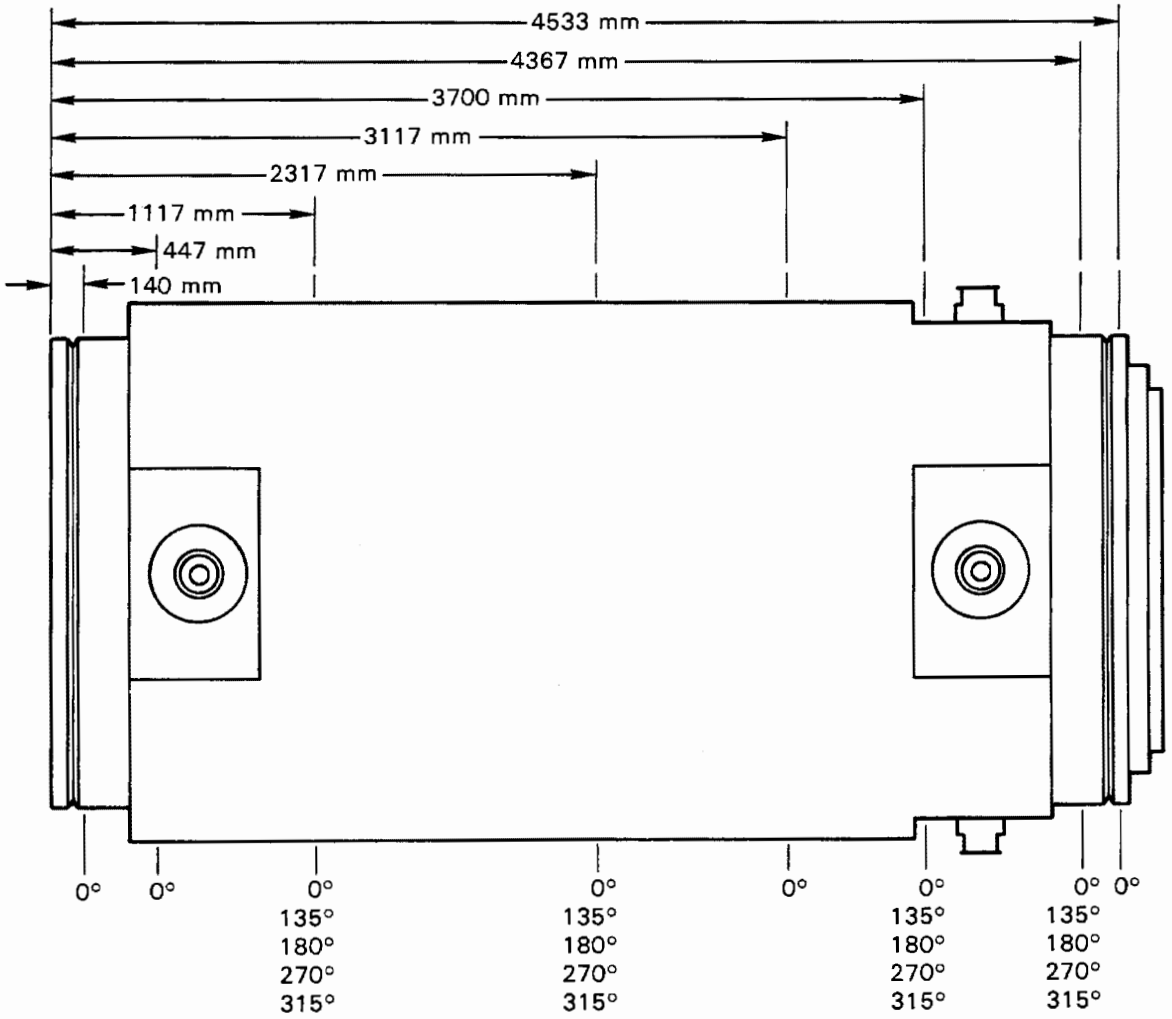

Figure 3-9. Cask Surface Thermocouple Locations

and with polyethylene spheres on the detector. The spheres are of five diameters: 76 mm (3 in.), 127 mm (5 in.), 203 mm (8 in.), 250 mm (10 in.), and 305 mm (12 in.). The polyethylene moderates the neutrons, and the resulting slow neutrons produce a distinct measurable peak. The incident neutron energy spectrum can be estimated by using the differences in slow neutron count rates produced by the different sizes of spherical moderators. A detailed discussion of the multisphere spectrometer is presented in (6).

Neutron spectra between thermal and 1 MeV were measured with a ^{3}He spectrometer. The ^{3}He spectrometer provides direct measurements of neutron flux as a function of energy and consists of a proportional counter filled with a mixture of ^{3}He and Ar. The neutrons interact with the ^{3}He to produce a triton and a proton. These charged

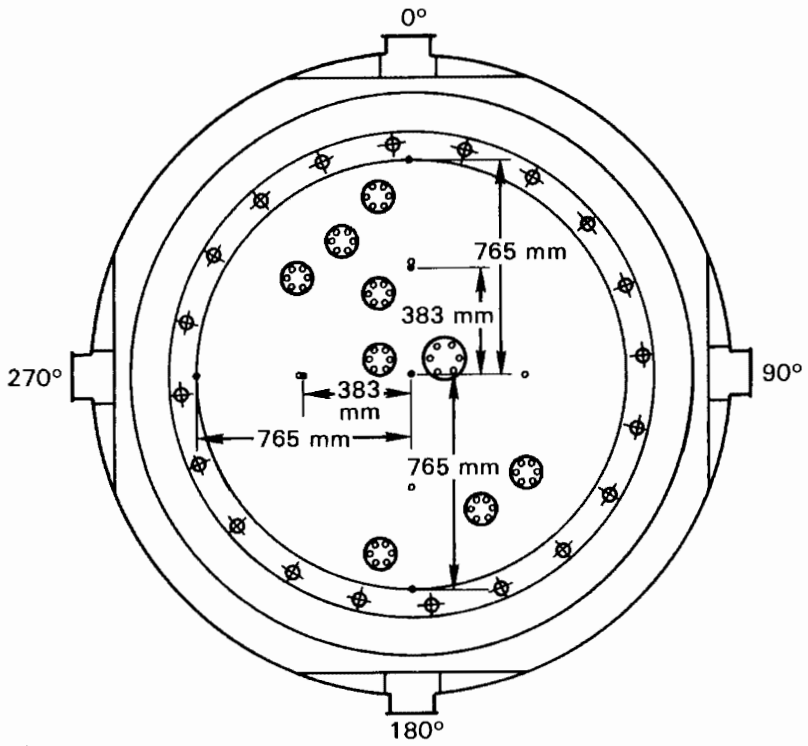

Cask Top

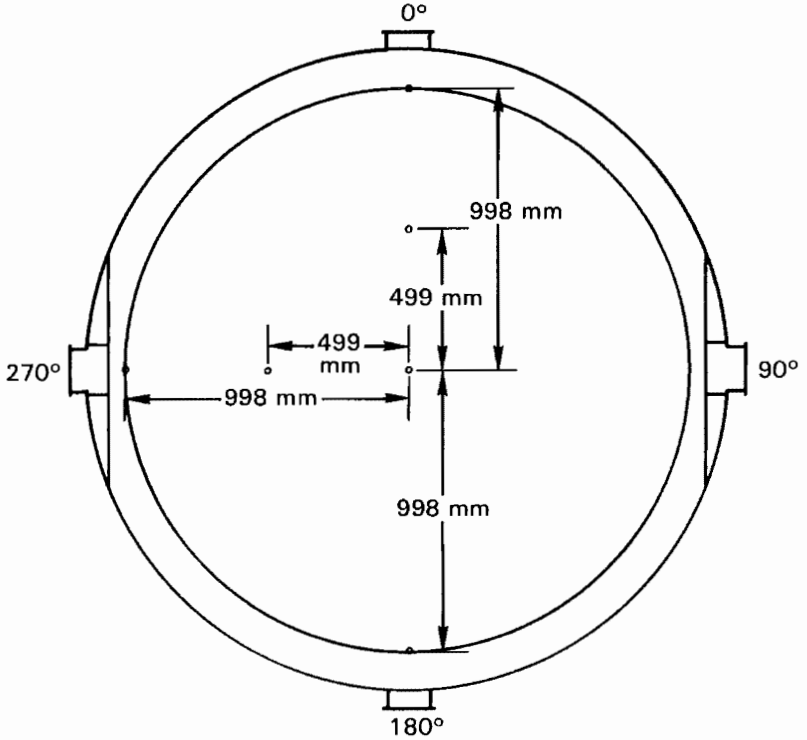

Cask Bottom

Figure 3-10. Cask Top and Bottom Thermocouple Locations

particles are slowed by the fill gas and deposit some or all of their energy in the detector. When the charged particles are completely stopped in the sensitive volume of the tube, the energy absorbed is directly proportional to the energy of the incident neutron plus 764 keV, the energy released by the nuclear reaction. The ^{3}He detector is most sensitive to thermal neutrons due to the 1/v cross section of ^{3}He for neutron absorption. This results in a large peak at 764 keV, which is used to calibrate the spectrometer. A detailed discussion of the ^{3}He spectrometer is presented in (6).

Thermoluminescent Dosimeters. Axial and radial gamma dose rate profiles on the cask surface were measured using thermoluminescent dosimeters (TLDs) at the 80 locations identified in Figures 3-11 and 3-12. An extra 15 dosimeters (6 on the lid and 9 on the side) were placed at various locations around the cask to detect possible streaming. Each TLD consisted of three ^{7}LiF chips placed in a gelatin capsule. Each capsule was attached to a 1-in. styrofoam cube to protect the dosimeter from the high temperatures at the very surface of the cask. The styrofoam blocks were attached to the surface of the cask with high-temperature tape. When heated, TLDs emit light in quantities proportional to the energy deposited in the material by the incident radiation; hence, the need to protect the dosimeters from high temperatures. The three chips per dosimeter were used to give good statistical results.

The TLDs were left on the cask for 3 to 4 days. The dates and times on and off were recorded for each dosimeter to determine exposure times. After exposure of the TLDs on the storage cask, the chips were removed from the gelatin capsules and read out.

Gamma dose rates from TLDs are calculated using a calibration factor derived by exposing a set of calibration dosimeters to 1000 milliroentgen of radiation from a 10-Ci ^{137}Cs National Bureau of Standards (NBS) certified source. The average of the readouts from all the calibration chips was used to convert the TLD output from nanocoulombs to milliroentgens. The results for the three chips in a given dosimeter capsule were averaged, and the background determined by a set of control TLDs was subtracted out. The resulting total doses in milliroentgens were divided by the length of time the TLDs were on the cask to determine total dose rates in milliroentgens per hour.

Track Etch Dosimeters. Track etch dosimeters (TEDs) were used to determine neutron dose equivalent rate profiles. The TED measurement locations consisted of 40 points

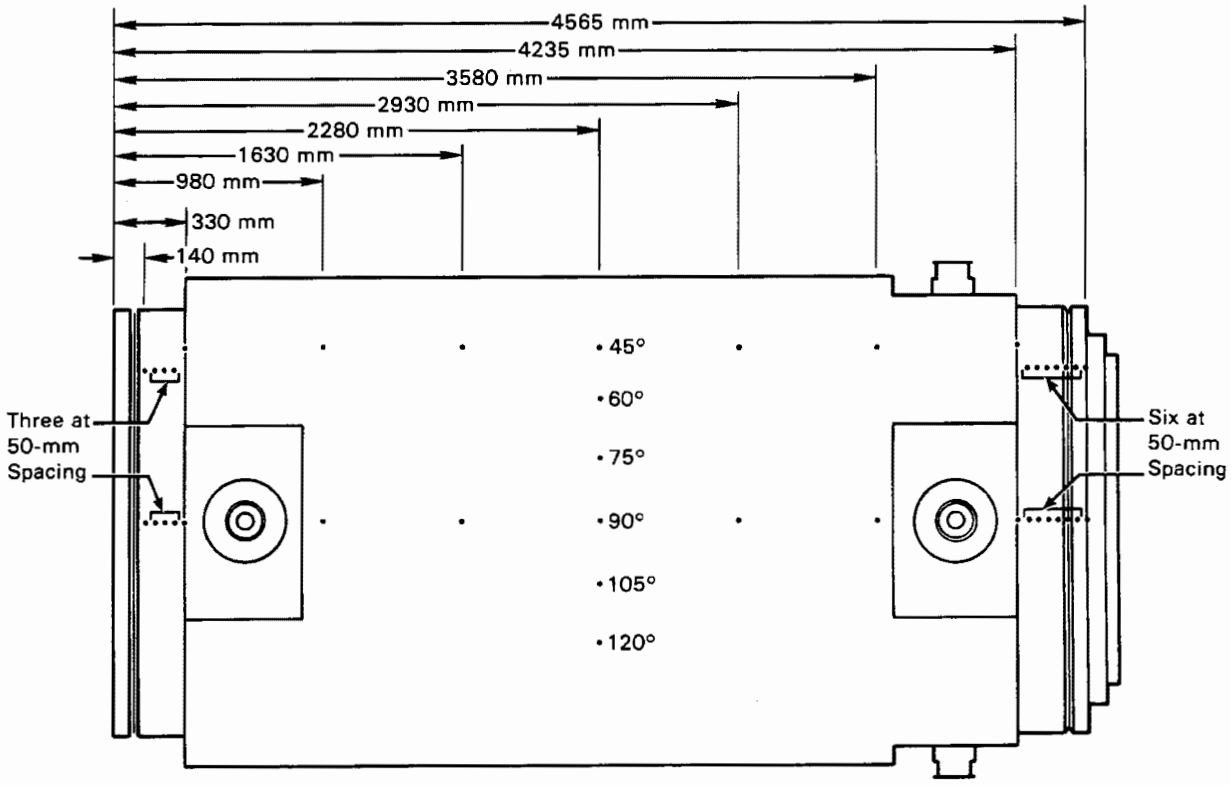

Figure 3-11. Cask Surface Dosimeter Locations

along the side of the cask, 20 on the top, and 20 on the bottom (Figures 3-11 and 3-12). The dosimeters were left on the cask for 3 to 4 days before being removed and processed.

The TEDs were made of strips of CR-39 plastic (allyl diglycol polycarbonate) 29 mm (1.125 in.) by 16 mm (0.625 in.) by 2 mm (0.07 in.). They were covered with an 8-mm (0.003-in.) layer of polyethylene to protect them from background alpha radiation. For dose rate measurements, the TEDs were attached to the same styrofoam cubes used for the TLDs, and the measurement times and locations were recorded individually. Upon exposure to radiation, damage sites are created through neutron bombardment of the polymer, causing proton recoil interactions and breaking some of the polymer crosslinkages. The TEDs were analyzed using a caustic solution and electrochemical etching to produce visible tracks of the damage sites. The number of tracks was counted, and the visible track density was related to dose equivalent using predetermined calibration factors.

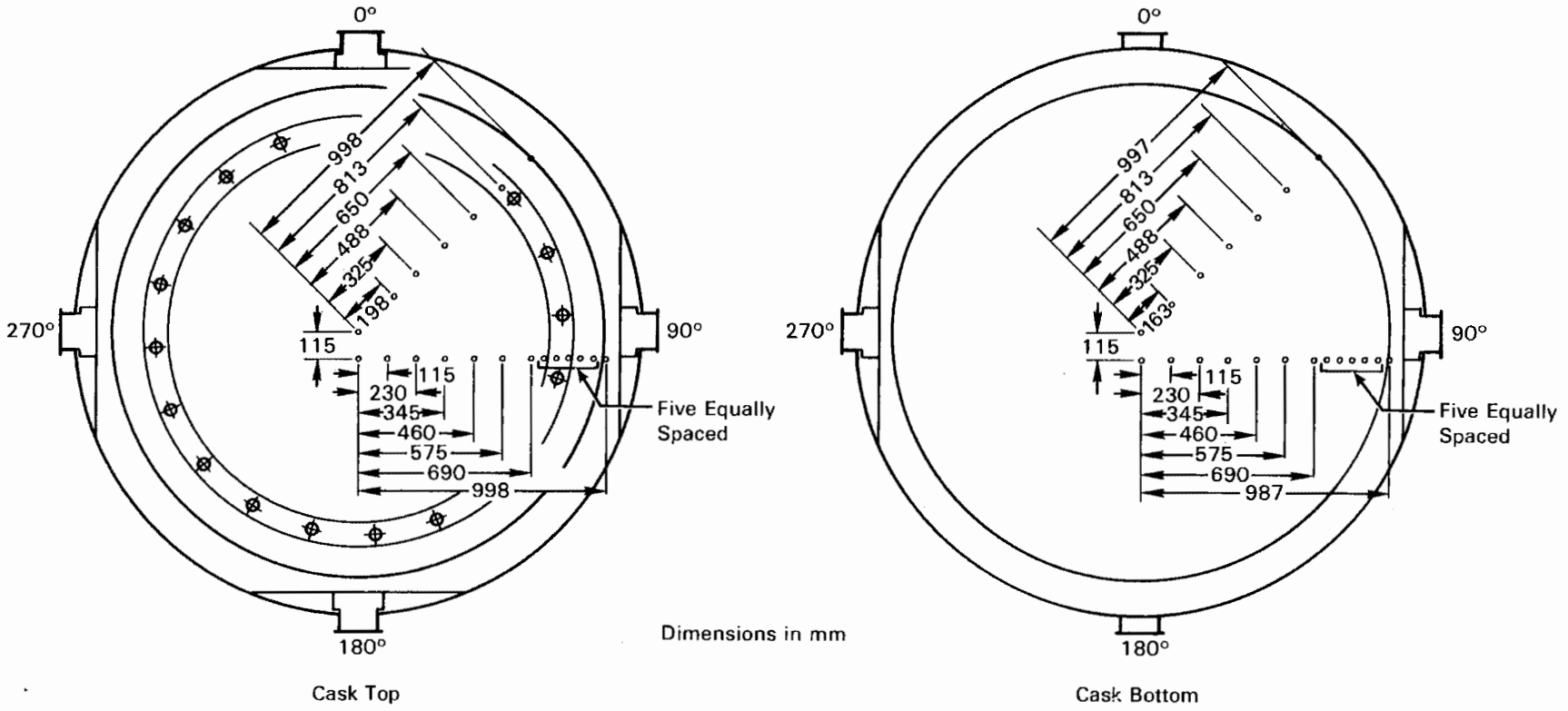

Figure 3-12. Cask Top and Bottom Dosimeter Locations

Several TEDs designated as controls were taken to the site and placed away from the cask to provide an indication of the background radiation received by the dosimeters. The neutron fluences from the TEDs were calculated from the track density (tracks/cm^2) using the energy response for an average neutron energy of 200 keV as given by the spectrometer results. The calibration factor was 5.0×10^{-6} tracks/neutron to convert tracks/cm^2 to neutron fluence (n/cm^2). Neutron dose equivalents were calculated from fluences using 6.11×10^{-6} mrem/(n/cm^2). The total dose equivalent in millirems was then divided by the time the dosimeter was on the cask to get the dose equivalent rate.

Tissue Equivalent Proportional Counter. A tissue equivalent proportional counter (TEPC) was used to directly measure the neutron dose rate at several of the locations indicated in Figures 3-11 and 3-12. The TEPC also provides information about the linear energy transfer and quality factor of the incident neutrons. It consists of a hollow sphere or cylinder of tissue equivalent plastic filled with a low-pressure tissue equivalent gas. Neutrons interacting within the wall of the TEPC produce recoil protons and heavy ions that travel through the fill gas, causing ionization. The electronic pulses created by the charged particles are collected on the counter anode. By definition, energy deposited in the gas divided by the mass of the gas is the absorbed dose. Using an appropriate algorithm, it is possible to determine neutron quality factors from the pattern of energy deposited in the counter; thus, it is possible to determine dose equivalent rates directly from the TEPC data. As a result, the TEPC is an absolute dosimeter and does not require independent calibration, so long as the size of the gas cavity is accurately known. Data taken with the tissue equivalent proportional counter were analyzed with the computer code TACI (7), which is run on an HP-87 desktop computer.

Portable Survey Instruments. Two standard portable survey instruments were used by INEL to measure gamma and neutron dose rates at the same locations where TLD and TED measurements were obtained (Figures 3-11 and 3-12). Gamma dose rate measurements were made using a Eberline RO-3A air ion chamber with a 3.5 mg/cm^2 Mylar window. Neutron dose rates were measured with an Eberline PNR-4. The PRN-4 consisted of a BF_3 tube moderated by a 9-in.-diameter polyethylene sphere.

Pacific Northwest Laboratory also performed radiation surveys of the cask to corroborate the results from the TLDs, TEDs, and spectrometers. The PNL gamma survey readings were taken with an Eberline RO-3B, which is the same type of instrument as

the RO-3A but with a different readout format. The neutron survey was performed using a SNOOPY, which consists of a BF_3 detector moderated by an 8-1/2-in.-diameter polyethylene cylinder.

The results of the PNL and INEL surveys provide a valuable comparison and example of how the same types of survey instruments can give consistently different readings, depending on the method and source used to calibrate the instrument and the source of radiation being measured. The INEL gamma survey instruments are calibrated using ^{137}Cs, and the neutron survey instruments are calibrated with an unmoderated ^{252}Cf source. The PNL gamma survey instruments also are calibrated with a ^{137}Cs source, but the SNOOPY is calibrated against an unmoderated PuBe source.

SURRY PWR SPENT FUEL AND ASSOCIATED INSTRUMENTATION

In this section, the design of the Surry spent fuel assemblies used in the TN-24P cask performance test is described. Results of predictions of the decay heat rates and associated average axial decay heat profile for the test assemblies are presented. A description of the instrumentation used to measure assembly guide tube temperatures is provided. The methods used to determine spent fuel integrity before, during, and after testing are discussed, along with results and findings obtained with each method.

Fuel Assembly Design

The fuel assemblies are square in cross section, nominally 214 mm (8.426 in.) on a side, and have a total length of 4058 mm (159.765 in.). The fuel column is 3658 mm (144 in.) long. The overall configuration is shown in Figure 3-13.

The fuel rods in a fuel assembly are arranged in a square array with 15 rod locations per side and a nominal rod-to-rod centerline pitch of 14.3 mm (0.563 in.), as shown in Figure 3-14. Of the total possible 225 rod locations per assembly, 20 are occupied by guide tubes for the control rods and burnable poison rods, and one central thimble is reserved for in-core instrumentation. The remaining 204 locations contain fuel rods.

In addition to fuel rods, a fuel assembly also includes a top nozzle, a bottom nozzle, and seven grid assemblies. The 21 guide tubes and central thimble, in conjunction with the grid assemblies and the top and bottom nozzles, comprise the basic structure of the fuel assembly. The top and bottom ends of the guide tubes

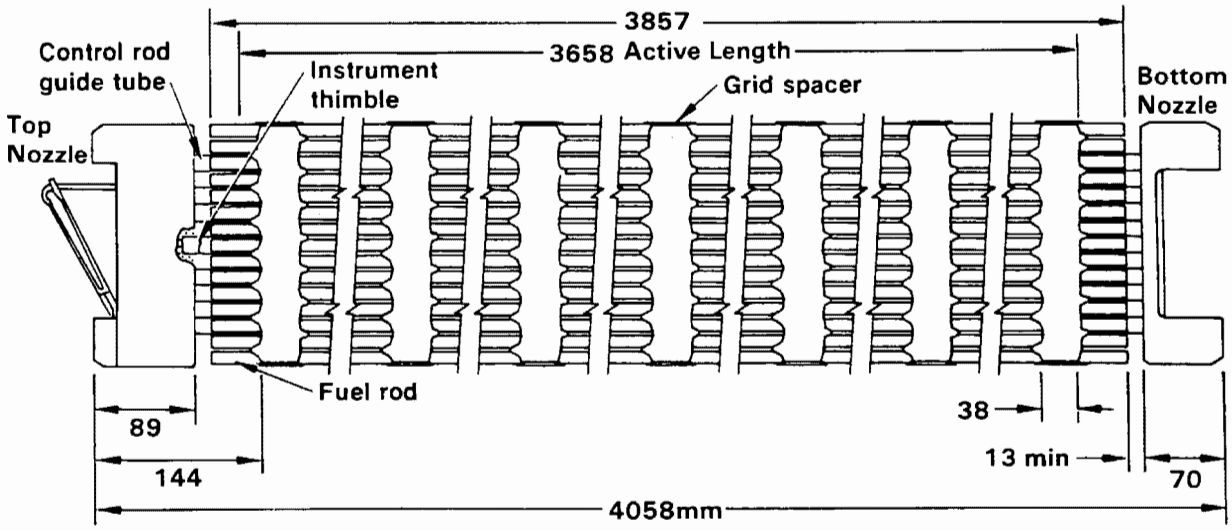

Figure 3-13. Surry 15 x 15 PWR Fuel Assembly

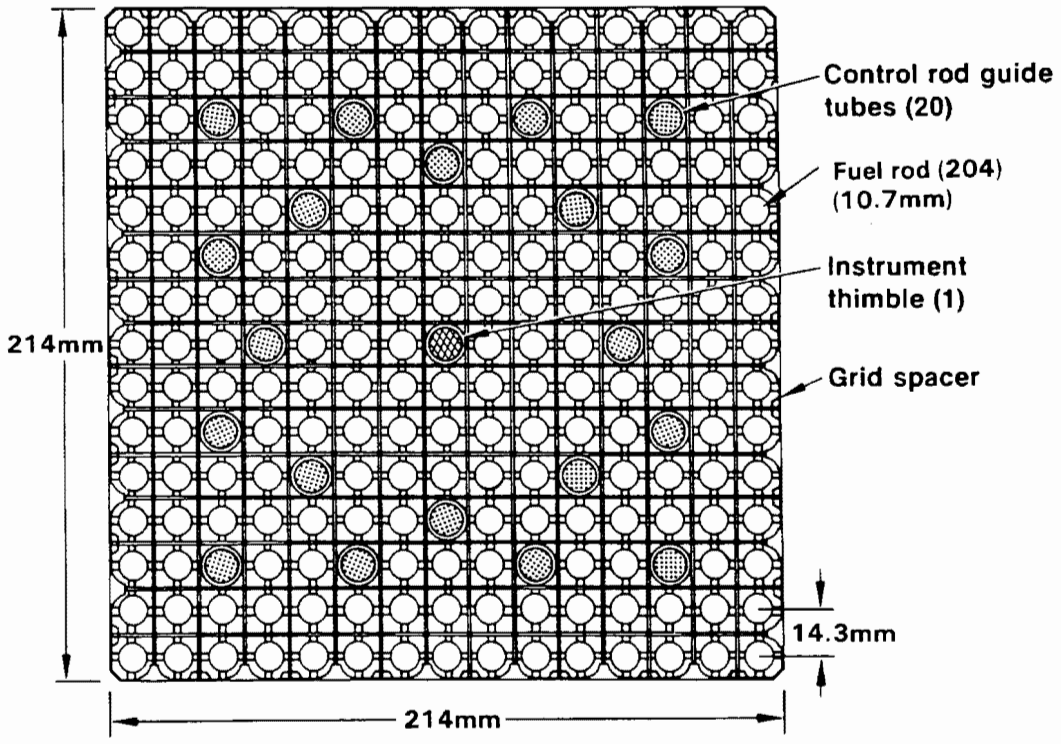

Figure 3-14. Surry 15 x 15 PWR Fuel Assembly Cross Section

are fastened to the top and bottom nozzles, respectively. The grid assemblies are fastened to the guide tubes at each location along the length of the fuel assembly at which lateral support for the fuel rods is required. Within this skeletal framework, the fuel rods are contained and supported, and the rod-to-rod centerline spacing is maintained along the assembly.

The bottom nozzle is a square pedestal structure that controls the coolant flow distribution to the fuel assembly and functions as the bottom structural element of the fuel assembly. The nozzle is fabricated from Type 304 stainless steel parts consisting of a perforated plate, four angle legs, and four pads or feet. The angle legs are welded to the plate to form a plenum space for the inlet coolant flow into the fuel assembly. The bottom support surface for the fuel assembly is formed under the plenum space by the four pads, which are welded to the corner angles.

The guide tubes, which carry axial loads imposed on the assembly, are fastened to the bottom nozzle plate. These loads, as well as the weight of the assembly, are distributed through the nozzle to the lower core support plate. Indexing and positioning of the fuel assembly in the core is fixed by two holes in diagonally opposite pads, which mate with two locating pins in the lower core plate. Lateral loads imposed on the fuel assembly are also transferred to the core support structures through the locating pins.

The top nozzle is a square, box-like structure that functions as the fuel assembly upper structural element and forms a plenum space where the heated reactor coolant mixes and is directed toward the flow holes in the upper core plate. The nozzle comprises an adaptor plate, nozzle enclosure, top plate, two clamps, double-leaf holddown springs, and assorted hardware. All parts except the springs and their holddown bolts are constructed of Type 304 stainless steel. The springs are made from age-hardenable Inconel 718, and the bolts from Inconel 600.

The control rod guide tubes in the fuel assembly provide guide channels for the control rods during insertion and withdrawal. The guide tubes are fabricated from a single piece of Zircaloy 4 tubing, which is drawn to two different diameters. The larger inside diameter at the top provides a relatively large annular area for rapid insertion during a reactor trip. It also accommodates a small amount of upward cooling flow during normal operation. The bottom portion of the guide tube has a smaller diameter to cause a dashpot action when the control rods approach the end of travel in the guide tubes. The transition zone at the dashpot section is conical so that there are no sharp changes in diameter in the tube. Flow holes are provided

just above the transition of the two diameters, to permit the entrance of cooling water during normal operation and to accommodate the outflow of water from the dashpot action during a reactor trip.

The control rod guide tubes are closed at the bottom with a welded end plug. The end plugs are subsequently fastened to the bottom nozzle during fuel assembly fabrication. Flow holes are provided in the end plugs to permit entrance of cooling water during normal operation and to regulate dashpot action during a control rod trip. The instrumentation thimble is left open at the bottom to receive the in-core instrumentation.

The spring clip grid spacers consist of individual slotted straps that interlock in an "egg-crate" arrangement. They are furnace-brazed to permanently join the straps at their points of intersection. Details such as spring fingers, support dimples, mixing vanes, and tabs are punched and formed in the individual straps prior to assembly.

Two types of grid spacers are used in the Surry PWR fuel assemblies. Grid mixing vanes that project from the edges of the straps into the coolant stream are used in the high-heat region of the fuel assemblies to promote mixing of the coolant. The grids located at the bottom and top ends of the assembly are of the nonmixing type. They are similar to the mixing type but do not have mixing vanes on the internal straps.

The outside straps on all grids contain mixing vanes that also aid in guiding the grids and fuel assemblies past projecting surfaces during handling or core loading and unloading. In addition, there are small tabs on the outside straps; the irregular contour of the straps is also for guiding.

Inconel 718 is used for the grid material because of its corrosion resistance and high strength properties. After the combined brazing and solution annealing temperature cycle, the grid material is age-hardened to obtain the material strength necessary to develop the required grid spring forces.

The fuel rods consist of uranium dioxide ceramic pellets contained in slightly cold-worked and partially annealed Zircaloy 4 tubing, which is plugged and seal-welded at the ends to clad the fuel. Nominal dimensions include 9.29-mm (0.3659-in.) pellet diameter, 10.71-mm (0.422-in.) tube OD, and 0.62-mm (0.0243-in.) tube thickness.

Sufficient void volume and clearances are provided within the rod to accommodate fission gases released from the fuel, differential thermal expansion between the cladding and the fuel, and fuel swelling due to accumulated fission products without overstressing of the cladding or seal welds. Shifting of the fuel within the cladding is prevented during handling or shipping prior to core loading by a carbon-steel helical compression spring that bears on the top of the fuel pellet column. The holddown force to prevent fuel shifting is obtained by compression of the spring between the top end plug and the top fuel pellet of the stack.

During assembly, the pellets are stacked in the cladding to the required fuel height. The compression spring is then inserted into the top end of the fuel, and the end plugs are pressed into the ends of the tube and welded. During the welding process, the fuel rods are internally pressurized with helium to about 27.6 bar (400 psia) for the "W" and "V" assemblies.

The fuel rod void space is sized to ensure adherence to the pressure criterion. The end-of-life pressure is evaluated for the worst rod under expected conditions of fuel operation and at the peak steady-state power. The model used to predict the quantity of fission gas in the gap at end-of-life is based on an extensive comparison to published performance of fuel rods under a variety of conditions. The composition of the gas in the gap at end-of-life is a maximum of approximately 50% fission.

The fuel pellets are right circular cylinders consisting of slightly enriched uranium dioxide powder, which is compacted by cold pressing and sintering to the required density. The ends of each pellet are dished slightly to allow the greater axial expansion at the center of the pellets to be taken up within the pellets themselves and not in the overall fuel length. The nominal design enrichment is 3.2 wt% and 2.9 wt% for the "W" and "V" assemblies, respectively. The nominal density is 95% of theoretical density for all of the fuel pellets.

Predicted Decay Heat Rates

The ORIGEN2 code (8) was used to predict decay heat generation rates of the Surry PWR spent fuel assemblies used in the TN-24P cask performance test. A brief description of ORIGEN2, a summary of the input, and the predicted decay heat rates and average axial decay heat profile are provided.

ORIGEN2 Computer Code. The ORIGEN2 computer code is widely used in the nuclear industry to predict decay heat rates of spent fuel assemblies. It is a general

purpose burnup and decay code featuring extensive data libraries containing information on over 1200 nuclides. The code can be used to perform transmutation calculations in steps of constant power or constant neutron flux level. The resulting nuclide concentrations can be decayed with user-specified time intervals. Output options are available for decay heat rate as well as spent fuel compositions and radioactivity.

Input Specifications. The Surry spent fuel assembly design data were provided in a previous section for the assemblies used in the TN-24P cask performance test. Additional input data used in the ORIGEN2 calculations for the assemblies included:

- reactor operating histories and decay times after final cycle of operation for each assembly
- monthly measured fuel assembly relative power density (RPD)
- measured end-of-cycle (EOC) fuel assembly burnups
- as-built fuel batch assembly average metric ton uranium (MTU) loadings and isotopics.

The Surry 2 reactor operating history for each cycle was based on the monthly core exposure log sheets obtained from the VP Nuclear Operations Department (NOD). The reactor operating histories for cycles 4 through 5 are given in Figure 3-15 and Appendix A. The monthly measured fuel assembly RPDs were extracted from the monthly INCORE (9) computer code maps produced by NOD. The measured EOC fuel assembly burnups were obtained from NEWTOTE (10) computer code results. A history of the assembly EOC average burnups is given in Table 3-2. The batch average assembly MTU loadings were obtained from Westinghouse as-built data. These data are provided in Appendix A.

The assembly-specific power for each irradiation step was calculated using three equations:

$$POWER(K) = (LOADF * RPDAVG * 2441) / 157 \quad (3\text{-}1)$$

$$BURNUP = (SUM(POWER(K) * DAYS)) / MTFUEL \quad (3\text{-}2)$$

$$IRP(K) = POWER(K) * AVGEOC / BURNUP \quad (3\text{-}3)$$

where POWER(K) = specific power for irradiation step K based on reactor operating history and measured RPDs

LOADF = reactor power level from reactor operation history for irradiation step K (fraction of 2441 MWth)

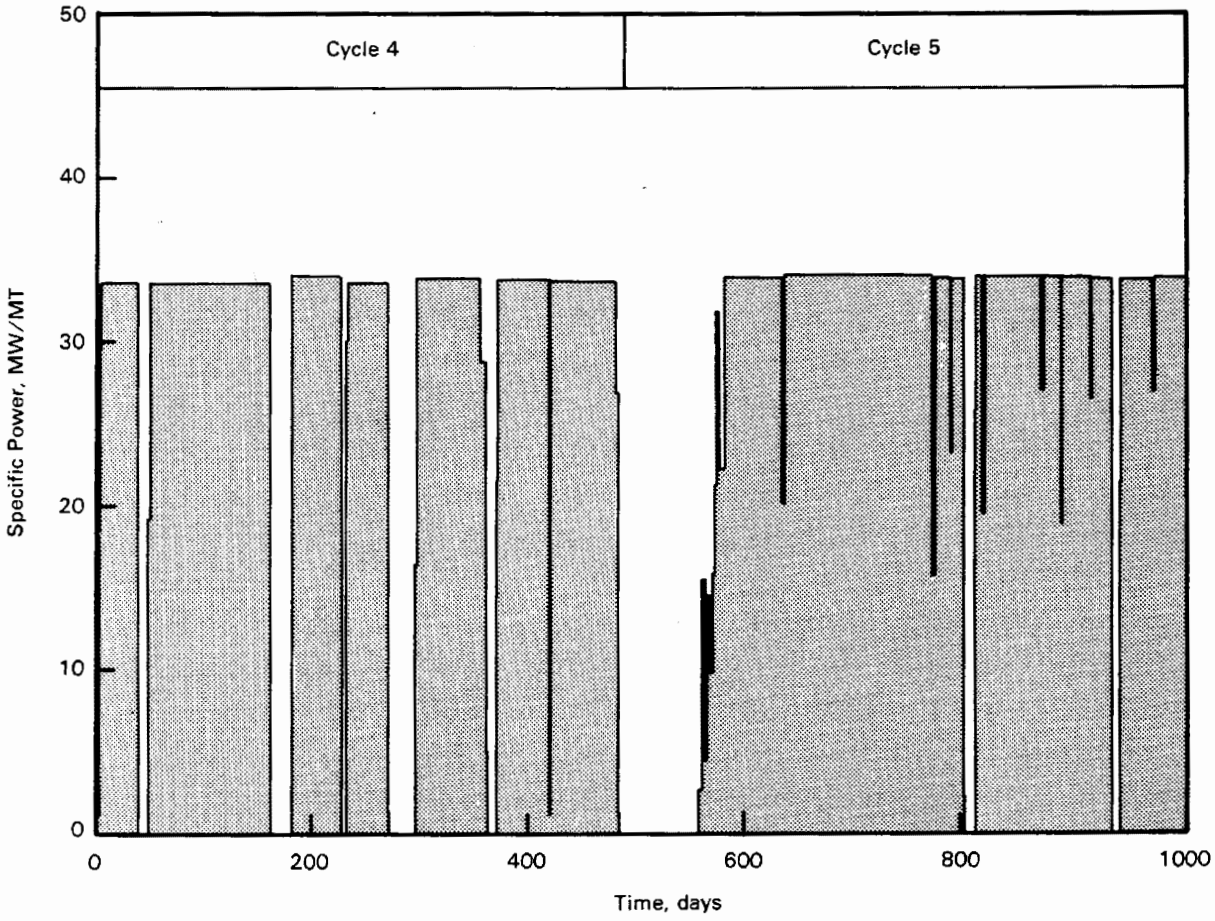

Figure 3-15. Surry 2 Reactor Operating History

Table 3-2

ASSEMBLY AVERAGE BURNUP HISTORIES (MWd/MTU)

Assemblies/Cycle	EOC S2C4	EOC S2C5
V18, V22	15,751	31,511
V03, V10, V16, V26	16,058	30,557
W02, W10, W16, W19, W23, W45, W49	14,087	29,795
W44, W17, W38, W01, W28, W46, W52	14,255	29,987
W13, W06, W27, W34	15,412	30,521
Cycle burnup, MWd/MTU	13,689	13,957
Cooling time between cycles, days	559	

RPDAVG = average RPD for symmetric fuel assemblies for irradiation step K
2441 = full power core heat output (MWth)
157 = total number of assemblies in Surry core
BURNUP = average EOC assembly burnup based on reactor operating history
SUM = summation over all irradiation steps
DAYS = number of days operated for irradiation step K
MTFUEL = metric tons uranium (MTU) loading per assembly
IRP(K) = specific power input for irradiation step K
AVGEOC = average measured EOC burnup for symmetric assemblies.

The above data were compiled for each assembly, and calculations were performed for each similar set of fuel assemblies. A typical assembly power history is shown in Figure 3-16.

Decay Heat Predictions. Using the data and technique described above, predictions of decay heat rates were made with ORIGEN2. The results of these calculations are given in Table 3-3 for the 24 assemblies that were used in the TN-24P cask during performance testing. Fuel assembly decay heat generation rates were predicted to total 20.6 kW at the start of testing and 20.3 kW at the end of testing, for an average of 850 watts per assembly. Decay heat from individual assemblies ranged from 830 to 919 watts per assembly.

The load pattern for the cask is shown in Figure 3-17. Assembly placements were selected to create quarter symmetry of heat generation within the basket and to produce a relatively flat temperature profile across the fuel assemblies.

Predicted Axial Decay Heat Profile

Measured axial decay heat profiles or gamma scans for the Surry spent fuel assemblies were not available as input data to the ORIGEN2 computer code to predict axial decay heat profiles. Axial gamma radiation scans previously obtained on Turkey Point reactor spent fuel assemblies were therefore used to develop a typical assembly axial burnup distribution (12). The Turkey Point and Surry PWR reactors and spent fuel assemblies are of the same designs, so axial decay heat profiles should be very similar.

The axial burnup distribution required as input to ORIGEN2 consisted of an average from gamma scans of 25 rods from five Turkey Point assemblies. ORIGEN2, with the measured gamma distribution and the appropriate Surry operating history, was then

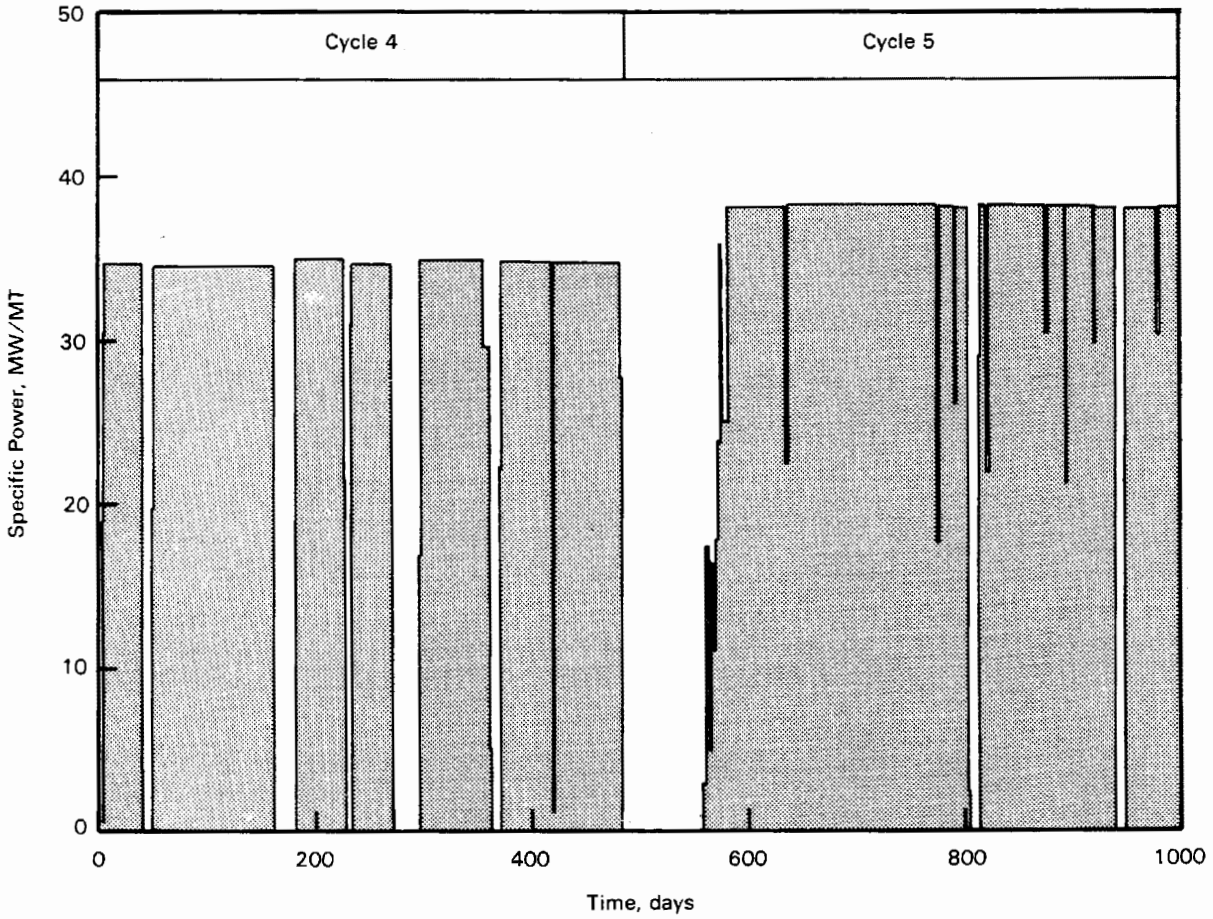

Figure 3-16. Assembly W02 Power History

Table 3-3

SURRY PWR SPENT FUEL CHARACTERISTICS

Assembly	Burnup, GWd/MTU	Cooling Time, months	Initial Enrichment, wt%	Decay Heat Prediction, W	
				Start 1/14/86	End 2/06/86
W02, W10, W16, W19, W23, W45, W49	29.8	50.3	3.20	845.5	832.3
W01, W17, W28, W38, W44, W46, W52	30.0	50.3	3.20	852.0	839.0
W06, W13, W27, W34	30.5	50.3	3.20	859.0	846.0
V03, V10, V16, V26	30.5	50.3	2.91	870.0	856.5
V18, V22	31.5	50.3	2.91	919.2	905.0

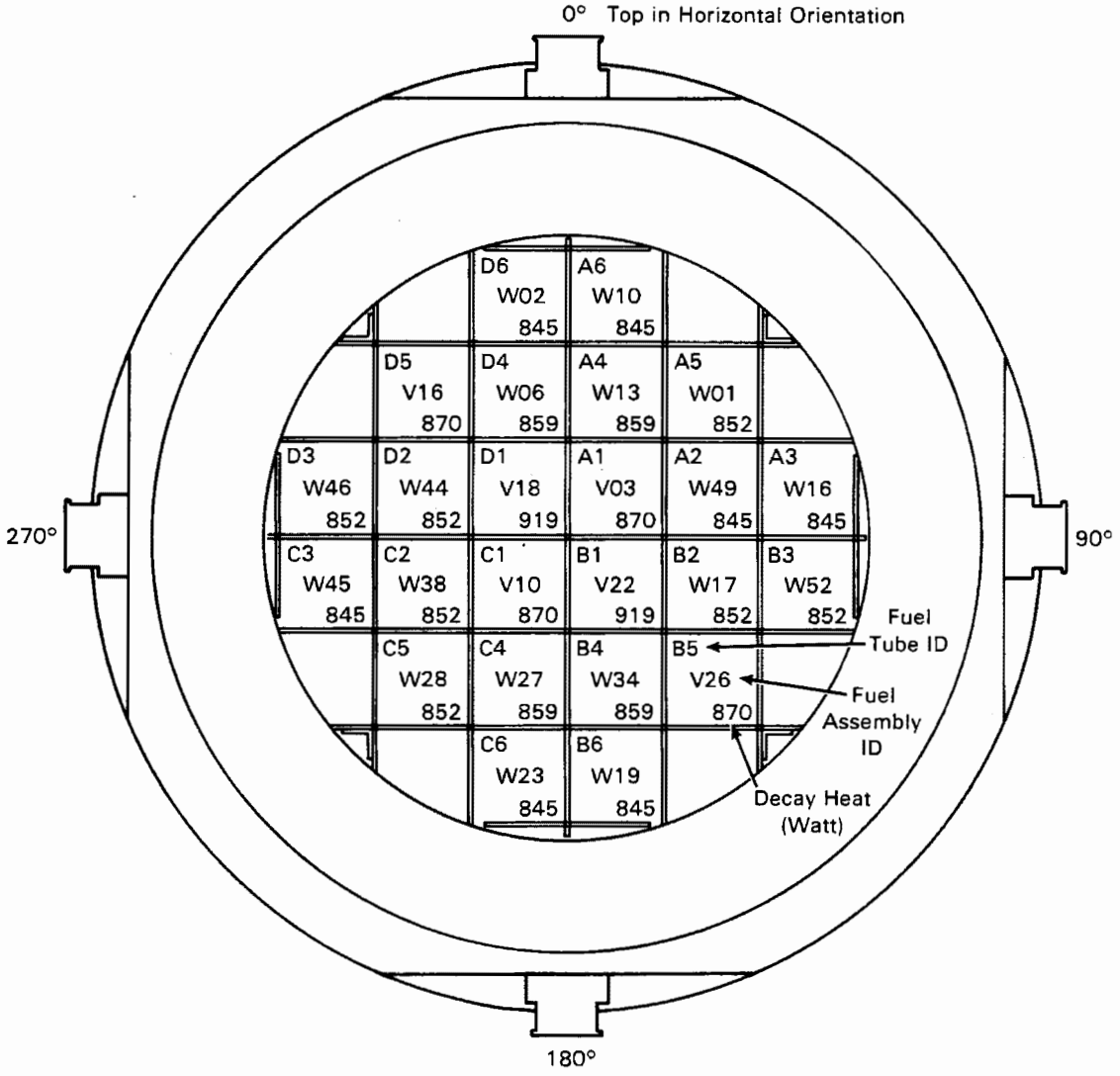

Figure 3-17. Spent Fuel Load Pattern

used to predict the relationship between burnup values and decay heat rates in specific axial regions (nodes) along the length of a fuel assembly. The measured gamma activity from Turkey Point assemblies and predicted Surry assembly decay heat axial profiles are shown in Figure 3-18. Both profiles are typical of those for spent fuel assemblies from PWR reactors. The dips in the profiles are a result of grid spacers at those locations.

Axial decay heat profiles are important because they strongly influence the shape of axial temperature profiles in the fuel assemblies, especially in vacuum and in a horizontal orientation where convection heat transfer is minimized. A smoothed

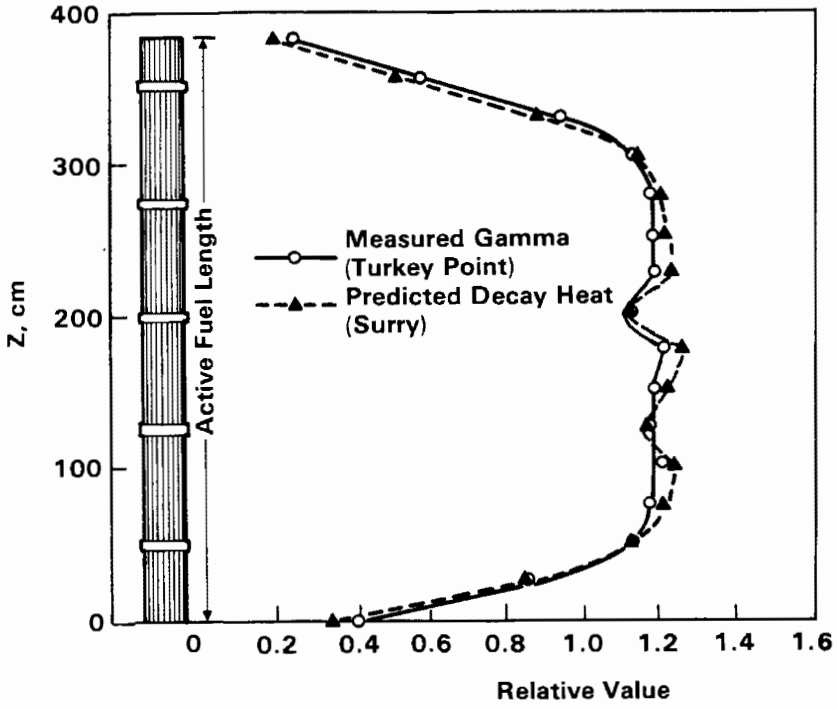

Figure 3-18. Predicted Axial Decay Heat Profile

representation of the predicted axial decay heat profile (Figure 3-18) was used as input to the COBRA-SFS heat transfer computer program to facilitate pre- and post-test temperature predictions (Section 5).

Spent Fuel Integrity

Selected spent fuel assemblies used in the TN-24P cask performance test were examined to determine the condition of the spent fuel prior to the test. Further examinations of the spent fuel assemblies upon completion of the long-term surveillance period will help determine whether long-term dry storage affected the spent fuel integrity or characteristics. Information on integrity is of interest in evaluating the impact of dry storage on the behavior of spent fuel rods during long-term dry storage and fuel-handling operations associated with dry storage. The main areas of interest for the spent fuel include the integrity of the fuel cladding, the condition of the spent fuel assembly hardware, and the character and condition of the crud. Specific information that was desired included the amount and type of damage, if any, to the cladding or fuel assembly hardware prior to fuel loading into the cask for performance testing and long-term dry storage; confirmation that no fission gas was being released from the spent fuel rods prior to the cask performance test;

and characterization of the crud from both the fuel rods and the shipping cask prior to performance testing and long-term dry storage.

Four examination methods were used to assess the integrity of the Surry fuel assembly rods prior to the performance test. These included ultrasonic examinations at VP; visual observations, including full-length black and white videos at both VP and INEL, and color photographs at INEL; and analyses of the cover gas in the TN-24P cask. Although crud behavior does not directly relate to fuel rod integrity, crud sampling was performed because crud spallation has been known to impact fuel-handling operations. Evidence that crud soaks loose during wet storage of some spent fuel rods has led to increased interest in crud behavior during rod consolidation and other dry operations.

Each fuel integrity examination is discussed in the following subsections. The results of the crud sample analyses for both the cask and fuel assemblies are also discussed.

In-Pool Ultrasonic Inspections. The Failed Fuel Rod Detection System (FRDS) is a portable system designed to be used underwater in spent fuel pools as shown in Figure 3-19. The system consists of an underwater manipulator (Figure 3-20), an ultrasonic probe (Figure 3-21), electronic controls, recording equipment, and a support plate (Figure 3-19). The manipulator with its probe (Figure 3-20) is attached to the support plate before it is submerged into the pool. The support plate, which rests upon the spent fuel pool storage racks, positions and stabilizes the fuel assembly being examined. The manipulator is doubly enclosed in a sealed steel casing, which reduces the chances of leakage and facilitates decontamination.

The FRDS is based upon ultrasonic techniques (UT) and is able to differentiate between sound and leaking rods by detecting the presence of moisture in the latter. The system uses a dual probe as shown in Figure 3-21. The probe incorporates a miniature ultrasonic transmitter and receiver on opposite sides of the probe arms. The probe is inserted in the gap between fuel rods while an ultrasonic pulse is transmitted between the arms of the probe. Defective fuel rods contain moisture, and even small amounts of water diffuse and attenuate the signals, providing distinctive traces on the oscilloscope and X-Y plotter (Figure 3-22). The arms of the

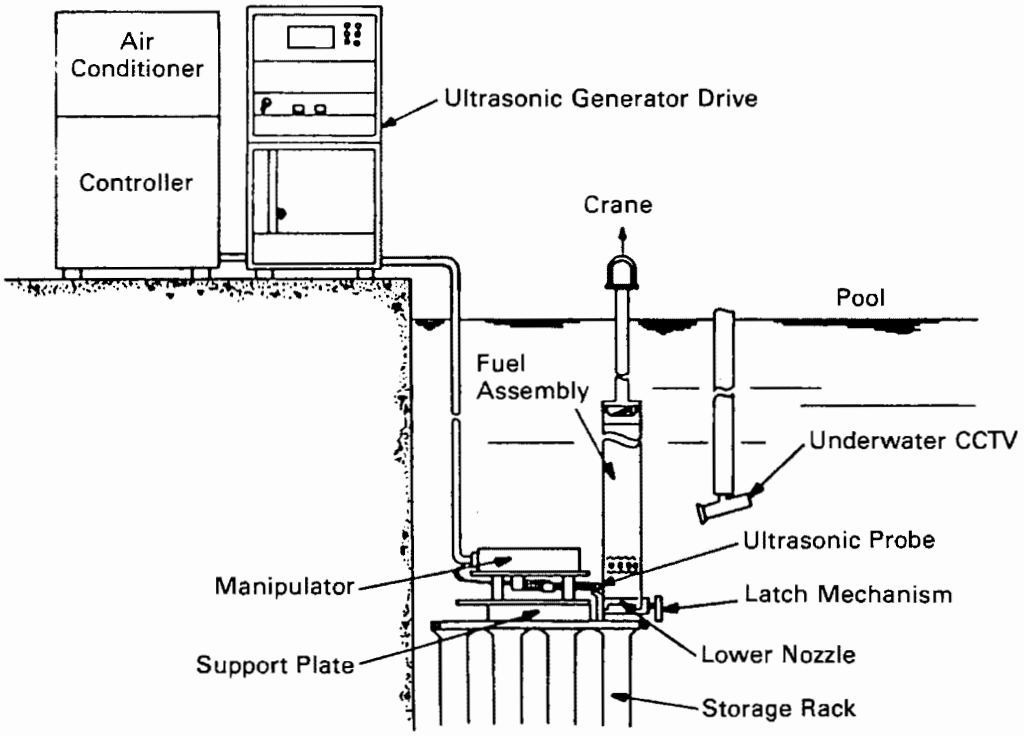

Figure 3-19. Failed Rod Detection System

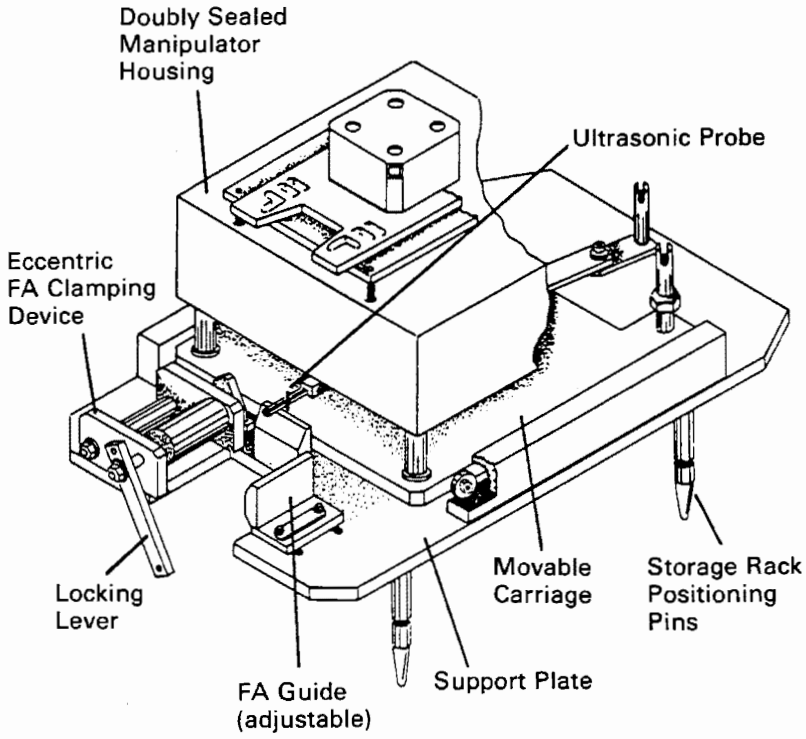

Figure 3-20. Failed Rod Detection System Manipulator and Support Plate

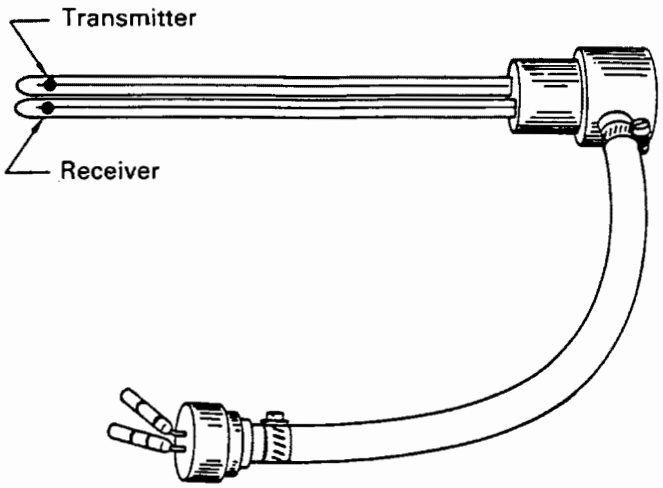

Figure 3-21. Failed Rod Detection System Ultrasonic Probe

test probe are quite flexible and able to accommodate differences between rod diameter and guide tube diameters as well as distortions that may have occurred in the fuel assembly. Contact between the probe arms and the fuel rods is minimal. In addition, the probing system incorporates a load-sensitive limit switch that stops the probe if resistance is encountered.

During examinations, the fuel assembly is suspended from the overhead crane and positioned so that the lower region of the fuel rods is located in front of the manipulator and probe. After initial alignment and calibration, the probe is automatically aligned with the rods and inserted and withdrawn sequentially in each gap between fuel rods. The fuel rods can be examined during both the insertion and withdrawal stroke; however, traces are normally taken during the withdrawal sequence only. After the entire side has been examined, the fuel assembly is rotated 90 degrees and each row of rods is reexamined, providing a cross-check on the ultrasonic indications. All of the fuel was examined from two faces during the initial scans; however, those assemblies considered suspect were later examined on the other two faces.

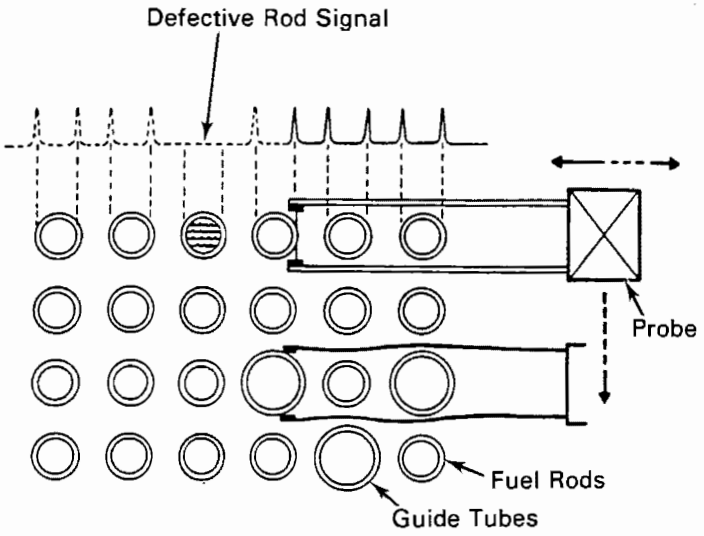

Figure 3-22. Typical Failed Rod Detection System Signal

Before the Surry fuel was inspected, a detailed inspection procedure was prepared and reviewed by all concerned parties, including the Surry Station Plant Review Committee. Only the salient points of that procedure are included here.

A. Equipment Pre-Test Checkout

- Before the FRDS equipment was moved into the spent fuel pool area, a radiation work permit was obtained and site health physics personnel prepared the necessary area corresponding to the needs of the FRDS equipment.

- All components of the FRDS, including electronic components, cables, and manipulator, were removed from their shipping cartons and placed in the prepared area adjacent to the spent fuel pool. The support plate, which had been previously used and stored at the Surry Station, was mated with the manipulator, and a television camera was affixed to the manipulator with a pre-prepared bracket.

- Electronic cables were interconnected between the controller, air conditioner, UT electronics, X-Y plotter, and the UT probes attached to the manipulator.

- Each of the electrical components was individually adjusted to conform to manufacturer's calibration standards, and the entire system was checked for continuity to ensure that the system operated as expected.

- Each of the detailed steps of checkout and inspection procedure required signoff by the individual responsible for the respective action, and each signoff was dated.

- At this point, before the manipulator/support plate was lowered into the spent fuel pool, a "site hold point" was initiated to allow health physics and site quality control staff to confirm that all procedural steps had been completed, that no site procedures were being violated, and that potential hazards had been considered.

B. System Calibration

- The overhead crane was used to lower the manipulator/support plate into the spent fuel pool and to position it in its predetermined location on the fuel storage racks.

- Following confirmation that the manipulator/support plate was properly located and secured in place, a calibration fuel assembly was moved into position in the support plate. Functional checkout of the FRDS system, consistent with the detailed inspection procedure, was then completed.

C. Fuel Examination

- The spent fuel assembly to be examined was moved from its position in the spent fuel storage rack to the manipulator/support plate using the spent fuel handling bridge. The fuel assembly was positioned in the support plate using the "Excenter," a device integral to the design of the support plate that accurately positions the fuel assembly in its proper position for inspection. Fuel rod inspections were performed at a level above the lower fuel assembly grid.

- The manipulator automatically moved the UT probe along the entire length of the first row of fuel rods in the assembly. It then automatically shifted its position to the second row of fuel rods and continued the inspection of the second row of rods in the same manner as the first. Subsequent rows of fuel rods were similarly examined until all 15 rows of rods had been examined.

- The fuel assembly was then removed from its position in the support plate, rotated 90 degrees, and repositioned in the support plate. The second face was then examined in the same manner as the first. Each fuel assembly was examined in 20 to 30 minutes in exactly the same manner as the first. Most of this time was spent in transferring the fuel assembly to and from the FRDs. Hard copy printouts of each fuel rod examined were produced on the X-Y plotter. Each face of each fuel assembly was recorded by the plotter and retained for record purposes.

- A number of the suspect fuel assemblies were reinspected from the two alternate faces of the assembly. The UT probes for those reinspected assemblies were located approximately 25 mm (1 in.) above the bottom grid of the fuel assemblies.

D. Equipment Disassembly and Decontamination

- When the fuel examinations were completed, the manipulator/support plate was removed from its position on the fuel storage racks to the periphery of the spent fuel pool. The equipment was removed with the overhead crane under guidance of the Surry Station site health

physics personnel. As the manipulator/support plate was removed from the water in the pool, it was thoroughly hosed down with clean station water to remove all loose radioactive contamination.

- After the manipulator/support plate was wiped dry, smear samples were taken by site health physics staff on all of the FRDS equipment including the electronics. The decontamination process resulted in no detectable radioactive contamination on the electronics and minor levels on the manipulator/support plate (approximately 1 to 3 milliroentgens).

- All components were returned to their respective shipping containers for offsite shipment.

All of the fuel assemblies inspected were examined from two adjacent faces. During the examination, fuel rods within the assemblies were determined to be CLEAR, SUSPECT, or leaking as indicated by the term INDICATION. Those assemblies that were CLEAR were not reexamined; however, all SUSPECT assemblies were reexamined from the remaining two faces. Those assemblies that clearly had INDICATIONS were not re-examined; however, several SUSPECT assemblies were reexamined to verify the validity of the initial examination.

The amplitude of pulses is the chief indication of the status of each fuel pin examined. Other factors tend to invalidate the results and must be considered. Specifically, crud buildup on a fuel pin may well distort the UT signal, resulting in a faulty indication. Rod bow, which causes variation in proximity of the probe to the fuel rod, may also result in a faulty indication.

The fuel examination findings are summarized in Table 3-4. No leaking fuel was identified from the fuel examination. A sample trace is shown in Figure 3-23.

Evaluation of data entailed the systematic interpretation of the output traces from the FRDS system. To ensure consistent and reliable interpretation of these traces, a calibration assembly was examined using the FRD system at the beginning and completion of each work shift. During the latter stages of fuel examinations, the calibration assembly was evaluated only once per shift. This was deemed acceptable due to the continuity between calibration traces obtained during the initial days of fuel examinations.

As previously noted, numerous factors must be considered when interpreting the X-Y plots of each fuel assembly examined. These factors include pulse height, crud deposits on the fuel rods, fuel assembly, and fuel rod bowing. Because the proximity of the UT probe to the fuel rods may vary with fuel rod bowing, pulse amplitudes

Table 3-4

FUEL INSPECTION RESULTS SUMMARY

Assembly ID	Date Inspected	Clear	Indication	Suspect	Faces
V03	08/19/84		X	1/4	
	08/26/84	X		2/3	
V10	08/20/84	X		1/4	
V16	08/19/84	X		1/4	
V18	08/20/84		X	1/4	
	08/25/84	X		2/3	
V22	08/19/84	X		1/4	
V26	08/19/84	X		1/4	
W01	10/02/84	X		1/4	
W02	09/30/84	X		1/4	
W06	09/30/84	X		1/4	
W10	10/01/84	X		1/4	
W13	10/02/84	X		1/4	
W16	09/30/84	X		1/4	
W17	09/30/84	X		1/4	
W19	09/30/84	X		1/4	
W23	10/02/84	X		1/4	
W27	09/30/84	X		1/4	
W28	10/01/84	X		1/4	
W34	10/02/84	X		1/4	
W38	09/30/84	X		1/4	
W44	10/02/84	X		1/4	
W45	10/01/84	X		1/4	
W46	09/30/84	X		1/4	
W49	09/30/84	X		1/4	
W52	09/30/84	X		1/4	

would also tend to vary in height. As a result of the inspections, all assemblies subsequently shipped from the Surry Station for TN-24P cask performance testing were determined to be free of defects.

Cask Cover Gas Sampling. The cask cover gas was sampled several times during performance testing, to evaluate the integrity of the spent fuel rods. Cover gas samples were taken as indicated in Table 3-5. Each sample was collected in a separate 500-cc stainless steel cylinder equipped with bellows-sealed valves as part of

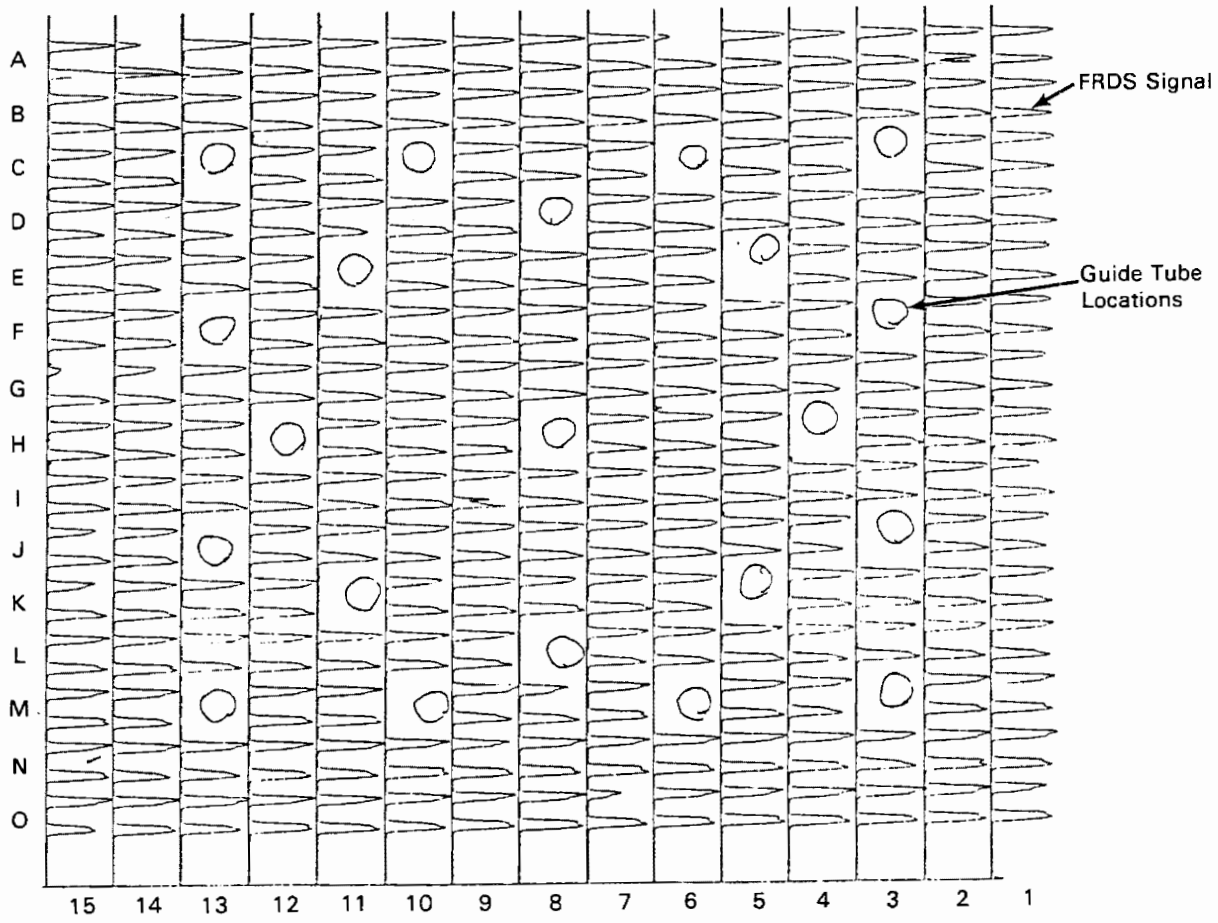

Figure 3-23. Sample Failed Rod Detection System Trace

the closure. The cylinders were checked for leaks prior to sampling. The addition of bellows valves to the same stainless steel cylinders used to take gas samples in the CASTOR-V tests has greatly improved sample quality for the TN-24P fuel storage cask in all but two cases. Samples 4C-PT and 4D-PT (bottles number 3 and 4, respectively) arrived at LLNL with one valve open on each. This mistake was discovered while processing sample 4C and caused more than half of the sample to be lost. However, this does not explain the percentage of air in the sample or the ratio of gross counts to percent He as compared to sample 4D. It is thought that sample 4C is not a representative sample of the cover gas.

Three types of gas analyses were performed at LLNL: sample pressure, mass spectra, and radionuclide concentration. To compare among the gas analyses, it was necessary to renormalize the concentrations measured to the cover gas content of the samples (helium or nitrogen excess after subtraction of air based on oxygen). The sample

Table 3-5

TN-24P CASK GAS SAMPLES

LLNL Number	Test Run Number	Sample Number	VP Bottle Number	Sample Cover Gas	Collection Time/Date	LLNL-Calculated Sample Pressure Absolute, mbar
17	1	1A-PR	19	He	1815/1-10-86	1434
18	1	1B-PR	22	He	1830/1-10-86	1422
19	1	1C-PT	23	He	0945/1-14-86	1396
20	1	1D-PT	24	He	0955/1-14-86	1402
21	2	2A-PR	26	N_2	1600/1-14-86	1441
22	2	2B-PR	29	N_2	1605/1-14-86	1443
23	2	2C-PT	20	N_2	1030/1-17-86	1433
24	2	2D-PT	25	N_2	1020/1-17-86	1436
27	4	4A-PR	11	He	1258/1-24-86	1442
28	4	4B-PR	12	He	1303/1-24-86	1429
29	4	4C-PT	3[a]	He	1245/1-27-86	(b)
30	4	4D-PT	4[a]	He	1255/1-27-86	939
31	5	5A-PR	6	N_2	1939/1-27-86	934
32	5	5B-PR	5	N_2	1947/1-27-86	917
33	5	5C-PT	7	N_2	1115/1-31-86	1460
34	5	5D-PT	8	N_2	1125/1-31-86	1443
37	-	TN-1A	10	He	1300/2-28-86	1342
38	-	TN-1B	15	He	1310/2-28-86	1352

[a]Bottles received with one open valve on each sample.

[b]Sample pressure was not calculated.

pressures shown in Table 3-5 were determined by assuming that the sample bottle volume was 500 cc, expanding the gas into a calibrated volume, and measuring the pressure in the calibrated volume. The pressure values given in Table 3-5 have been reduced to the equivalent pressure at 0°C and may be corrected to the cask internal pressure at sampling time when corrected for cask and system temperatures and expansion volumes during sampling. The estimated overall accuracy of these measurements is on the order of ±1% and derives principally from bottle volume uncertainty. These pressures should equal the test pressures at sampling time when corrected for

cask and system temperatures and expansion volumes during sampling. The data in Table 3-5 were obtained from information supplied with the sample bottles.

The results of the LLNL gas analyses are presented in Table 3-6. Mass spectra were analyzed for all common gases with masses less than 100. Only N_2, O_2, He, Ar, and CO_2 concentrations above 0.01% are detected in any of the samples. Analyses of the other species reported are of marginal reliability. Water is reported as a lower limit due to absorption on vessel walls. The accuracy of the mass spectra measurements is noted in Table 3-6.

Table 3-6

CASK GAS SAMPLE COMPOSITION

LLNL Sample Number	Test[a] Run Number	Volume Percent[b]							
		He	N_2	O_2	Ar	CO_2	CO	H_2O	H_2
17	1A-PR	99.97	<0.01	0.020	<0.01	<0.01	<0.01	>0.01	<0.01
18	1B-PR	99.96	0.037	<0.01	<0.01	<0.01	<0.01	>0.09	<0.01
19	1C-PT	99.92	0.056	0.017	<0.01	<0.01	<0.01	>0.01	<0.01
20	1D-PT	99.93	0.057	<0.01	<0.01	<0.01	<0.01	>0.06	<0.01
21	2A-PR	<0.01	99.99	<0.01	<0.01	<0.01	<0.01	>0.01	<0.01
22	2B-PR	<0.01	99.99	<0.01	<0.01	<0.01	<0.01	>0.04	<0.01
23	2C-PT	<0.01	99.94	<0.01	<0.01	<0.01	0.052	>0.01	<0.01
24	2D-PT	<0.01	99.98	<0.01	<0.01	<0.01	<0.01	>0.01	0.011
27	4A-PR	99.99	<0.01	<0.01	<0.01	<0.01	<0.01	>0.01	<0.01
28	4B-PR	99.93	0.077	<0.01	<0.01	<0.01	<0.01	>0.05	<0.01
29	4C-PT	0.379	77.73	20.83	0.931	0.058	0.071	>0.03	<0.01
30	4D-PT	87.42	9.792	2.592	0.118	0.014	0.060	>0.01	<0.01
31	5A-PR	0.063	98.93	0.937	0.063	<0.01	<0.01	>0.01	<0.01
32	5B-PR	0.058	98.68	1.162	0.074	<0.01	0.027	>0.01	<0.01
33	5C-PT	<0.01	99.95	<0.01	0.028	0.012	<0.01	>0.01	<0.01
34	5D-PT	<0.01	99.93	<0.01	0.029	<0.01	<0.027	>0.01	<0.01
37	TN-1A	99.99	<0.01	<0.01	<0.01	<0.01	<0.01	>0.01	<0.01
38	TN-1B	99.99	<0.01	<0.01	<0.01	<0.01	<0.01	>0.01	<0.01

[a]Number indicates run, letter following run number differentiates samples, and letters following dash indicate Pre-Run or Post-Test.

[b]Species present in mass spectra at 0.01% or more. Accuracy of these measurements is ±0.2% of the concentration or 1 unit in the least significant digit, whichever is greater.

Table 3-7 presents measured concentrations and detection limits for ^{85}Kr and ^{14}C from the cover gas samples. The radionuclide concentrations ^{85}Kr, $^{14}CO_2$, and ^{14}CO were determined in two stages. The first stage involved screening analyses, which were done by thin window beta counting to find ^{85}Kr activity greater than 1 nCi/ml. Activity can be measured as low as 1 pCi/ml. At least one of each sample pair was processed for ^{85}Kr and at least one sample from each test run was processed for ^{14}C as both CO_2 and CO. The second stage involved elution chromatography to obtain the

Table 3-7

RADIONUCLIDE CONCENTRATION OF GAS SAMPLES (pCi/ml)[a]

LLNL Sample Number	Test[b] Run Number	^{85}Kr Screening Analysis	^{85}Kr	$^{14}CO_2$	^{14}CO
17	1A-PR	≤0.08	--	--	--
18	1B-PR	≤0.06	≤0.01	--	--
19	1C-PT	0.44 ± 0.06	≤0.02	0.10 ± 0.02	≤0.02
20	1D-PT	0.65 ± 0.24	≤0.02	--	--
21	2A-PR	≤0.07	--	--	--
22	2B-PR	≤0.07	≤0.02	--	--
23	2C-PT	2.05 ± 0.29	--	--	--
24	2D-PT	2.65 ± 0.13	≤0.02	16.8 ± 1.0	≤0.01
27	4A-PR	≤0.07	--	--	--
28	4B-PR	≤0.07	≤0.02	--	--
29	4C-PT	2657 ± 37	--	--	--
30	4D-PT	7269 ± 166	7506 ± 82	1.54 ± 0.04	0.04 ± 0.02[c]
31	5A-PR	277 ± 7	--	--	--
32	5B-PR	251 ± 6	252 ± 3	0.12 ± 0.01	0.05 ± 0.01[c]
33	5C-PT	2132 ± 30	--	--	--
34	5D-PT	2110 ± 24	2077 ± 38	4.96 ± 0.07	0.02 ± 0.01[c]
37	TN-1A	7.31 ± 0.10	--	--	--
38	TN-1B	7.09 ± 0.12	7.24 ± 0.54	2.19 ± 0.02	0.05 ± 0.01[c]

[a]Picocuries per milliliter of sample at 760 torr, 0°C, decay corrected to 1-1-86. Indicated errors are one standard deviation of the mean of replicate measurements.

[b]Number indicates run, letter following run number differentiates samples, and letters following dash indicate Pre-Run or Post-Test.

[c]Marginally detectable. Detection limit defined as sample count rate greater than 25% that of the detector background. For ^{85}Kr, the detection limit is increased by 5% of the observed krypton carrier background.

separated, pure gases for radioassay. In all cases, inactive carrier gases were added to the samples prior to processing and were recovered in good yield. The separated krypton gas was analyzed either by thin window beta counting for high levels or by internal proportional counting for low levels. Carbon-14 was measured as $^{14}CO_2$ by internal proportional counting. The CO was separated from the gas sample, converted to CO_2 over CuO at 500°C, and also analyzed by internal proportional counting. Typically, activities above 0.02 pCi/ml can be detected by this method. The amounts of ^{85}Kr and ^{14}C in test runs 4 and 5 (horizontal helium and nitrogen), and TN-1A and 1B (post-test) indicate a leaking fuel rod was present during this portion of the test. The relatively low amounts of ^{85}Kr and ^{14}C in the other samples are what would be expected to result from crud, not a leaking fuel rod. The increase in ^{85}Kr and ^{14}C content coincides with the cask being rotated from vertical to horizontal, which suggests that a fuel rod(s) may have started leaking due to the change in position. The decay in the leak rate, run 5 sample concentrations being less than run 4 samples and sample TN-1B being less than run 5 samples, indicates that the leak was small (or most of the gas had already been lost) and took several days to vent the gas from the fuel rod(s).

Video and Photographic Examinations. The fuel assemblies were examined visually, to establish their general condition after shipment from VP and before TN-24P cask performance testing. Two kinds of visual examinations were used: black and white videos and color photography of three fuel assemblies (V16, V18, and W02). The fuel examination test plan specified that any fuel assemblies with unusual characteristics also be scanned and that unusual areas be photographed. However, no such characteristics were identified, so no additional photography was required.

The black and white videos taken at both VP and INEL did not provide sufficient detail to characterize the crud or very small features on the fuel rods. However, they did indicate no significant variations in the fuel rods after either shipment or handling. The videotapes alone did not provide enough detailed information to adequately determine the integrity and condition of the fuel and fuel cladding. Examination of the video scans shows that all of the fuel assemblies and fuel rods look basically the same when viewed from the outside of the assemblies. There was some discoloration of the fuel rod cladding in the area of the grid spacers, which was expected.

Color photographs were taken at six levels on each of four sides of fuel assemblies V16, V18, and W02. A typical orange/reddish crud (probably Fe_2O_3) was evenly deposited on all of the Zircaloy 2 cladding and fuel assembly hardware. A

photograph showing typical fuel assembly conditions near the lower hardware and lower portions of the fuel assemblies is presented as Figure 3-24. There were no noticeable changes in the characteristics or adherence of the crud during handling operations involving the spent fuel assemblies at INEL. Figure 3-25 shows typical details of the fuel rods in the spacer grid area. Some scratches and worn spots were apparent on the spacer grids and some fuel rods, but these features did not change as a result of examination or handling operations. In general, the fuel rods were in excellent condition, with a very adherent crud layer.

Crud and Smear Sampling. The crud from the fuel assemblies was sampled to establish its characteristics and determine if any crud spallation occurred during the fuel shipment and fuel-handling operations. If crud spallation had occurred during dry storage testing or in the basin after the long term testing, then the characteristics of the crud might prove useful in evaluating the performance and long-term dry storage data. Crud and smear samples were also collected from the bottom and side of a TN-8L shipping cask after the first and after the final shipment of fuel to INEL.

The results of the analysis of 12 smear and crud samples are given in Table 3-8. The values in parentheses are estimates of the precision of the measurement expressed as a percentage. The only fission product present is ^{137}Cs but only marginally to the extent of a few thousand disintegrations per minute in these spectra. The crud and smear sample data from the TN-8L shipping cask show an increase in the buildup of crud in the bottom of the cask during the shipping campaign while the cask wall appears to have become cleaner during this same time period. The fuel shows a relative small spread in the results of the smear samples with assembly V18 being the cleanest. The samples were counted in the as-received condition at an ill-defined (nominally 5 cm) distance from the detectors. Because of this, the relative amounts of species detected in the swipes should be reliable, but absolute amounts are of questionable accuracy. Data were processed by the GAMANAL code (11), which finds peaks, calculates photons per minute, identifies radionuclides, and outputs disintegrations per minute for various species. The absence of a result for any given species means only that the code was unable to identify its characteristic gamma rays in the spectra. The detection and quantification of less abundant species was precluded or reduced by the presence of large quantities of ^{60}Co in the samples.

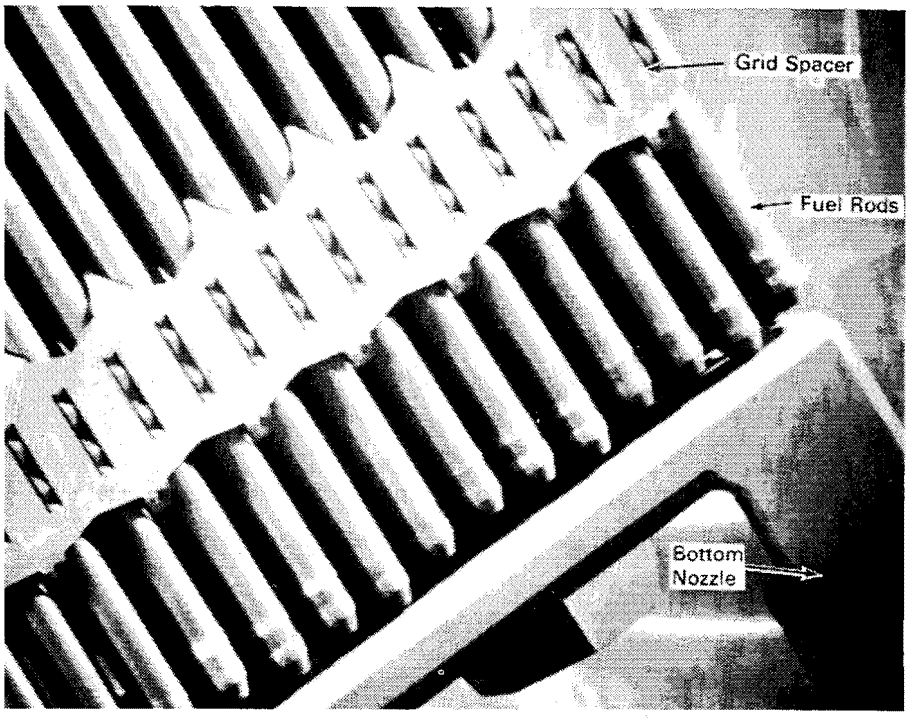

Figure 3-24. Typical Fuel Assembly Condition Near Lower Hardware

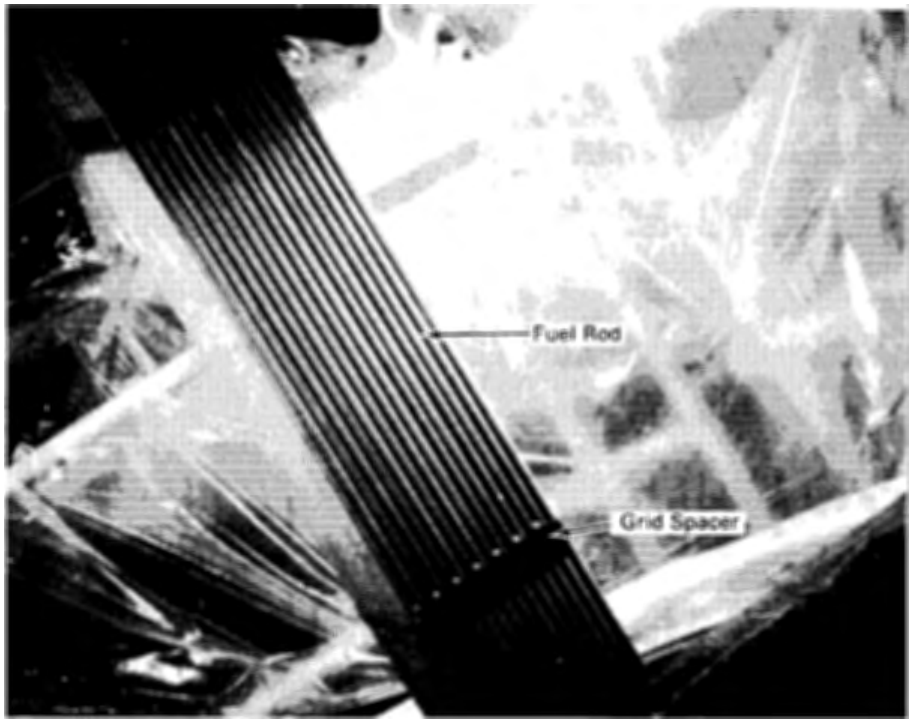

Figure 3-25. Fuel Assembly Condition Near Spacer Grids

Table 3-8

ANALYSIS OF CRUD AND SMEAR SAMPLES FROM A TN-8L SHIPPING CASK AND SURRY FUEL

Sample Data		10^4 dpm at 00:00 hours 10/27/85 (±%)[a]			
Swipe or Crud Sample	Sample Date	^{54}Mn	^{60}Co	^{94}Nb	^{125}Sb
TN-8L, First Shipment, Side Smear	11/19/85	0.65(8)	114.(1)	--	--
TN-8L, Seventh Shipment, Side Smear	12/26/85	0.12(16)	26.3(1)	--	--
TN-8L, First Shipment, Bottom Smear	11/19/85	1.00(8)	136.(1)	--	--
TN-8L, Seventh Shipment, Bottom Smear	12/26/85	42.3(6)	10060.(1)	--	6.77(28)
TN-8L, First Shipment, Bottom Crud	11/19/85	26.3(4)	3431.(1)	--	--
TN-8L, Seventh Shipment, Bottom Crud	12/26/85	374.(4)	36740.(1)	--	--
Fuel Assembly (V18 @ 0°)[b]	11/18/85	4.83(2)	280.(1)	0.16(12)	5.71(1)
Fuel Assembly (V18 @ 180°)	11/18/85	2.12(2)	131.(1)	0.04(24)	2.31(1)
Fuel Assembly (V16 @ 0°)	11/21/85	10.6(2)	655.(1)	0.33(15)	17.5(1)
Fuel Assembly (V16 @ 180°)	11/21/85	7.23(3)	458.(1)	0.25(16)	10.3(1)
Fuel Assembly (WO2 @ 0°)	12/16/85	5.86(2)	361.(1)	0.18(19)	8.99(1)
Fuel Assembly (WO2 @ 180°)	12/16/85	13.2(3)	959.(1)	0.37(26)	20.7(1)

[a]Values in parentheses are estimates of measurement precision in percent.

[b]Smear samples taken between the 2nd and 3rd grid spacer from the fuel assembly top.

DATA ACQUISITION SYSTEM

The data acquisition system (DAS) used to receive and process signals from the cask and fuel TCs and the cask pressure transducer is shown schematically in Figure 3-26. The system consisted of extension leads from the respective sensors to a junction box (JB#1). Additional extension leads were required from junction box 1 (JB#1) to junction box 2 (JB#2) located near the Keithly Series 500 DAS.

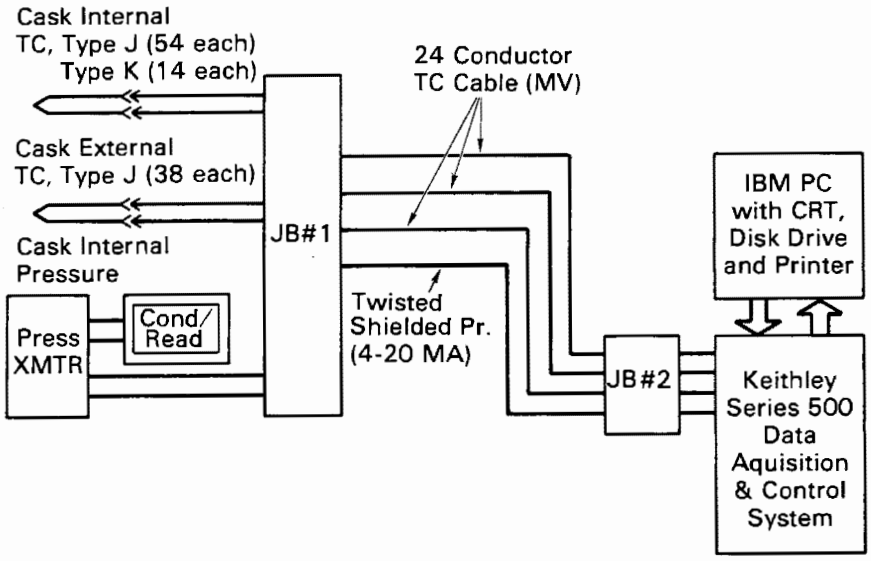

Figure 3-26. Data Acquisition System

The Keithly Series 500 DAS is a general-purpose data acquisition and control device consisting of a Keithly Series 500 mainframe and a standard IBM PC with a CRT display, floppy disk drive, and printer (13). The Keithly Series 500 mainframe provides an interface between an IBM PC and the real world (instrumentation sensors). Therefore, any IBM PC can be used for direct data acquisition and intelligent process control.

The Keithly Series 500 mainframe is a modular system, centered around a low-noise chassis containing a precision power supply and baseboard with slots for 10 plug-in modules. The module family provides all of the conditioning, conversion, and control capabilities needed for laboratory and industrial automation. All four kinds of real-world signals--analog input, analog output, digital input,and digital output--are accepted by the Keithly Series 500.

Analog input from the cask instrumentation pressure and temperature sensors was processed in two stages. The initial conditioning and selection of all signals was provided by a series of the analog input module (AIM). Different modules offer amplification, isolation, bridge detection, excitation, and cold junction reference. Programmable gain allowed the range of the signal to match that of the converter. Signals were then directed to a single analog-to-digital module (ADM) that accesses the level of the signal with an A/D converter, returning a digital value understood by the IBM computer.

Signals from the Keithly Series 500 were received, converted to engineering units, stored on floppy disks, and printed out on hard copy by the IBM PC. Further processing of the pressure and temperature data consisted of applying appropriate calibrations to the raw temperature data and plotting selected data presented in Section 4.

DATA UNCERTAINTY ESTIMATES

Temperature uncertainties for the internal TC lance temperature measurements are within ±4°C, and external temperature measurements are within ±4.5°C based on the combined uncertainties of the thermocouples, extension wires, and data acquisition system. The higher accuracy of the internal measurements results because the TC lance thermocouples were calibrated, whereas the thermocouples attached to the casks surface were not. Where independent calibration data were not obtained, vendor certifications were used to estimate the TC contribution to temperature measurement uncertainty.

Pressure measurement uncertainties were within 1.5 mbar for the low-pressure vacuum measurements and within ±6 mbar for the readings near 1500 mbar. The pressure measurement uncertainty is a combination of the uncertainty in the pressure transducer's 4- to 20-milliampere output and the voltage drop across a precision resistor (1%) in the data acquisition system. Detailed uncertainty calculations for both pressure and temperature measurements are presented in Appendix B.

The passive dosimeters were used primarily to give more detailed dose rate profiles on the surface of the cask than are possible with the portable survey instruments, which average counts over relatively large areas. The TLDs are individually selected to have a dose response within 5% when exposed to 1 R of ^{137}Cs gamma rays, and should respond within 10% when exposed on the cask. The TEDs were used only for obtaining a relative profile of the cask, because they are not very sensitive to low- and intermediate-energy neutrons and require long exposures.

Survey instruments are field instruments and can have large overresponses depending on the energy spectrum of the calibration source and the energy spectrum being measured. The gamma survey instruments should be accurate to within 10% for room temperature measurements. For measurements not in the range of 15 to 26°C, an appropriate temperature correction should be applied. This was not necessary for the cask survey where the front of the instrument was 1 in. from the surface at about 25°C. The neutron survey instruments can overrespond by a factor of 1.5 to 2 for neutrons with energies in the hundreds of kiloelectronvolts (the average energy

on the surface of the cask was between 150 to 200 keV). They overrespond by a factor of 3 to 4 for lower-energy neutrons; for 14-MeV neutrons, they underrespond by a factor of about 3.

The TEPC directly measures absorbed neutron dose, and neutron dose equivalent can be determined using the pattern of energy deposition. The TEPC has demonstrated a response to monoenergetic neutrons between 0.1 and 17 MeV that, on the average, falls within 3% of the calculated or known dose. The multisphere spectrometer has low energy resolution but is responsive to neutrons over a very large range of energies (thermal to 20 MeV). Neutron dose and dose equivalent rates can be determined from the measured spectra to within 20%. The ^{3}He spectrometer directly measures neutron energy spectra between 30 KeV and 1 MeV and is dependent only on the neutron capture cross section of ^{3}He over that range. For determining neutron energy spectra, the ^{3}He spectrometer is accurate to within 3%, but because of the neutrons that fall outside the range used, the total neutron fluence and dose equivalent determined are not always extremely accurate.

INEL CASK TESTING FACILITY

The primary INEL facilities are shown in Figure 3-27. The spent fuel storage cask performance tests are being performed at the Test Area North (TAN) facilities. The TAN is a large, multi-purpose testing and support area near the northern boundaries of INEL. Storage casks arrive at the INEL Central Facilities Area (CFA) by rail and are transported by heavy haul transporter to the TAN facility where all fuel-handling and testing activities are performed.

TAN-607 Facility

The primary cask testing facility is Building TAN-607 (Figure 3-28). This building includes several large shops: a high-bay hot shop area with unique capabilities for remote handling of highly radioactive materials involving either delicate and precise work or massive, industrial-sized operations; a water pit for interim storage of radioactive materials and components; a hot cell for observation and analysis of small radioactive objects, as well as for disassembly and examination of fuel rods; and a high-bay warm shop for receipt, assembly, and decontamination of low contaminated items, and testing. The two shops used for cask testing are the hot shop and warm shop at the north end of TAN-607 (Figure 3-29). In addition, a pad was constructed west of TAN-607 for long-term surveillance of the cask.

TAN-607 Hot Shop. The TAN-607 hot shop shown in Figure 3-30 is a shielded cell designed for the remote handling of large radioactive components. The shop is

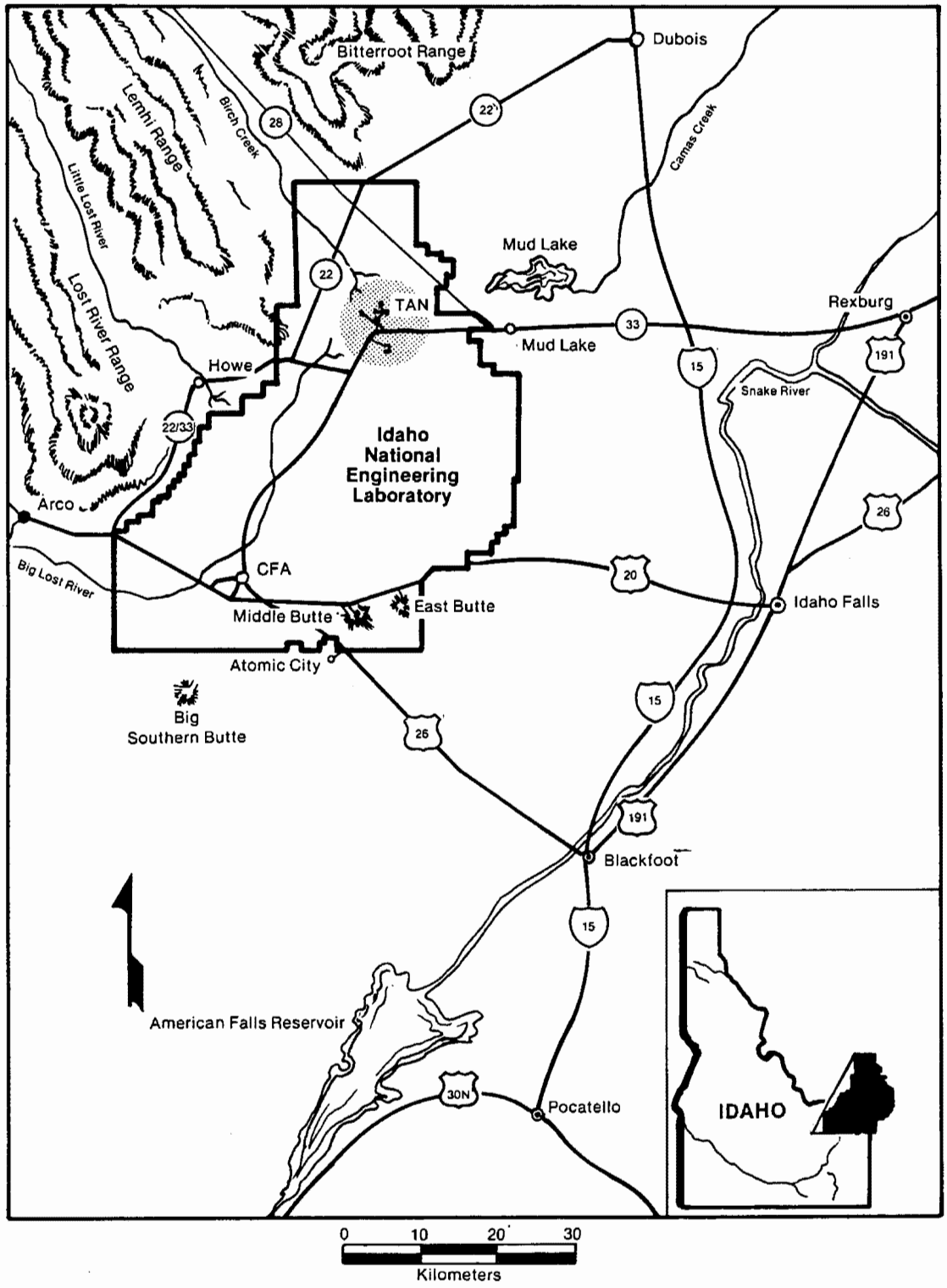

Figure 3-27. INEL Facility

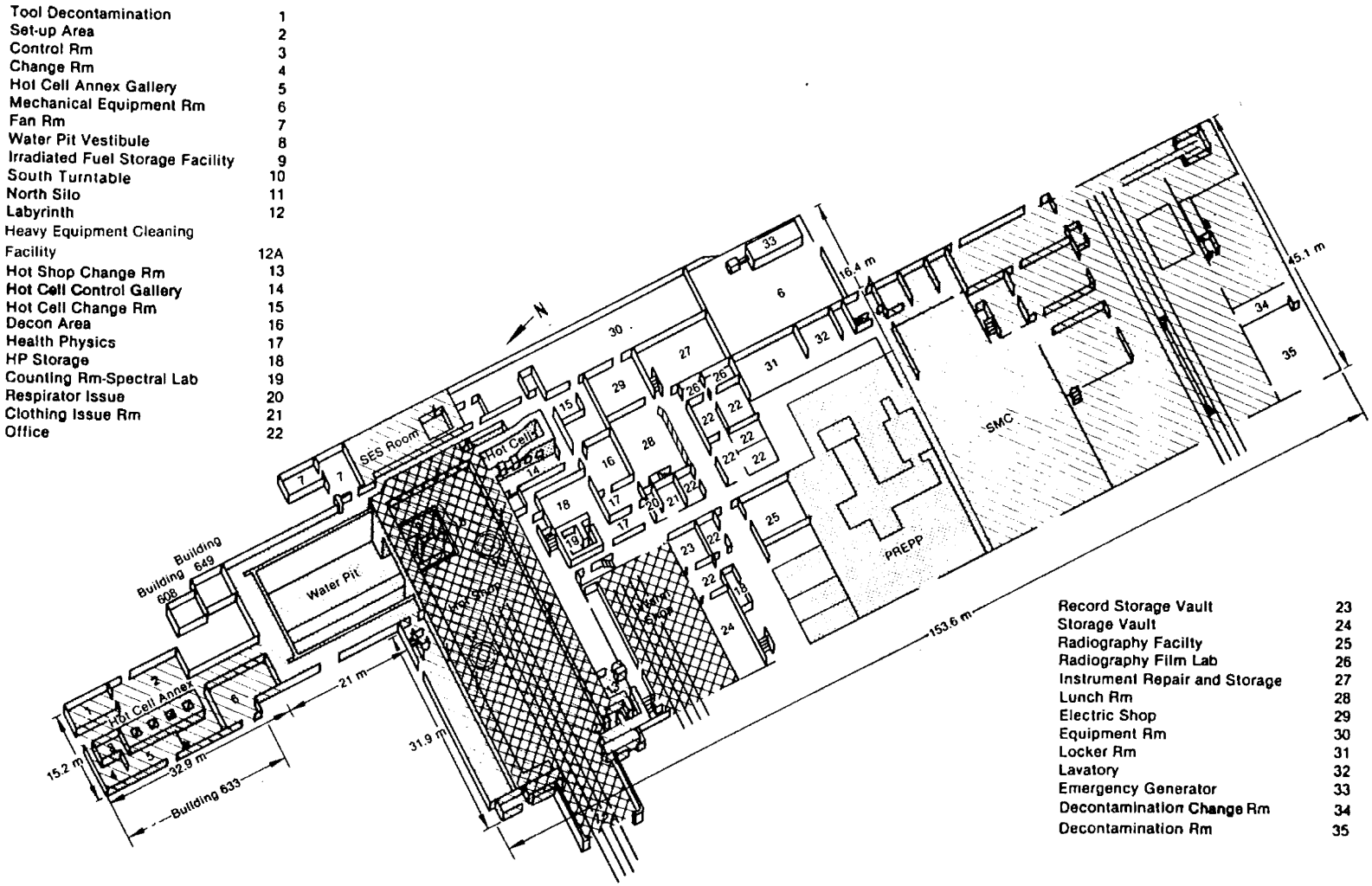

Figure 3-28. TAN-607 Facility

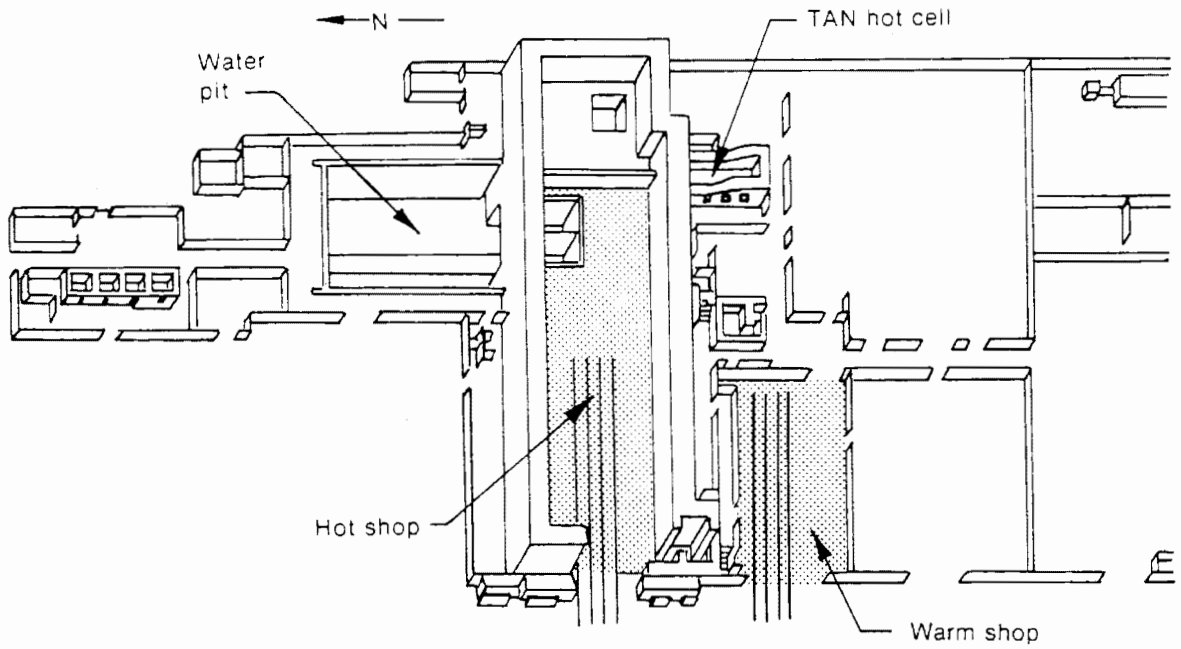

Figure 3-29. North End of TAN-607

15.5 m (51 ft) wide by 48.8 m (160 ft) long by 16.8 m (55 ft) high and constructed with 2-m-thick (7-ft) thick concrete walls. Shielded viewing is provided by nine 1.8-m-thick (6-ft) glass windows. The main door to the hot shop is 8.5 m (28 ft) wide by 9.8 m (32 ft) high, allowing the entry of large vehicles including rail cars. The hot shop is serviced by a four-rail railroad system. The TAN hot shop is designed to a Uniform Building Code (UBC) Seismic Zone 2. The floor loading for the shop is 1222 kg/m^2 (250 lb/ft^2), but heavily concentrated loads can be located within the hot shop by positioning them over specific support areas. The ventilation system exhausts the hot shop air through prefilters, HEPA filters, and silver zeolite absorbers to a 45.7-m (150-ft) stack. A negative pressure is maintained in the hot shop to ensure constant air flow into the shop. The hot shop is not a sealed alpha-containment facility. Appropriate hot and warm waste systems are provided in the facility.

The hot shop is served by a variety of remotely operated handling equipment as shown in Figure 3-31. The largest piece of equipment is the 100/10-ton bridge crane, which is currently upgraded for 125-ton lifts. The crane services the entire shop and has a maximum lift height of approximately 15.5 m (51 ft). A bridge-mounted overhead electromechanical manipulator can also cover the entire shop. The manipulator can lift a 272-kg (600-lb) load with its hand, and has a shoulder hook

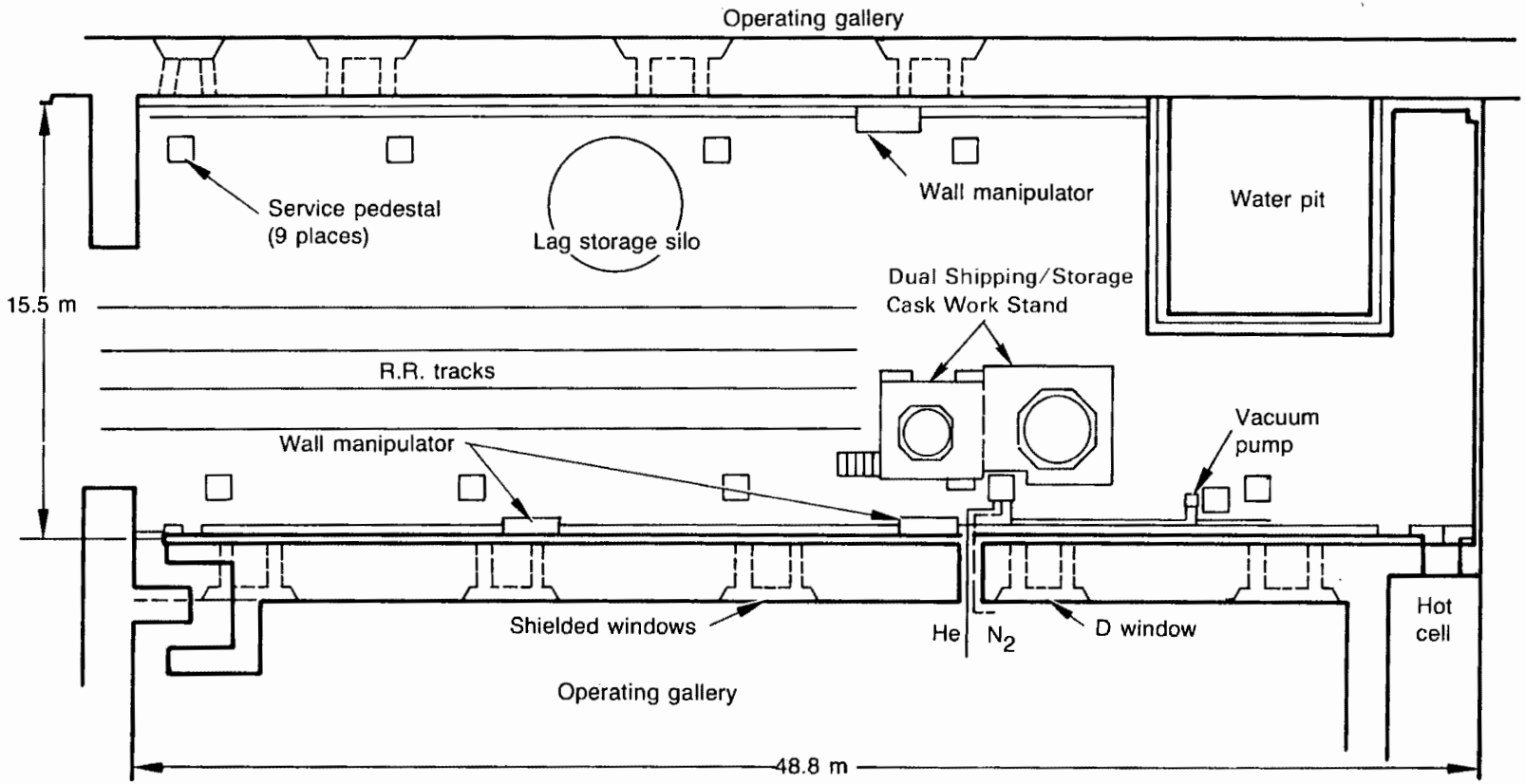

Figure 3-30. TAN-607 Hot Shop

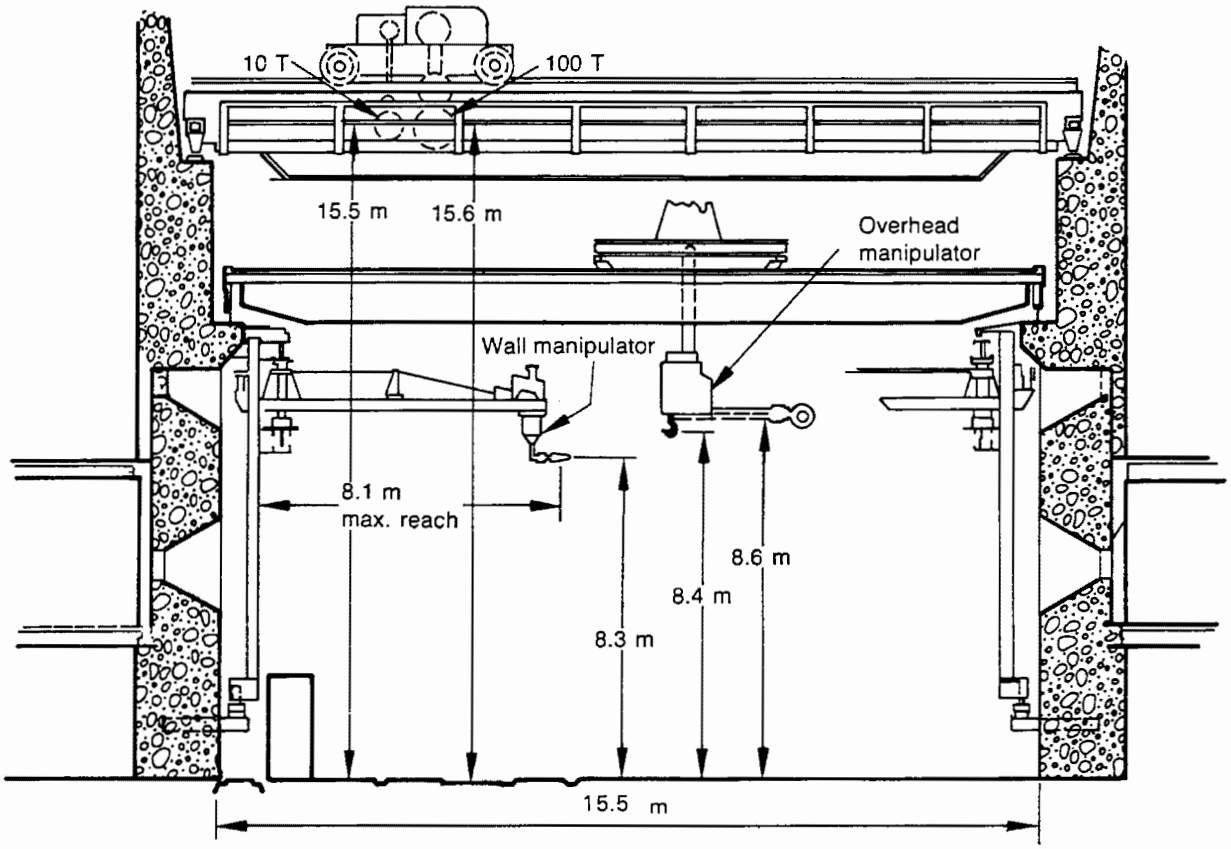

Figure 3-31. Elevation View of Hot Shop and Handling Equipment

capable of lifting 2270 kg (5000 lb) to a height of 9.1 m (30 ft). Three wall-mounted manipulators are installed for lighter-duty work. These manipulators can travel both horizontally and vertically [up to about 9.1 m (30 ft)] along the hot shop walls, and have jib booms that can be swung from the wall to the center of the shop. The shielded window in the northwest corner of the hot shop contains heavy-duty master-slave manipulators.

Service pedestals are located on the hot shop floor to provide all of the utilities normally used in the hot shop operations, including compressed air, oxygen, acetylene, demineralized water, raw water, electricity, telephone, and intercom. All are conveniently accessible via quick-disconnect couplings designed for remote manipulation. Remotely operated power tools are plugged into these service pedestals by the manipulators when needed. Pedestal "D" has been expanded to include helium and nitrogen gas supplies, a vacuum system to evacuate the casks, instrument hookups to a DAS, and electrical hookups for the video camera pan-tilt controls and light system.

Visual access to the hot shop is gained through a series of 1.8-m-thick (6-ft) windows arranged and installed on either side of the shop and in two rows corresponding roughly to second- and third-story heights. Binoculars, mirrors, periscopes, remote microscopes, and closed circuit television are all used to enhance the visual observation and control of the remote functions within the hot shop. At each window is located a control pedestal for controlling the functioning of the crane and the pertinent manipulators. All of the stations on a given side and level are housed in a common "operating gallery."

A vestibule has been extended from the main doorway of the hot shop to provide an enclosed area for equipment preparation and truck-trailer deicing before they enter the hot shop (Figure 3-32). A work platform was fabricated and installed below control window "D" in the hot shop to contain a shipping and storage cask during fuel transfer between the two (Figure 3-33 and 3-34). The work platform is divided into two sections; one section services the shipping cask, while the other services the storage cask. The two sections are joined to permit personnel travel between them.

Figure 3-32. TN-8L Shipping Cask and Trailer in Hot Shop Vestibule

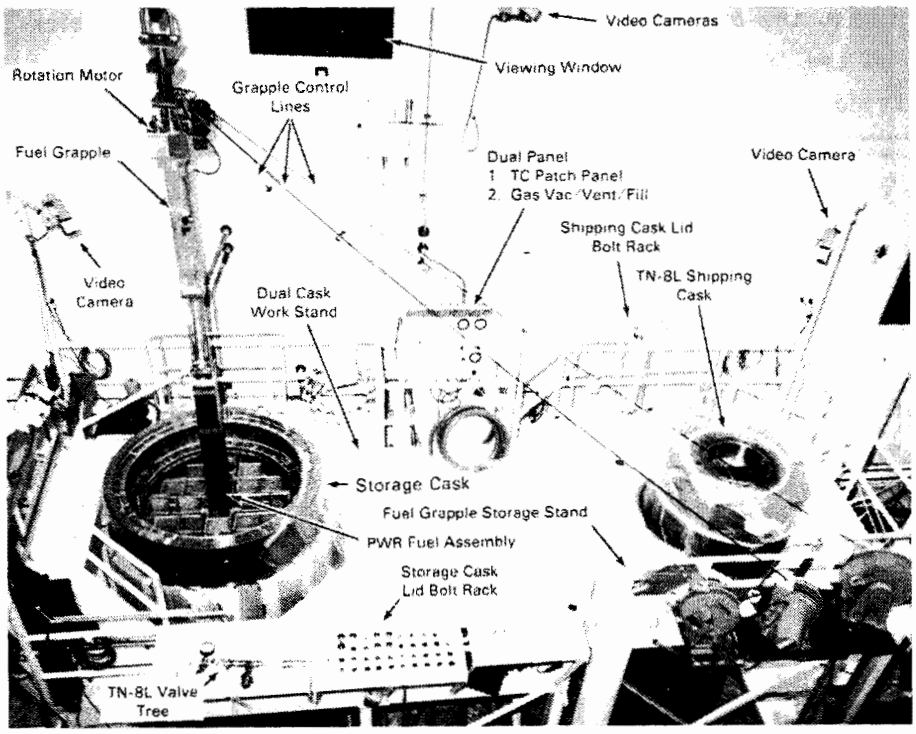

Figure 3-33. Dual Work Stand for Spent Fuel Transfers

The working level of the platform is 4 m (13 ft) above the hot shop floor. The top of the cask is approximately 1 m (3 ft) above the platform's working level, thus allowing operators easy access to the cask lid bolts and gas connections.

The casks are placed into the work platforms using a lifting yoke attached to the 100-ton hot shop crane (Figure 3-35). Each half of the work platform has a removable section of grating that permits side access, thus precluding lifting the cask above the platform's working level (Figure 3-36). The grating is removed and replaced using the 10-ton hot shop crane and lifting slings attached to lifting lugs on the removable sections.

Access to the working level is via a stairway located on the south side of the platform. A notch in the storage cask side of the platform allows easy access to utility pedestal "D" from the platform level.

The assembled work stand contains six posts that support TV cameras with a pan and tilt mechanism (Figure 3-33). Two cameras are mounted on the outer end of the shipping cask stand and two on the outer end of the storage cask stand. Mounts are also

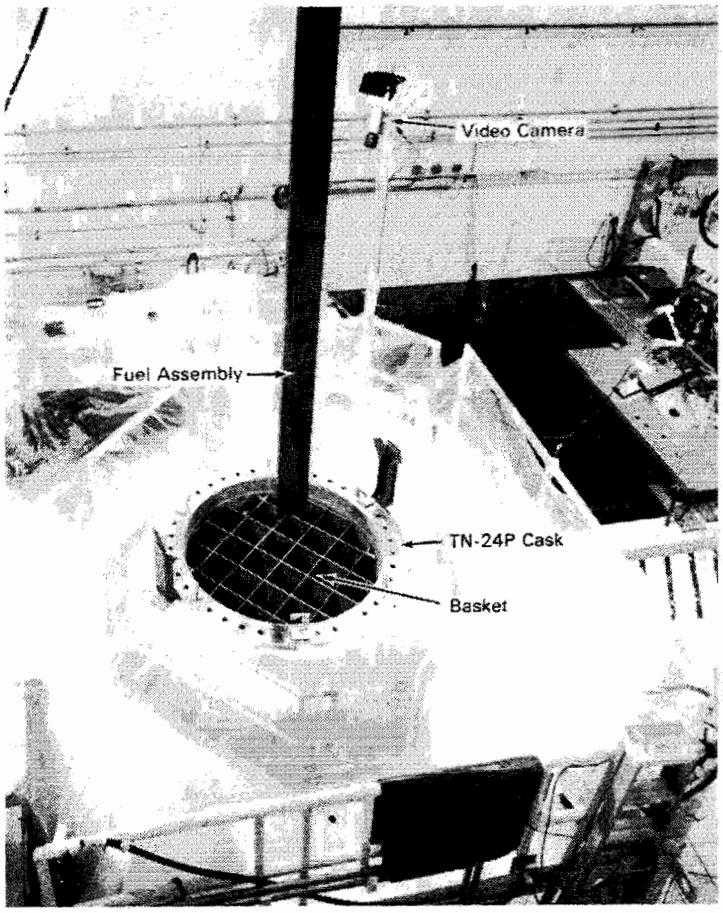

Figure 3-34. Loading TN-24P Cask with Fuel in Work Stand

provided at the midsection of the assembly. The cameras are used for assisting operations with fuel transfer and for fuel assembly inspection.

The work platform also contains platforms for storing cask lid bolts and tool boxes, and for temporarily storing TC lances before and after installation into the casks (Figure 3-33).

TAN-607 Warm Shop. The TAN-607 warm shop is located south of the hot shop as shown in Figure 3-29. The warm shop is designed as a service area for handling test assemblies with low to medium radiation or contamination. It is currently used as an area for familiarization and training on casks upon receipt, instrumenting casks, and testing casks in a controlled environment. The warm shop is 15.5 m (51 ft) wide by 24 m (80 ft) long by 15 m (50 ft) high. It has a main door 8.5 m (28 ft) wide by

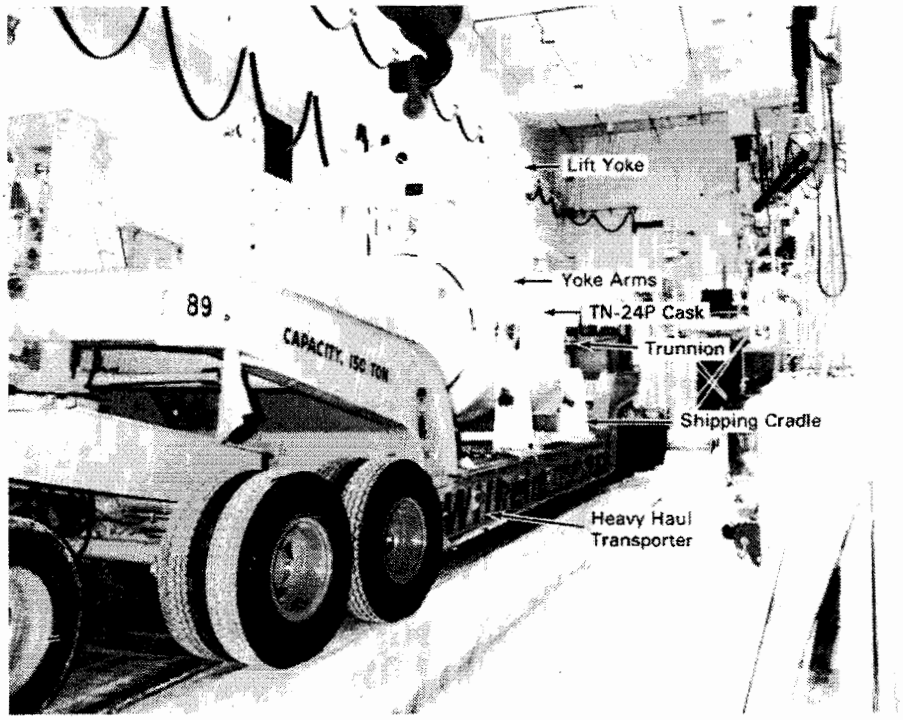

Figure 3-35. Cask with Lift Yoke Attached

10 m (33 ft) high as shown in Figure 3-37. The warm shop is served by a 30/5-ton overhead bridge crane. The warm shop is designed to UBC Seismic Zone 2 requirements. The floor drains for the facility are connected to a hot waste holding tank.

The warm shop was modified to include helium and nitrogen gas supply systems and a vacuum system for use in cask performance testing. These systems interface with corresponding hot shop systems. Two gas cylinder banks, one helium and one nitrogen, were installed against the north wall of the TAN warm shop. These banks supply gas to either the hot shop control panel at the work platform or the warm shop control panel that is also mounted on the north wall (Figure 3-38).

The warm shop control panel provides connection to a vacuum system. The vacuum suction line and a pressure relief line are routed from the control panel, out of the warm shop, and into the hot shop, where they join the hot shop systems. The control panel also provides a connection between an instrumented cask in the warm shop and the DAS located in the hot shop control room at "D" window.

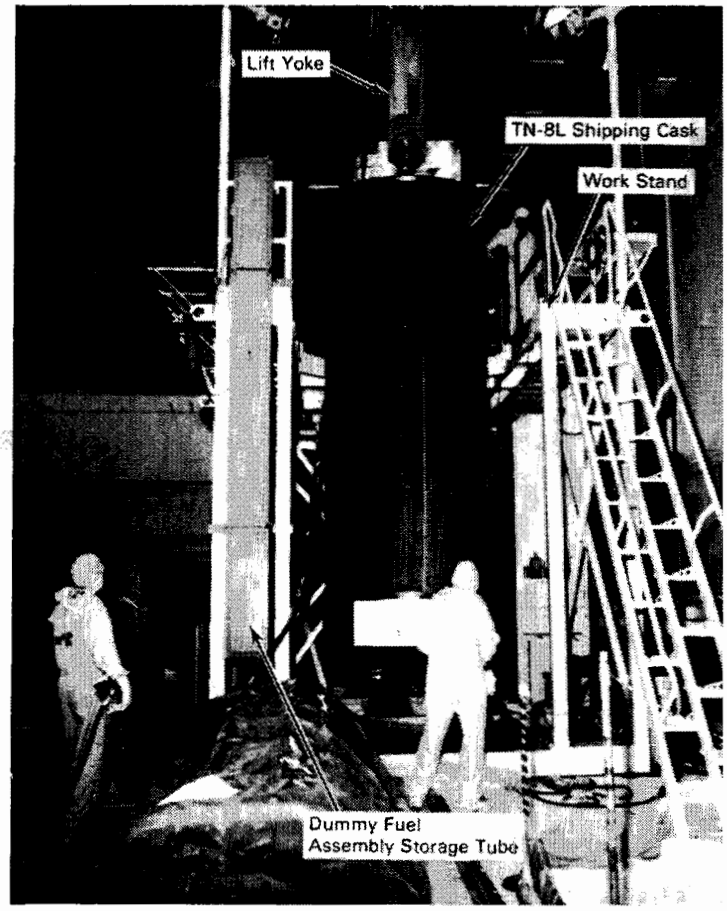

Figure 3-36. Installing Loaded TN-8L Shipping Cask in Work Stand

A radiation shielding wall was added to the warm shop to protect personnel in adjoining hallways and change rooms from exposure when a loaded cask is being tested.

TAN Railroad System

Movement of casks between the TAN hot shop, warm shop, and pad is accomplished by means of a special shielded locomotive and rail-car dolly over a four-track standard gauge railroad system (Figure 3-39). A 27-m-diameter (90-ft) turntable is located just west of the hot shop and pad in the four-track railroad system. Indicators for showing the position of the turntable, turntable alignment, controls for positioning the turntable, and turntable locking controls are located in the Turntable Control Building adjacent to the turntable.

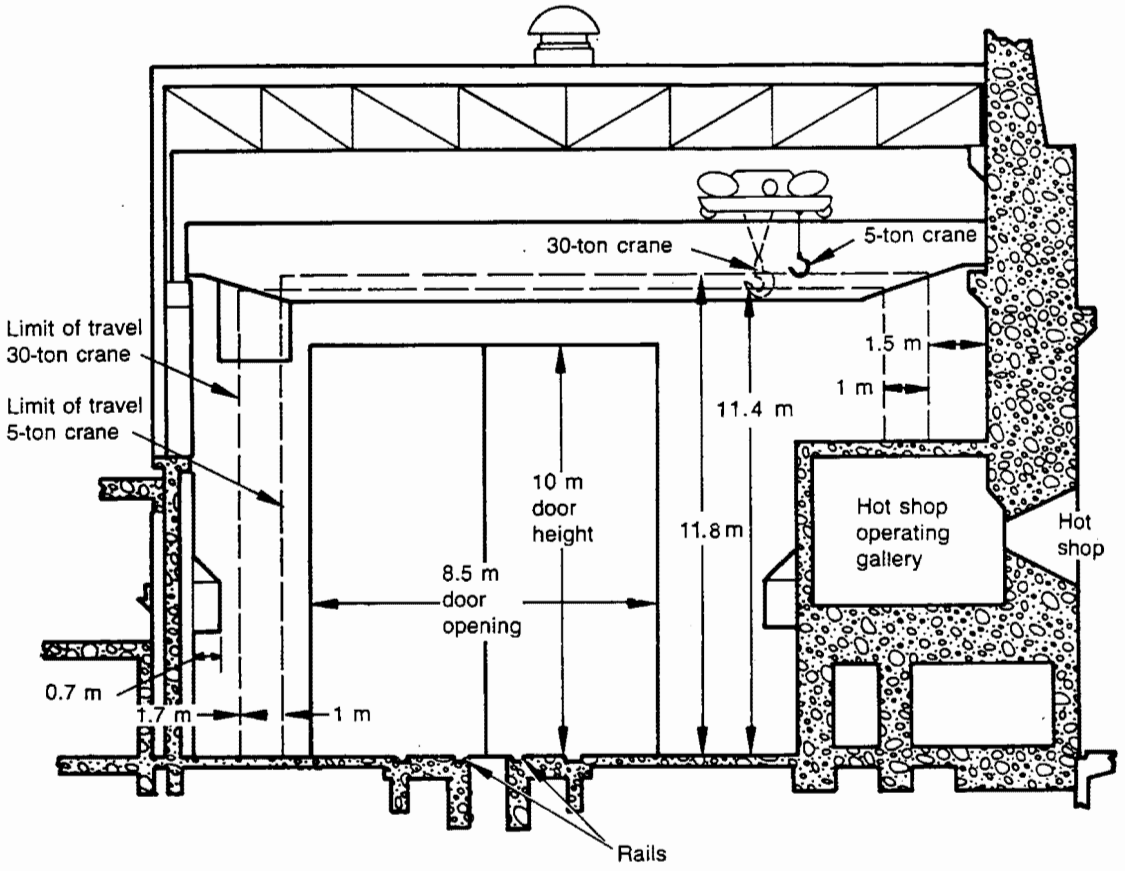

Figure 3-37. Elevation View of TAN Warm Shop

The double-wide rail-car dolly used to move the casks was modified with a heavier underframe to support the weight of the storage casks (Figure 3-40).

Long-Term Surveillance

Facilities for conducting long-term surveillance of the casks were constructed west of TAN-607 (Figure 3-41). These consist of a concrete long-term surveillance pad, data acquisition building, and weather station. A photograph of the TN-24P cask on the pad with the data acquisition building in the background is shown in Figure 3-42.

The long-term surveillance pad is located adjacent to the rail track that exits the TAN hot shop. It is sized to hold six spent fuel storage casks, four from the VP project and two from the Nuclear Fuel Services (NFS) project. The pad is 0.6-m-thick (2-ft) reinforced concrete, 28.7 m (94 ft) long by 12 m (40 ft) wide. Its elevation is the same as the railroad bed, to facilitate crane transfers from rail cars to the pad. An asphalt paved apron surrounds the pad to permit vehicle

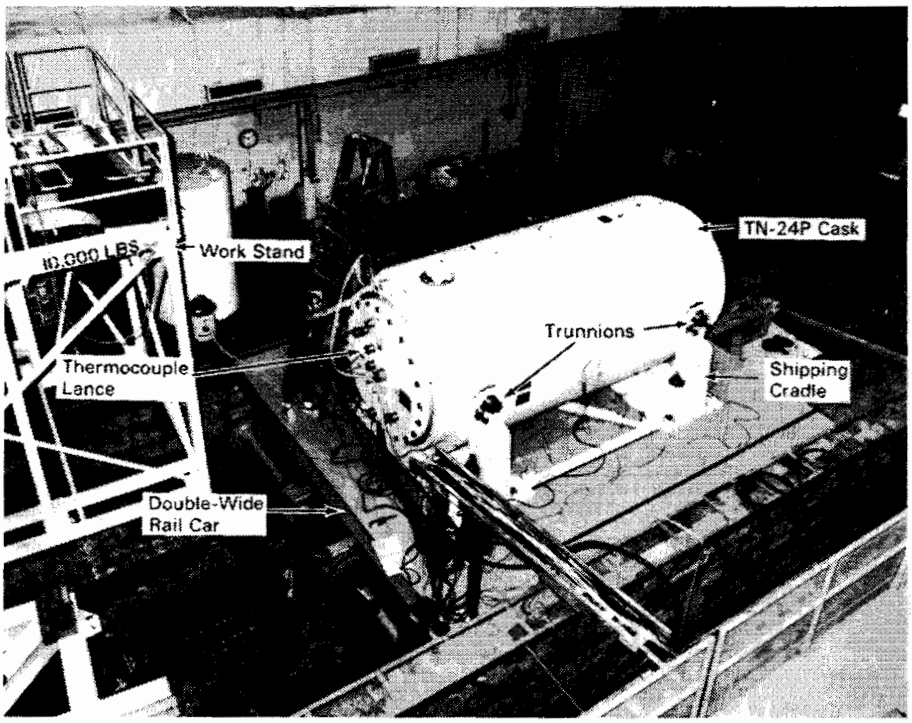

Figure 3-38. Warm Shop Test Area

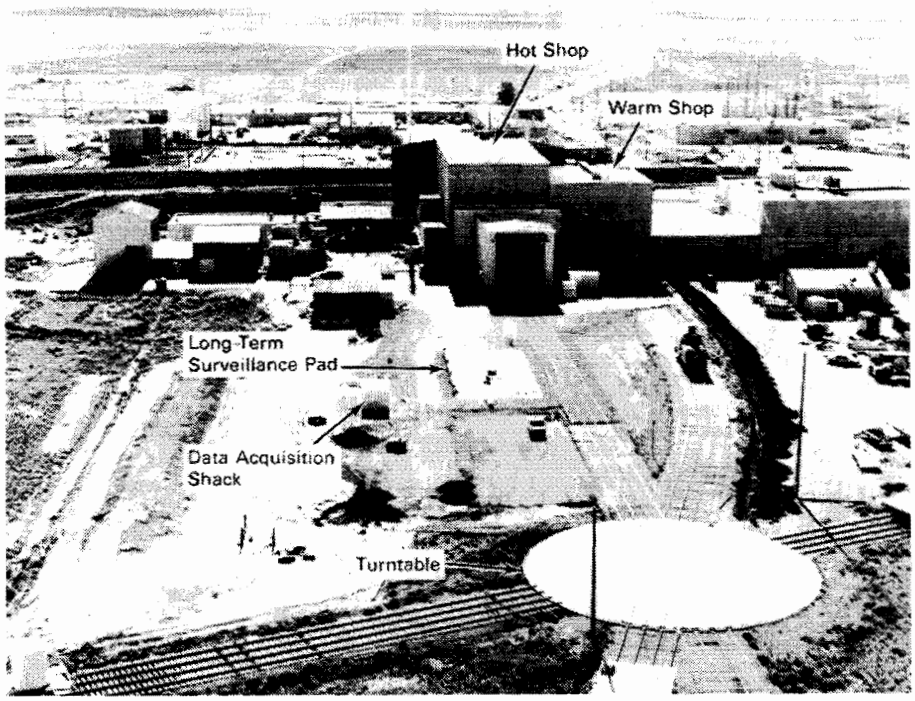

Figure 3-39. Hot Shop Complex and Four-Track Rail System

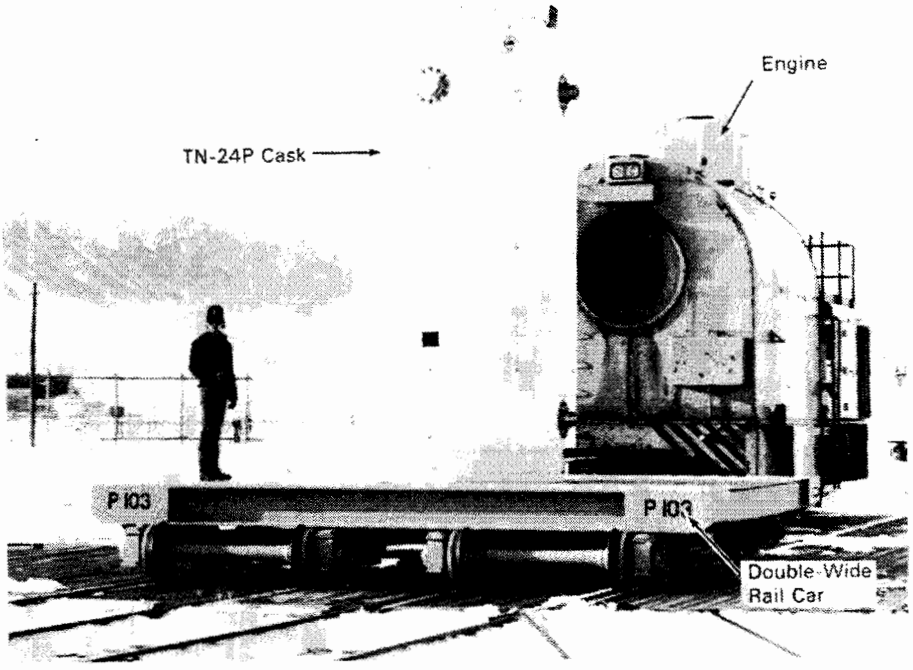

Figure 3-40. Moving TN-24P Cask Between Hot Shop and Warm Shop on Modified Rail-Car Dolly

access. A fence will be constructed to limit access and provide radiation area exclusion after the casks are placed on the pad.

The data acquisition building rests on a small concrete pad near the test pad. The building, constructed of metal framework and siding, is 3.35 m (11 ft) square by 2.75 m (9 ft) tall. Instrumentation leads pass through underground conduit from the pad to the building. Inside the building are a Keithly DAS with an IBM XT personal computer. The PC will be used for storing and reporting monitored data. The building is heated during winter to protect the electronic equipment.

The weather station is located adjacent to the data acquisition building. The small, self-contained unit measures wind speed and direction, atmospheric pressure, air temperature, precipitation, relative humidity, and solar insolation (6). Instrument cables connect the weather station to the DAS.

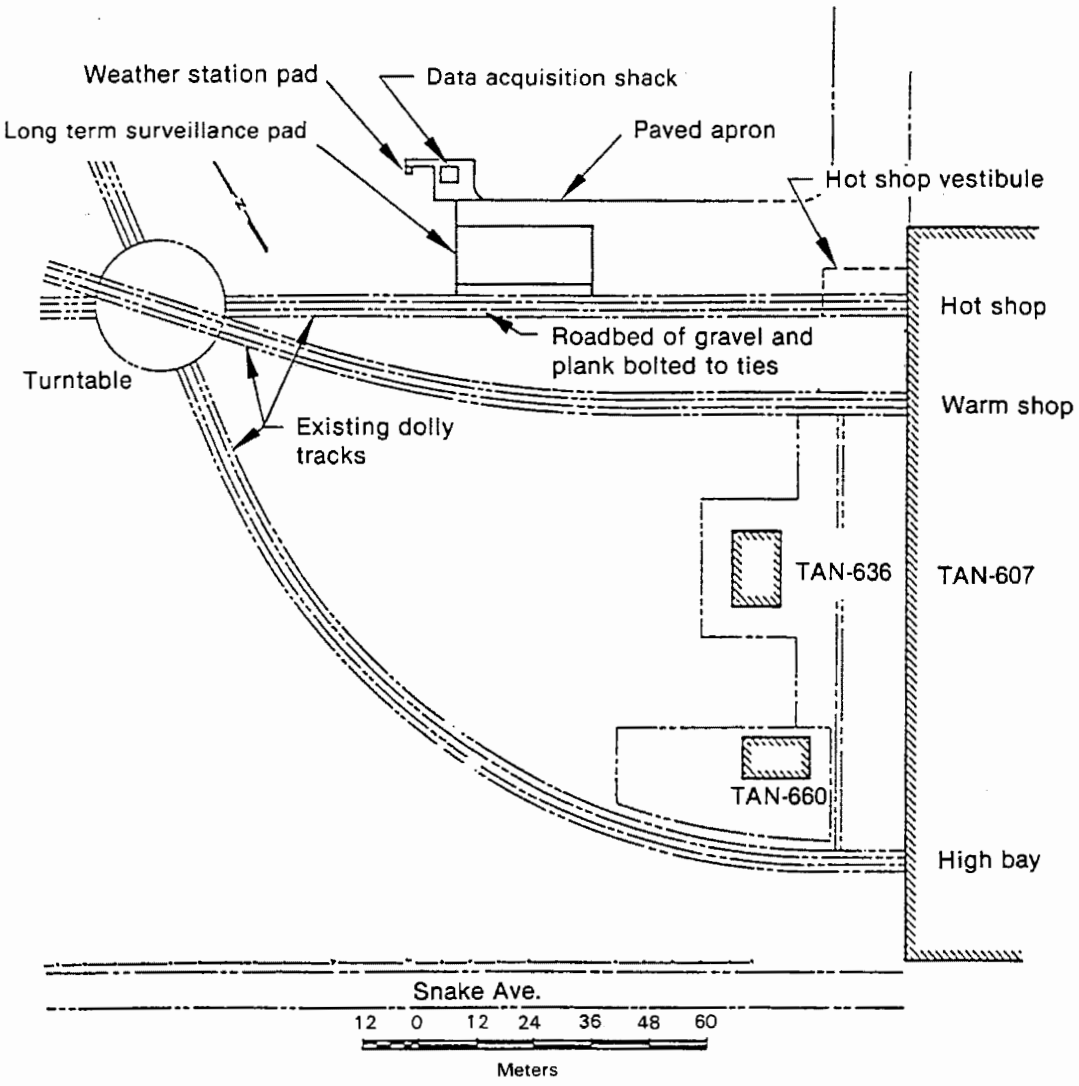

Figure 3-41. Long-Term Surveillance Pad and Data Acquisition System Building Location

TEST PLAN

The TN-24P cask performance test consisted of the six runs indicated in Table 3-9. The test runs involved a fully loaded cask (24 spent fuel assemblies), three backfill media (vacuum, nitrogen, and helium), and two cask orientations (vertical and horizontal). A test plan specified the order of the runs, the fuel assembly load pattern (see Figure 3-17 in Fuel Assembly Section), instrumentation/measurement locations, calibration requirements, and gas and crud sampling intervals. The test plan also addressed cask-handling and fuel assembly characterization activities that were required before, during, and after performance testing.

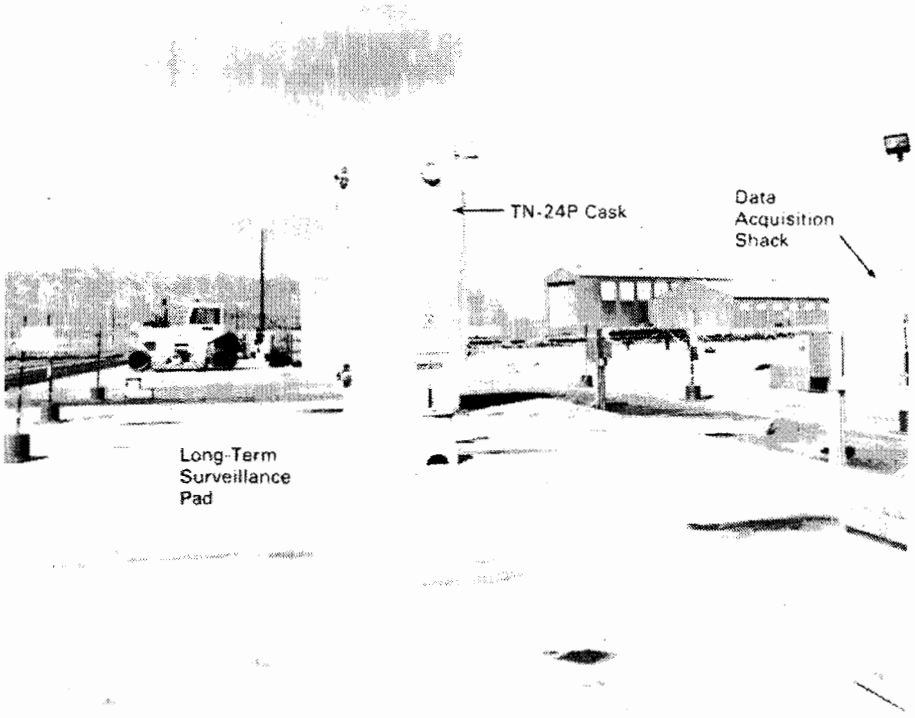

Figure 3-42. TN-24P Cask on Long-Term Surveillance Pad with Adjacent Data Acquisition System Building

Table 3-9

CASK PERFORMANCE TEST MATRIX

Run Number[a]	Cask Orientation	Backfill Medium
1	VerticalHelium[b]	
2	VerticalNitrogen[b]	
3	VerticalVacuum	
4	HorizontalHelium[b]	
5	HorizontalNitrogen[b]	
6	HorizontalVacuum	

[a]All runs were performed with a fully loaded cask (21 assemblies). The total predicted cask heat load was 28.4 kW at the beginning of the month-long test and 27.5 kW at the end of the test.

[b]Gas samples were taken at the beginning and end of each of these test runs.

Before loading the cask with fuel at INEL, VP inspected each fuel assembly using ultrasonic scanning and video (see Fuel Integrity Section). The assemblies were then shipped from Surry to TAN, three at a time, in Transnuclear TN-8L shipping casks. Upon receipt at TAN, the three assemblies were unloaded from a TN-8L cask and transferred directly into the TN-24P cask in the TAN hot shop without first being temporarily stored in lag storage (see section on INEL cask testing facility). After the eighteenth assembly was loaded in the TN-24P cask, a TC lance was installed in a center assembly and the temperatures were intermittently monitored to ensure safe fuel rod operating temperatures. This procedure was followed until the cask was fully loaded. Once the TN-24P storage cask was fully loaded, the remaining 8 TC lances were inserted through the primary test lid into guide tubes of selected fuel assemblies and basket locations. The cask was then moved from the hot shop to the warm shop on a double-wide rail car. Instrumentation leads were connected to appropriate sensors, and the test matrix shown in Table 3-9 was completed.

The fuel assembly load pattern used during testing was previously shown in Figure 3-17. The load pattern maintained 1/8 symmetry in the cask, to evaluate temperature and dose rate symmetry and to simplify the analytical modeling effort.

The test plan required that gas samples be taken shortly after the cask was filled with a different gas, and immediately prior to evacuating a gas from the cask. The gas samples obtained during the test are indicated in Table 3-9. Each time the cask backfill medium was changed, the cask was pumped down, backfilled with the desired medium, pumped down again, and finally backfilled. This ensured purity of all backfill media to >99%. Nitrogen was used immediately prior to vacuum test runs to obtain a low-pressure (1 to 3 mbar), low-conductivity, vacuum/nitrogen environment.

The test plan formed the basis for developing a set of detailed operating procedures by INEL that outlined the steps required to perform the cask performance test. The procedures are discussed in the next section.

INEL CASK HANDLING AND OPERATING EXPERIENCE

This section describes the cask handling and operating experience gained during cask performance testing. The tasks required to conduct cask performance testing included performing storage and shipping cask handling studies, assessing the use of existing facilities and equipment, installing cask ancillary and research equipment at the INEL TAN cask testing facility, operation preparations, storage cask receipt and preparations, operational dry runs, a facility readiness review, fuel transfers and

loading, cask performance testing, fuel assembly inspections, and long-term surveillance. INEL personnel performed a dry run to train personnel and check out equipment. After the dry run was evaluated, necessary equipment and procedure changes were made. The cask performance test was then conducted.

When they arrived from the Surry reactor at the INEL TAN-607 Hot Shop in TN-8L shipping casks, the fuel assemblies were transferred in air to the TN-24P cask. Operations personnel monitored the cask during this time. Preliminary testing began when the cask was partially loaded with 18 fuel assemblies. When the cask was fully loaded with fuel, the cask was transferred to the warm shop test bay where formal testing began.

As the TN-24P cask was being loaded with fuel, certain selected fuel assemblies were visually characterized by video and still photograph. Crud and smear samples were also collected and analyzed.

At the conclusion of the formal testing in the warm shop, the TN-24P cask was moved to the hot shop were the cask was prepared for temporary storage and monitoring. The cask was then placed on the long-term surveillance pad and connected to the data collection system.

Each of the tasks required to conduct the TN-24P cask performance testing is described in the following subsections.

Storage and Shipping Cask-Handling Studies

Two detailed cask-handling studies were performed. One study developed the handling logic for the TN-24P storage cask, and the other defined handling of the Transnuclear TN-8L shipping cask and fuel. The handling studies identified how the shipping and storage casks would be received at INEL and how fuel could be handled. They compared test requirements of the approved test plan with INEL site capabilities. The specific equipment and systems required to accomplish the cask performance test were defined. The studies identified modifications or upgrades to base facility equipment needed to accomplish the performance test. The two handling studies became the bases for identifying the equipment and operational preparation subtasks required to accomplish the cask performance test.

Facilities and Equipment

Existing INEL equipment and facilities were used as much as possible. Those at the Central Facility Area (CFA) and Test Area North (TAN) were the most extensively

used. Facility equipment capability, modification requirements, and maintenance requirements were evaluated. Equipment at CFA--the rail system, gantry crane, and heavy haul trailers, roads, and bridges--were identified. Equipment located at the TAN-607 hot shop was also evaluated. Equipment systems evaluated included the hot shop crane; manipulators; direct viewing shielding windows; floor loading; hot cell transporter; in-shop utility pedestals; operating galleries and shielding; in-shop rail track; shield doors; hot shop lighting; cask gas venting system; and facility safety support systems. Equipment and systems evaluated outside the hot shop were the local in-plant rail track; turntable; locomotive; and the warm shop capability for cask testing. Areas along and adjacent to the hot shop were evaluated as a site for the long-term surveillance pad. These base facility systems and equipment were previously discussed in the section on the INEL cask testing facility.

Two types of project-specific equipment were identified: cask test support and cask-handling/operation equipment. Cask test support equipment was that required to gather test data. It consisted of the gas/vacuum/vent system and the data acquisition system. Cask handling/operation equipment was that required to handle the cask, such as lift yokes, cask lid lifting fixtures, cask surface seal protectors, thermocouple lance template, and the cask gas/vacuum/vent valve tree.

The base facility equipment modifications and project-specific equipment systems were designed, procured, and installed concurrent with performance of the tasks to prepare the facility for operation. After a review of the TN-24P cask manual and drawings, specialized handling fixtures and tools were developed for hands-on and remote cask operation. Thermocouple lance insertion was closely reviewed. Special semiremote insertion tools were developed to reduce personnel radiation exposure and contamination spread while installing and removing the lances.

Both base and project-specific equipment were operationally tested before they were actually used for remote operation. The equipment was tested either during a dry run training task or by an independent, formal system-operation test. When problems were encountered, they were resolved, and the equipment or system was retested.

Operational Preparations

Numerous tasks were required to prepare the facilities for the cask testing project. Operating documentation was developed, personnel were trained, the TN-24P storage cask was received and moved to the TAN test facility, and a dry run was performed to check out the equipment and operating procedures. A facility readiness

review, held prior to the first storage cask test, approved the facility for cask testing. No formal readiness review was held for the TN-24P cask test.

Documentation Development. Reviews compared the base facility safety and standard operating documentation with the TN-24P cask testing work scope. A facility fuel criticality analysis was performed on the TN-24P cask, which indicated that, during air loading of the cask in the TAN hot shop, if water from facility sources were to enter the cask, a multiplication factor above the limiting value (0.95) would occur. Poison rods were placed into 16 of the 20 fuel assembly guide tubes at the reactor loading facility to provide the required INEL site criticality safety margin. Operational sequences were verified, and revised addendums to the facility Safety Analysis Report (SAR) and Operation Safety Requirements Document (OSRD) were prepared and approved. Facility Standard Operating Practices were also reviewed and revised as required to meet the cask-testing requirements.

Site Work Releases (SWRs) or Hot Cell Work packages controlled all operating tasks performed at the facilities. The SWR work, general work using craft labor, does not require rigorous control and review. It usually involves equipment installation or maintenance. Hot Cell Work packages identify the tasks or subtasks required to accomplish a specific scope of work, and delineate a specific sequence for facility operating tasks. These work packages usually contain one or more detailed operating procedures (DOP), which are step-by-step instructions for performing a specific task. The SWRs, work packages, and DOPs are controlled documents. As such, they must be revised and approved, should a work step need changing. Work stops while the package is being revised, and does not resume until the revision is approved.

The overall project statement of work and the TN-24P test plan were used to develop this operating documentation. Information for preparing the procedures came from the cask vendor, safety analysis, equipment drawings, and operating and maintenance manuals. Safety, quality, project, independent safety, and operations personnel rigorously reviewed these work packages and DOPs.

Three Hot Cell Work packages were prepared to provide operating instructions for the operating personnel. The first consisted of training procedures to familiarize personnel with the cask, check out and perform the cask operating equipment fit-up, and check the operating procedure. The second work package provided instructions for actual fuel receipt and cask loading. The third package instructed personnel in cask testing and long-term surveillance at the pad.

The Detailed Operating Procedures used for handling, operating, and testing the TN-24P dry fuel storage cask are listed in Table 3-10.

A document control office managed the release and change control of the cask operating and safety procedures and documents. The document control office maintained the facility operating project, research data, research photographs, project equipment, and operating cost and schedule files.

Operational Training. Personnel training requirements were developed for the TN-24P cask and the Transnuclear TN-8L shipping cask. Training consisted of both classroom and hands-on training. Operation technicians and supervisory personnel received personal training packages before beginning the classroom instruction.

Storage Cask Receipt and Preparation. The TN-24P storage cask was received at the CFA in late September 1985. It had traveled from the west coast to the INEL on a special heavy depressed-center rail car. The cask, attached to a horizontal shipping and storage cradle, was off-loaded from the rail car (Figure 3-43). The 200-ton gantry crane was used for this operation. The cask remained at CFA while the TAN area was being prepared.

A heavy-haul transport plan was prepared to coordinate moving the cask from the CFA to TAN. An over-the-road 150-ton heavy-haul trailer was leased to transport the cask (Figure 3-44). The cask was transported to TAN in mid-October and moved to the TAN-607 hot shop preparation area.

Operations technicians uncrated the cask from its special hardwood container and prepared to off-load it at TAN (Figure 3-45). While the cask was being prepared, the hot shop was readied for lifting the cask. A contamination-free zone was established inside the hot shop. The heavy-haul trailer containing the cask was moved into the hot shop and located parallel to the bridge crane (Figure 3-35). The cask-lifting yoke was attached to the crane hook and connected to the top trunnions of the cask.

Operations technicians used the crane bridge travel and hoist motion to rotate the cask to a vertical orientation (Figure 3-46). The rigging and crane hook were kept vertical throughout cask rotation. Then, the cask was suspended from the crane off to the side of the heavy-haul trailer, and the trailer was removed from the hot shop. The horizontal cask storage cradle was removed and placed into temporary storage.

Table 3-10

DETAILED OPERATING PROCEDURES FOR TN-24P CASK HANDLING AND TESTING

DOP Number	Title
1.13.24	TAN SFSC Program Grid Marking for Instrumentation of TN-24P Storage Cask
1.13.25	TAN SFSC Program Thermocouple Block Mounting for TN-24P Storage Cask
1.13.26	TAN SFSC Program Transfer TN-24P Storage Cask from Transporter to P103 Dolly and Move to Warm Shop
1.13.27	TAN SFSC Program TN-24P Storage Cask Training Equipment Fit-Up in Warm Shop
1.13.28	TAN SFSC Program Transfer TN-24P Storage Cask from P103 Dolly to Hot Shop Storage Cask Work Platform. Move CASTOR-V/21 Storage Cask to Warm Shop
1.13.29	TAN SFSC Program TN-24P Storage Cask Training Fuel Assembly Fit-Up, and Fuel Transfer Dry Run in Hot Shop
1.13.30	TAN SFSC Program Fuel Receipt and Transfer from TN-8L Shipping Casks to TN-25 Storage Casks.
1.13.31	TAN SFSC Program Checkout of Lance and Basket Thermocouples for the TN-24P Storage Cask
1.13.32	TAN SFSC Program Installation and Operational Check of Data Acquisition System (DAS) and Transducers TN-24P Storage Cask
1.13.33	TAN SFSC Program Dosimetry Installation and Removal for TN-24P Storage Cask
1.13.34	TAN SFSC Program Install TC Lances in TN-24P Test Lid and Leak Check
1.13.35	TAN SFSC Program Move TN-24P to W/S Move CASTOR-V/21 to HS
1.13.36	TAN SFSC Program TN-24P Cask Vertical Test Matrix Runs 1, 2, and 3
1.13.37	TAN SFSC Program Rotate TN-24P Cask to Horizontal
1.13.38	TAN SFSC Program TN-24P Cask Horizontal Test Matrix Runs 4, 5, and 6
1.13.39	TAN SFSC Program Move TN-24P to HS Move CASTOR-V/21 to WS
1.13.40	TAN SFSC Program Remove TC Lances from TN-24P Test Lid and Leak Check Penetrations
1.13.41	TAN SFSC Program TN-24P Cask Interim Monitoring at Test Pad
1.13.42	TAN SFSC Program TN-24P Cask Interim Gas Sampling at Test Pad

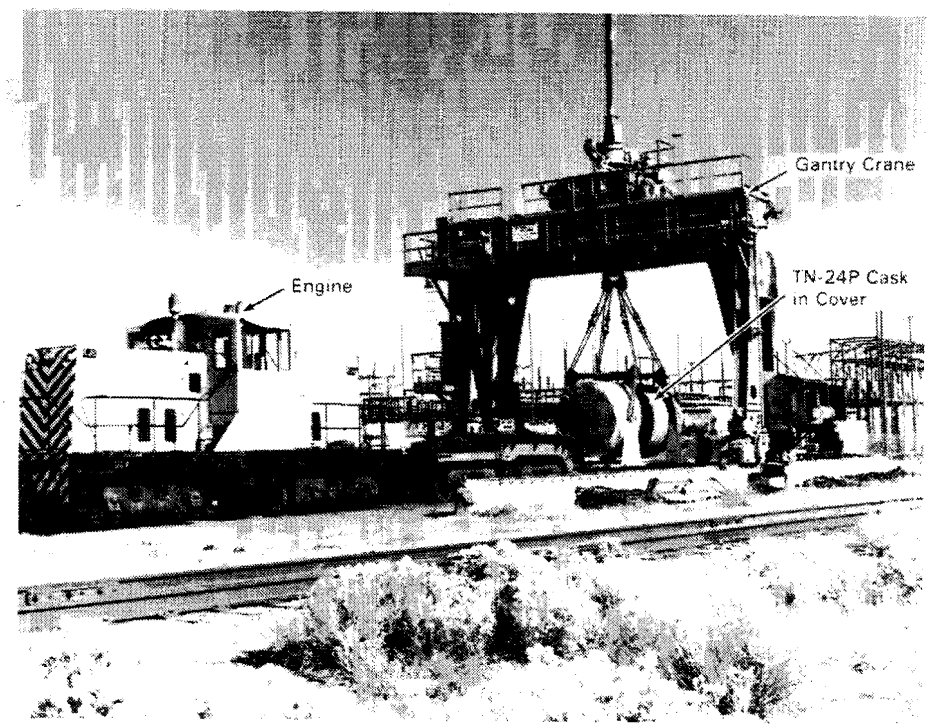

Figure 3-43. TN-24P Cask Receipt and Off-Loading at Central Facilities Area

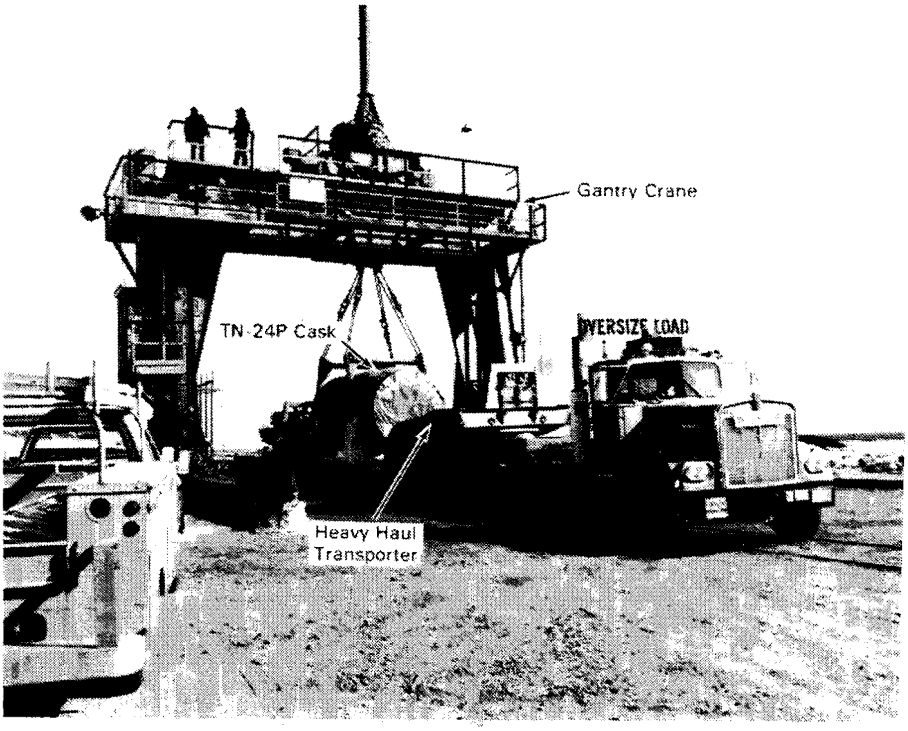

Figure 3-44. Loading TN-24P Cask Onto Heavy-Haul Trailer for Transport to TAN

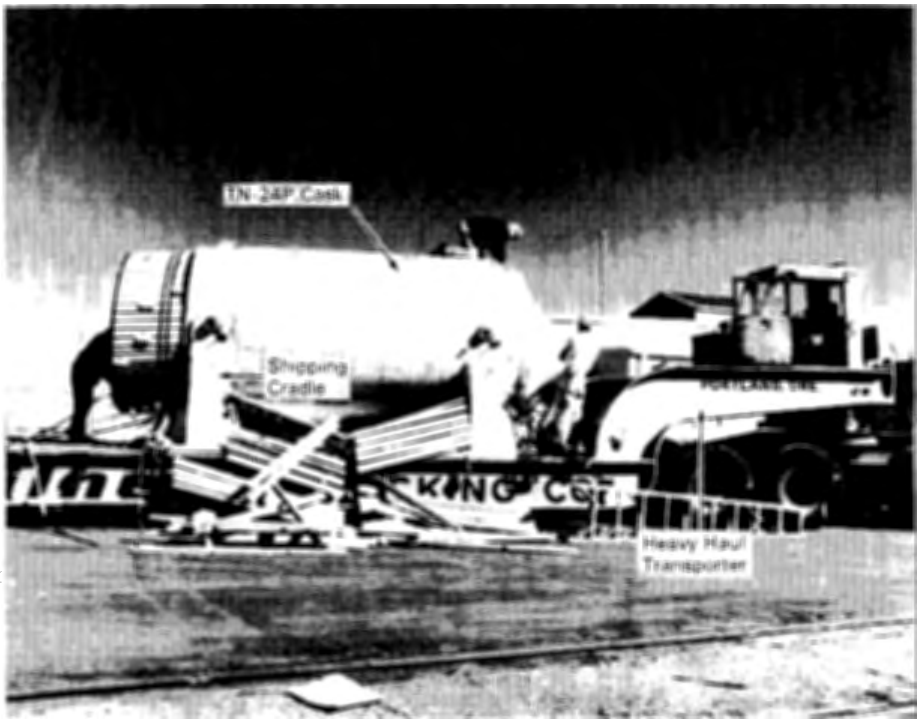

Figure 3-45. Preparing TN-24P Cask for Off-Loading at TAN-607 Hot Shop

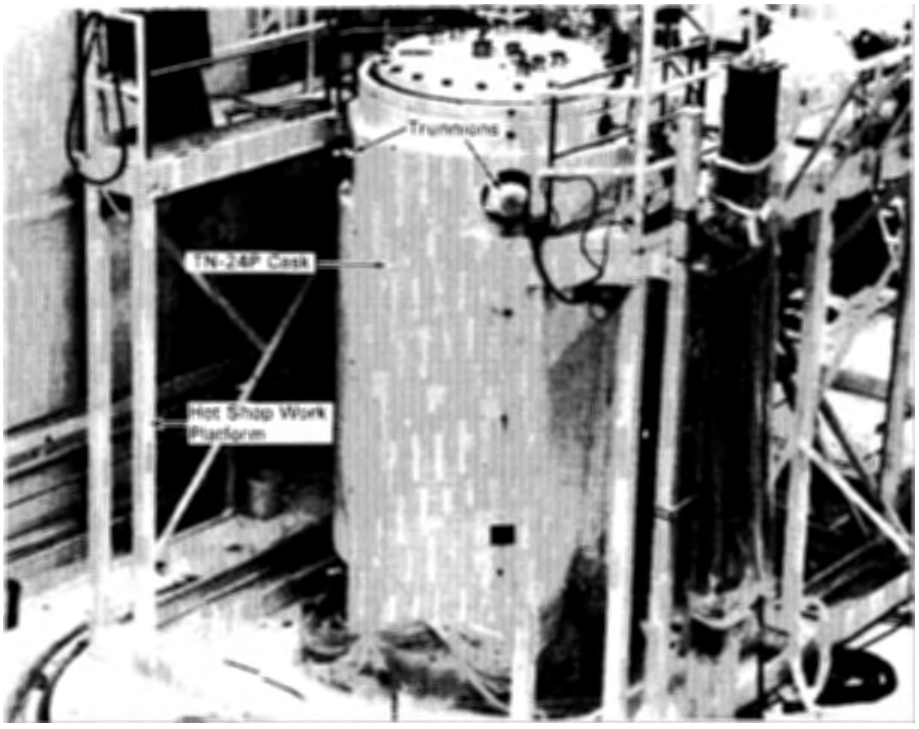

Figure 3-46. TN-24P Cask Hoisted to Vertical Position

The cask was then placed into the hot shop work platform. Shims were used to level the cask so the lid surfaces would be as level as possible. Level lid surfaces facilitate remote lid removal and fuel assembly loading. Because the fuel assemblies were transferred in air, a contamination barrier was required to reduce the possibility of contaminating the outer cask surfaces. Teflon was used for this because of its high melting point. Teflon sheets were attached to the cask with Teflon tape. Cask familiarization, training, and ancillary equipment/tool checkout was performed. Using the personnel work platform for access and the hot shop crane for hoisting, operations technicians vented the cask cavity and removed the cask rain cover, pressure-monitoring accessories, and standard shield lids. Seals and seal surfaces were inspected, and the lid surface seal protectors were installed.

The lid seals were inspected, and a shipping basket restraint was removed. Clearances were checked to ensure they would allow a TC lance position template to be installed on top of the fuel basket. The template was used to verify the test lid lance penetration locations and assist in lance insertion training. The test lid was then reinstalled. Thermocouple lance blind flanges covering the test lid penetrations were removed one at a time with a semiremote reach tool. A mockup TC lance was inserted through each lid penetration and template location hole. A rope block and tackle and remote reach tools for positioning the tip of the lance were used for installing the lances. When the TC lance installation training was completed, the blind flanges were replaced and the test lid and the TC lance template were removed.

A remote shield lid-lifting fixture was attached to the shield lid, which provided a cylinder-into-cylinder sliding handling effect rather than a disk-into-cylinder effect. This helped prevent the lid from binding when it was placed into the cask lid cavity.

Operational Dry Run. An operational dry run was performed in the hot shop. Because the hot shop personnel were trained previously on the TN-8L shipping cask, the dry run concentrated on the TN-24P storage cask handling and spent fuel loading into the storage cask. The dry run trained personnel and checked out the operating facility, project-specific equipment, and procedures.

The dry run began with the TN-24P in the hot shop work platform (Figure 3-47). The cask was vented through a controlled gas/vacuum/vent system. Technicians then removed the lid bolts and installed the lid-lifting fixture. Numerous equipment checkout procedures were performed to verify that all cask-handling equipment and facility safety systems were ready for remote operation.

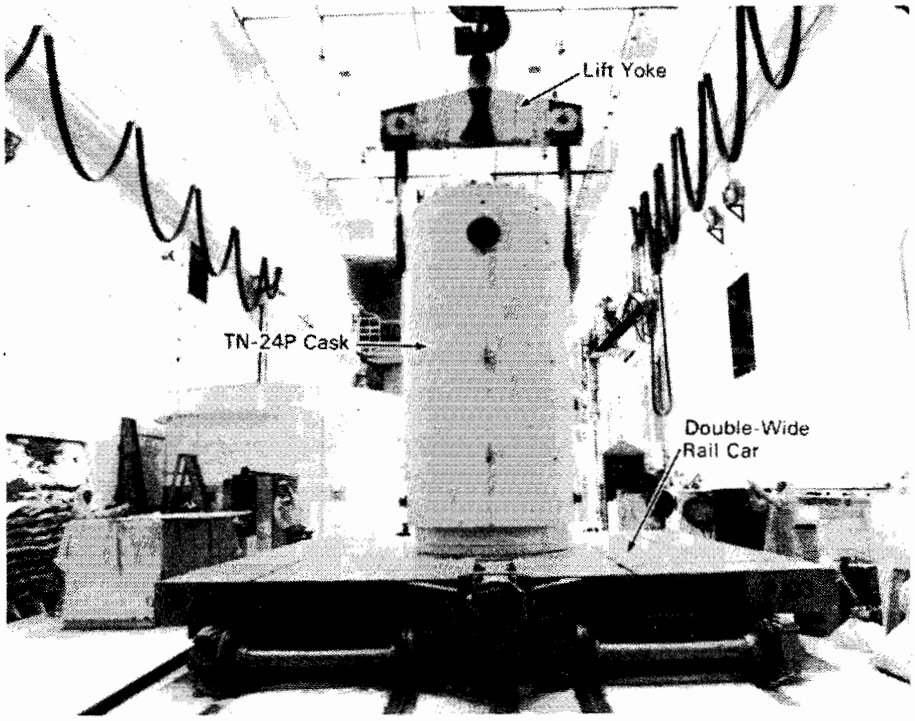

Figure 3-47. TN-24P Cask in Hot Shop Work Platform

Although the actual procedure would ensure that all personnel were evacuated from the hot shop, certain personnel remained in the hot shop for the dry run to observe the operation. However, they did not assist any of the remote operations. During the dry run, different operating technicians repeated the following handling sequences several times:

- removing the TN-24P storage cask lid and placing it on lid support stands on the hot shop floor
- installing the lid seal surface protectors on the storage casks
- connecting the crane to the fuel grapple and attaching the grapple to the mockup fuel assembly
- using the power rotate on the grapple to align the fuel assembly vertically and rotationally
- lowering the fuel assembly into the storage basket (Figure 3-48).

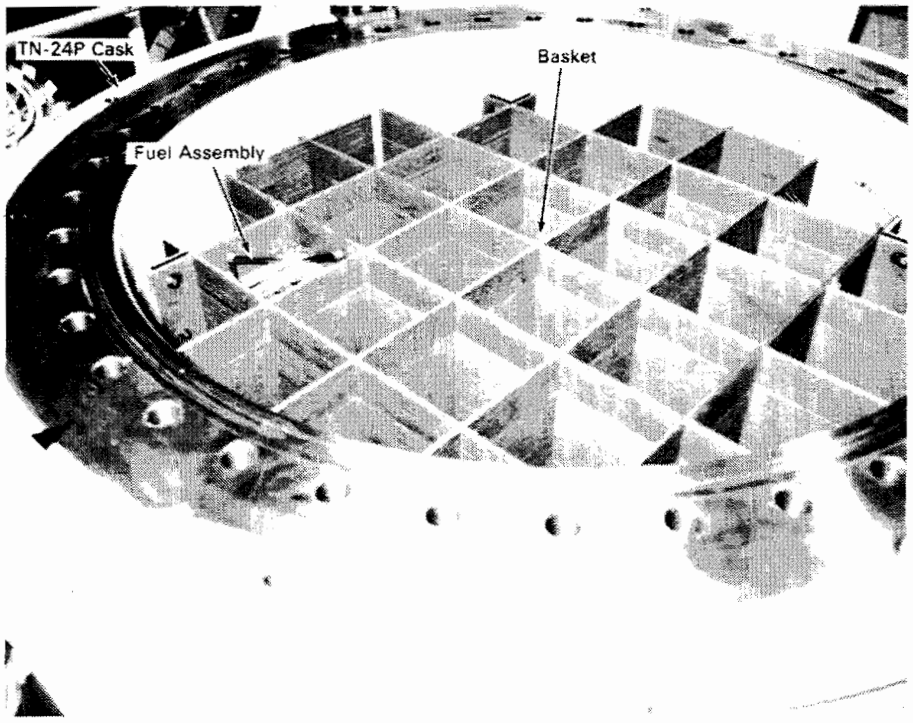

Figure 3-48. Mockup Fuel Assembly Installed into TN-24P Cask During Dry Run

During these operations, the fuel grapple load cell was monitored closely to prevent the possibility of hanging up the fuel assembly, which could cause the grapple system to fail. When the mockup fuel assembly had been inserted into each tube of the storage cask basket, the assembly and grapple were returned to their storage racks.

The operations technicians then remotely removed the cask seal surface protector from the storage cask. Using a tool held in the overhead manipulator, the seal surfaces were wiped down to remove any foreign material from the mating surface. The test shield lid was then reinstalled on the storage cask.

At this point in the handling sequence, hands-on work was performed in the hot shop. Operations technicians installed and torqued the cask lid bolts. The cask was evacuated and backfilled with nitrogen.

Fuel Transfers and Loading

The TN-24P storage cask was loaded with fuel during November and December 1985. Loading fuel into the TN-24P cask was routine, and no problems were encountered. The fuel transfers and loading followed the procedures verified during the dry

run. The loading, vacuum pumpdown, and decontamination operations and experience are discussed in this section. Personnel radiation exposure levels estimated to have occurred during fuel transfers, loading, and testing are also presented.

Cask Loading. The eight TN-8L shipping casks arrived at the TAN facility at any hour of the day or night. Because each cask shipment was tracked along the shipping route, facility operations personnel received the estimated time of arrival. They then could schedule the unloading with other facility project work. Generally, if the cask arrived on the weekend or late at night, it remained at the TAN guard gate. Sometimes the area health physicist would escort the shipment to the TAN hot shop annex building, where it was parked inside. The cask would be unloaded during the next regular work shift. The cask unloading turnaround time usually required two and one-half shifts or about 20 h. Planned overtime and weekend work supported a shorter cask shipping schedule.

Eight shipments, with three fuel assemblies each, were received to fully load the TN-24P storage cask. No handling problems were encountered, and the cask-handling equipment and operating ancillary equipment performed well.

Gas samples were taken from each shipping cask and analyzed before the cask was vented. No fission product gases were detected. The shipping cask radiological surveys were below legal shipping limits. The INEL shipping requirements made minor decontamination necessary before casks could be shipped from INEL.

The first and seventh shipments arrived in the same cask. The cask internals were radiologically smeared after the first and seventh shipment to determine if contamination had increased. Standard smears with 4.25-cm-diameter (1.67-in.) tabs over an area of 100 cm^2 (15.5 $in.^2$) with an applied force of 35 kPa (5 psi) were taken from the fuel basket bottom and near the bottom on the side wall. Crud collection samples were also taken from the bottom surface of the cask fuel basket. The samples were sent to LLNL from the bottom surface of the cask fuel basket. The samples were sent to LLNL to compare the samples from the seventh shipment with those from the first (see Table 3-8).

TN-24P cask surface temperatures reached 90°C. Therefore, Teflon sheeting with a high melting point replaced the standard polyethylene sheeting. The sheeting served

as a barrier to prevent storage cask contamination. Teflon sheeting in the temperature range required was available only in rolls 0.9 m (34 in.) wide. The sheeting was attached to the cask with Teflon tape. The seams were loosely overlapped and taped.

To prevent other top surfaces of the work platform near the cask from being contaminated, the following arrangement was used. Teflon sheeting was attached to areas contacting the cask. Polyethylene sheeting was taped to the Teflon at a safe distance from the cask. The contamination barrier also acted as a thermal barrier, preventing some heat transfer from the cask. However, the contamination barrier was used only while the cask was being loaded. It was removed during formal thermal cask testing.

The TN-24P storage cask operations were very satisfactory. Cask-handling and loading operations were easy. Vendor service and information response were good.

Vacuum Pumpdown. A valve tree connected to a cask monitoring port allowed cask vacuum pumpdown and gas backfilling. The valve tree was connected by quick-disconnects and vacuum hose to the gas/vacuum/vent system. A pressure transducer, teed into the valve tree, monitored cask cavity pressure.

The cask vacuum pumpdown system required approximately 3/4 to 1 h to pump the cask from 850 mbar atmosphere pressure (12.25 psi) at 1463 m (4800 ft) elevation down to less than 1 mbar (0.01 psi). Backfilling the cask with cover gas required about 15 min.

Decontamination. Contamination spread was not a major problem during the fuel assembly air transfers between the shipping and storage casks. However, minor contamination did occur. The contamination was localized to the personnel work platform between the casks. About 4 h of decontamination were required before personnel could continue hands-on work for cask shipping and interim storage activities.

The fuel assembly grapple lower assembly and tool fingers became highly contaminated after each fuel unloading. The lower assembly was decontaminated and bagged between use.

Estimated Personnel Radiation Exposures. During the 3 months personnel were loading and testing the TN-24P cask, operational radiation and temperature monitoring were

performed. The monitoring provided current actual data for personnel safety. Temperatures and radiation increased with each fuel loading, and more personnel safety equipment was used. A combination of materials was used to reduce personnel exposures on top of the cask for lid bolt removal, lance installation, and gas samples. Thermal blankets were placed on the top and down the sides of the cask to reduce the effect of the high temperature hazards. Blankets for thermal insulation were 0.61 m x 1.2 m x 2.5 cm (2 ft x 4 ft x 1 in.) thick. Borated poly sheets, 2.5 cm thick (1 in.) were used for neutron shielding, and 1.27-cm-thick (1.5-in.) lead wool blankets provided gamma shielding. This-loose laid protective material was repositioned as required for access to different cask penetrations and for lid bolt installation. When it was not practical to use shielding, every effort was taken to reduce personnel exposures by reducing time in the radiation field.

Personnel radiation exposures during the handling, loading, and testing of the TN-24P cask were:

- fuel receipt and loading- 0.3 man-rem
- thermocouple lance installation and removal - 0.3 man-rem
- cask handling - 0.3 man-rem
- testing (instrumentation) - 0.3 man-rem.

Loading and testing the cask required extensive hands-on operation. For example, thermal testing, radiation dose rate monitoring, multiple gas backfilling, and sampling were hands-on operations. These operations were performed to support the cask performance test, but they would not be required for commercial power plant underwater fuel loading. Hence, radiation exposures under actual storage scenarios would be much lower than those encountered during this cask performance testing effort.

Cask Performance Testing

Preliminary thermal testing was started when the TN-24P storage cask was loaded with 18 fuel assemblies. This was done to ensure that fuel would not exceed maximum allowable temperatures during the cask loading and to obtain early cask heat transfer data. The preliminary data ensured that fully loaded cask surface temperatures and fuel temperatures would not exceed allowable values.

Fuel temperature data were collected using TC lances inserted through a penetration in the test lid and into the guide tube of a selected fuel assembly (Figure 3-49). The TC lances were connected to the data acquisition system. The DAS collected temperature and pressure data during cask pumpdown and interim storage between fuel

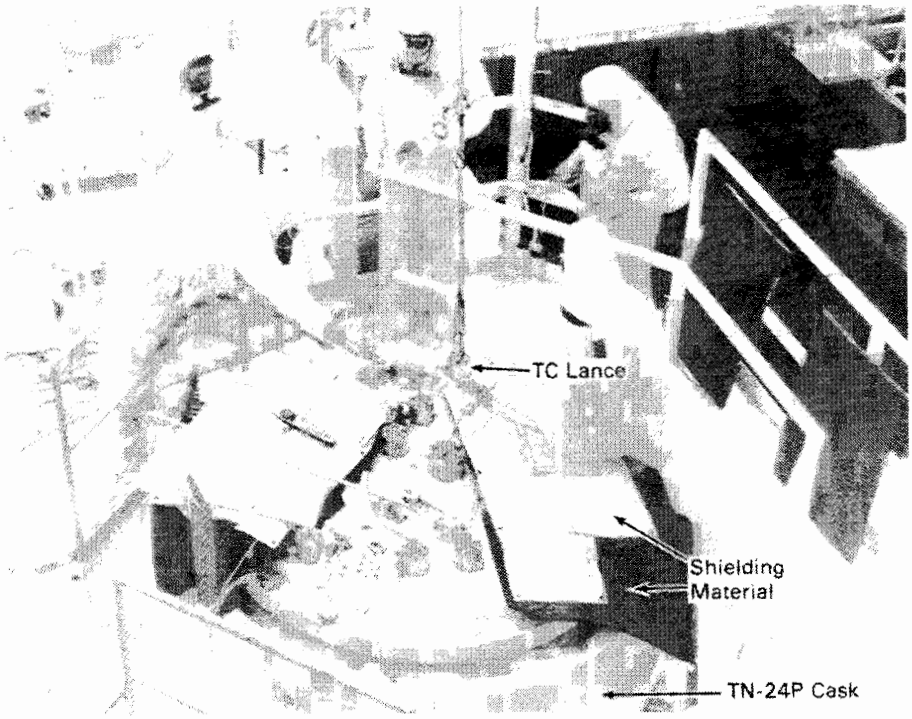

Figure 3-49. Installing Thermocouple Lances into the Fuel Assembly Guide Tubes Through the TN-24P Test Lid

loadings. Cylindrical spacers 8.0 cm (3.5 in.) long were placed between TC lance flanges and the cask primary test lid to permit proper installation.

A TC lance was installed after each subsequent fuel loading until the cask was fully loaded. Data were collected weekly and transmitted to PNL.

When the TN-24P storage cask was fully loaded, it was tested according to the approved test plan. The test lid was bolted on. Operations personnel installed all nine TC lances through the test lid into seven fuel assembly guide tubes and two basket locations. The cask was double-pumped and backfilled with helium cover gas to ensure gas purity. Then the cask was moved into the warm shop test bay, where it was externally instrumented with TCs at predetermined locations (Figures 3-50 and 3-38). All TCs and the pressure monitor were connected to the DAS.

The cask was already near the equilibrium temperature because of heat buildup during the cask loading period. Only a short period was required to reach the peak equilibrium temperature. Monitoring continued for at least 24 h after steady-state

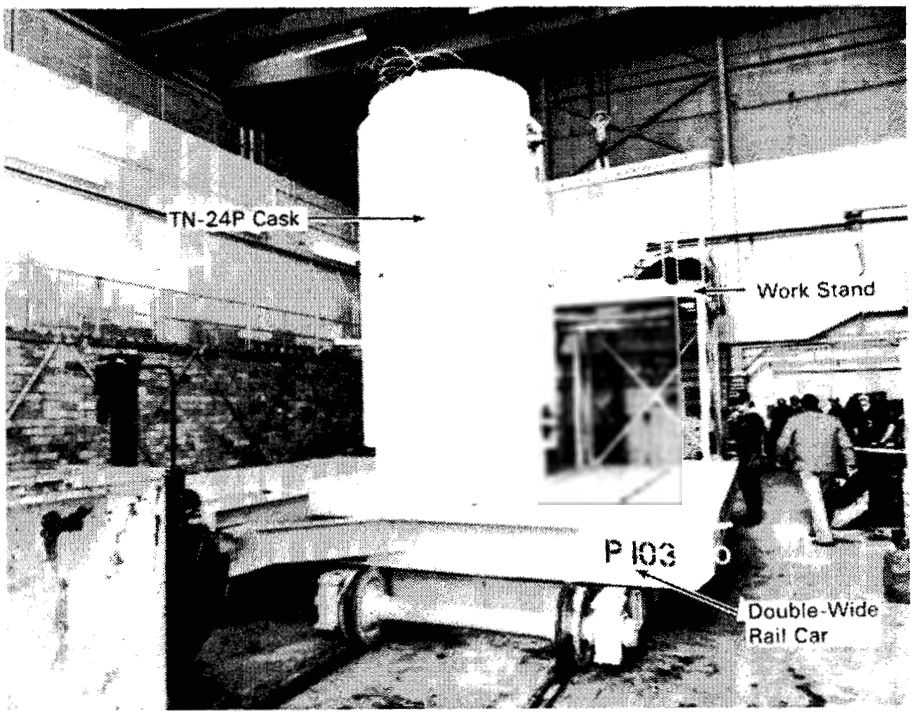

Figure 3-50. TN-24P Cask Being Moved to the Warm Shop Test Bay

temperatures had been reached, to verify that the peak temperature had been obtained. Cask cavity gas samples were taken before and after each test run.

Once the vertical helium test run data had been verified, the cask cover gas was changed to nitrogen. Gas samples were taken at the beginning and end of the vertical nitrogen test run. Temperature and pressure monitoring continued throughout the vertical nitrogen test run. A vertical vacuum test run was conducted in a similar manner.

Two to three days were required for the cask to reach steady-state temperature after a position or cavity backfill gas change.

When the cask was rotated from the vertical to the horizontal orientation during the performance test, the cask TCs had to be disconnected from the DAS. The cask was moved to the hot shop where the cask was rotated to the horizontal position with the hot shop crane. When the cask was back in the warm shop test bay, the TCs were reconnected and the test run monitoring began.

During the vertical and horizontal test runs, neutron/gamma radiation dose rate measurements were taken on all cask surfaces using both portable survey instruments and dosimeters. EG&G Idaho, Inc. health physics technicians conducted the portable surveys, and PNL technicians conducted the dosimetry.

At the completion of initial cask testing, the TN-24P cask was prepared for interim storage at the test pad. The TC lances were removed, and the cask cover gas pressure was adjusted to 1.5 mbar. The cask was placed vertical on the P103 dolly and moved to the long term surveillance test pad area on March 13, 1986. Two locally available cranes were used to off-load the cask from the dolly onto the test pad (Figure 3-51).

Figure 3-51. Off-Loading the TN-24P Cask onto the Long-Term Surveillance Pad

Fuel Assembly Inspections

During TN-24P cask loading, selected fuel assemblies were inspected. A color TV camera system performed a four-surface video characterization examination while the fuel assemblies were being removed from the TN-8L shipping cask. Two of the eight assemblies were color photographed using a periscope for high resolution to confirm the condition of the fuel rods and crud buildup (Figures 3-24 and 3-25).

Crud and smear samples were collected from these two fuel assemblies. A 2.54-cm-diameter (1-in.) rubber bottle stopper with a 2.54-cm-diameter (1-in.) smear filter attached to one side was used to take the smear samples. The rubber stopper was held in the overhead manipulator hand and remotely pressed against a fuel rod. It was then moved vertically about 20 to 26 cm (8 to 10 in.). The rubber stopper was remotely placed in an open plastic bag. When hands-on operations began inside the hot shop, the smear filters were manually removed from the stopper, placed in small shielded pigs, and sent to LLNL for analyses.

Crud collection samples were taken in a similar manner. A large-diameter rubber stopper with double-sided sticky tape was remotely pressed against a fuel rod and then retracted. The sample was then placed in a plastic bag, and the bag was manually placed into a shielded shipping pig.

Section 4

CASK HEAT TRANSFER AND SHIELDING PERFORMANCE

Heat transfer and shielding performance data obtained for the TN-24P PWR spent fuel storage cask are presented and discussed in this section. Both cask and fuel assembly peak temperatures and associated temperature profiles are presented to assess heat transfer performance. Cask exterior surface peak dose rates and corresponding dose rate profiles are provided to evaluate shielding performance. The thermal and shielding performance of the TN-24P does not represent the performance of a standard TN-24 cask because of structural differences between the two casks as described in Section 3. Spent fuel integrity results were previously presented and discussed in Section 3.

HEAT TRANSFER

The cask heat transfer performance test consisted of the six runs discussed in detail in Section 3. Test runs were performed inside the TAN warm shop, in both vertical and horizontal orientations, and with vacuum, nitrogen, and helium backfills. The predicted total decay heat generation of the spent fuel was approximately 20.5 kW during the month-long performance test. A vacuum environment was used to determine the maximum temperature that could be encountered in the cask and to assess the radiation heat transfer performance of the cask. Nitrogen runs were performed to determine the effects of convection heat transfer in the TN-24P basket. In addition, studies are underway to provide the technical basis for using nitrogen as a long-term storage medium (14). The use of helium as a backfill gas permitted determination of the minimum expected operating temperature of the cask because of the relatively high thermal conductivity (five times higher than nitrogen) of helium. Both vertical and horizontal orientations were incorporated in the test to determine differences in performance. Heat transfer data in the three backfills and both orientations are presented in the following sections, along with discussions of cask performance.

Heat Transfer Performance Overview

The cask performance test matrix was developed to determine the effects of cask orientations and backfills. Table 4-1 presents the peak measured guide tube

Table 4-1

TN-24P CASK TEST MATRIX AND PEAK TEMPERATURES

Run #	Orientation	Backfill	Cask Heat Load, kW	Ambient Temp, °C	Side Surface Temp, °C	Meas. Guide Tube Temp, °C	Est. Peak Clad. Temp, °C
1	Vertical	Helium	20.6	18	69	214	221
2	Vertical	Nitrogen	20.6	20	67	232	241
3	Vertical	Vacuum	20.6	20	69	278	290
4	Horizontal	Helium	20.5	18	67	208	215
5	Horizontal	Nitrogen	20.4	21	69	247	256
6	Horizontal	Vacuum	20.3	19	66	268	280

temperatures for all six test runs. Peak cladding temperatures were estimated by using 1) a cubic spline fit to the lance temperatures to estimate the peak axial temperature in a guide tube, 2) assuming a parabolic temperature profile across a fuel assembly, and 3) using the center basket temperature and the adjacent fuel assembly (basket location D1) lance temperatures to extrapolate to the maximum fuel temperature. Average ambient and cask surface temperatures are also shown in Table 4-1. All temperature data are contained in Appendix C.

As can be seen from Table 4-1, fuel cladding temperatures were well below the 375°C design temperature for all six runs (4). The high thermal conductivity of the helium resulted in the lowest measured peak temperature (208°C), and the low-conductivity vacuum run produced the highest measured temperature (278°C), as would be expected. It is interesting to note that the measured peak temperature in the vertical nitrogen run was not much higher (<18°C) than in the vertical helium run. This indicates that the added convection heat transfer in nitrogen nearly compensated for the higher thermal conductivity of helium.

A comparison of measured peak temperatures in vertical (214°C) and horizontal (208°C) helium runs indicates that the enhanced conduction heat transfer resulting from fuel assemblies contacting basket fuel tubes in a horizontal orientation did compensate for the loss of convection in helium. A comparison of vertical and horizontal nitrogen runs shows the opposite effect to be true; i.e., the additional

conduction in a horizontal orientation due to assemblies contacting fuel tubes (peak equal 247°C) is not nearly as significant as convection in vertical nitrogen (peak equal 232°C).

In general, the cask heat transfer based on peak temperatures can be concluded to be exceptionally good because peak temperatures in helium, when the cask was dissipating 20.6 kW, were about 100°C less than specified for the cask operating limit of 24 kW (4). Contributions of the different modes of heat transfer are discussed further in the following sections.

Vacuum Runs

Two vacuum runs were conducted during the performance test, one in the vertical orientation and one in the horizontal orientation. The vertical vacuum run (Run 3) resulted in the selected axial temperature profiles presented in Figure 4-1 and the additional data contained in Appendix C. For clarity, lines are used to connect points in Figure 4-1 and all subsequent illustrations in Section 4; however, these lines do not represent actual temperature profiles. Axial temperature profiles shown in Figure 4-1 are for the lances in four fuel assembly guide tubes and one basket guide tube, the center basket thermocouples, the inner wall thermocouples, and the outer surface thermocouples as shown in the insert to Figure 4-1. The predicted relative axial decay heat profile previously shown in Figure 3-18 is included with the temperature profiles to show similarities between temperature and decay heat profiles.

The temperature profiles are symmetrical relative to the active fuel length. The measured peak temperature of 278°C occurred at an elevation of 2.3 m (7.5 ft). Based on a cubic spline fit to the data from the hot lance in basket location A1, the maximum fuel rod temperature in the cask for the vacuum runs occurred at an elevation of 1.9 m (6.2 ft). The temperature difference within a fuel assembly can be estimated if a parabolic temperature profiles is assumed to exist across the fuel assembly. A parabolic temperature profile will give zero slope at the center of the fuel assembly and an increasing slope with distance from the center, as would be expected for a body generating heat with conduction in the radial direction. The above calculation resulted in the conclusion that the maximum fuel rod temperature was about 12°C above the temperature in fuel assembly lance D1-5 for the vacuum runs.

A crossover between the basket and fuel assembly lance temperatures is observed near the top of the cask. This is caused by the relatively close proximity of the upper

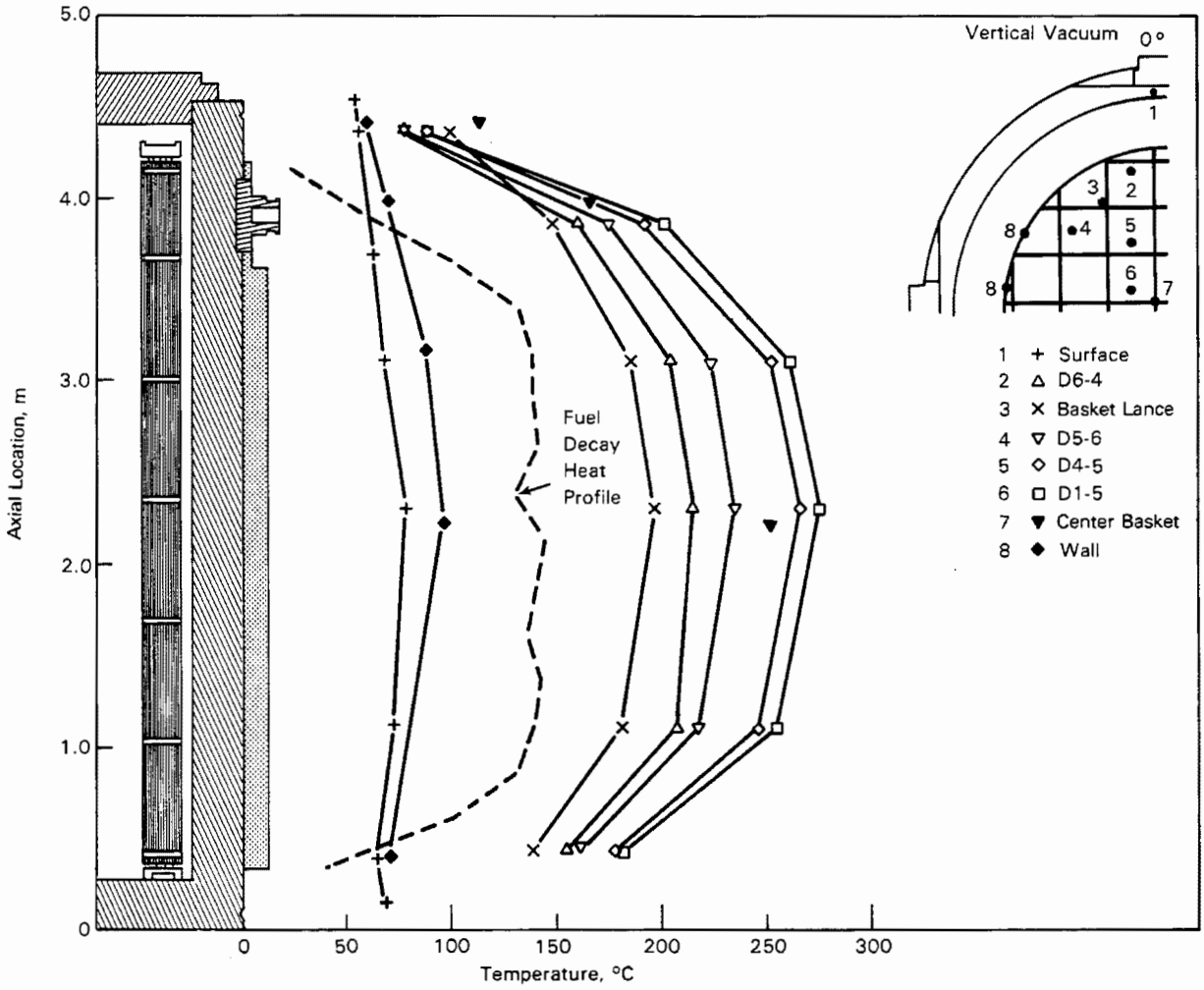

Figure 4-1. Axial Temperature Profiles for Vertical Vacuum Run

lance TCs [elevation 4.37 m (14.3 ft)] to the basket, lid, and fuel assemblies (Figure 4-2). The upper fuel assembly lance TCs are below the top of the basket but do not contact it. They are about 6 cm (2.4 in.) below the bottom of the lid, 3 cm (1.2 in.) below the top of the basket, and 10 cm (2.5 in.) above the fuel. Conduction from the lances in the fuel assembly guide tubes to the lid causes the upper fuel assembly lance TCs to read low. The upper basket lance TC is located in a simulated guide tube made of aluminum and stitch-welded to the basket. This TC is 3 cm (1.2 in.) below the top of the basket. Conduction of heat from the upper basket through the guide tube to the lance TC causes higher temperatures in this basket lance than at the respective location in the fuel assembly lances. This is consistent with what happens in the basket. Figure 4-1 shows that conduction through the basket causes the upper basket to be significantly hotter than an

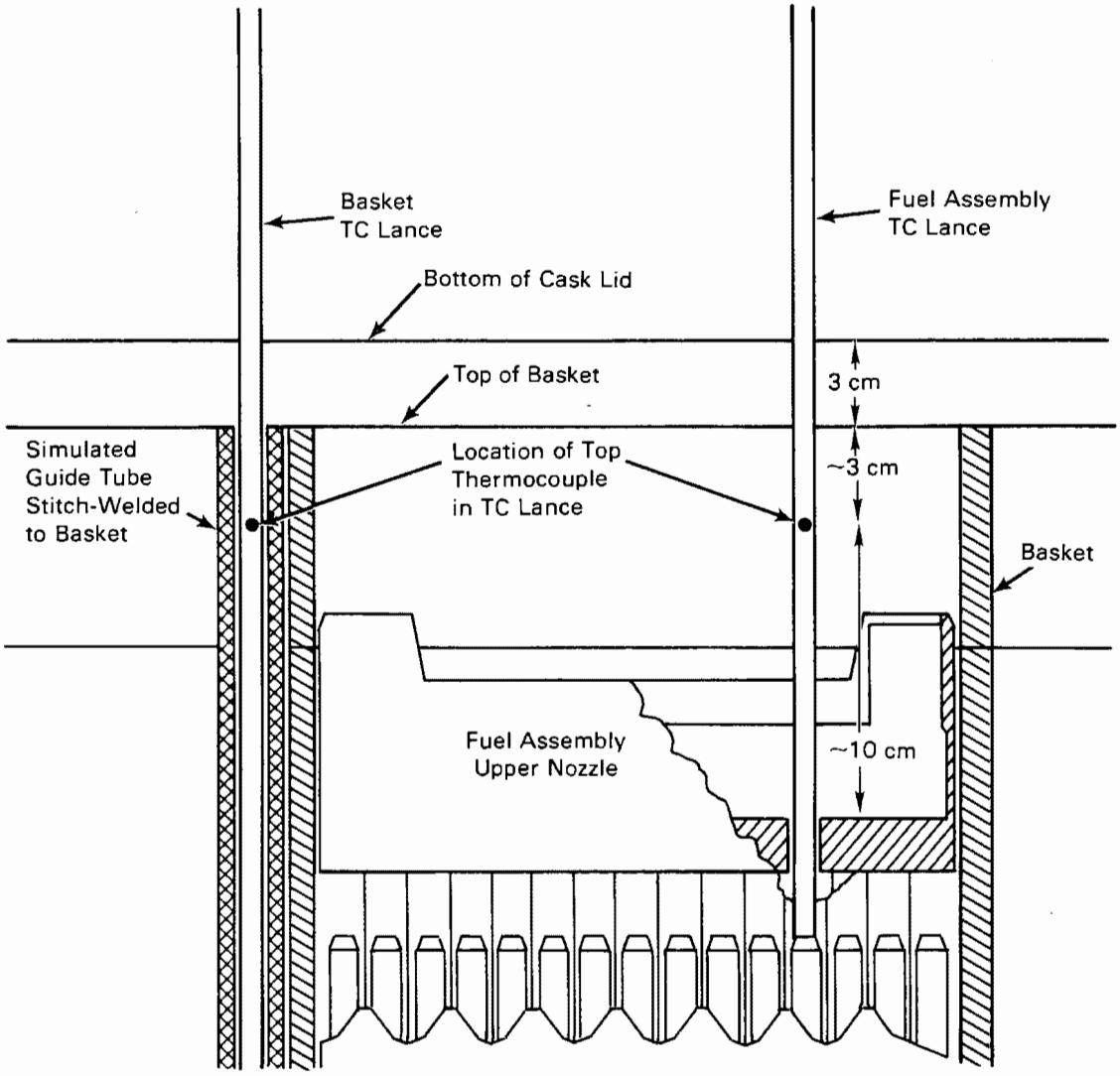

Figure 4-2. Relationship of Cask Lid to Topmost Thermocouple in Thermocouple Lance

adjacent fuel assembly (compare the center fuel assembly D1 with the center basket temperature). At the midplane of the cask, the center basket temperature is 26°C less than the center fuel assembly temperature, while at the top of the basket the basket temperature is 25°C hotter than the center fuel assembly lance temperature.

Axial temperature profiles for the horizontal vacuum run (Run 6) are shown in Figure 4-3. Except for a small change in magnitude (the peak temperature in the horizontal run was 268°C compared to 278°C for the vertical run), the profiles are similar in shape to those shown in Figure 4-1 for the vertical vacuum run. It can

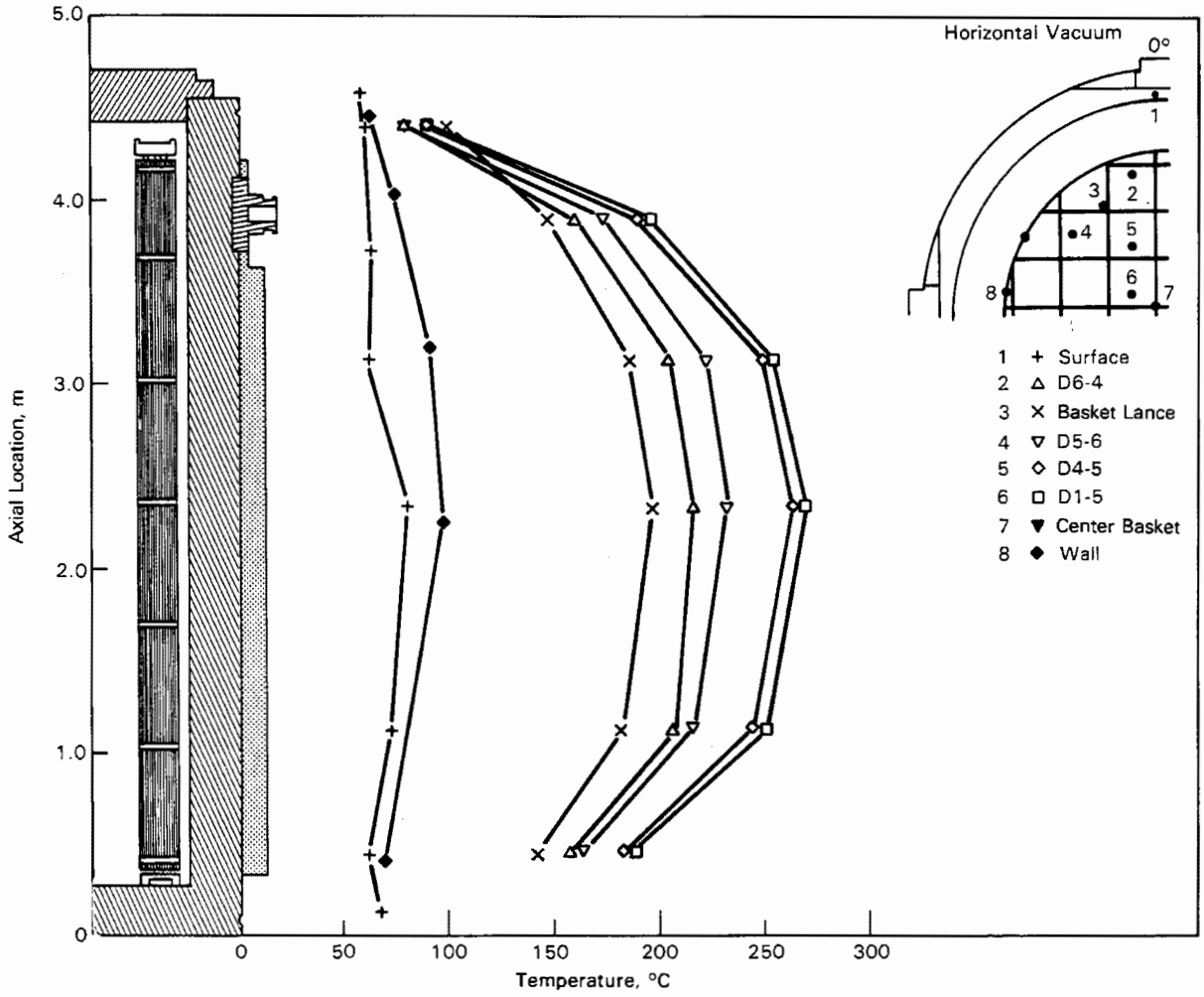

Figure 4-3. Axial Temperature Profiles for Horizontal Vacuum Run

be concluded that convection was negligible in the vacuum runs as would be expected because of the absence of a gas to convect. This absence of convection causes the similarity between the horizontal and vertical axial temperature profiles and the similarity between the decay heat and temperature profiles. Both are symmetrical about the active fuel length. The vertical run temperature profiles are not skewed toward the top of the fuel assemblies as would be expected if significant convection were present.

Temperature symmetry in the cask can be assessed from the axial temperature profiles shown in Figure 4-4 for the vertical and horizontal vacuum runs. The cask basket insert is included on Figure 4-4 to locate the temperature measurement locations. Both sets of axial profiles are for the lances in symmetric locations with respect

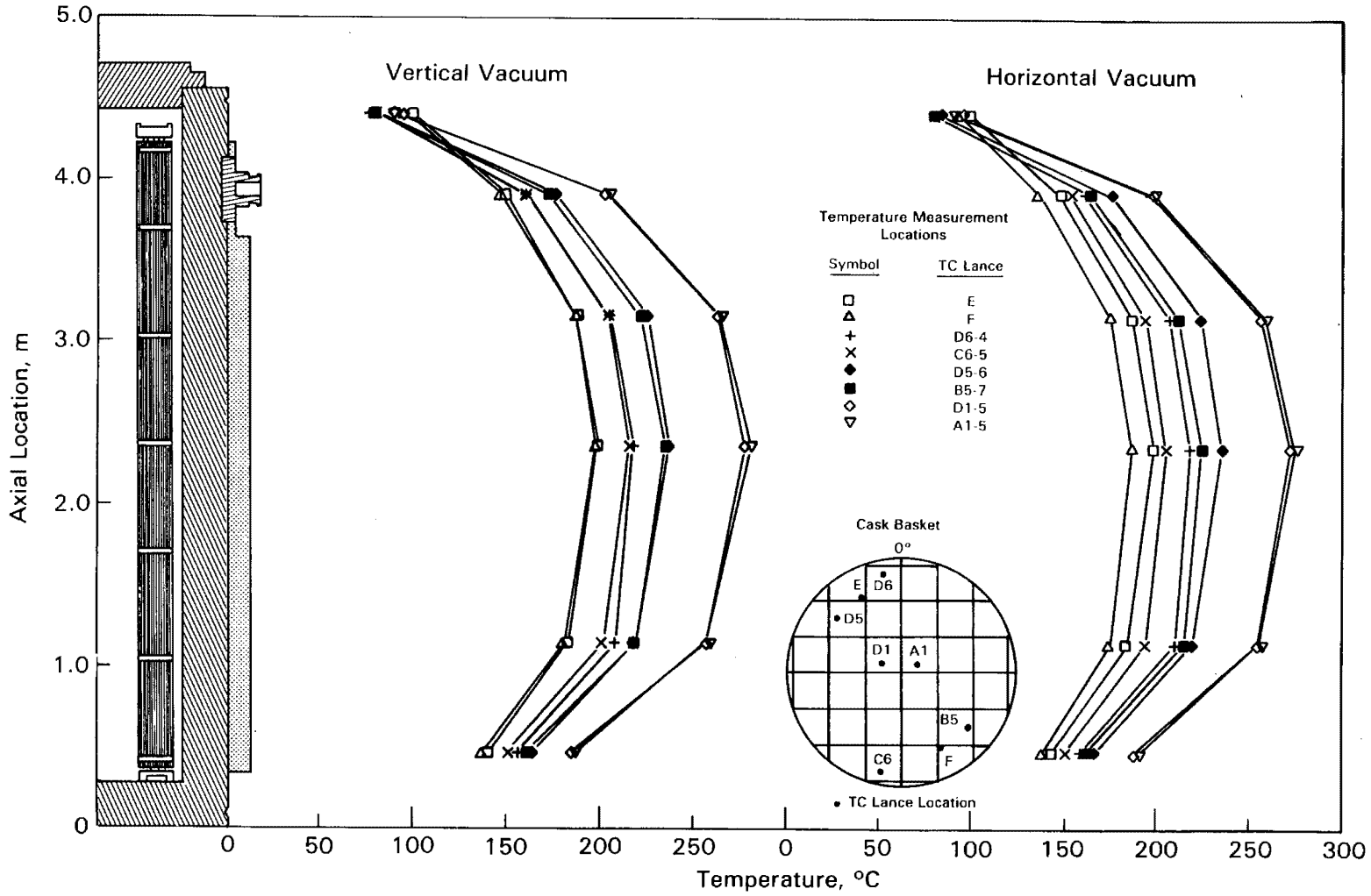

Figure 4-4. Comparison of Temperature Profile Symmetry for Vacuum Runs

to an axis or center of the cask. The vertical temperature profiles are very close for similar locations. In the horizontally oriented cask, the temperature profiles in the two center fuel assemblies (A1 and D1) are nearly the same, as would be expected. Their temperature difference changes by less than 1°C with a change in cask orientation.

However, the basket and outer assembly profiles for the horizontal cask are significantly different from those for the vertical cask. The higher temperatures occur in the more elevated portions of the horizontal cask. In the vertical cask, the temperature difference between the fuel assembly lances in location D6 and C6 is less than 2°C. In the horizontal cask, this difference is about 13°C, with upper location D6 being the hottest. Likewise, the temperature difference between the lances in basket locations E and F are 1°C and 12°C for the vertical and horizontal orientations, respectively. Again, the hotter temperatures occur in the more elevated location in the horizontal cask (lance E). Similar effects are seen for the lances in fuel assembly locations D5 and B5.

Temperature differences between vertical and horizontal orientations are associated with the change in the thermal contact resistance between the cask basket and the inner wall. In the vertical orientation, contact between the basket and cask inner wall should be fairly uniform and independent of basket quadrant. In the horizontal orientation, the weight of the basket and fuel assemblies will increase the contact between the basket and the inner wall in the lower portion of the horizontal cask at 180°. Likewise, this weight will cause the basket to pull away from the upper portion of the horizontal cask at 0°. This will decrease the thermal conductance between the basket and the upper portion of the horizontal cask and increase it between the basket and lower portion of the cask. Hence, the lower portion of the horizontal basket will cool and the upper portion of the horizontal basket will experience an increase in temperature, as has been seen by comparing the vertical and horizontal data shown in Figure 4-4.

Radial temperature profiles for the vacuum backfill runs are shown in Figure 4-5 for the vertical cask and in Figure 4-6 for the horizontal run. The solid lines in Figures 4-5 and 4-6 connect the temperatures taken at common axial distances from the bottom of the cask using fuel assembly TC lances. Temperature measurements made in basket locations have not been connected with lines. Their elevation is indicated by the type of symbol used. The radius used represents the distance the TC was located from the center of the cask with the positive distance representing positions in the upper quadrants. A negative radius represents a position in the

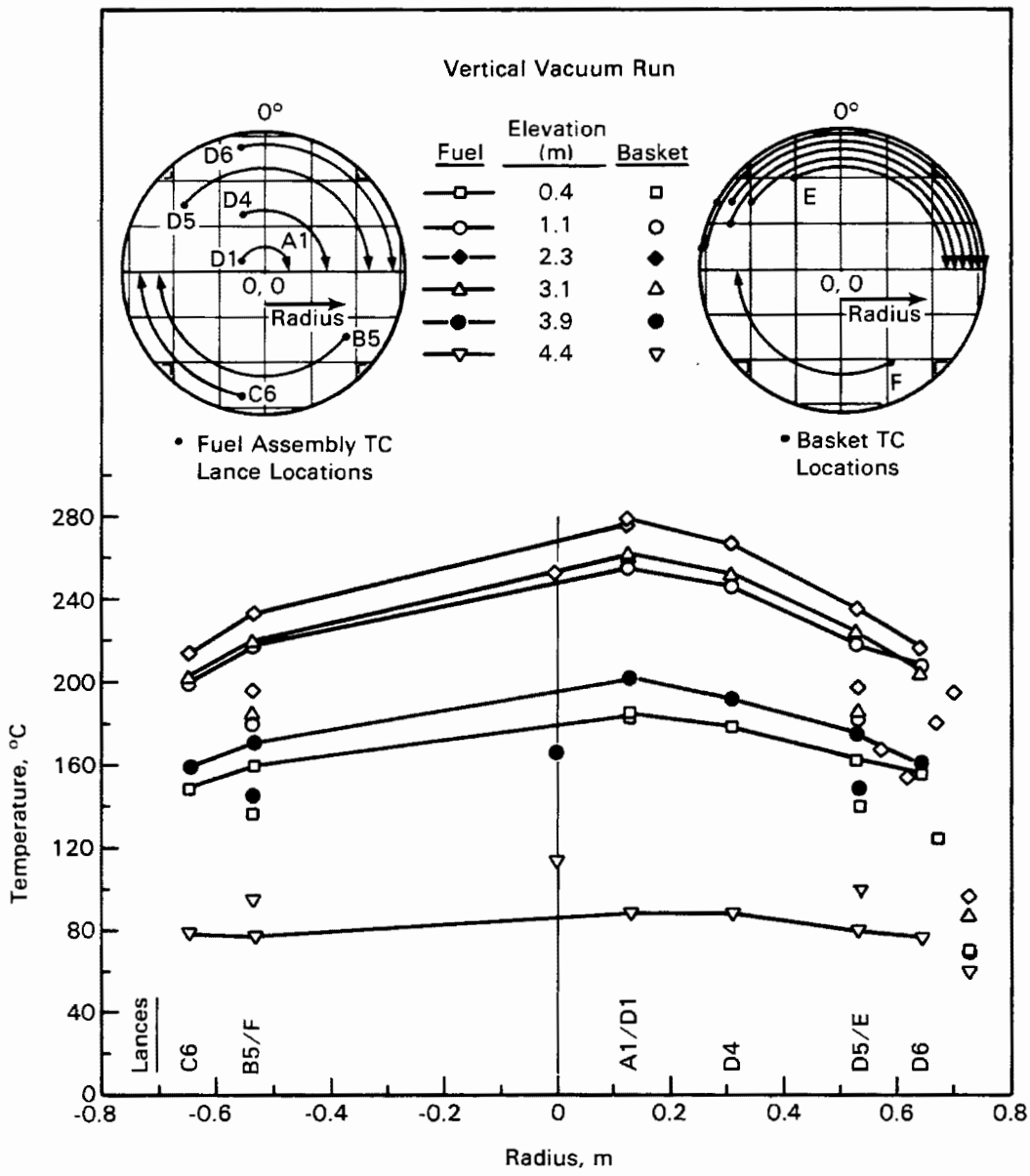

Figure 4-5. Radial Temperature Profiles for Vertical Vacuum Run

lower quadrants of the horizontal cask. The inserts show how this was done. The differences in the shape and magnitude of the radial temperature profiles between the vertical and horizontal vacuum runs are quite small. There is a slight skewing of the temperature profile in the horizontal run with the hotter temperature in the upper quadrants. However, this effect is more apparent from symmetry plots of Figure 4-4 than it is from comparing Figures 4-5 and 4-6. The major change in the

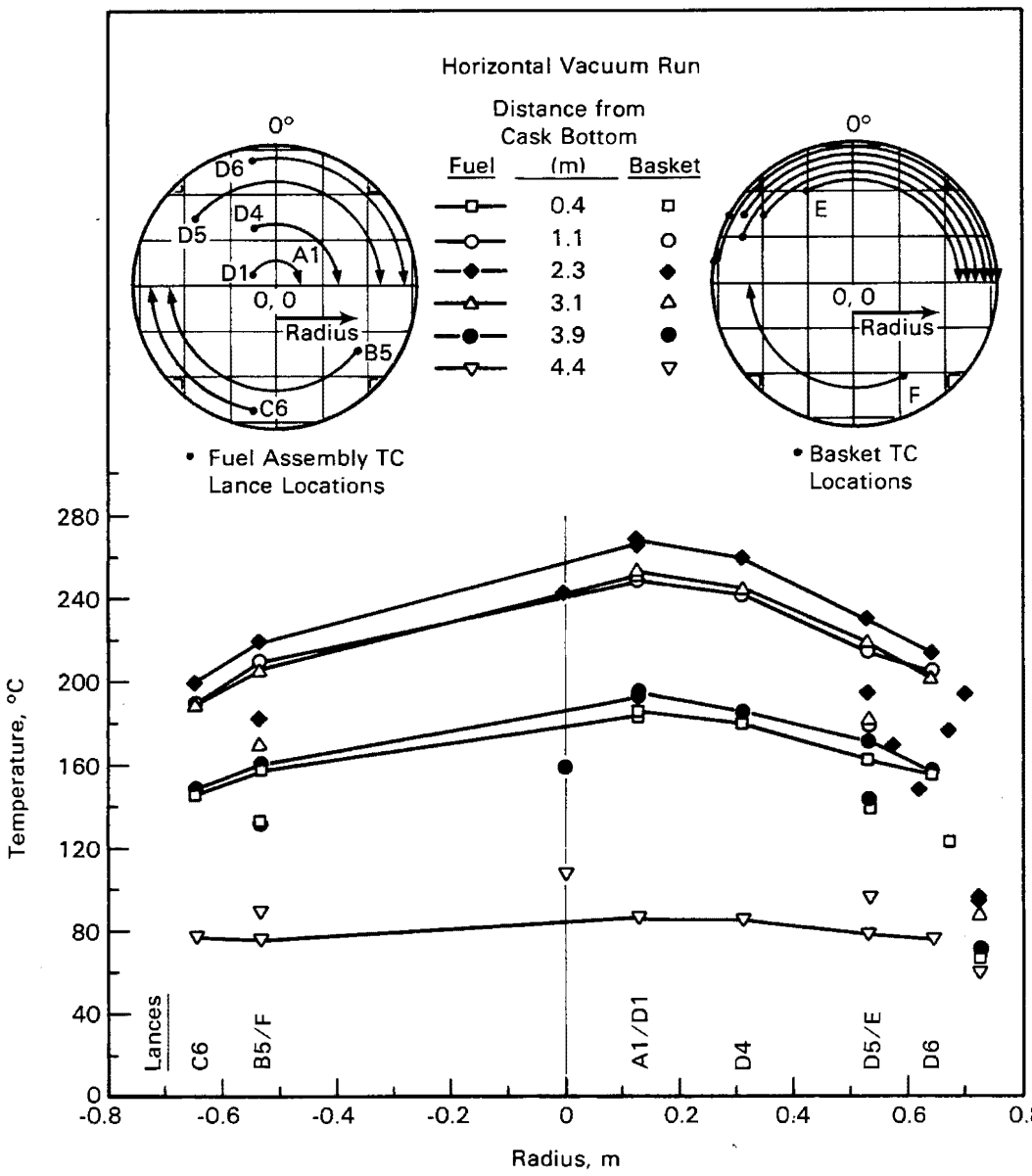

Figure 4-6. Radial Temperature Profiles for Horizontal Vacuum Run

heat transfer mechanism between the horizontal and vertical vacuum runs is due to a change in the contact resistance between the basket and the cask, as previously discussed.

Another item of interest observed in Figures 4-5 and 4-6 is the temperature drop from the basket to the cask inner wall. Based on the information at an elevation of 2.3 m (7.5 ft), this temperature drop can be 50 to 100°C. This represents a

significant portion of the temperature drop from the center of the cask to the ambient (ambient temperature of about 20°C).

Nitrogen Runs

Axial temperature profiles for the vertical nitrogen run are presented in Figure 4-7 for the TC lances of the upper left-hand quadrant. As shown in Figure 4-7, the axial temperature profiles are clearly skewed toward the upper portion of the fuel assemblies in the vertical cask, indicating significant convection heat transfer. Measured peak assembly guide tube temperatures occurred at an elevation of 3.12 or 3.87 m (10.2 or 12.7 ft). The highest measured peak temperature (232°C) occurred in center assembly A1. Using a cubic spline fit to the lance temperatures in assembly

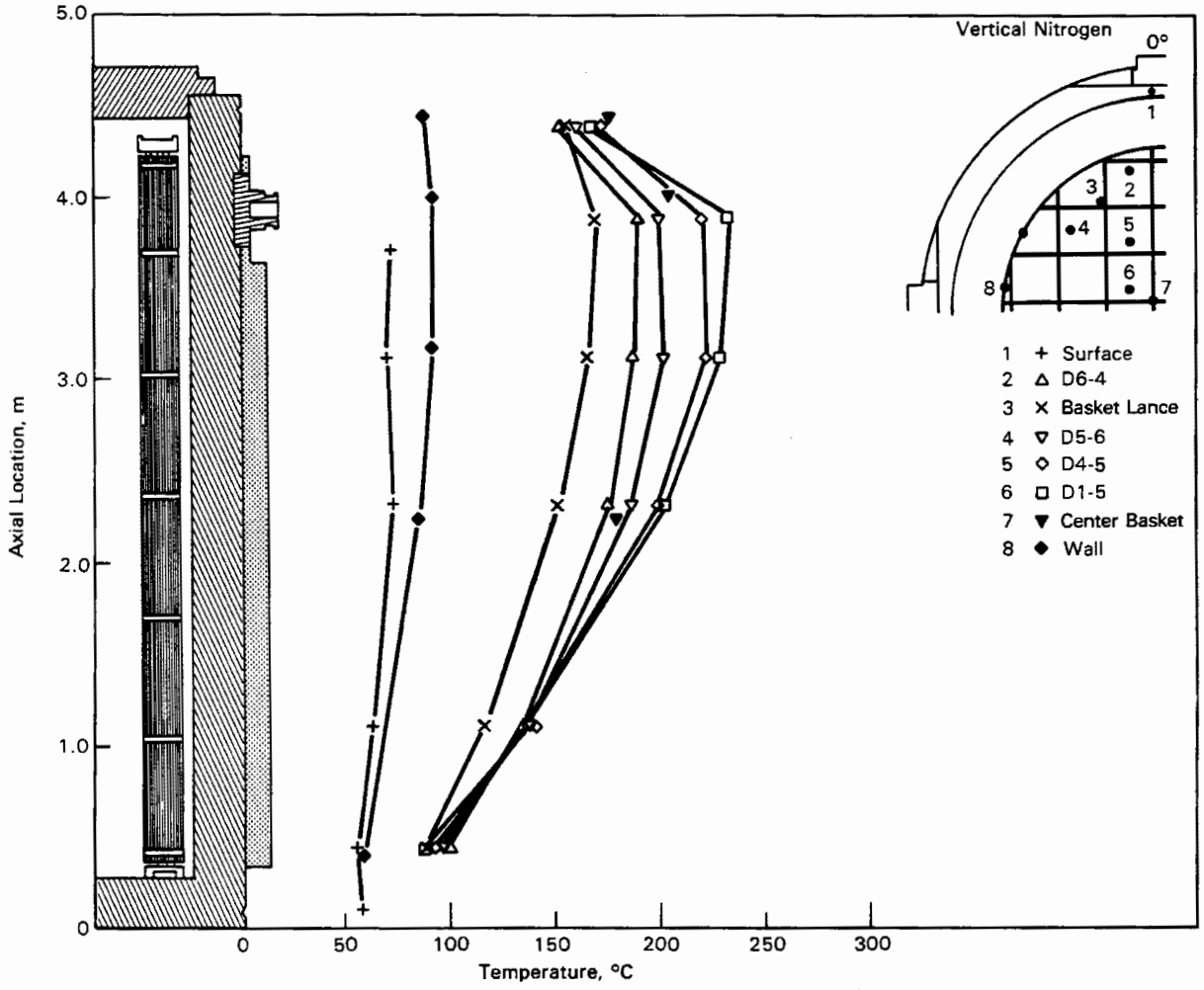

Figure 4-7. Axial Temperature Profiles for Vertical Nitrogen Run

A1 indicates the peak temperature in the cask occurred at an elevation of 3.7 m (12.1 ft). The peak temperature in an outer assembly (D6) was 189°C. The maximum fuel rod temperature in the cask for the nitrogen runs can be estimated as it was for the vacuum runs. The estimate uses the center basket temperature and the adjacent fuel assembly lance temperatures (assembly D1) with an assumed parabolic profile across a fuel assembly to predict a peak cladding temperature that was about 9°C above the maximum temperature along the fuel assembly TC lance.

Temperatures measured in center assembly D1 indicate the largest axial temperature gradient rise (146°C) of any fuel assembly. This is based on the difference between the peak temperature and the temperature measured at the lowest elevation (0.45 m/ 1.5 ft) in instrumented fuel assembly locations. The assembly in D1 had the lowest and the highest temperature of any instrumented fuel assembly. Temperature profiles for outer assemblies D6 and C6 had much smaller axial temperature rises (89°C). This is not too surprising, because in the center of the cask, the surrounding fuel assemblies act as guard heaters and limit the radial heat flow due to radiation heat transfer. The primary modes of heat loss for the inner assemblies must be conduction and convection where the conduction path to the ambient is longer than for the outer assemblies. The outer assemblies can take advantage of radiation heat transfer to the wall of the cask, conduction through the gas and basket, and convection. The side of the basket next to the cask inner wall can act as a counterflow heat exchanger, which is more efficient than the parallel flow heat exchanger arrangement seen by the inner assembly. Convection patterns in the cask are discussed in more detail in Section 5.

Figure 4-7 shows that the basket temperature at the top of the basket is relatively close to the temperature measured in the fuel assembly TC lance for the center assembly at nearly the same elevation. Likewise, the top basket lance temperature is relatively close to the top fuel assembly lance temperature of the outer assemblies. This indicates that convection to the lances and basket in these locations is large enough to lessen the effects of conduction from the fuel assembly guide tube to TC lance to the lid. As a result, the basket and fuel assembly lance temperatures are closer together at elevation 4.4 m (14.4 ft) in the vertical nitrogen run than they were for the vacuum runs.

A better appreciation for the degree of convection in the vertical cask with nitrogen backfill can be attained by comparing axial temperature profiles for a horizontal orientation (Figure 4-8) with those for the vertical orientation (Figure 4-7). The horizontal nitrogen temperature profiles are similar in shape to the

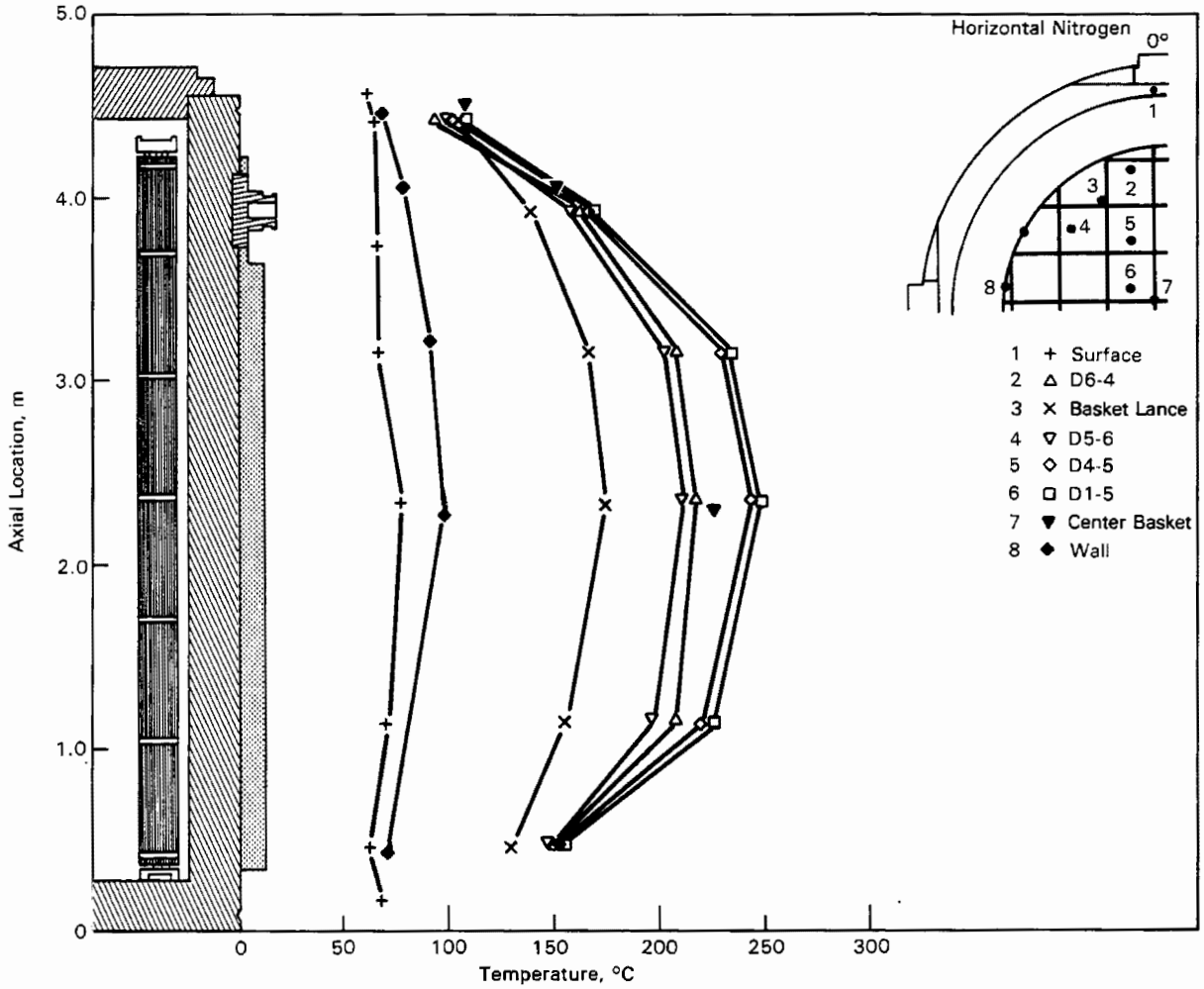

Figure 4-8. Axial Temperature Profiles for Horizontal Nitrogen Run

vacuum runs and do not show a skewing of the temperature profiles toward the top of the cask as was seen in the vertical profiles, Figure 4-7. The change in shape of the axial temperature profiles with a change in the cask orientation is due to a change in the heat transfer mechanism within the cask.

Rotating the cask to the horizontal orientation can cause at least three changes in the heat transfer mechanisms inside the cask. First, fuel assemblies will rest on one side of basket fuel tubes. This will increase the contact and heat conduction between the fuel assemblies and the basket. However, the contact is limited due to the spacer grids in the fuel assembly. These spacer grids will tend to hold the fuel rods off the basket. Second, gravity will shift the basket in the cask from resting on the bottom of the cask in the vertical orientation to resting on the side of the cask in the horizontal orientation. When the basket is resting on the side

of the cask, its weight will increase contact between the basket and inner wall of the cask on the lower side of the cask (180°) and decrease the contact on the upper side (0°). The effect of this shift was seen in the symmetry plots of Figure 4-4, where the temperatures were higher in the upper quadrants of the horizontal cask than they were in the lower quadrants. The third and most important effect for the nitrogen runs is that axial convection will be significantly reduced for the horizontal runs. This is confirmed by comparing the axial profiles for the horizontal nitrogen run with those for the vacuum runs. The shapes of the profiles are similar, indicating a lack of axial convection in the horizontal nitrogen run. The difference in magnitude results from the added conduction through the nitrogen and possibly the creation of some small localized convective cells in the fuel assemblies and open basket enclosures.

A crossover in the fuel and basket lance temperatures is seen at the top of the horizontal cask. With axial convection significantly reduced, conduction to the lid is sufficient to cool the fuel assembly lances enough to change the relationship between the temperatures measured close to the lid in the basket and those measured in the TC lances. Conduction from the fuel assembly guide tube to the TC lance to the cask lid will cool the fuel assembly lance TC close to the lid, resulting in lower lance (measured) temperatures than gas (actual) temperatures at this elevation (see Figure 4-2). Conversely, conduction from the basket will cause the basket lance temperatures to be close to the basket temperature.

Figure 4-9 shows temperature symmetry in the cask for the vertical and horizontal orientation. The vertical run shows good symmetry, whereas the horizontal run shows a significant temperature difference between symmetrical locations. In the horizontal run the effect of increased contact between the basket and the cask in the lower portion of the cask and decreased contact between the basket and the upper portion of the cask results in a diametrical temperature gradient with the hotter temperatures at the top. This is seen by the increased distance between profiles at similar locations in the horizontal runs than was observed in the vertical run (E versus F, D5 versus B5, and D6 versus C6). Locations A1 and D1 are symmetrical irrespective of cask orientation.

Radial temperature profiles for the vertical and horizontal nitrogen runs are shown in Figures 4-10 and 4-11, respectively. The solid lines in Figure 4-10 and 4-11 connect the fuel assembly lance temperatures taken at common axial distances from the bottom of the cask. Points not connected by lines show temperatures taken in basket TC lances or with TCs attached to the basket. Their elevation is indicated

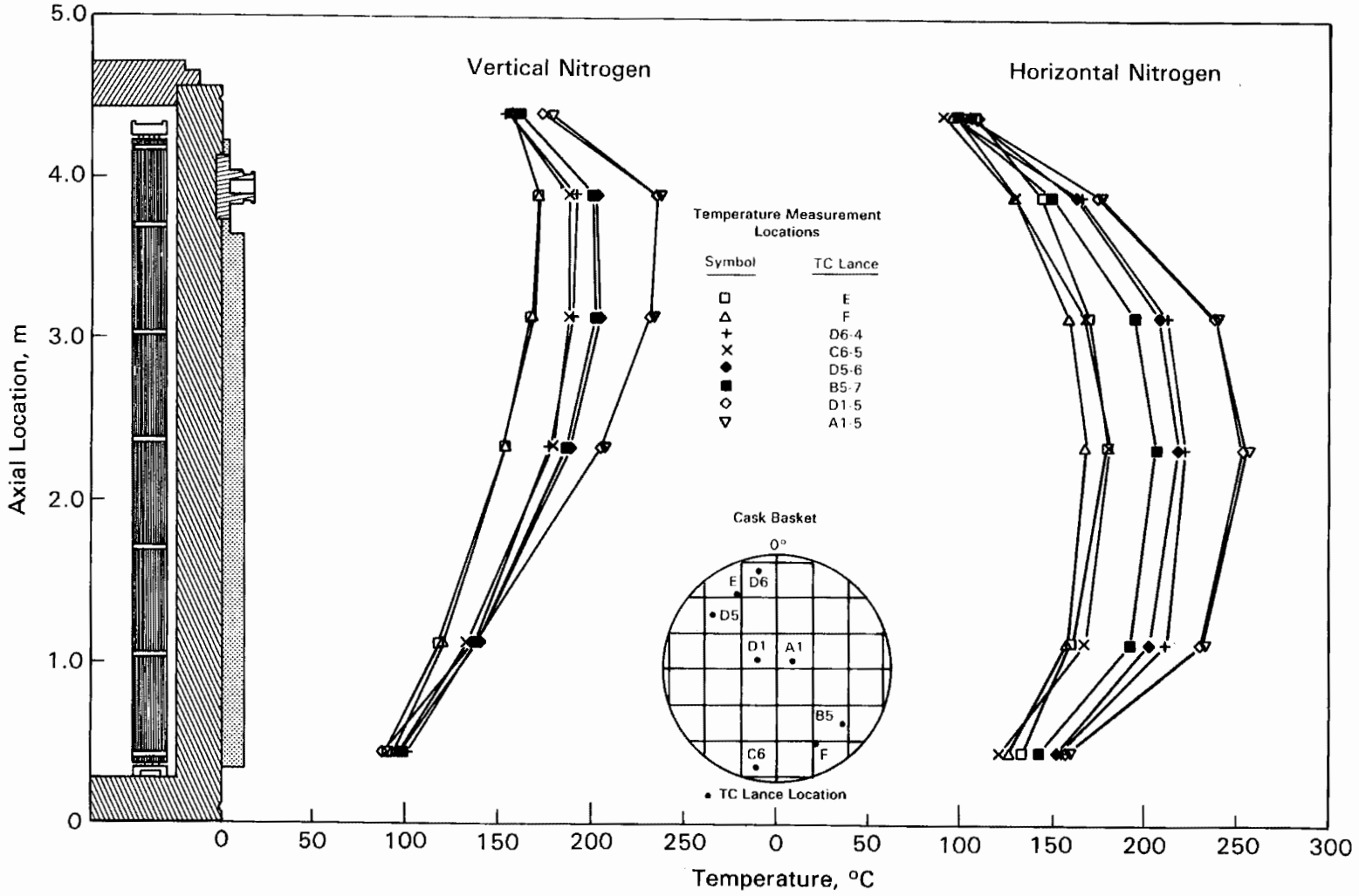

Figure 4-9. Temperature Symmetry for the Vertical and Horizontal Nitrogen Runs

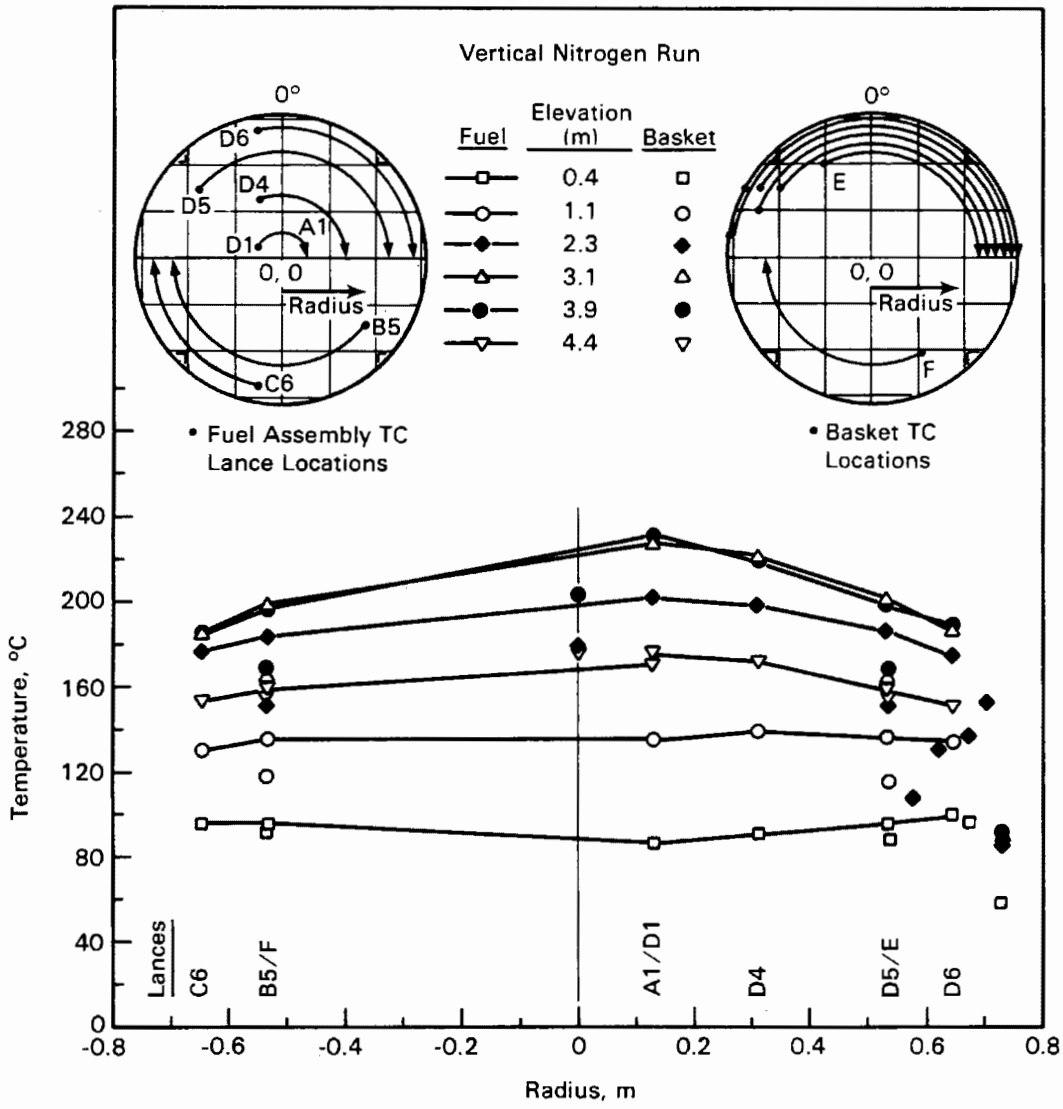

Figure 4-10. Radial Temperature Profiles for Vertical Nitrogen Run

by the symbol used. The radius used represents the distance from the center of the cask at which the TC was located, with the positive distance representing positions in upper quadrants. A negative radius represents positions in the lower quadrants of the horizontal cask.

The vertical nitrogen run, Figure 4-10, shows good symmetry between the upper and lower quadrants of the cask. Comparing Figures 4-10 and 4-11 shows two differences between the horizontal and vertical runs. The first is a skewing of the temperature profile with the hotter temperatures in the upper portion of the cask. This was seen more graphically in the symmetry profiles of Figure 4-9 and is caused by

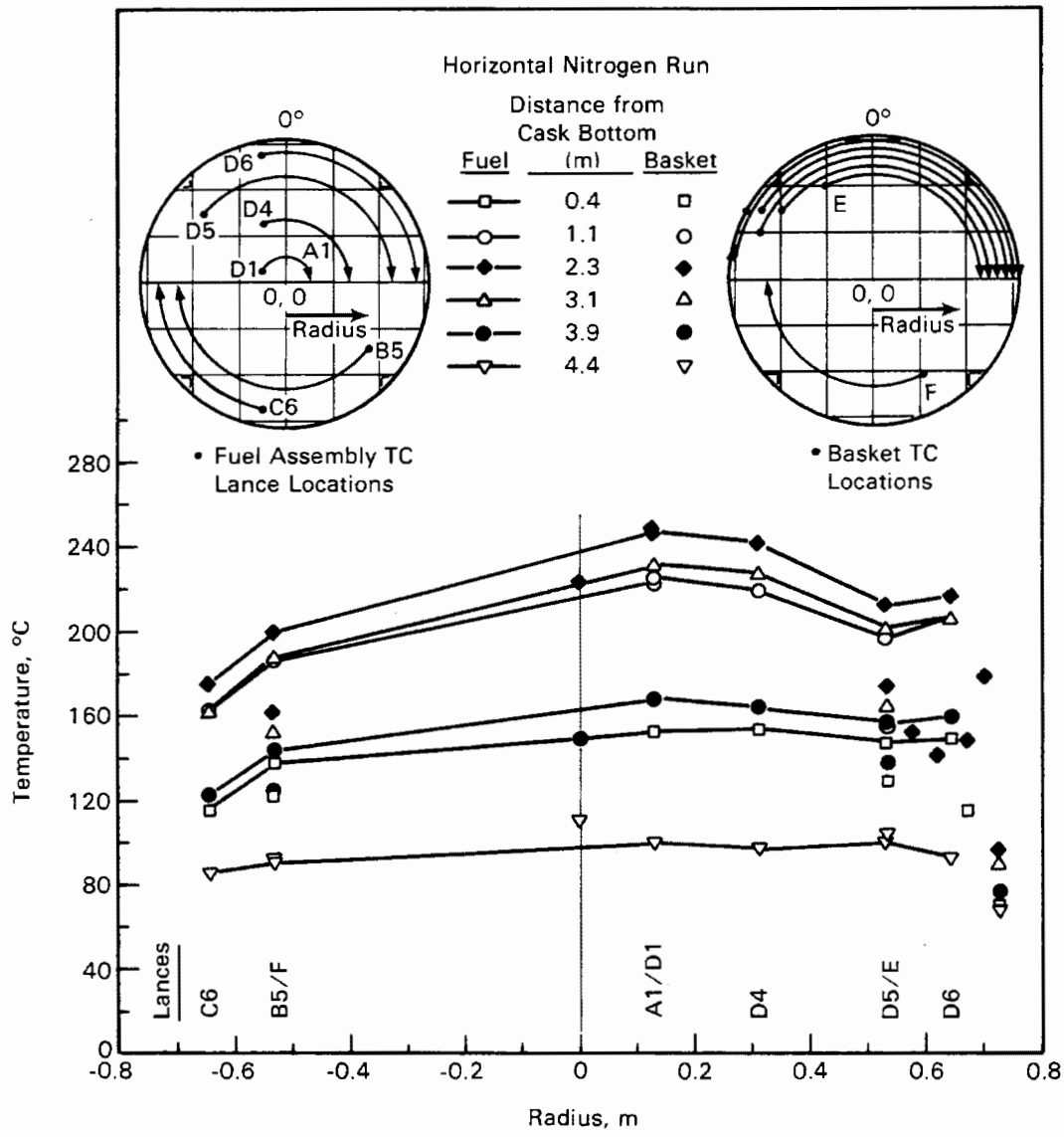

Figure 4-11. Radial Temperature Profiles for Horizontal Nitrogen Run

the change in contact resistance between the cask and basket. The weight of the basket and fuel assemblies causes the contact resistance between the basket and cask wall to decrease on the lower side and increase on the upper side of the horizontal cask. This, in turn, causes the temperature of the basket to increase on the upper side and decrease on the lower side. The second difference between Figures 4-10 and 4-11 is the temperature differences between the lances in assembly positions D5 and D6 (radius 0.532 and 0.645 m) and those in assembly locations B5 and C6 (radius -0.532 and -0.645 m). In the vertical nitrogen run, the difference in temperatures between lances in locations D5 and D6 is about the same as that between B5 and C6.

In the horizontal nitrogen run, the temperatures at the lower elevation decrease with respect to the temperatures at the higher elevation; i.e., lance temperatures in location B6 and D5 decrease with respect to lance temperatures in C5 and D6 respectively. Because this change in temperature difference between the upper and lower quadrants of the cask is seen for only the horizontal nitrogen run it is assumed to be caused by convection. If it had been caused by a change in contact resistance between the cask and basket, it should have been seen in the horizontal vacuum runs. If it had been caused by a change in the gas conductivity, it should have been seen in the vertical nitrogen runs. Because this temperature change was not seen in either of the vacuum runs or the vertical nitrogen run, it must be caused by convective cells set up in the horizontal nitrogen runs. Figure 4-12

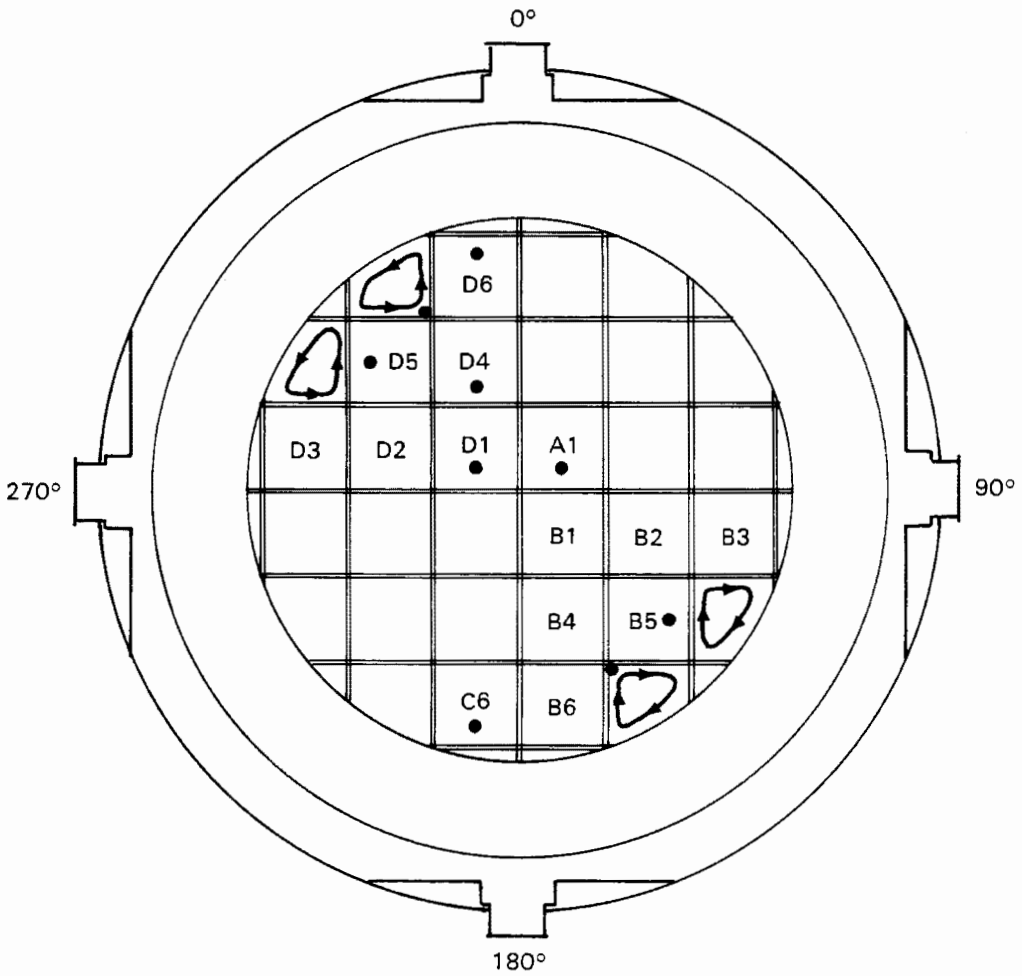

Figure 4-12. Hypothesized Convection Cells for Horizontal Nitrogen Runs

shows a possible convective cell arrangement that could cause the temperature profiles seen in Figure 4-11. The convective currents near D5 should be strong because the heated surfaces are lower or vertical (top of D3 and side of D5) and will drive convection. The heated nitrogen will try to rise along the heated vertical surfaces and then be cooled and fall at the cask wall setting up the convective cooling current that will cool basket location D5. At the lower side of the cask, only the vertical surfaces (side of B6) will tend to drive convection. The horizontal surface (bottom of B3) will heat the nitrogen and could cause temperature stratification. This would elevate the temperature in B5. Hence, B5 lance temperatures rise with respect to C6 lance temperatures, and D5 lance temperatures fall with respect to D6 lance temperatures.

Another item of interest observed in Figure 4-10 and 4-11 is the temperature drop from the basket to the inner cask wall. Based on the information at an elevation of 2.3 m (7.5 ft), this temperature drop can be 25 to 65°C in the vertical case and 50 to 80°C in the horizontal case. This represents a significant portion of the temperature drop from the center of the cask to the ambient (ambient temperature of about 20°C).

Helium Runs

Axial temperature profiles for the vertical helium run are presented in Figure 4-13 for the TC lances of quadrant D. As shown, the axial temperature profiles are skewed toward the upper ends of the assemblies, indicating the presence of some convection heat transfer. However, the shift in the temperature peak is not as pronounced as it was for the vertical nitrogen run. This may be due to the combined effect of a decrease in convection with helium and an increase in the thermal conductivity of helium. Measured peak temperatures occurred at an elevation of 2.3 m (7.5 ft) in each TC lance. The maximum measured temperature of 214°C for the vertical helium run occurred in assembly A1. A cubic spline fit of the six measured temperatures from the fuel assembly hot lance (A1-5) indicates that the peak temperature in the cask would have occurred at an elevation of 2.4 m (7.9 ft). The maximum fuel rod temperature in the cask for the helium runs can be estimated as it was for the vacuum and nitrogen runs. The estimate uses the center basket temperature and adjacent fuel assembly lance temperatures (assembly D1) with an assumed parabolic profile across a fuel assembly to estimate a peak cladding temperature that is about 7°C above the maximum temperature along the TC lance.

A crossover between the basket and fuel assembly lance temperature profiles is observed near the top of the cask. The crossover is not as large as that observed

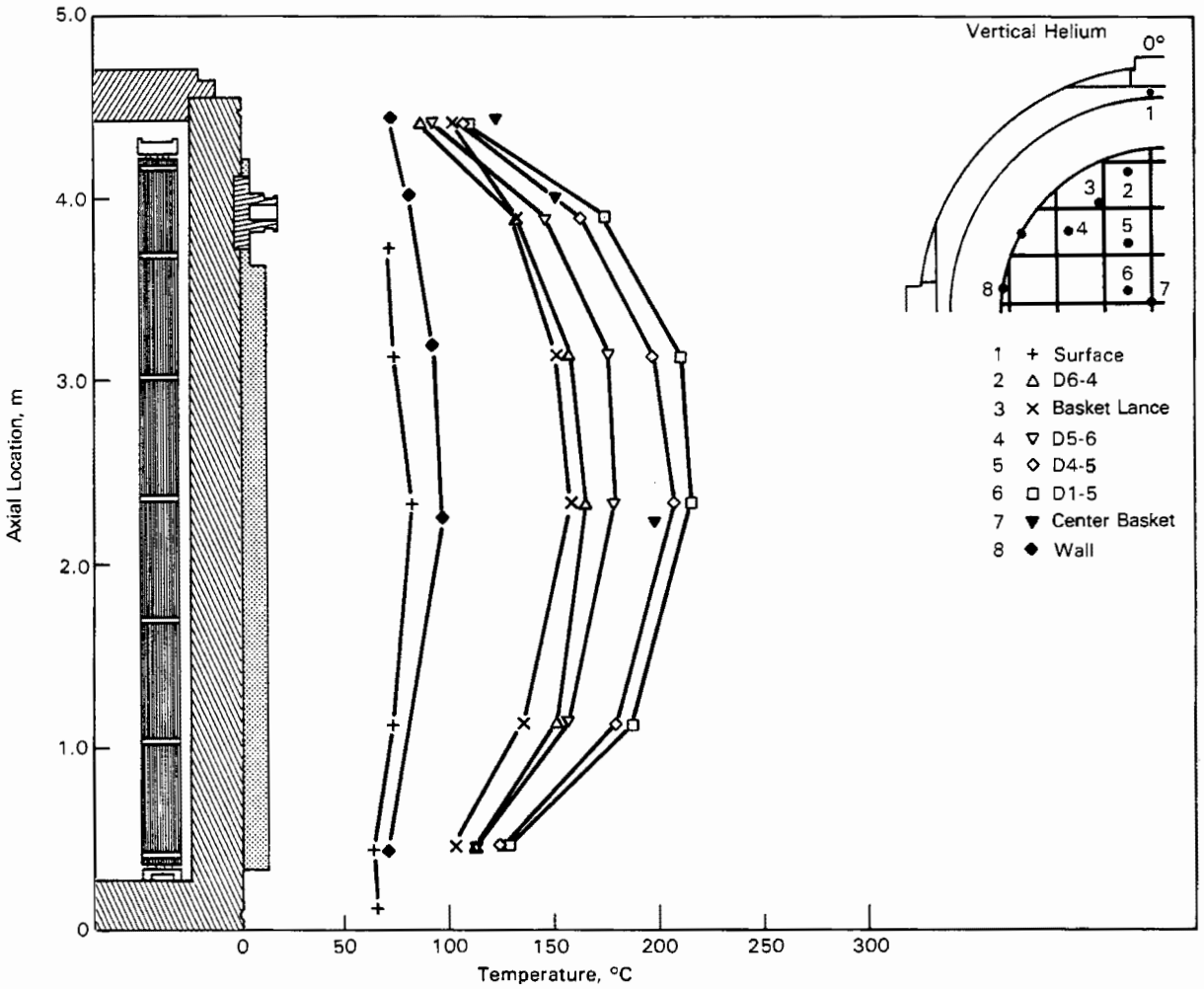

Figure 4-13. Axial Temperature Profiles for Vertical Helium Run

for the vacuum runs, but is larger than that observed for the vertical nitrogen run. It is caused by conduction of heat through the fuel assembly lances to the cask lid. This artificially lowers the lance temperature in the vicinity of the upper fuel assembly lance TC. If a lot of convection were present, then the heat flow to the rod due to convection would lessen the cooling effect on the rod by conduction to the lid. The aluminum guide tube containing the basket thermocouple is stitch-welded to the basket, providing a good conduction path between the basket and the upper basket lance TC. Therefore, temperatures measured with the basket lance should be relatively close to that of the basket.

A better appreciation for the degree of convection in the vertical cask with helium backfill can be gained by comparing the axial temperature profiles for a horizontal cask shown in Figure 4-14 with those for the vertical cask shown in Figure 4-13.

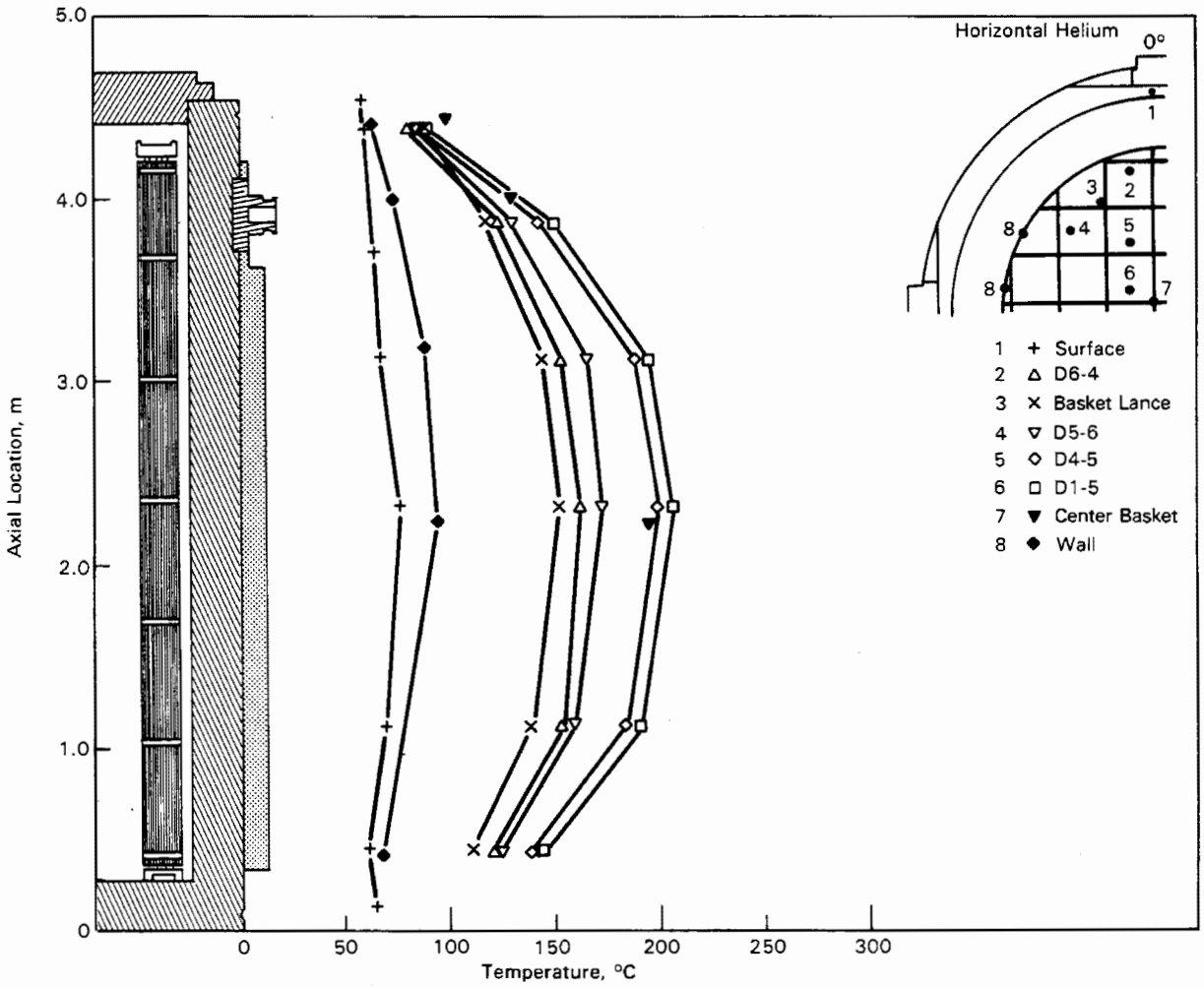

Figure 4-14. Axial Temperature Profiles for Horizontal Helium Run

The shapes of the temperature profiles for the horizontal helium run are similar to the shapes of the vertical vacuum run and the horizontal nitrogen and vacuum runs, indicating that convection is limited or nonexistent in the horizontal helium run. The measured peak temperature in the horizontal helium run was 208°C compared to 214°C for the vertical run. A cubic spline fit to the hot lance temperature data indicates that the peak temperature in the horizontal cask occurred at an elevation of 1.9 m (6.2 ft). This elevation is the same as that for the vertical vacuum and other horizontal runs and is 0.5 m (20 in.) lower that the indicated for the vertical helium run.

It is interesting to note that although the locations of the peak temperatures in the assemblies in the two orientations are significantly different, with the horizontal being at approximately 1.9 m (6.2 ft) and the vertical being at approximately

2.4 m (7.9 ft), the peak temperature magnitudes do not differ significantly. The measured peak guide tube temperature in the vertical orientation was 214°C; in the horizontal orientation, it was 208°C, only 6°C lower. The additional conduction heat transfer gained by the assemblies contacting their basket fuel tubes in the horizontal was noticeable and compensated for the convection heat transfer that existed in the vertical helium run.

Again, a crossover is seen between temperature measurements at the top of the cask. The crossover is similar to that seen for the horizontal vacuum and nitrogen runs. Conduction of heat through the basket to the basket lance causes the lance to record a higher temperature at the upper elevation than do the fuel assembly lances that communicate by conduction with the relatively cold lid.

Figure 4-15 shows the symmetry of temperatures in the cask for the vertical and horizontal orientations. The vertical run shows good symmetry, whereas the horizontal run shows significant temperature differences in the cask due to a shift in the basket and fuel assemblies when the cask is rotated. Again, the effect of increased contact between the basket and the cask at the lower portion of the cask and decreased contact between the basket and the upper portion of the cask results in diametrical temperature gradients, with the hotter temperatures at the top. However, the difference between the upper and lower quadrant temperatures for the horizontal helium run is significantly less than was observed for the horizontal nitrogen run, showing the effect of increased thermal conductivity of helium. Figure 4-15 also shows the change in axial temperature profile with orientation, as well as the peak measured temperatures in the cask. The vertical helium run is slightly skewed toward the top of the cask. The horizontal helium run is similar to the vacuum runs and the horizontal nitrogen run in which the temperature profiles are somewhat symmetrical with respect to the active fuel length.

Radial temperature profiles for the vertical helium run are shown in Figure 4-16. Figure 4-17 shows the results for the horizontal helium run. The solid lines connect the fuel assembly lance temperatures taken at common axial distances from the cask bottom. Points not connected with lines represent basket temperature measurements taken with the TC lances or TCs directly to the basket attached at other axial locations. Their elevation is indicated by the symbol used. The radius used represents the distance the TC was located from the center of the cask. The positive distance represents a position in the upper quadrants of the cask. A negative radius represents a position in the lower quadrants of the horizontal cask.

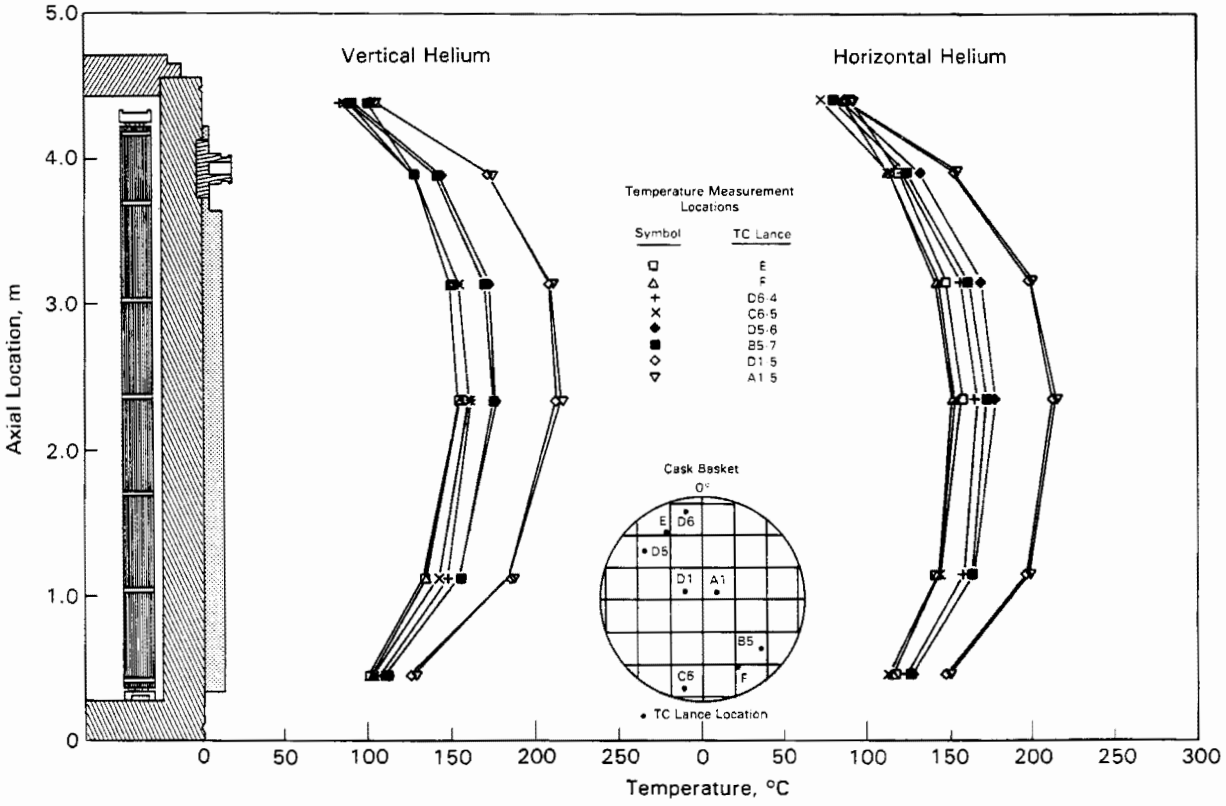

Figure 4-15. Temperature Symmetry for Helium Runs

The vertical helium run (Figure 4-16) shows good symmetry with almost the same relative relationship between the lance temperatures in the upper quadrants of the cask as those in the lower quadrants. That is, the temperature differences between the lances in assembly positions D5 and D6 (radius 0.532 and 0.645 m) are about the same as those between the lances in assembly locations B5 and C6 (radius -0.532 and -0.645 m). Figure 4-17 shows an increase in the temperature difference between measurements in locations B5 and C6 (radius -0.532 and -0.645 m) for the horizontal run when it is compared to the temperature difference between the same locations in the vertical run. The small change in temperature difference between assembly location C6 and B5 in the upper quadrant is due to the convection current set up in the open basket location adjacent to basket location D5. The small change in temperature difference between assembly locations C6 and B5 in the lower quadrants is attributed to either small convection currents or temperature stratification in the open basket location next to B5. There is also a slight skewing of the temperature profile in the horizontal run, with an increase in temperature in quadrants A and D. However, this effect is more apparent from comparing the curves of Figure 4-15. The

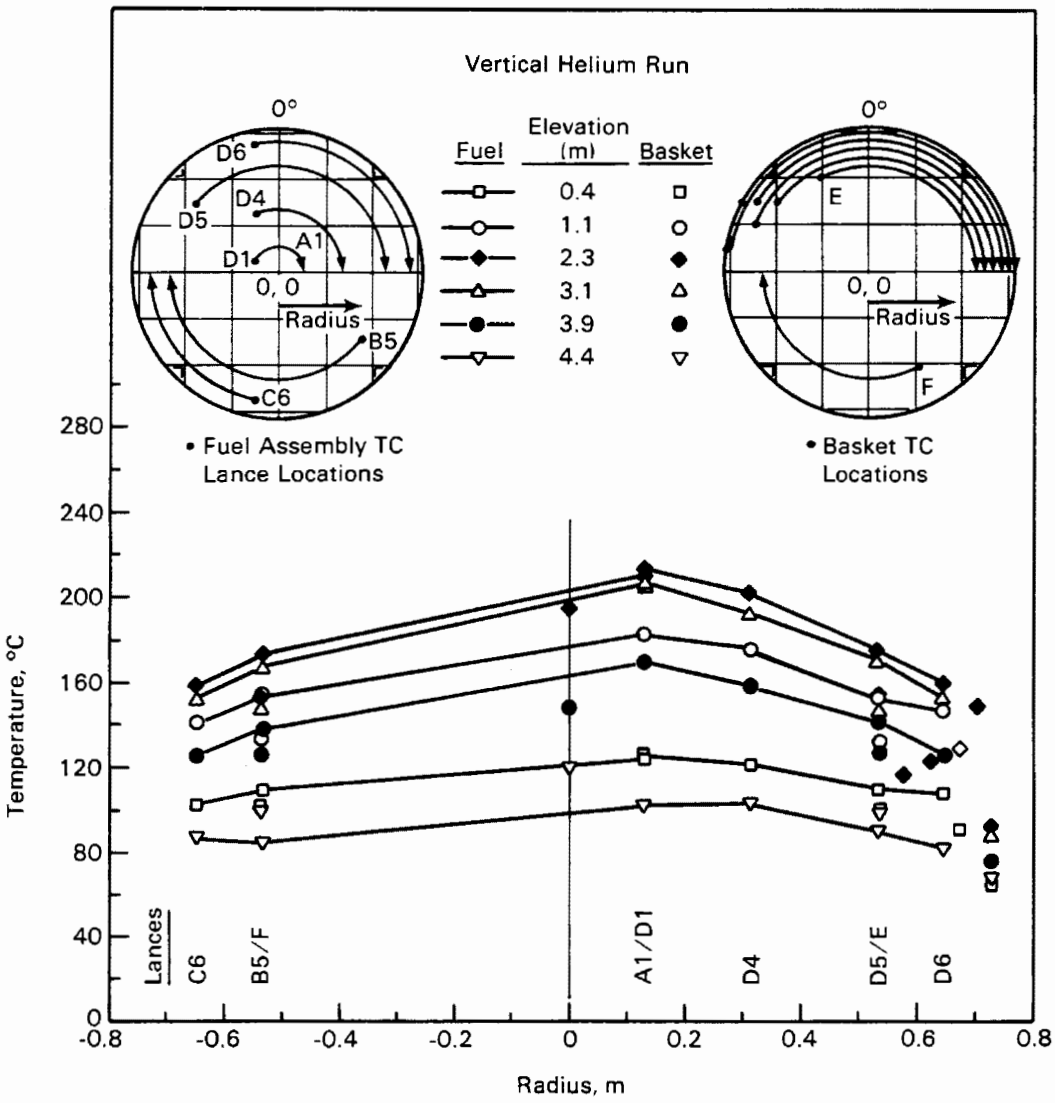

Figure 4-16. Radial Temperature Profiles for Vertical Helium Run

temperature skewing between the lower and upper quadrants is attributed to the change in contact resistance between the basket and the cask inner wall due to the weight of the basket and fuel assemblies.

Figures 4-16 and 4-17 show a significant temperature drop from the basket to the cask inner wall. At an elevation of 2.3 m (7.5 ft), this temperature drop is 20 to 55°C in the vertical and 30 to 55°C in the horizontal helium run, representing a significant portion of the temperature drop from the center of the cask to the ambient.

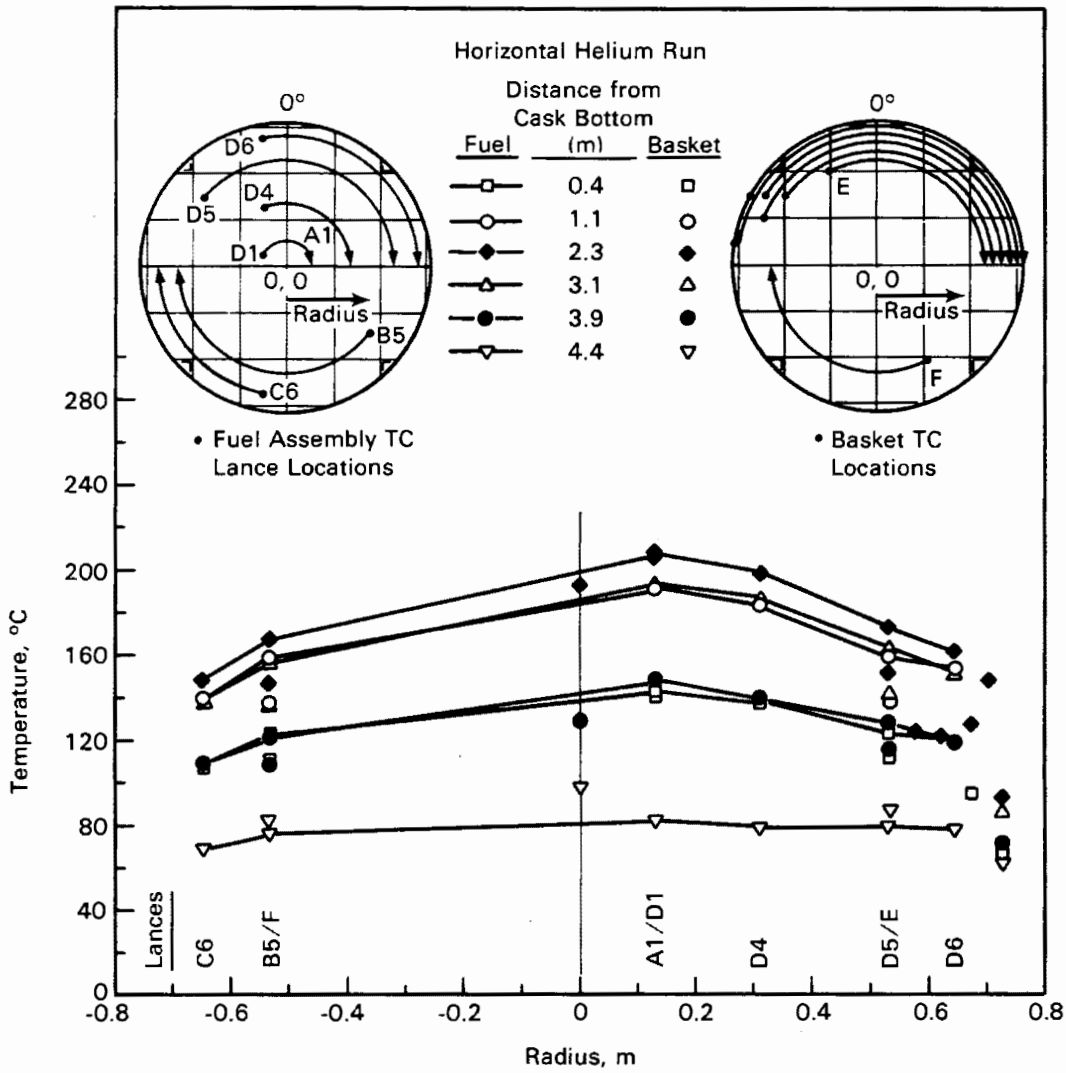

Figure 4-17. Radial Temperature Profiles for Horizontal Helium Run

Effects of Backfill Environment

Effects of backfill environment on guide tube temperatures are discussed in this section. Both axial and radial temperature profiles are compared for the different fill conditions and cask orientations.

Temperature data demonstrate that helium is the most effective backfill. Peak guide tube temperatures were significantly less (60 to 64°C) than temperatures in vertical vacuum and less (18 to 39°C) than temperatures in nitrogen. Some convection occurred in the vertical helium runs, although not with as dramatic an effect as in the vertical nitrogen run. Axial temperature profiles were skewed toward the tops of the

fuel assemblies, but not as much as they were for nitrogen. Peak fuel temperatures in a horizontal orientation occurred slightly below [estimated to be 0.5 m (20 in.) below] those in a vertical orientation, but the peak measured lance temperature was only 6°C (208°C versus 214°C) lower in the horizontal orientation. Therefore, the added conduction heat transfer resulting from assemblies contacting their basket fuel tubes was just enough to replace the axial convection that occurred in a vertical orientation.

Figure 4-18 shows the effect of gas environment and cask orientation on the hot fuel assembly lance temperature profile. The hot lance in each case was found in assembly D1. The vacuum profiles serve as a base for determining the effect of convection in the cask. Both vacuum runs show similarly shaped profiles, with a small difference in magnitude caused by the difference in conduction paths between the basket and the cask due to orientation. The temperature profiles for the horizontal nitrogen and helium runs are similar in shape but significantly lower in magnitude than for the vacuum runs. The similar profile shape leads to the conclusion that there was no axial convection in the horizontal nitrogen and helium runs. The difference in magnitude is a result of the different gas thermal conductivities. The vacuum case has the lowest conductivity, resulting in the highest temperature. Nitrogen and helium follow with their increasing thermal conductivities, resulting in decreasing peak temperatures. Axial convection is apparent in the vertical nitrogen and helium runs. Convection skews the temperature profiles, moving the location of the peak temperature upward in the cask. Skewing of temperature profiles is more apparent with vertical nitrogen than with vertical helium because of higher temperatures and the greater density of nitrogen that result in larger buoyancy forces and more convection in nitrogen than in helium. In the nitrogen case, convection moves the location of the peak axial temperature from an elevation of 1.9 m (6.2 ft) to 3.6 m (11.8 ft); in the helium case, convection moves the location of the peak axial temperature from an elevation of 1.9 m (6.2 ft) to 2.4 m (7.9 ft).

Figure 4-19 shows the radial temperature profiles at the elevation of the peak axial temperature from each of the six runs. Temperatures for all three backfill conditions show good radial symmetry when the cask is in the vertical orientation. In the horizontal orientation, the temperatures are skewed for all three fill conditions; the temperatures in the upper quadrants of the cask are hotter than those in the lower quadrants of the cask. In the vacuum runs, the temperature differences between assembly locations C6 and C5 and between D5 and D6 do not change with orientation. However, these temperature differences do change for the nitrogen and

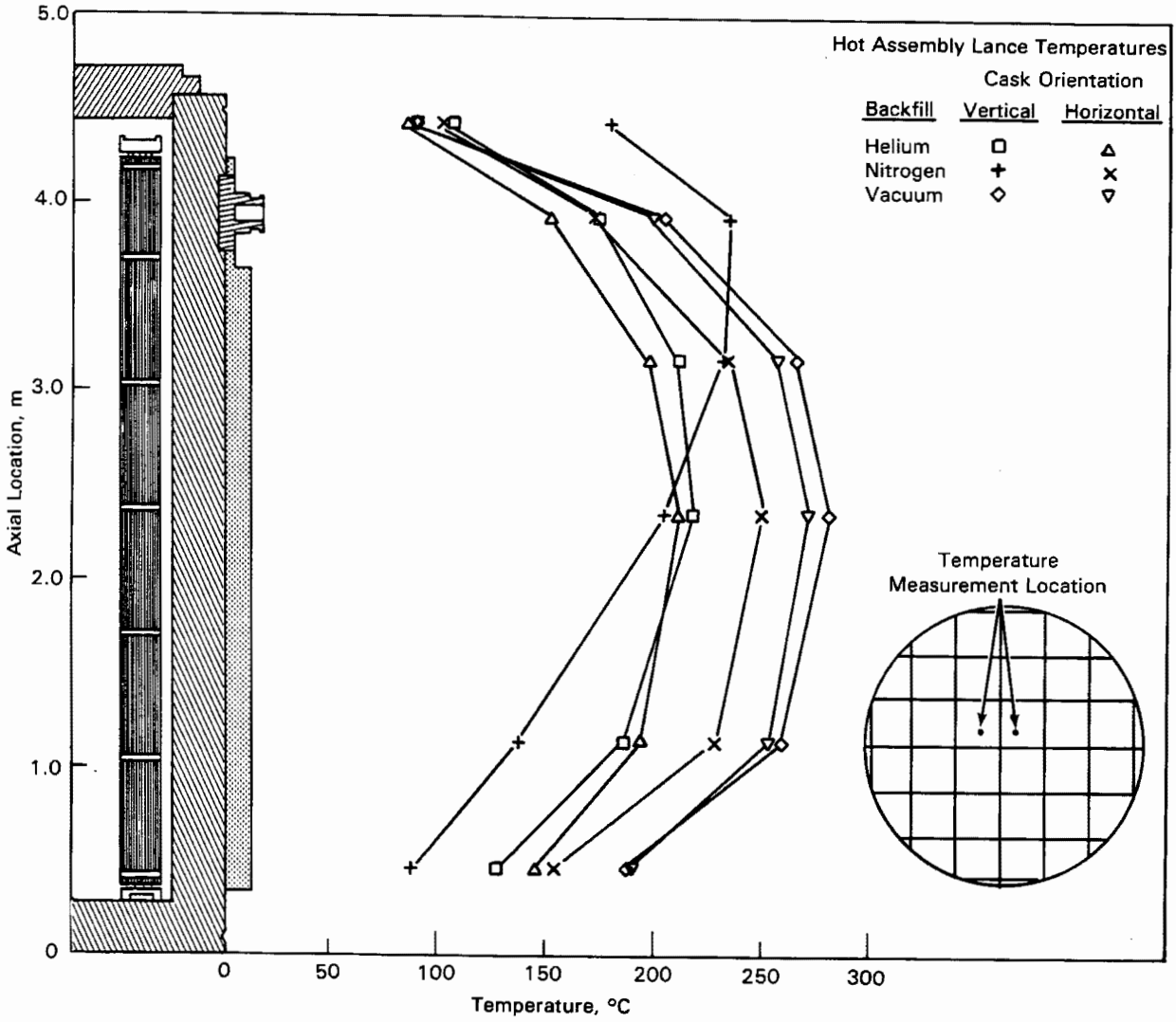

Figure 4-18. Effect of Gas Environment and Cask Orientation on Axial Temperature Profiles

helium fill conditions. The change is very apparent for the nitrogen case and quite subtle for the helium fill condition. These changes in the temperature relationship between assembly locations C6 and B5 and between D5 and D6 are felt to be a result of convection currents set up in the open basket space next to D5 and to convective currents or temperature stratification in the open basket slots next to B5, as was shown in Figure 4-12. Change in contact resistance between the basket and the cask is ruled out as a cause of the difference between vertical and horizontal orientation because the change in temperatures between C6, B5, D5, and D6 was not seen in

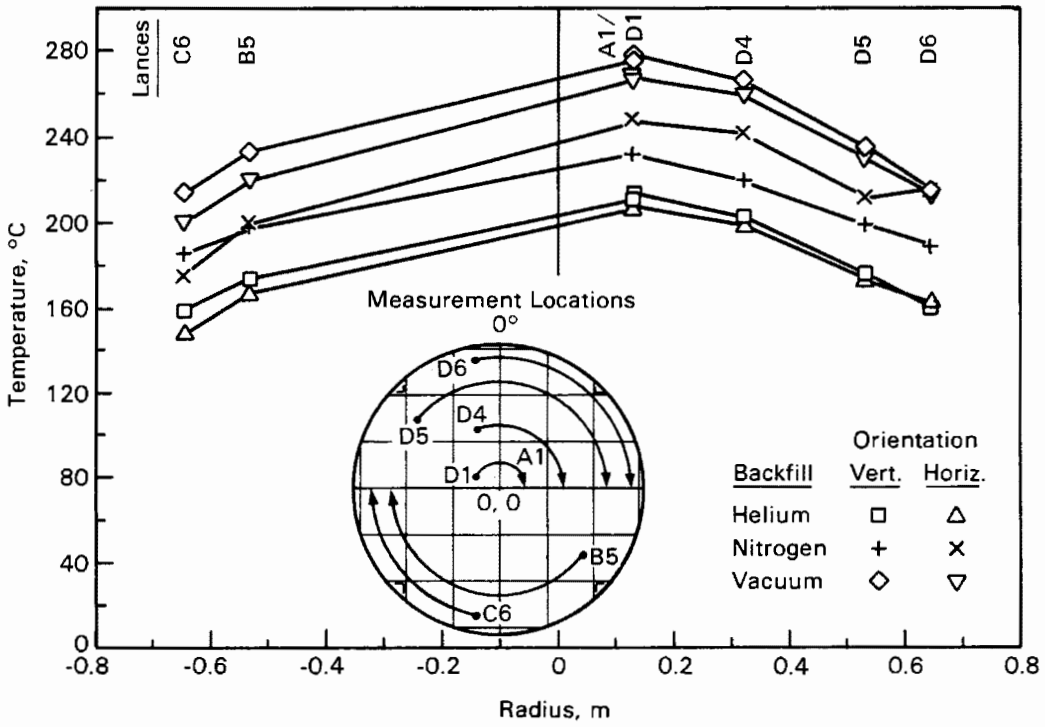

Figure 4-19. Radial Temperature Profiles Measured Near Peak Axial Temperatures

the vacuum run. Increased conductivity of the gas is ruled out because the difference is not observed in the vertical runs. Convection is the only heat transfer mode remaining; hence, convection must be the source of the observed temperature difference in a horizontal orientation.

Backfill also affects the temperature drop between the basket and the inside wall of the cask. For the vacuum run this drop was 50 to 100°C. In the nitrogen runs it was between 25 and 80°C, and for the helium runs it was between 20 and 55°C. This temperature drop represents a significant portion of the total temperature drop from the peak temperature in the cask to the ambient temperature.

Surface Temperatures

Cask surface temperatures are important from an operation and maintenance standpoint. Selected axial temperature profiles measured on the cask surface are shown in Figure 4-20; the remaining surface temperature data are provided in Appendix C. The peak surface temperature was measured during the vertical vacuum run and was 79°C. The axial surface temperature profiles reflect the temperatures inside the

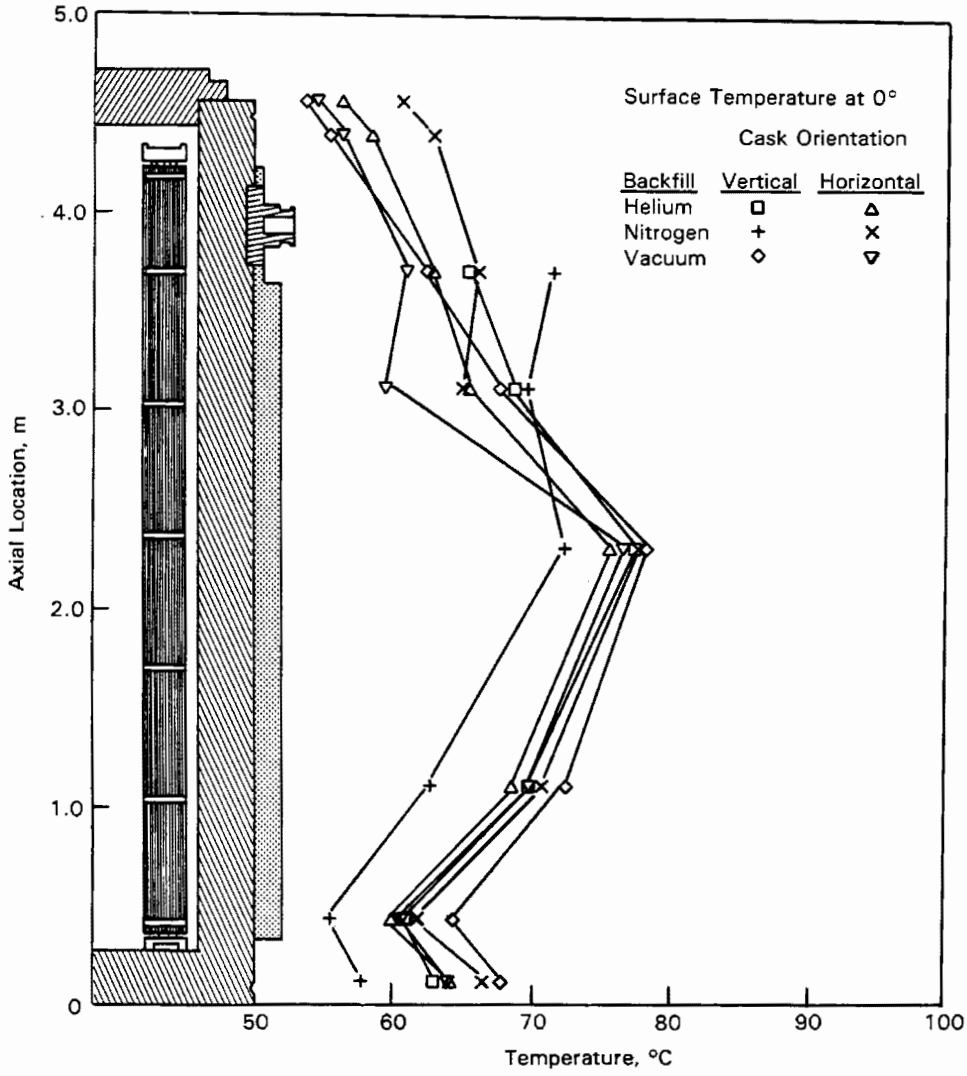

Figure 4-20. Axial Surface Temperature Profiles

cask. There is not a distinct indication of significant convection on the cask outer surface. However, surface temperatures during the vertical helium and nitrogen runs are hotter near the top of the cask. Skewing of the axial surface temperature profile toward the top of the cask was probably due to convection inside the cask rather than on the outer surface. Had the skewing of the temperature profile been caused by external convection, there should have been a larger difference between the vertical and horizontal vacuum runs. It appears that a TC may have come loose at an elevation of 3.2 m (10.5 ft) for the horizontal nitrogen and vacuum runs. This would explain the apparently low temperature for these two runs at this

elevation; when TCs loosen, they read closer to the ambient temperature. In general, the cask surface temperatures are thought to be satisfactory, because they range between 49°C and 79°C and are less than 100°C.

Corresponding circumferential temperature profiles at an elevation of 2.3 m (7.5 ft) are presented in Figure 4-21. The circumferential temperature profiles show some modest effect of orientation on cask surface temperature. The vertical nitrogen run profile is cooler than the others and reflects the effect of convection inside the cask, decreasing the heat flux through the cask at this elevation. The difference in temperature around the cask in the vertical runs was less than 5°C, with the temperatures at 0° being the hottest. In the horizontal runs the temperature difference around the cask was about 8°C, with the temperatures at 180° being the hottest. This amounts to an average change of about 13°C between the 0° and 180° locations. The hotter temperatures at the bottom of the horizontal cask (180°) are due to the better contact between the basket and the cask wall at this location during the horizontal run. A larger portion of the decay heat flows from the basket to

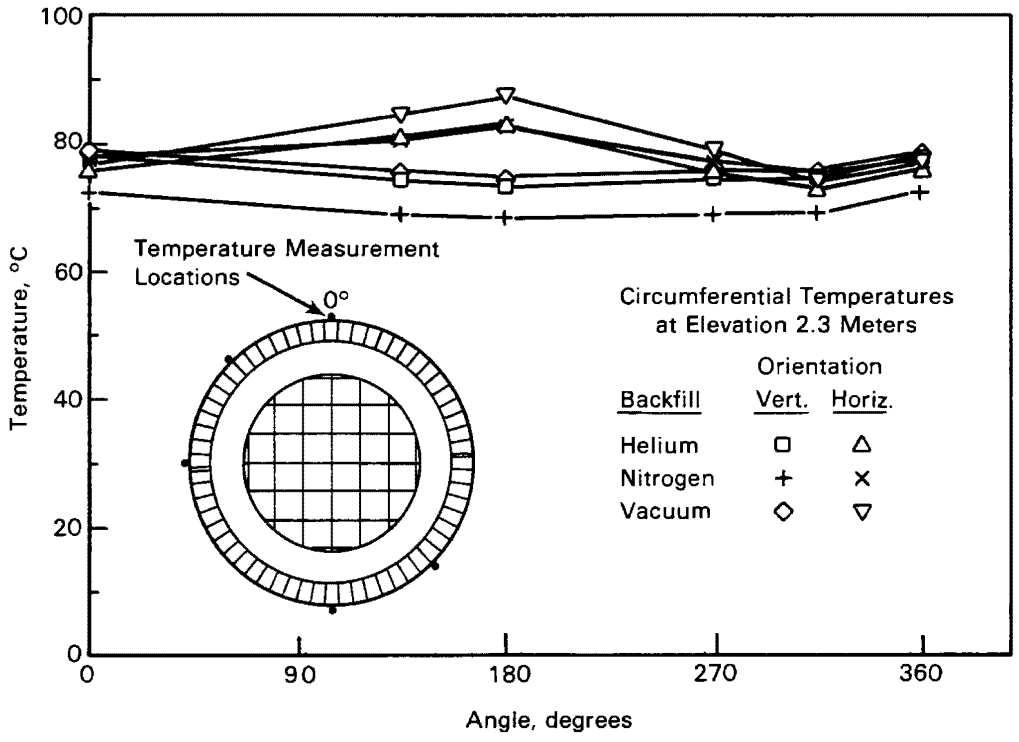

Figure 4-21. Circumferential Surface Temperature Profiles

the cask at 180° during the horizontal runs than it does during the vertical runs. This results in the higher cask surface temperatures at this location during horizontal runs.

Temperature Transients

Temperature transients occurred during testing as a result of changes in backfill environments and rotation of the cask from a vertical to a horizontal orientation. As much transient temperature data as practical were collected, but because the TC lances were disconnected when the cask was being rotated, continuous data scanning was not possible.

Temperature histories for the TCs in the center assembly (D1), cask surface, and ambient are presented in Figure 4-22. The internal cavity pressure is also shown in Figure 4-22. The data indicate that temperature transients were very mild. The steepest transient temperature rise occurred immediately following the change of gas when the cask was in a vertical orientation. The transient was on the order of 12°C/h. The steepest measured temperature transient was on the order of 30°C/h and was measured following the vacuum run when the cask was cooling after being backfilled with helium. It is interesting to note how the temperature transient curves at the various elevations exchange position during vertical runs, while in the horizontal runs the curves maintain their respective positions as their magnitudes change from one fill condition to another. The reason for the change of position during the vertical runs is the effect of convection on locations of peak temperatures.

It can be concluded that abrupt changes in backfills from or to environments of significantly different thermal conductivities or convection characteristics did not result in significant temperature transients in the spent fuel rods. Transients that result from replacing a gas backfill with a vacuum can be reduced in severity by having a vacuum/helium environment instead of a vacuum/nitrogen environment. That is, the cask can be backfilled with high conductivity helium prior to attaining a vacuum-drying environment. Of course, this was not done during the cask performance test because one test objective was to determine maximum temperatures possible in the cask.

Long-Term Surveillance

At the conclusion of the TN-24P performance test, the cask was put on the long term-surveillance pad as shown in Figure 3-51. At monthly intervals, 3 days of cask surface temperature, pressure, and weather data were collected. The cask response to the ambient conditions is discussed in this section.

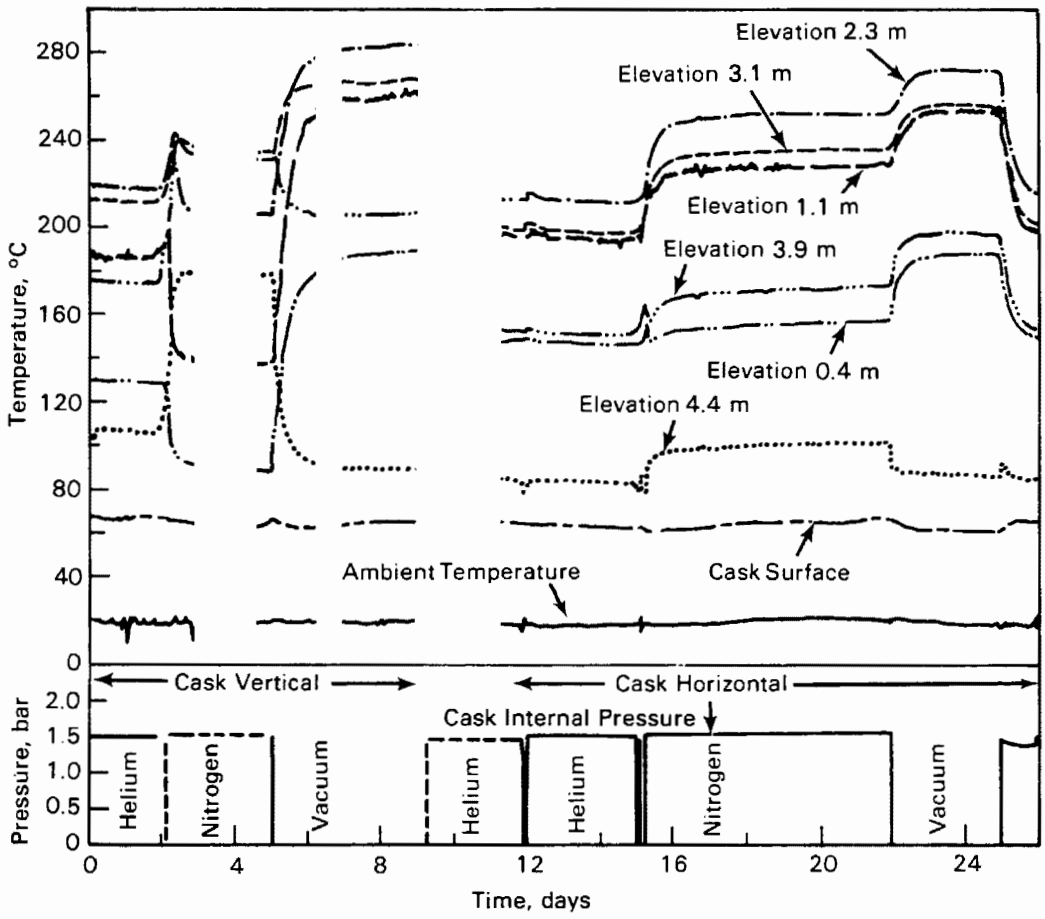

Figure 4-22. Hot Lance, Cask Surface, and Ambient Temperature Histories

Figure 4-23 shows the response of the cask surface temperature to ambient temperature, wind speed, and solar insolation for four surveillance periods. The cask surface temperature represents the average of four TCs attached to the surface of the cask. Figure 4-23 shows a definite relationship between the wind velocity and the cask surface temperature. The relationship between wind speed and surface temperature is most apparent during the May and June surveillance periods when the ambient temperature was somewhat stable. During these periods (around 40 h into the May period and 48 h into the June period), changes in the cask surface temperature were inversely proportional to the wind speed; i.e., the cask surface temperature decreased for increases in wind speed. At other times it is more difficult to separate the effect of wind speed from the effect of ambient temperature. This is because a constant multiplied by the product of the convective heat transfer coefficient and the temperature difference (between the cask surface and the ambient temperature) is equal to the heat lost from the cask. The heat transfer coefficient is

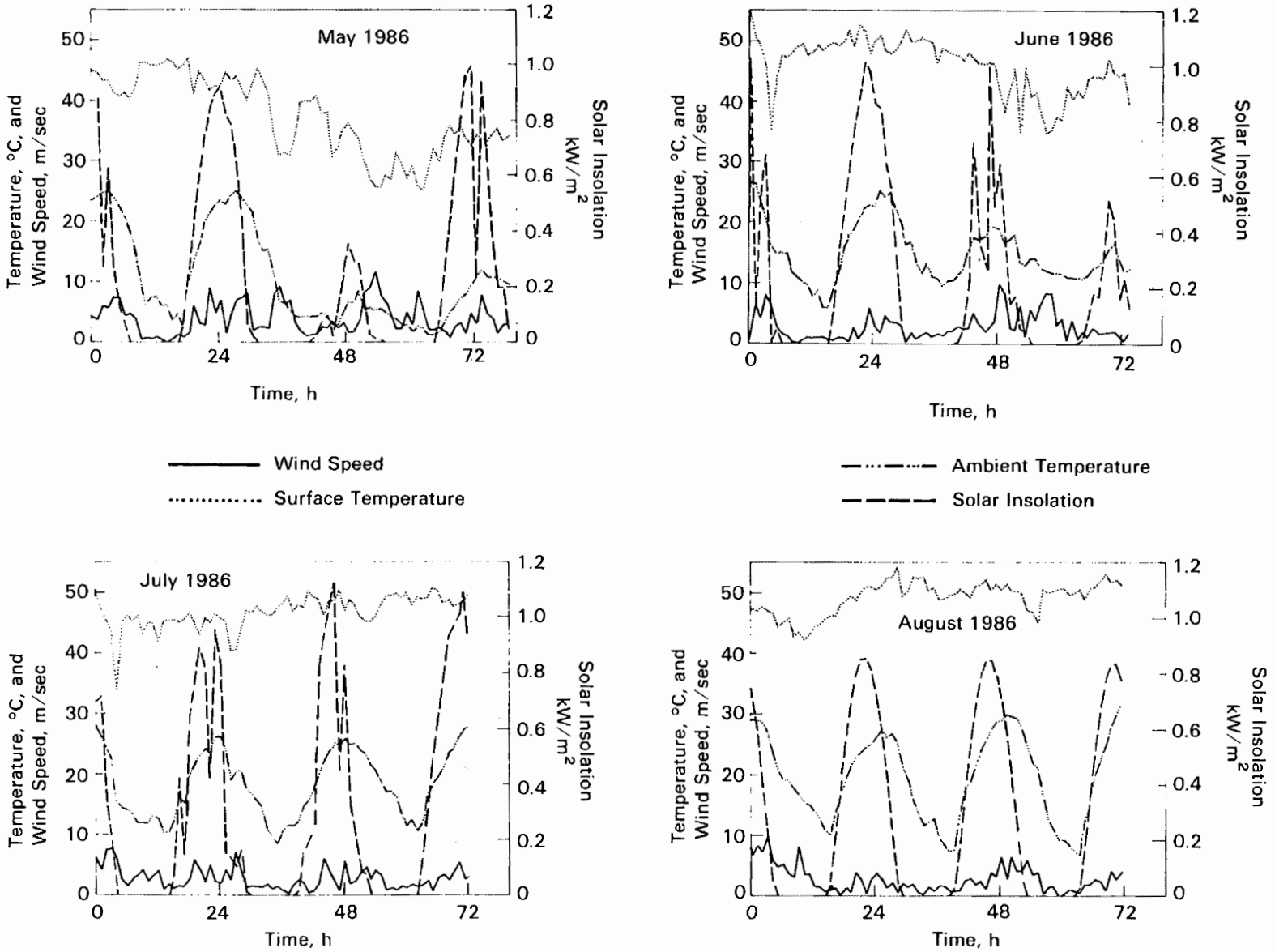

Figure 4-23. Cask Surface Temperature Response to Ambient Temperature, Wind Speed, and Solar Insolation

directly proportional to the wind speed. Hence, when the ambient temperature rose and the wind increased, the effect of increased ambient temperature on cask surface temperature tended to cancel the effect of increased wind speed. However, the effect of shutting off the wind is seen during the August surveillance period. The wind stopped at a little over 50 h into the surveillance period. At this time, the surface temperature increased significantly, even though the ambient temperature was decreasing.

An effort to correlate the relationship between the wind speed and surface-to-ambient temperature drop is shown in Figure 4-24. Heat transfer considerations indicate that velocity to some power multiplied by temperature drop should equal a constant multiplied by the heat lost from the cask. A log-log plot was used to plot

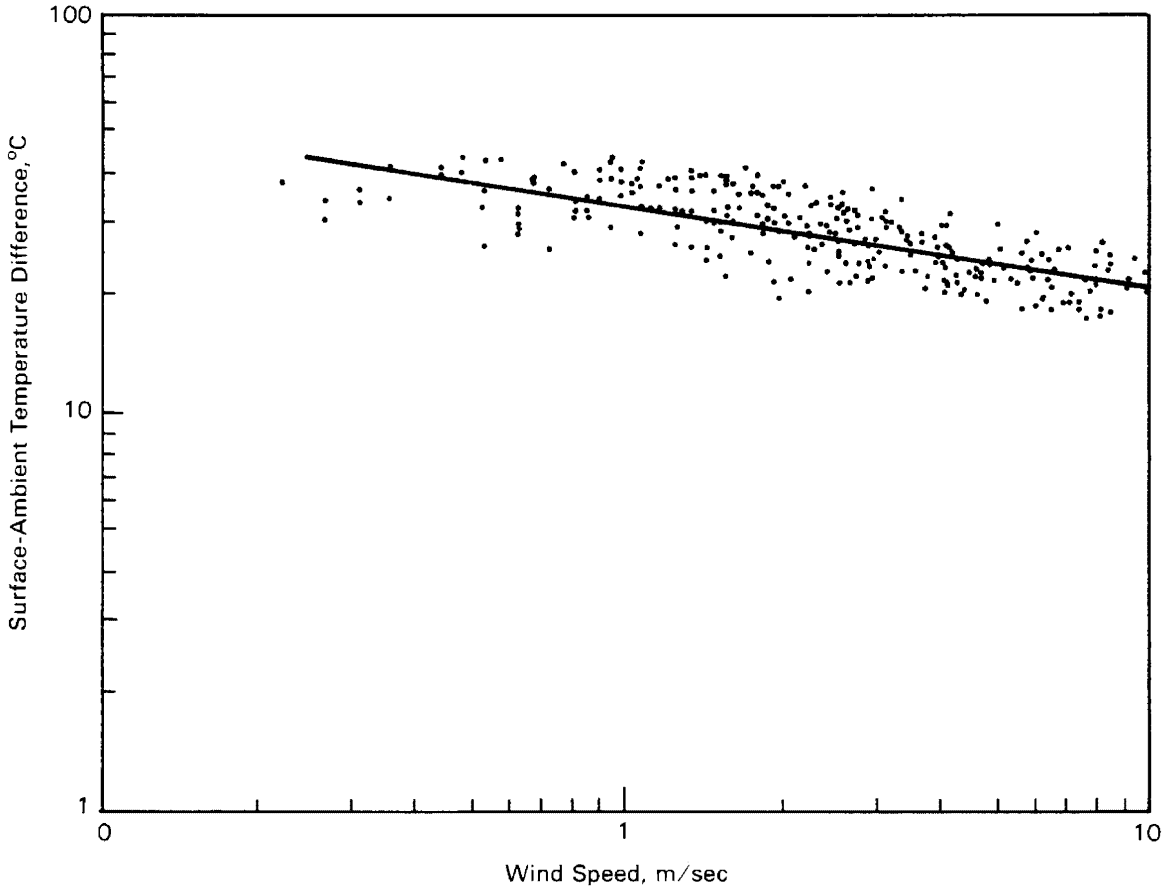

Figure 4-24. Correlation Between Temperature Drop at Cask Surface and Wind Speed

these variables, and the heat loss from the cask was assumed to be constant. A best-fit straight line to the data gives

$$(\text{delta T})*(\text{wind speed})^{0.21} = \text{Constant}$$

The effect of solar insolation on the cask temperatures is not readily apparent from the long-term surveillance data. Solar insolation is so closely coupled to ambient temperature that it may not be possible to separate the effects. Swings in ambient temperature followed the solar insolation, as would be expected. The August surveillance period yielded the most uniform solar insolation data collected. Based on these data, the solar load on the cask could be between 4 and 10 kW during the peak of the day. Compared to 20 kW generated in the cask, this solar load should have resulted in significant daily swings in cask surface temperature. However, they are not seen in the data. These results are similar to those observed for the REA cask (6), where no correlation between solar insolation and cask temperatures could be derived. It is felt that proper accounting of the effect of ambient temperature on convection from the cask surface will take care of the effect of solar insolation on the cask.

The cask internal pressure was monitored during the surveillance periods shown in Figure 4-25. It was found to be very stable during the 4-month period, indicating the absence of gas leakage from the cask. The apparent decrease in cask pressure

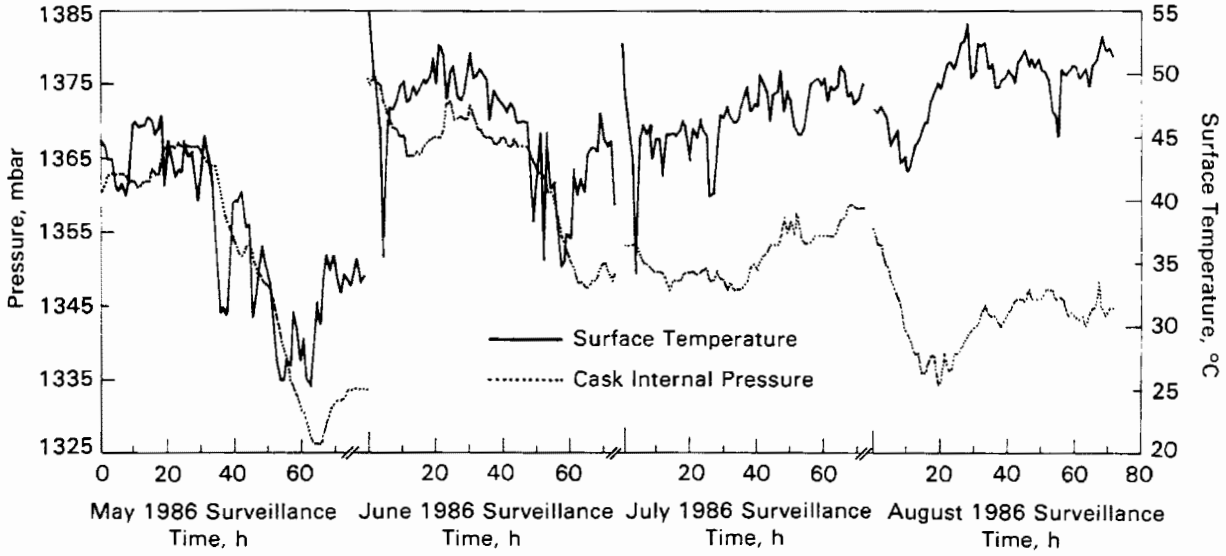

Figure 4-25. Surface Temperature and Internal Cask Pressure History for Cask on Long-Term Surveillance Pad

over time shown by the increased separation of the temperature and pressure data is caused by the removal of gas from the cask during monthly gas sampling activities. Other changes in the cask internal pressure followed changes in cask surface temperature, as would be expected from laws governing a perfect gas in a fixed volume; i.e., increases in temperature cause corresponding increases in pressure. Based on the data shown in Figure 4-25, the internal pressure changes lag behind the surface temperature changes by 9 to 10 h.

SHIELDING PERFORMANCE

Dose rates (gamma and neutron) were measured at selected locations (see Figures 3-11 and 3-12 of Section 3) on the cask surface. Energy spectrum instruments identified and discussed in Section 3 were used to obtain reference dose rates and energy spectra at a few selected locations. The spectral measurement locations were 1) the center of the primary lid of the cask, 2) the center of the bottom of the cask, and 3) the side of the cask at a 90° angle and an elevation of 2.3 m (7.5 ft) from the bottom of the cask. These reference energy measurements were used to calibrate thermoluminescent dosimeters (TLDs) and track etch dosimeters (TEDs) to permit accurate gamma and neutron dose rates to be determined with TLDs and TEDs, respectively.

Measurements were obtained with TLDs and TEDs at 26 points on the lid, 49 points along the cask side, and 20 points on the cask bottom. In addition, INEL obtained gamma and neutron portable survey instrument readings at each of the TLD/TED locations, and PNL obtained portable survey instrument readings at selected TLD/TED and spectrometer locations. Selected data obtained during dose rate measurements are discussed in the following subsections; the remainder of the data are presented in Appendix C.

Reference Energy Spectra and Dose Rates

The neutron dose equivalent rate data obtained from the spectrometer measurements are presented in Table 4-2. Survey instrument and dosimeter measurements have also been included for comparison. It should be noted that the measurements were made as close to the cask surface as practical, but because of the size of the detectors, the actual measurement location in some instances was several centimeters away from the surface and averaged over a large volume. Results from the ^{3}He spectrometer, tissue equivalent proportional counter (TEPC), multisphere spectrometer (M/S), track etch dosimeter (TED), and SNOOPY survey instrument measurements are in relatively good agreement. The multisphere results are consistently low on the side of the cask. This finding is due to the very low dose rate and the low count rate measured with each sphere, which caused large convergence errors in the computer analysis.

Table 4-2

REFERENCE NEUTRON DOSE EQUIVALENT RATE MEASUREMENTS

Location	Dose Equivalent Rate, mrem/h					
	Spectrum-Based			Survey Instruments		
	^3He[a]	TEPC[b]	M/S[c]	TED[d]	PNL SNOOPY	INEL PNR-4[e]
Top of Cask - Centerline						
at contact	18.6	16.9	f	31.1	30	37
at 1 meter	10.5	4.5	6.4	f	12	f
Bottom of Cask - Centerline						
at contact	40.3	57.0	42.7	63.8	90	100
at 1 meter	27.6	16.2	14.9	f	25	f
Side of Cask - 90°, 228 cm						
at contact	1.62	1.13	0.2	2.1	2	1.5
at 1 meter	f	1.06	0.3	f	1.8	1.5

[a]Helium-3 neutron spectrometer.

[b]Tissue equivalent proportional counter.

[c]Multisphere neutron spectrometer.

[d]Track etch dosimeter.

[e]Eberline PNR-4.

[f]Not measured.

The neutron energy spectra measured by the ^3He spectrometer at the top, bottom, and side of the cask are given in Figure 4-26. The neutron flux distribution is given in 20-keV energy bins for energies between 40 keV and 1 MeV. The well-defined minima in the spectra correspond to absorption resonances in the neutron cross sections for iron and oxygen. The more minor fluctuations at the high energy end of the spectra for the top and bottom are due to poor counting statistics; however, the two spectra have the same general pattern overall. The ^3He tube used for these two measurements was a small-diameter tube that has a low efficiency for high-energy neutrons and requires very long run times to obtain sufficient data at high energies.

The average neutron energies at the top, bottom, and side were estimated to be 173, 193, and 87 keV, respectively, from the ^3He data. The multisphere spectrometer

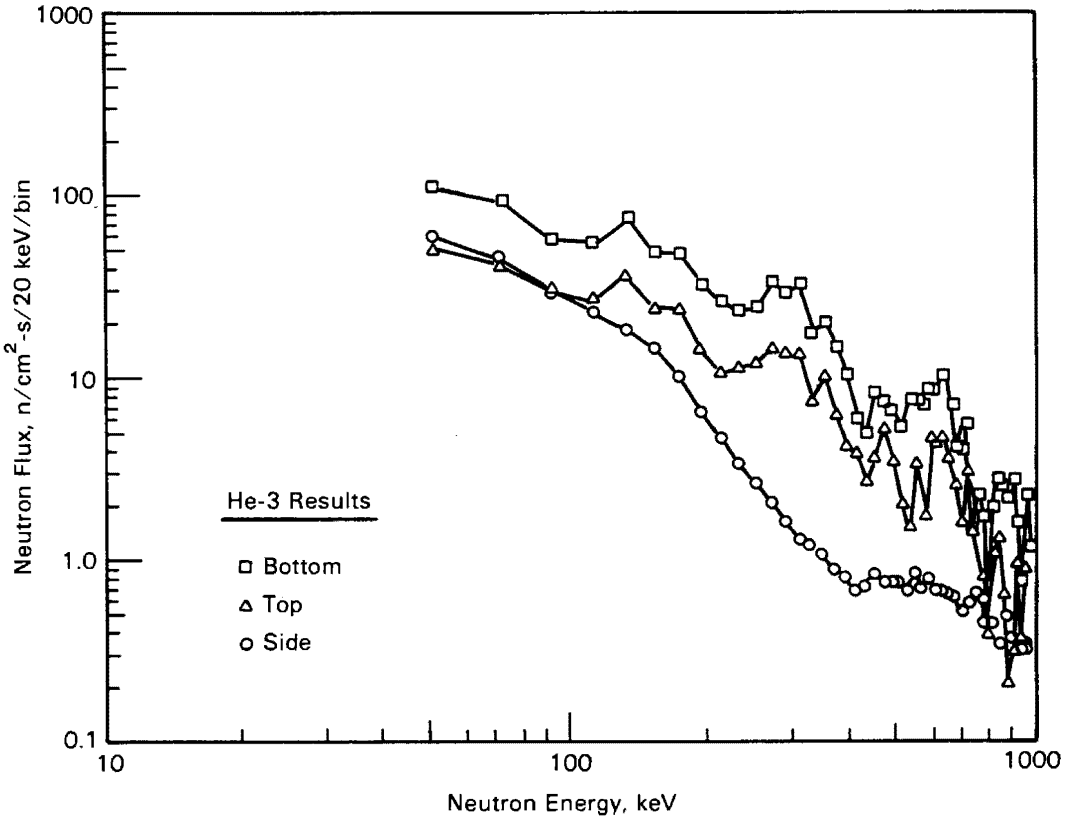

Figure 4-26. Neutron Spectra Measured on Cask

determined the average energies to be 110, 138, and 8 keV at the top, bottom, and side, respectively. Average neutron energies of 183 and 112 KeV were used to obtain factors to convert the TED data from tracks per square centimeter to neutrons per square centimeter. Because the sources used to calibrate the neutron survey instruments have average neutron energies above 1 MeV (1000 KeV), the instruments overrespond at lower energies. This causes the survey readings to be consistently higher than the TEPC or TED results.

A comparison of gamma dose rate measurements can be made from the data presented in Table 4-3. The gamma dose rate measurements were made with TLDs and ion chamber survey instruments, which are both somewhat energy-dependent. Good agreement exists between all gamma dose rate data.

An intrinsic germanium spectrometer was used to determine the gamma energy spectrum and confirm the appropriate calibration for the TLDs and gamma survey instruments. The gamma energy spectra measurements were made at the top, bottom, and side of the cask as well, but they were made at some distance back from the surface, to prevent

Table 4-3

REFERENCE GAMMA EXPOSURE RATE MEASUREMENTS

Location	Exposure Rate, mR/h		
	TLD[a]	RO-3B[b]	RO-3A[c]
Top of Cask - Centerline at contact	50.6	52	70
Bottom of Cask - Centerline at contact	126.4	145	170
Side of Cask - 90°, 228 cm at contact	13.1	13	18

[a]Thermoluminescent dosimeter.

[b]Eberline RO-3B used by PNL.

[c]Eberline RO-3A used by INEL.

pulse pile-up in the detector. The germanium spectrometer was used only to look at the energies of the source gammas. A representative gamma energy spectrum with the gamma energy peaks identified for the source radionuclides is shown in Figure 4-27. The major radionuclides identified were ^{60}Co and $^{144}Ce/Pr$ at the top and bottom of the cask, and $^{144}Ce/Pr$, ^{134}Cs, and ^{154}Eu on the side. The dominance of ^{60}Co at the top and bottom is due to the activation of the stainless steel on the ends of the fuel assemblies. The primary contributor at the side is $^{144}Ce/Pr$, a fission product present in the spent fuel.

Based on the measured gamma energy spectra, the TLD measurements did not require a modified calibration factor to account for differences in the energy spectra between the cask and laboratory calibration sources. Measurements with the survey instruments are quite close to the TLD results.

Dose Rate Profiles

Gamma and neutron dose rate profiles measured on the primary lid (the outer neutron shield and protective cover were not used during testing) at a 45° angle are presented in Figure 4-28; additional data are included in Appendix D. Data from TLDs (gamma), TEDs (neutron), INEL portable survey instruments, and PNL portable survey instruments are shown.

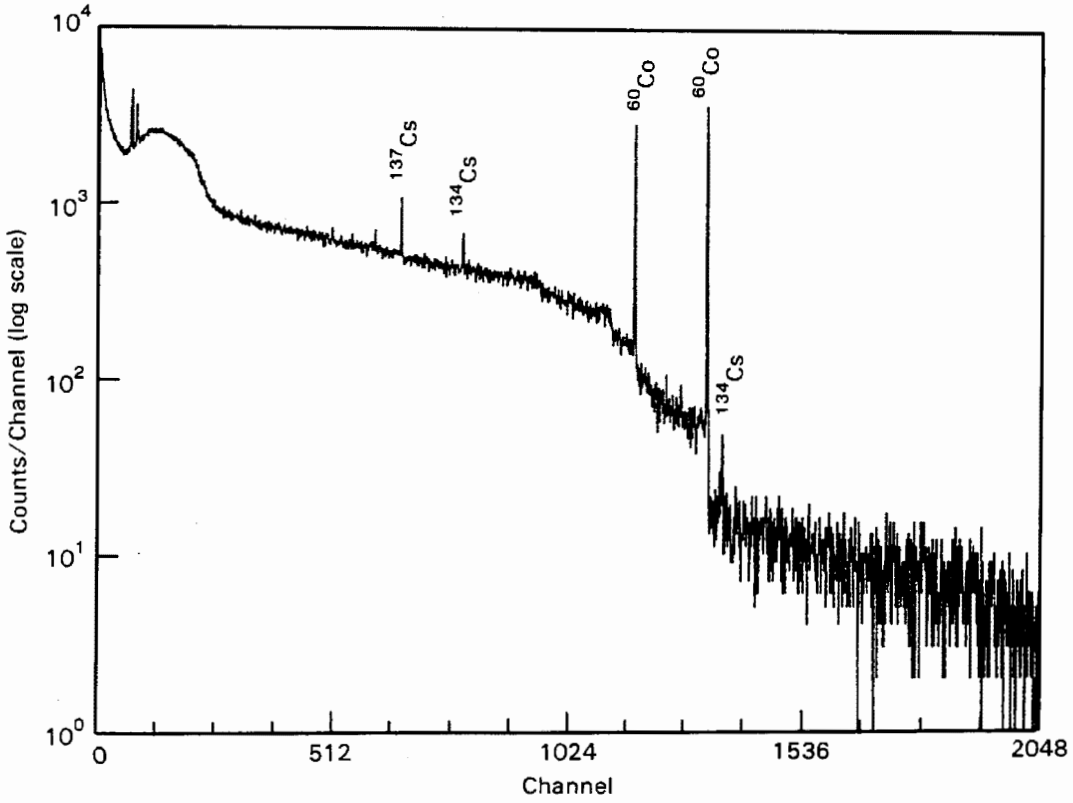

Figure 4-27. Representative Gamma Energy Spectrum

The gamma dose rates are higher than the neutron dose rates by almost a factor of 2 toward the center of the lid, but the two converge as the radius increases until the neutron dose rates eventually become higher at the edge of the lid. The neutron profile is reasonably flat from r = 0 to r = 0.57 m (22.4 in.), then decreases sharply. This decrease in dose rate corresponds to the absence of fuel assemblies directly below measurement locations along the 45° diagonal near the radius of the cask inner cavity. The gamma profile decreases steadily with increasing radius except near the centerline where the dose rate is lower. This trend shows up in the neutron dose rate as well, but to a lesser degree. This decrease may be due to the absence of a fuel assembly directly in the center of the cask. The total (gamma and neutron) dose rate measured with the TLDs and TEDs peaks at 91 mrem/h at r = 0.14 m (5.5 in.). Profiles obtained with TLDs and TEDs generally have lower magnitudes than those obtained with portable survey instruments, but agreement among measurement techniques is exceptionally good. The profiles indicate that portable survey instruments, if properly calibrated and operated, can be used to obtain accurate

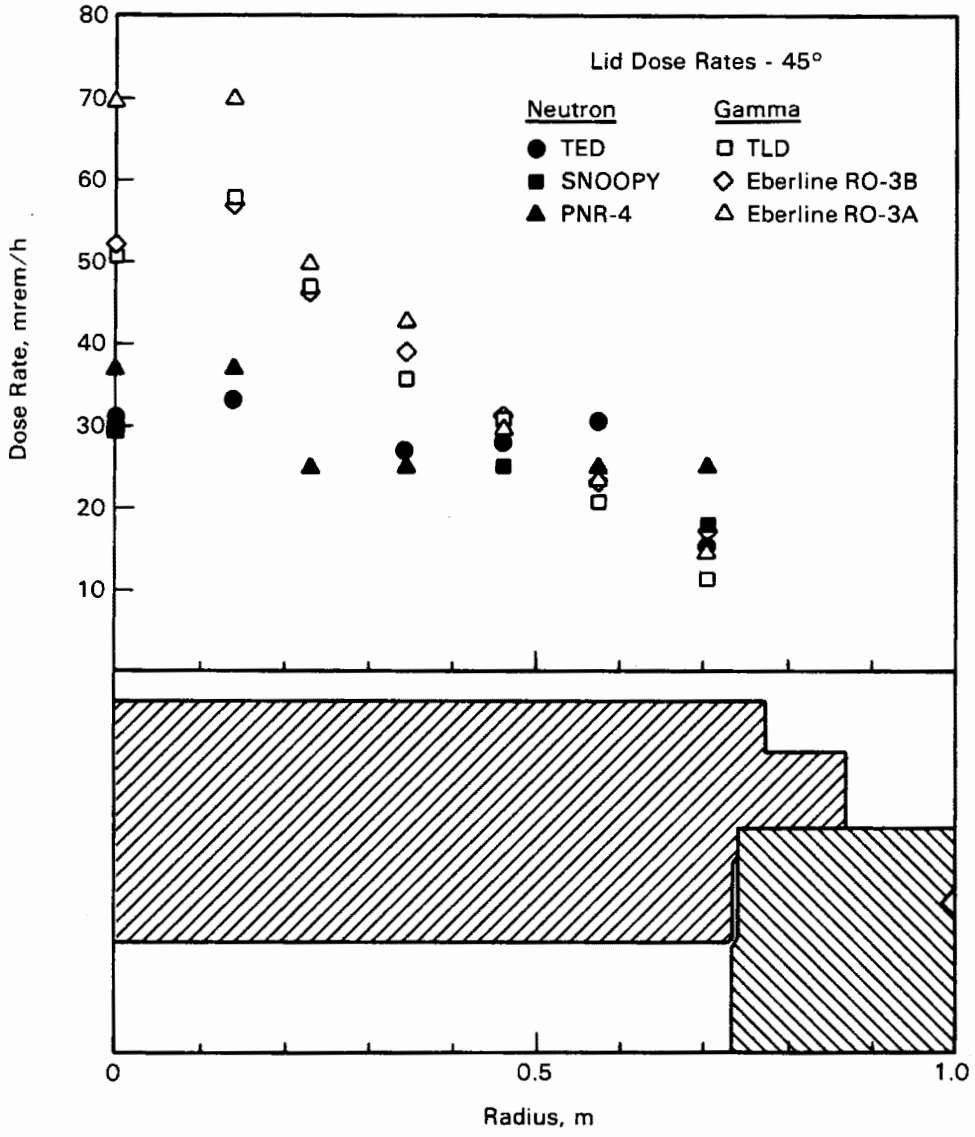

Figure 4-28. Gamma and Neutron Dose Rate Profiles Measured on Cask Primary Lid

gamma and neutron dose rates for the energy spectra associated with spent fuel in the TN-24P cask. It does not appear that the additional time and expense associated with TLD and TED measurements is necessary to determine personnel exposure rates.

Additional dose rate measurements on the top edges and parting plane of the primary lid (Appendix C) resulted in a peak gamma dose rate of 297 mrem/h measured at 115 mm down from 90° at a radius of 0.89 m (35 in.). The neutron dose rate increased only slightly to 19 mrem/h. This dose rate is not shown in Figure 4-28 or Figure 4-29

and is caused by an empty bolt hole under the test lid. During normal operation, with a standard lid, this hole will have a bolt in it and the peak gamma dose rate should be substantially reduced.

Dose rates measured on the side of the cask at 90° are presented in Figure 4-29; the tabulated data are included in Appendix D. Measurements from portable survey instruments agree exceptionally well with TLD and TED dose rate measurements. Gamma dose rate profiles near the ends of the cask show several peaks (33 and 54 mrem/h). These peaks correspond to the upper and lower end fittings of the Surry PWR spent fuel assemblies. If reduction of these peaks is desired, a minor refinement involving adding gamma shielding is required. Neutron dose rates near the cask ends show slightly smaller peaks (<21 and 37 mrem/h). Dose rate measurements obtained near lifting trunnions indicated no increase due to streaming. Total gamma and neutron dose rates on the remainder of the side of the cask are relatively low, less than 20 mrem/h.

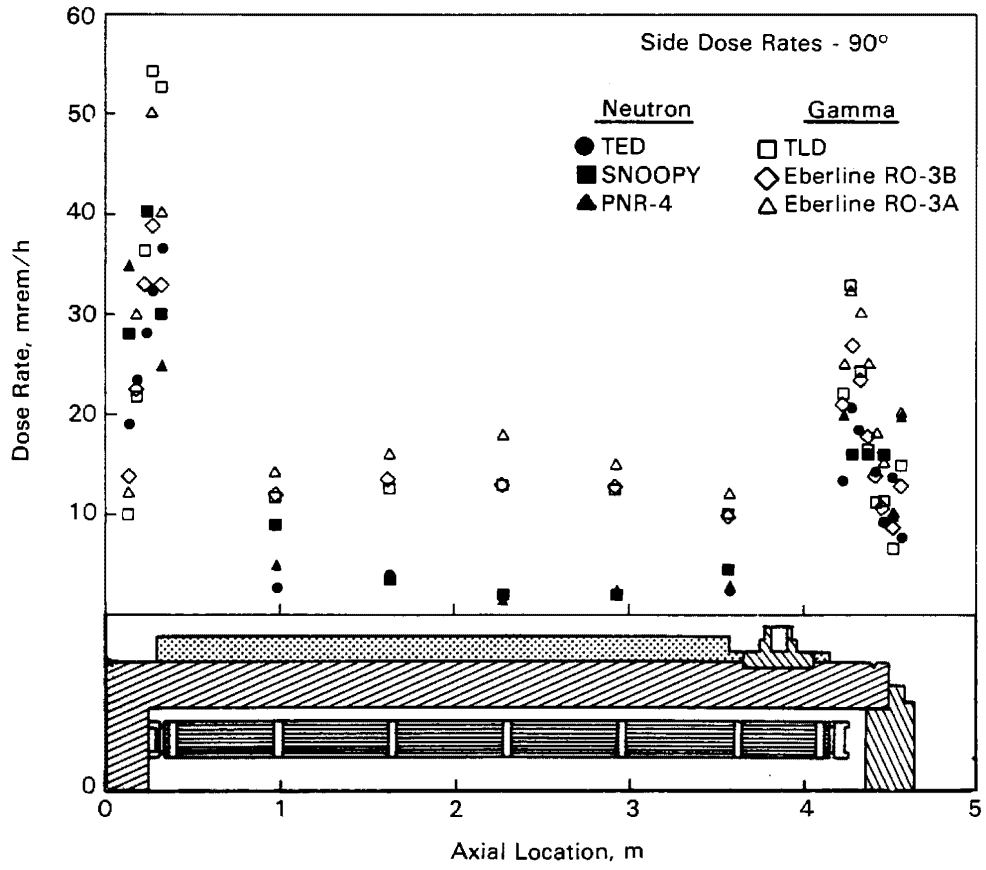

Figure 4-29. Gamma and Neutron Dose Rate Profiles Measured on Cask Side

Circumferential dose rate profiles obtained at 2.3 m (7.5 ft) elevation are shown in Figure 4-30. Both the gamma and neutron dose rate profiles measured with TLDs and TEDs are reasonably uniform (10 mrem/h to 13 mrem/h for gammas and 2.1 mrem/h to 3.4 mrem/h for neutrons). The gamma dose rate does show a slight increase at 90°. Additional TLDs and TEDs were placed continuously along the circumference of the cask at an elevation of 2.3 m (7.5 ft) between the 80° and 90° angles as shown in Figure 4-31. Dose rates were measured here to determine if local peaks in neutron or gamma dose rates resulted from the internal fins used to conduct heat through the neutron shield. As shown in the dose rate profiles of Figure 4-31, no significant peaks were detected, although it appears that the minor neutron dose rate peaks and gamma dose rate valleys correspond to the fins as would be expected.

Dose rate profiles measured on the bottom of the cask at 45° are shown in Figure 4-32; additional data are included in Appendix D. Measurements from portable survey instruments are slightly higher than those made with TLDs and TEDs, but not enough to justify the added time and expense required to obtain good TLD and TED data. The gamma dose rate profile obtained with TLDs is reasonably uniform (103 to

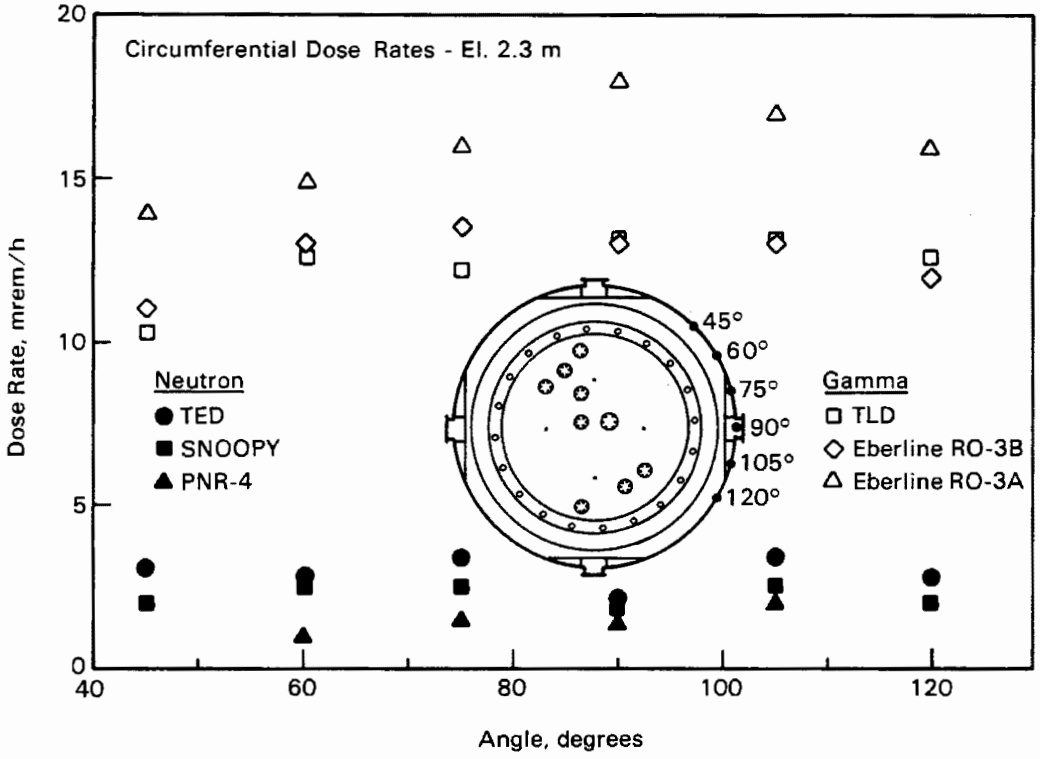

Figure 4-30. Circumferential Dose Rate Profiles

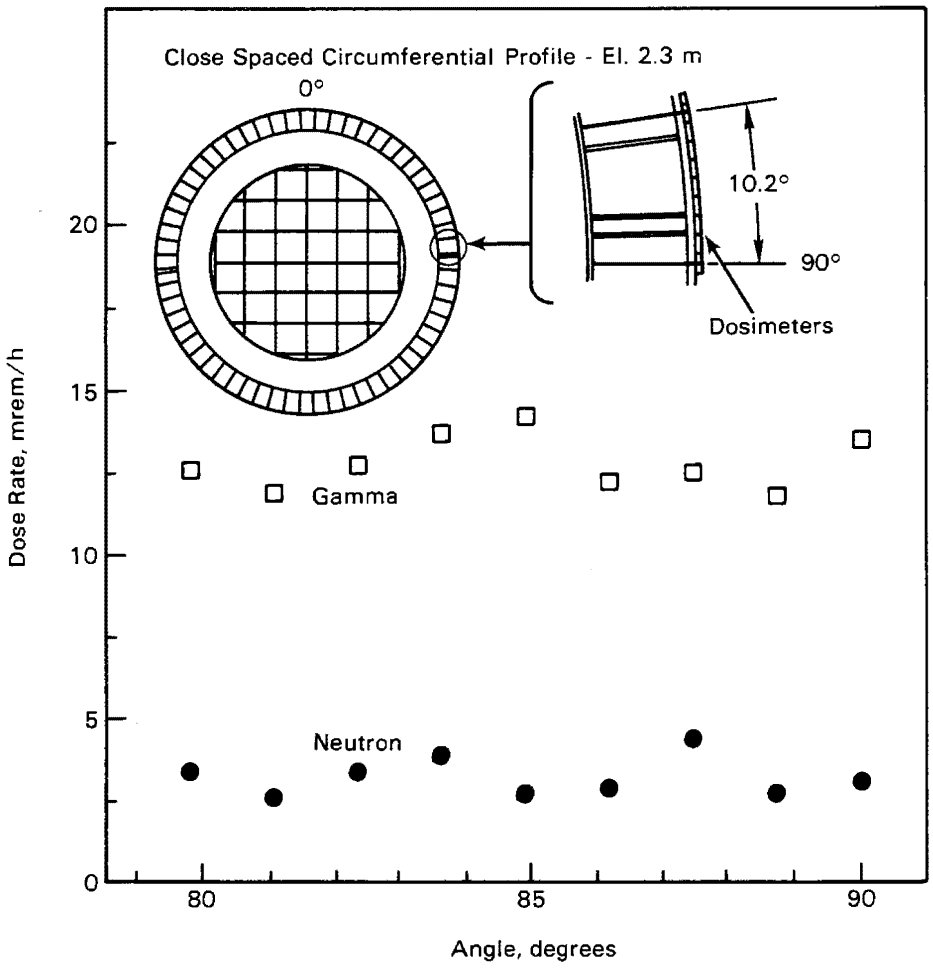

Figure 4-31. Close-Spaced Circumferential Dose Rate Profile

135 mrem/h) from the centerline of the bottom to a radius of 0.46 m (1.5 ft), but drops off to less than 5 mrem/h near the edge of the bottom. The neutron dose rate profile peaks at the centerpoint of the bottom (64 mrem/h) and decreases to less than 10 mrem/h at the edge of the bottom. The total (gamma and neutron) dose rate peaks at about 200 mrem/h near the center of the cask and decreases to <10 mrem/h at the edge of the bottom.

Dose rates at selected locations on the cask surface and in air 1 m (3.3 ft) and 2 m (6.6 ft) adjacent to the cask were measured with survey instruments. Figure 4-33 indicates the attenuation that can be expected from the cask surface to 2 m away from the cask.

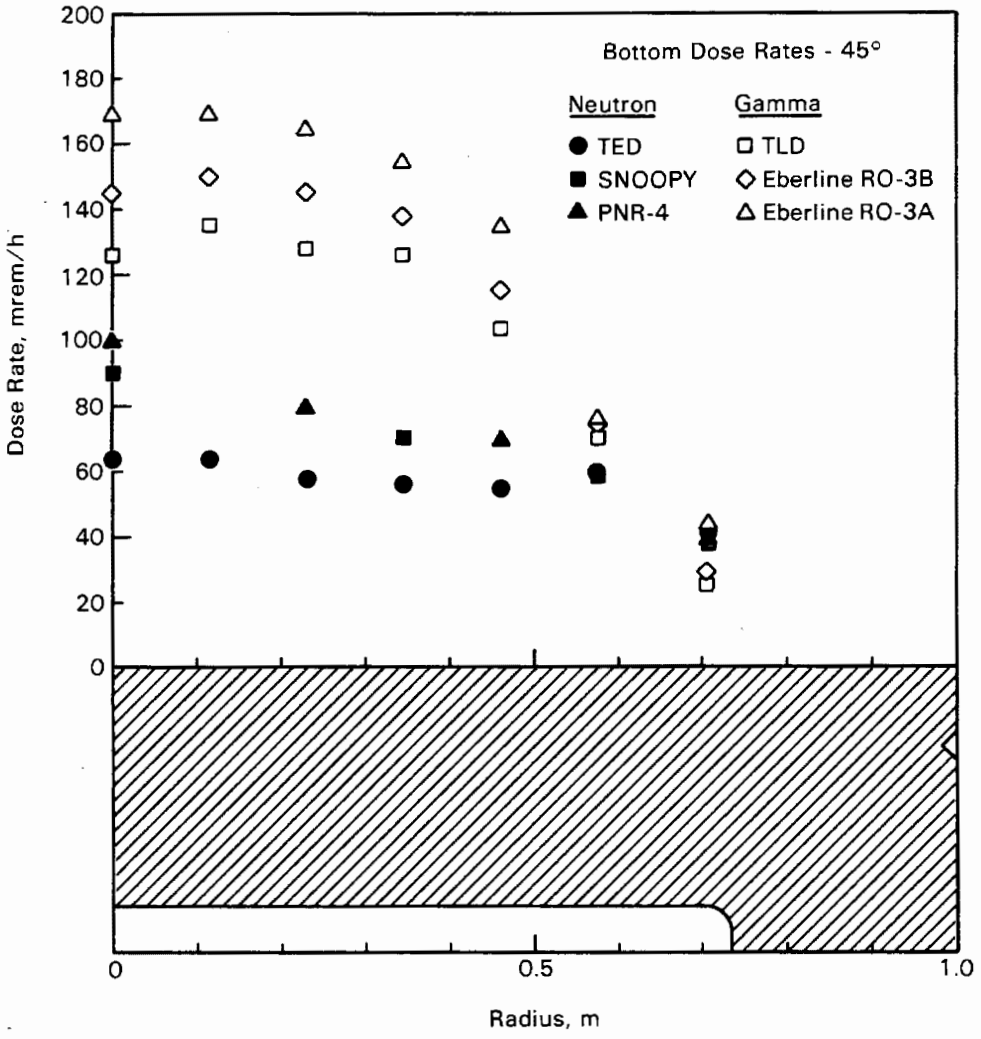

Figure 4-32. Gamma and Neutron Dose Rate Profiles Measured On Cask Bottom

Near the top of the cask, neutron surface dose rates adjacent to the centerline were attenuated from 30 mrem to 12 mrem at a distance of 1 m (3.3 ft) from the cask surface. Gamma surface dose rates were attenuated from 52 mrem to 23 mrem at 1 m (3.3 ft). At r/2 (one-half radius out from the center) the neutron dose rate fell from 30 mrem/h at the surface to 3 mrem/h at 2 m (6.6 ft). The gamma dose rates at r/2 and r decreased from 30 mrem/h and 160 mrem/h to 3 mrem/h and 8 mrem/h (outside edge), respectively. The bottom shows the same trend with distance. Note that the neutron shield and protective cover were not on the cask during these dose rate measurements because test lid and TC lances were being used. When the neutron shield and protective cover are in place, their presence will significantly reduce dose rates near the cask top.

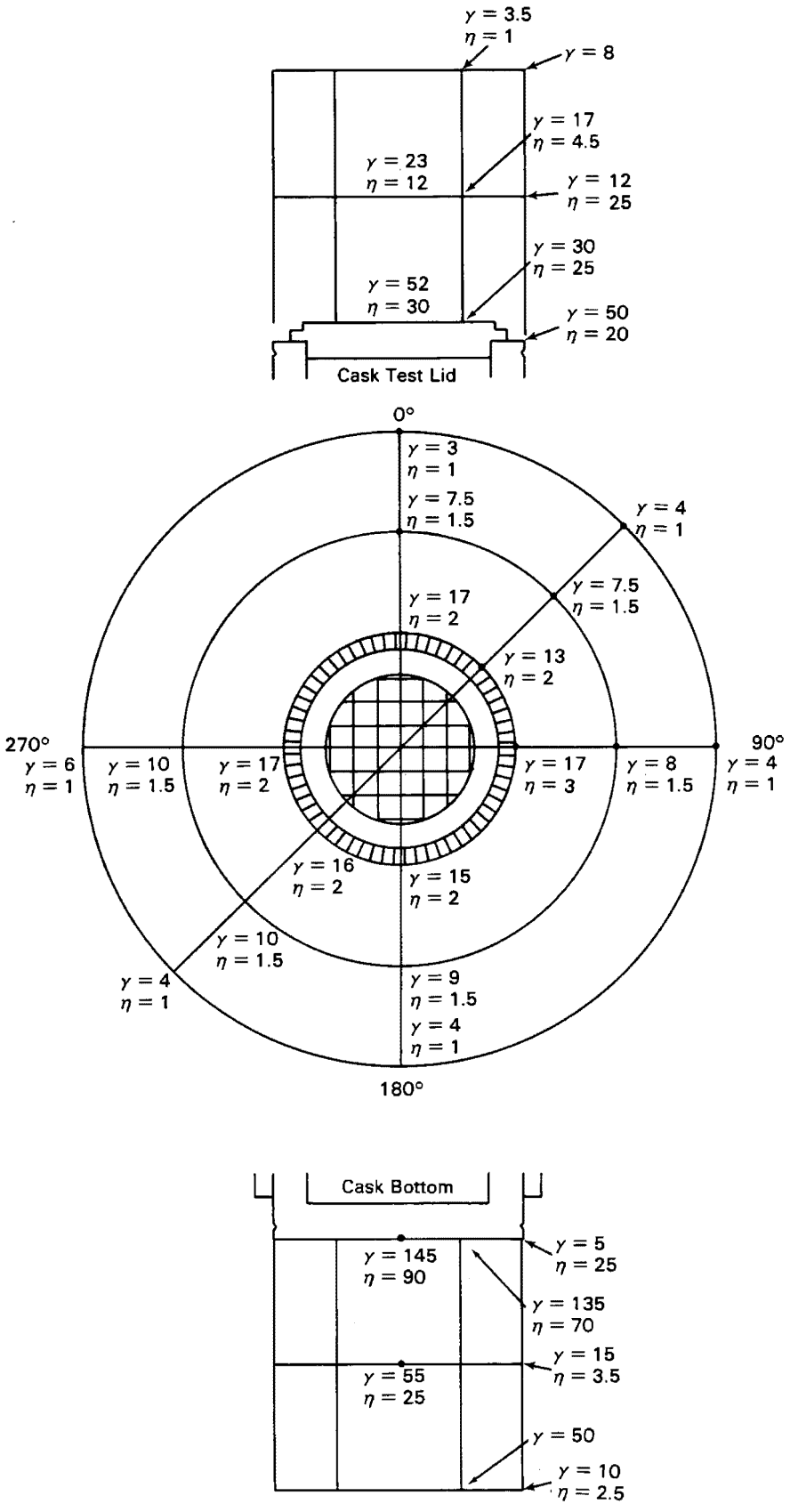

Figure 4-33. Dose Rates Measured On and Near Cask Surface (mrem/h)

Near the side of the cask at an elevation of L/2 (halfway up the cask) and peripheral angles of 0, 45, 90, 180, 225, and 270°, neutron dose rates were attenuated from 2 mrem/h at the surface to 1 mrem/h at a distance 2 m (6.6 ft) away. Likewise, gamma dose rates were attenuated from 13 to 17 mrem/h at the surface to 3 to 6 mrem/h at 2 m (6.6 ft). On the side, all peaks occurred within 2 m (6.6 ft) of the cask because all values at 2 m (6.6 ft) were less than those at 1 m (3.3 ft) adjacent to their respective peripheral locations.

The shielding performance of the cask met the design goal of less than 60 mrem/h on the side of the cask (4), except for peaks as high as 89 mrem/h near the ends. These peaks could easily be reduced with minor refinement involving adding gamma shielding adjacent to the top and bottom end fittings of the PWR spent fuel assemblies. In general, the dose rates on the lid were less than 90 mrem/h and should be less than 60 mrem/h when the neutron shield and protective cover are used during long-term storage. However, total dose rates on the top of the cask were as high as 316 mrem/h near the drain/fill flange. Total dose rates on the bottom of the cask were generally less than 200 mrem/h and should not be a problem during vertical storage. During horizontal storage or handling, temporary shielding could be placed near the bottom of the cask.

Section 5

COBRA-SFS ANALYSIS

The COBRA-SFS (Spent Fuel Storage) computer code was used to predict temperature and velocity distributions in the TN-24P spent fuel storage cask to assure allowable temperatures would not be exceeded and to further evaluate the code. Results were obtained for cask operation with vacuum, nitrogen, and helium backfills in vertical and horizontal orientations. Descriptions of the COBRA-SFS code, its modeling capabilities, the conservation equations, and geometry models and input are presented, as are comparisons of pretest and post-test code predictions with test data.

COBRA-SFS COMPUTER PROGRAM

The COBRA-SFS code is a steady-state, lumped-parameter, finite-difference computer code that predicts flow and temperature distributions in spent fuel storage systems and fuel assemblies under mixed and/or natural convection conditions. Derived from the COBRA family of codes (15, 16, 17, 18), which have been extensively evaluated against in-pile and out-of-pile data, COBRA-SFS retains all the important features of the COBRA codes and extends the range of application to problems with two-dimensional radiation and conduction heat transfer. This capability permits analyses of single- and multiassembly spent fuel storage systems with unconsolidated or consolidated fuel, with a variety of fill media (19, 20, 21, 22, 23, 24).

COBRA-SFS provides finite-difference solutions to the equations governing mass, momentum, and energy conservation for incompressible flows. Analyses are conducted using a subchannel approach in which the flow areas of assemblies or storage systems are divided axially into discrete control volumes for which the conservation equations of mass, momentum, and energy are written. These equations are then solved using an iterative implicit method. The energy equations for the coolant, rod cladding, fuel, and structural members (slabs) are solved implicitly by iteration, but simultaneously in a plane. Axial conduction in the structural members is considered. A nonparticipating media, gray body radiation heat transfer model also allows two-dimensional radiant heat exchange among all solid members in an enclosure and is iteratively coupled to the rod and wall energy equations.

The flow field may be either user-prescribed or internally calculated as a function of the gravitational and dynamic pressure losses. Specifications of heat losses from the boundary may vary circumferentially and/or axially, and can include both radiation and convection heat transfer. Axial heat transfer from the subchannel model to plenum regions (regions above and below the fuel assemblies) also can be modeled.

In the following sections, the COBRA-SFS modeling capabilities are outlined, and a brief description of the conservation equations is given.

Modeling Capabilities

COBRA-SFS allows simulations of a wide range of dry storage systems via input instructions. In addition to the multiassembly cask analysis described in this report, applications have included analyses of single-assembly spent fuel storage systems under multiple orientations and fill media (20), multiassembly systems with unconsolidated spent fuel (22, 23), and analyses of both single- and multiassembly consolidated fuel storage systems (19, 21, 24). The code contains thermal-hydraulic models for pressure drop, turbulent mixing, diversion crossflow, buoyancy-induced flow recirculation, and conduction and radiation heat transfer. A versatile fuel rod model allows simulation of consolidated fuel assemblies. The code's capabilities and limitations are outlined in Table 5-1.

Conservation Equations

The COBRA-SFS code solves the conservation equations of mass, momentum, and energy in a fuel assembly or fuel storage system using finite difference equations derived by performing suitable balances on finite control volumes. Empirical relationships are used where needed to close the set of equations.

The fluid control volume for continuity, axial momentum, and energy is characterized by a flow cross-sectional area, A; an axial length, Δx; and a gap width, S, for the connection between itself and adjacent control volumes. Figure 5-1 shows the relationship of a subchannel control volume to a fuel storage system; a typical subchannel control volume is also displayed. Any series of control volumes connected axially is considered a subchannel. In the following equations, the finite-difference terms are presented with the corresponding word definitions given in brackets immediately below each equation. The list of symbols in the Nomenclature section of this document should be referred to for explanation of the notation.

Table 5-1

COBRA-SFS CAPABILITIES AND LIMITATIONS

Modeling Capabilities	Lumped parameter	Multiple flow regions
	Steady state	Fluid conduction and turbulent mixing
	Triangular, square, or consolidated rod arrays	Pressure drop model (network and subchannel)
	Recirculating flows	Variable property rod model
	Zero net flow solution	Prescribed heat flux
	Interassembly and intra-assembly heat transfer	Plenum heat flux
	Nonparticipating radiation (planar)	Use of specified or prescribed flow regions
	Mixed geometry	Variable fluid properties
	Variable axial grid spacing	
Program and I/O Control	Constant prescribed flow	
	Zero net flow	
	Restart and post-processing dump	
	Decoupled hydrodynamics (no buoyancy)	
	Fully coupled hydrodynamics	
	Echoed input	
	Result execution and time monitoring	
	Variable/constant fluid properties	
	Pressure drop initialization scheme	
	Data "roll" option for large problems	
Limitations and Assumptions	Incompressible flow	
	Lumped parameter approach	
	No free-field capability	
	One-dimensional boundary heat transfer	

Continuity Equation (for subchannel i)

$$\overline{A}\,\frac{\rho - \rho^{n}}{\Delta t}\,j = \frac{v_{j-1}A_{j-1}\rho^{*}_{j-1}}{\Delta x_j} - \frac{v_j A_j \rho^{*}_j}{\Delta x_j} - \sum_{k\epsilon\Psi_i} e_{ik}(u_k S_k \rho^{*}_k)_j$$

$$\begin{bmatrix}\text{mass}\\ \text{storage}\end{bmatrix} = \begin{bmatrix}\text{mass transported}\\ \text{axially}\end{bmatrix} + \begin{bmatrix}\text{mass transported}\\ \text{laterally}\end{bmatrix} \qquad (5\text{-}1)$$

The asterisk denotes that donor cell values are convected by the velocity v.

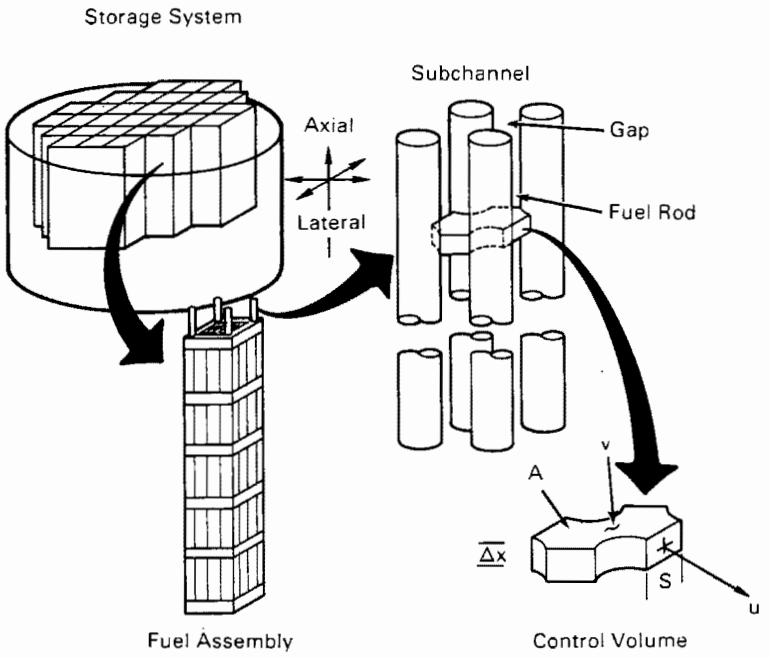

Figure 5-1. Subchannel Definition

Fluid Energy Equation (for channel i)

$$\overline{A}\,\frac{\rho h - (\rho h)^{n}}{\Delta t}\,j = \frac{v_{j-1}A_{j-1}\rho^{*}_{j-1}h^{*}_{j-1}}{\Delta x_j} - \frac{v_j A_j \rho^{*}_j h^{*}_j}{\Delta x_j} - \sum_{k\epsilon\Psi_i} e_{ik}\left(u_k S_k \rho^{*}_k h^{*}_k\right)_j$$

$$\begin{bmatrix}\text{energy}\\ \text{storage}\end{bmatrix} = \begin{bmatrix}\text{energy transported}\\ \text{axially}\end{bmatrix} + \begin{bmatrix}\text{energy transported}\\ \text{laterally}\end{bmatrix}$$

$$+ \sum_{n\epsilon\lambda_i} \frac{A_{HTR}H_R}{\Delta x_j}\left(T_{c_n} - T\right) + \sum_{m\epsilon\tau_i} \frac{A_{HTW}H_W}{\Delta x_j}\left(T_{w_m} - T\right)$$

$$+ \quad [\text{rod heat flux}] \quad + \quad [\text{wall heat flux}]$$

$$+ \sum_{k\epsilon\Psi_i} e_{ik}S_k K_k \frac{T_{II} - T_{JJ}}{\ell_k Z_k} + \sum_{k\epsilon\Psi_i} e_{ik}W_T\left(h_{II} - H_{JJ}\right)$$

$$+ \begin{bmatrix}\text{conductive heat}\\ \text{transfer laterally}\end{bmatrix} + [\text{turbulent energy exchange}] \qquad (5\text{-}2)$$

All other forms of energy transport that are not explicitly represented in Equation (5-2) (e.g., potential and kinetic energy) have been neglected.

Axial Momentum Equation (for channel i)

$$\overline{A}\,\frac{\rho v - (\rho v)^n}{\Delta t}_j = \frac{A_{j-1} v_{j-1} v^*_{j-1} \rho^*_{j-1}}{\Delta x_j} - \frac{A_j v_j v^*_j \rho^*_j}{\Delta x_j} - \sum_{k\varepsilon\Psi_i} e_{ik} \left(u_k S_k v^*_k \rho^*_k\right)_j$$

$$\begin{bmatrix}\text{axial}\\ \text{momentum}\\ \text{storage}\end{bmatrix} = \begin{bmatrix}\text{axial momentum}\\ \text{transported}\\ \text{axially}\end{bmatrix} + \begin{bmatrix}\text{axial momentum}\\ \text{transported}\\ \text{laterally}\end{bmatrix}$$

$$+ \overline{A}_j \frac{P_{j-1} - P_j}{\Delta x_j} + \sum_{k\varepsilon\Psi_i} e_{ik} w_T \left(v_{II} - V_{JJ}\right)$$

$$\begin{bmatrix}\text{pressure}\\ \text{gradient}\end{bmatrix} + \begin{bmatrix}\text{turbulent momentum}\\ \text{exchange}\end{bmatrix}$$

$$- \frac{1}{2}\left(\frac{f}{D_h} + \frac{C}{\Delta x_j}\right) \rho_j v_j |v_j| A_j - A\,\rho g \cos\theta$$

$$- \begin{bmatrix}\text{irreversible friction}\\ \text{and form losses}\end{bmatrix} - [\text{gravitational head}] \qquad (5\text{-}3)$$

In the derivation of the axial momentum equation, it is assumed that all irreversible losses can be obtained by use of suitable friction factors and loss coefficients applied to the bulk velocity. Also, it is assumed that pressure changes linearly along the control volume, and the shear stress terms due to flow in the adjacent subchannels can be neglected.

Transverse Momentum Equation

$$S\Delta x_j \frac{\rho u - (\rho u)^n}{\Delta t}_k = S_k v_{j-1} \rho^*_{j-1} u^*_{j-1} - S_k v_j \rho^*_j u^*_j$$

$$\begin{bmatrix}\text{lateral}\\ \text{momentum}\\ \text{storage}\end{bmatrix} = \begin{bmatrix}\text{transverse momentum}\\ \text{transported axially}\end{bmatrix}$$

$$+ \left(P_{II} - P_{JJ}\right)_{j-1} \frac{S_k \Delta x_j}{\ell_k} - C_T u_k u_k \frac{\rho S \Delta x_j}{2\ell_k}$$

$$+ [\text{pressure gradient}] - \begin{bmatrix}\text{irreversible form and}\\ \text{friction loss}\end{bmatrix} \qquad (5\text{-}4)$$

The momentum control volume length, ℓ, and gap width, S, define a transverse momentum control volume as shown in Figure 5-2. Inside this control volume, the transverse velocity is normal to the transverse gap; the flow is assumed to have no transverse component outside the transverse momentum control volume. A further assumption in the transverse momentum equation is that there are no applied body forces in the transverse direction.

Fuel Rod and Cladding Energy Equations

$$y_c \rho_c c_c \frac{T_c - T_c^n}{\Delta t} = \sum_{n \epsilon \gamma_i} H_r (T_{c_n} - T) - H_g \frac{R_f}{R_c} (T_{fs} - T_c)$$

$$\begin{bmatrix}\text{energy} \\ \text{storage}\end{bmatrix} = \begin{bmatrix}\text{convective} \\ \text{transfer to} \\ \text{the fluid}\end{bmatrix} + \begin{bmatrix}\text{heat transfer} \\ \text{from fuel}\end{bmatrix}$$

$$+ \sigma \sum_{n \epsilon \zeta_i} F_{in} (T_c^4 - T_{c_n}^4) + \sigma \sum_{m \epsilon \beta_i} F_{im} (T_c^4 - T_{w_m}^4)$$

$$+ \begin{bmatrix}\text{radiation heat} \\ \text{transfer from} \\ \text{rods}\end{bmatrix} + \begin{bmatrix}\text{radiation heat} \\ \text{transfer from} \\ \text{walls}\end{bmatrix} \quad (5\text{-}5)$$

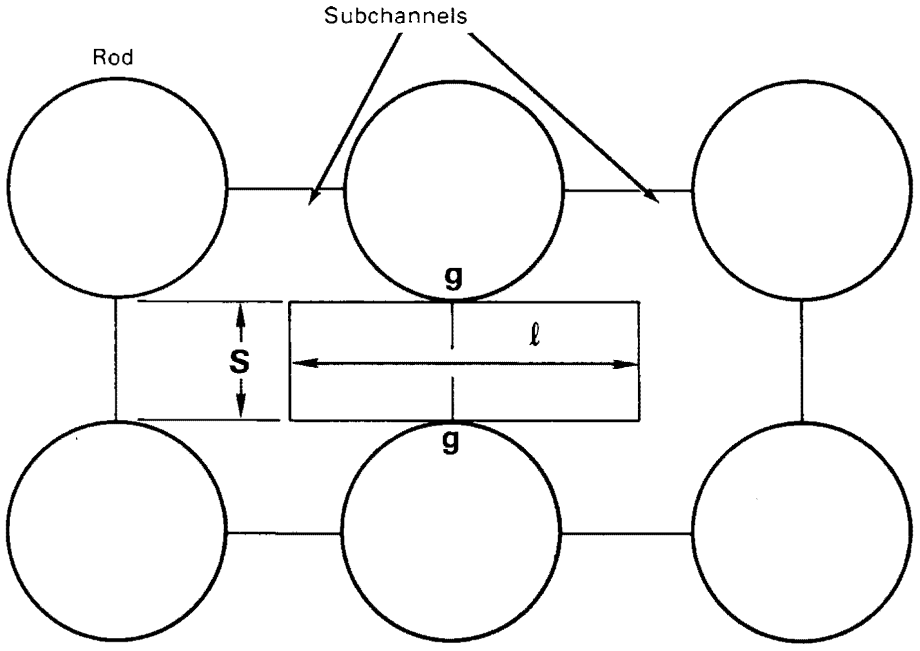

Figure 5-2. Transverse Momentum Control Volume

By assuming that 1) there is no heat transfer axially, 2) the heat is generated uniformly throughout the fuel at a given axial location, and 3) the fuel properties do not vary with the radial variation in temperature, the cladding temperature is obtained by performing a lumped energy balance on the cladding material at each axial level. In Equation (5-5), it is assumed that the temperature is uniform around the circumference of the cladding. The film coefficient, H_R, is given by user-specified correlations, and the gap conductance between fuel pellet and cladding, H_g, is assumed constant. F_{in} and F_{im} are gray body radiation exchange factors that account for multiple reflections within an enclosure. F_{in} is a coefficient for rod-to-rod heat transfer, while F_{im} is a coefficient for rod-to-slab heat transfer. Both are derived by assuming constant surface emissivity. The gray body exchange factors can be user-prescribed or calculated internally by specifying black body view factors and surface emissivity values.

Slab Energy Equations

$$\rho_w c_w t_w \frac{T_w - T_w^n}{\Delta t} = \sum_{n\varepsilon\xi_i} U\left(T_w - T_n\right) + \sigma \sum_{m\varepsilon\sigma_i} F_{im}\left(T_w^4 - T_m^4\right)$$

$$[\text{energy storage}] = \begin{bmatrix}\text{heat transfer}\\ \text{from adjacent}\\ \text{channels}\end{bmatrix} + \begin{bmatrix}\text{radiation heat}\\ \text{transfer from}\\ \text{walls}\end{bmatrix}$$

$$+ \sigma \sum_{n\varepsilon\kappa_i} F_{in}\left(T_w^4 - T_{c_n}^4\right) + q'''$$

$$+ \begin{bmatrix}\text{radiation heat transfer}\\ \text{from rods}\end{bmatrix} + \begin{bmatrix}\text{heat}\\ \text{generation}\end{bmatrix}$$

$$+ U_{j-1}\left(T_w - T_{w_{j-1}}\right) + U_{j+1}\left(T_w - T_{w_{j+1}}\right) + \sum_{m\varepsilon\alpha_i} U\left(T_w - T_{w_m}\right)$$

$$+ [\text{axial conduction heat transfer}] + \begin{bmatrix}\text{heat transfer}\\ \text{from adjacent}\\ \text{walls}\end{bmatrix} \qquad (5\text{-}6)$$

As before, F_{im} and F_{in} are the gray body exchange factors from wall node i to wall node m and rod node n, respectively. Axial heat transfer from the walls to a plenum region can be included at the end axial levels.

COBRA-SFS MODELS AND INPUT

The TN-24P cask was analyzed using two different three-dimensional models. A one-eighth section model was used to investigate the cask thermal response in a vertical orientation, while a one-half section model was used to analyze the cask when in a horizontal orientation. The smaller, less expensive model was designed for cases in which the cask internals are centered within the cask, an assumption applied only when the cask was in an upright position. For the horizontal orientation, it is important to model basket shift and the effect of fuel assemblies moving against basket fuel tube walls. For this reason, the one-half symmetry model was also developed. These models, along with boundary specifications and properties used, are described in the following sections.

One-Eighth Section Cask Model

The COBRA-SFS one-eighth section model consisted of 18 uniform axial levels as depicted in Figure 5-3. Each axial level comprised 51 wall nodes, 386 subchannels, and 450 rod nodes (Figure 5-4).

The wall nodes included 27 basket nodes, 12 cask body nodes, 4 neutron shield nodes, and 8 cask shell nodes. The four outermost shell nodes are zero-thickness nodes that represent the cask surface temperature for the purpose of accurately calculating the contribution of radiation and convection heat transfer to the environment.

One of the lines of symmetry used to define the one-eighth section model runs through two of the basket fuel tubes. Fuel assemblies in these locations were modeled with one rod surface node per rod, for a total of 120 rod surface nodes. This representation, along with the layout of the 136 fluid subchannels used to describe the flow, is shown in Figure 5-5. In the noding of the full fuel assemblies, the flexibility of the COBRA-SFS subchannel approach was used to selectively lump rods together and channels together to decrease the size of the computational model, as displayed in Figure 5-6. The 225 rods were represented by 105 lumped rods. The flow area within the assemblies was modeled by 57 channels. Previous work (24) has demonstrated the validity of combining together rods with surface temperatures of near the same magnitude to form a single rod surface node. Before the rod lumping pattern was selected, a simulation was carried out with one-rod/one-surface node logic. The lumping pattern was then developed based on the predicted rod surface temperatures. The thermocouple lance locations were modeled individually as shown in Figure 5-6. This facilitated data comparison with the thermocouple measurements.

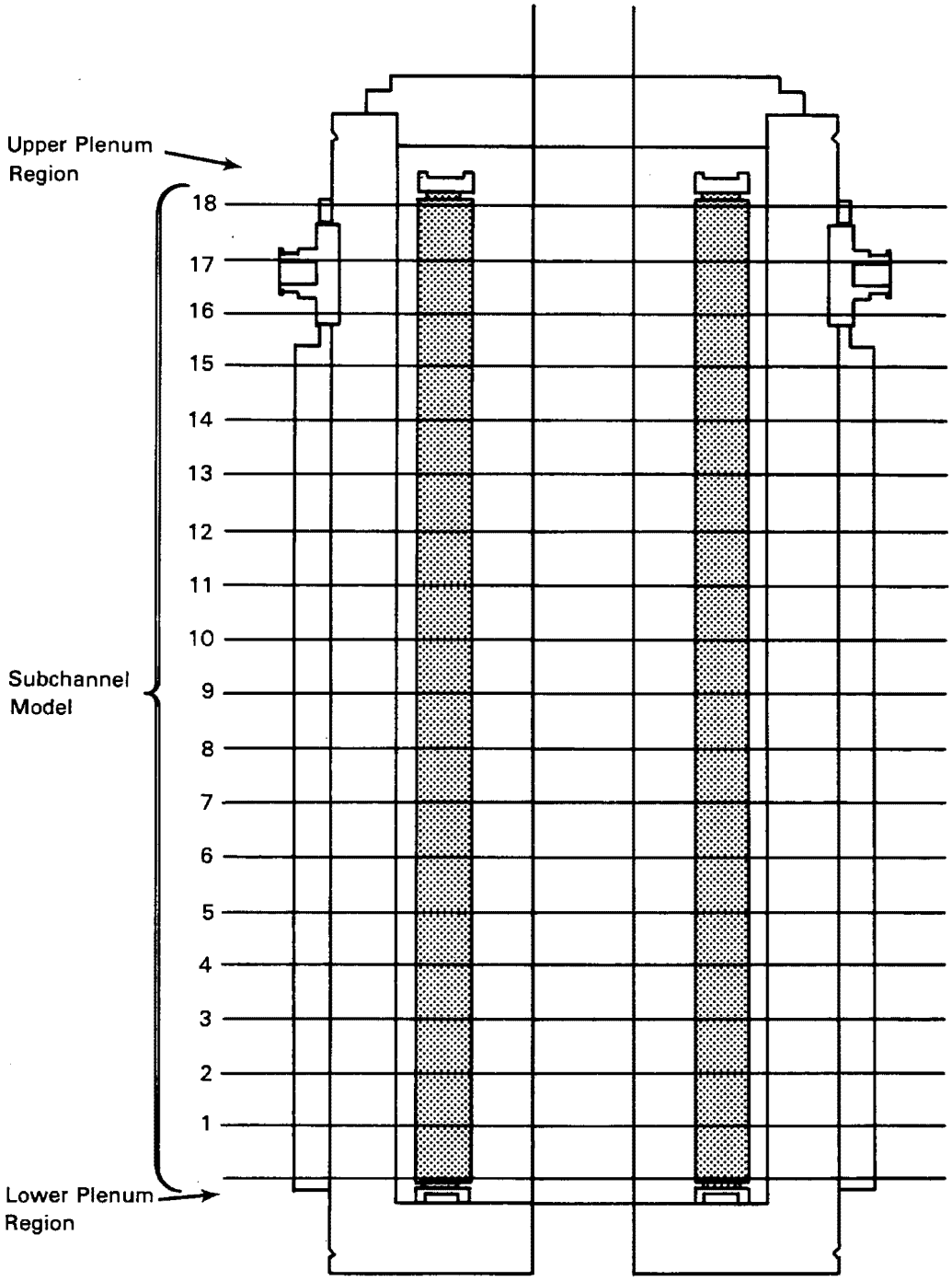

Figure 5-3. Axial Computational Cask Model

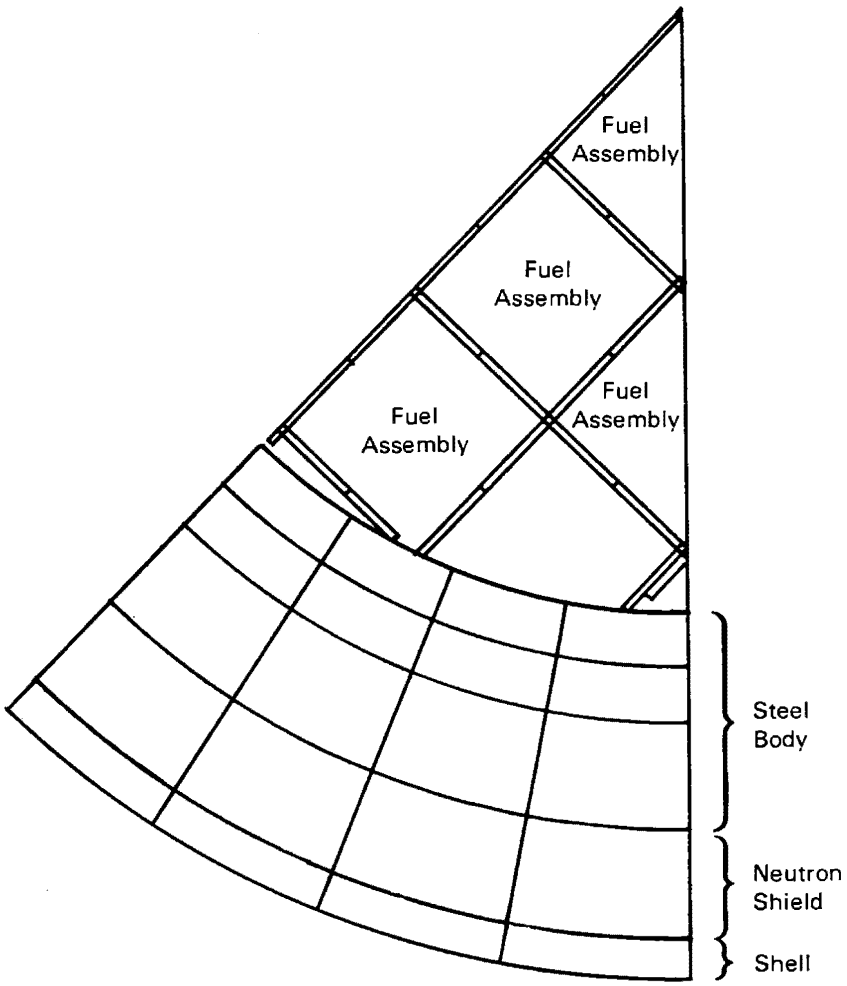

Figure 5-4. One-Eighth Transverse Section Computational Cask Model

One-Half Section Cask Model

An expanded model was necessary to account for asymmetries in heat transfer paths that occurred when the cask was in a horizontal orientation. The asymmetries resulted from two effects: 1) the unconstrained basket shifting downward to contact the lower inner cask surface, and 2) the fuel assemblies shifting within the basket fuel tubes. The one-half symmetry model that accounts for these effects is presented in Figure 5-7. In this model, 191 wall nodes were used; 95 of those were basket nodes, 48 were cask body nodes, 16 were neutron shield nodes, and 32 were cask shell wall nodes. All of the fuel assemblies in the one-half symmetry model were represented by the same lumping logic as used in the one-eighth symmetry full fuel assembly representation.

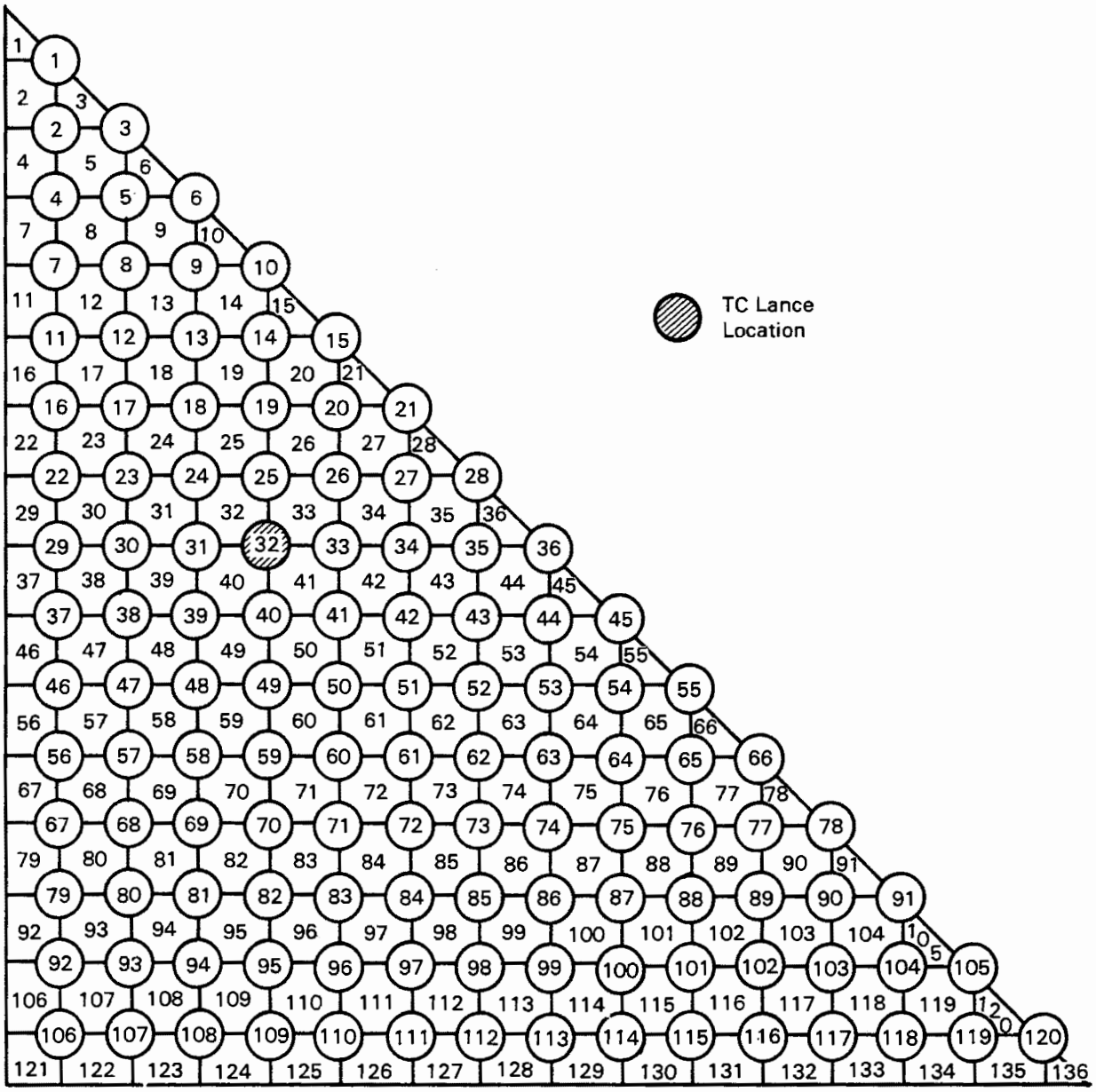

Figure 5-5. One-Half Transverse Fuel Assembly Rod and Subchannel Computational Model

Heat Transfer Models

The axial decay heat profile displayed in Figure 3-18 was applied to all of the assemblies. The assembly decay heat profiles were calculated by the ORIGIN2 computer code (8), based on average gamma scans from similar Turkey Point PWR spent fuel assemblies. The one-eighth section model incorporated the decay heat rates

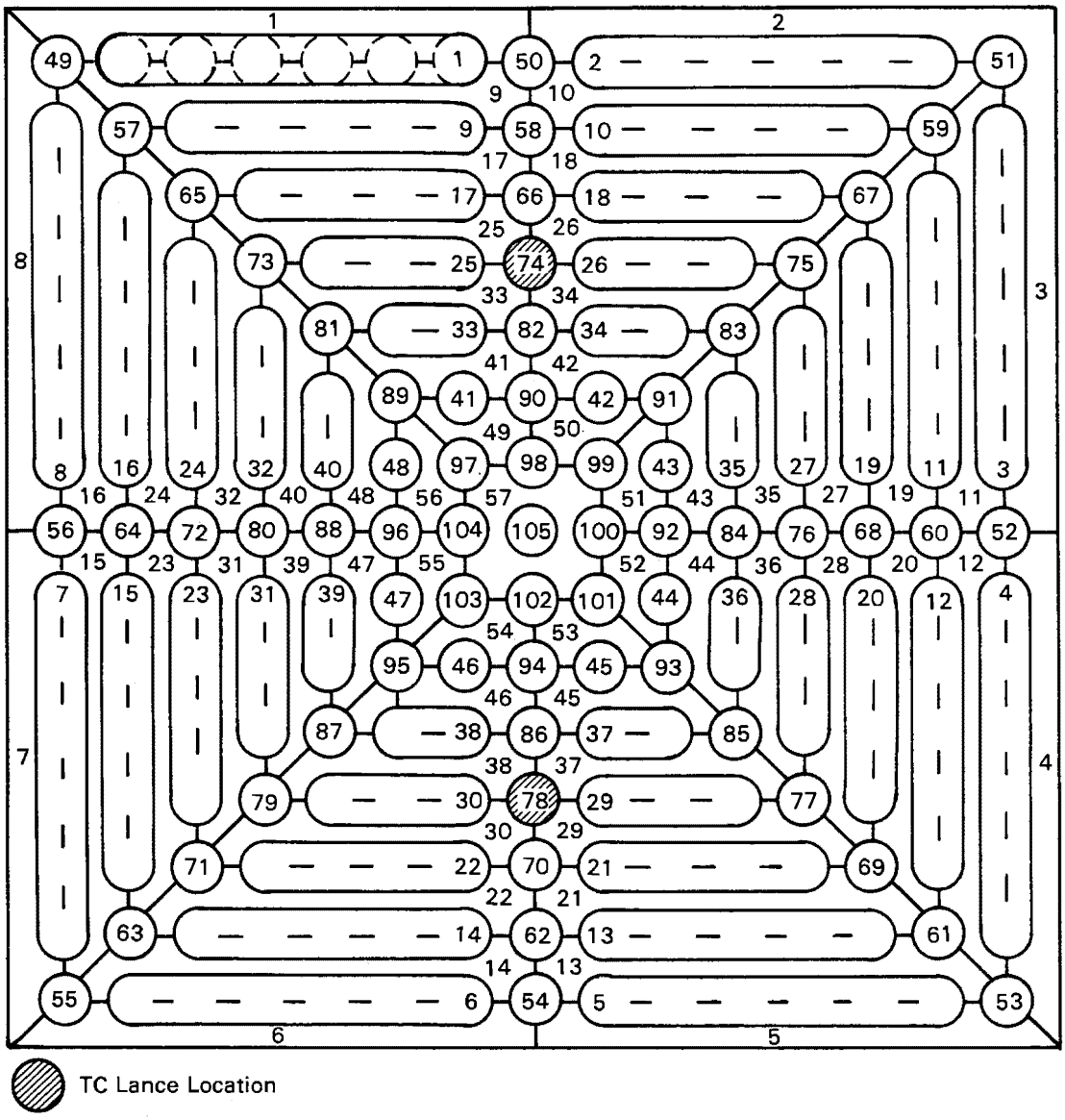

Figure 5-6. Full Transverse Fuel Assembly Lumped Rod and Lumped Channel Computational Model

from quadrant D shown in Figure 3-17. Assembly decay heat rates for the one-half section model were representative of quadrants C and D. The total decay heat rates ranged from 21 kW to 23 kW, and a uniform radial power distribution within each fuel assembly was assumed.

Decay heat from the fuel assemblies is removed by conduction, convection, and radiation heat transfer. The following is a discussion of COBRA-SFS modeling of each of these modes.

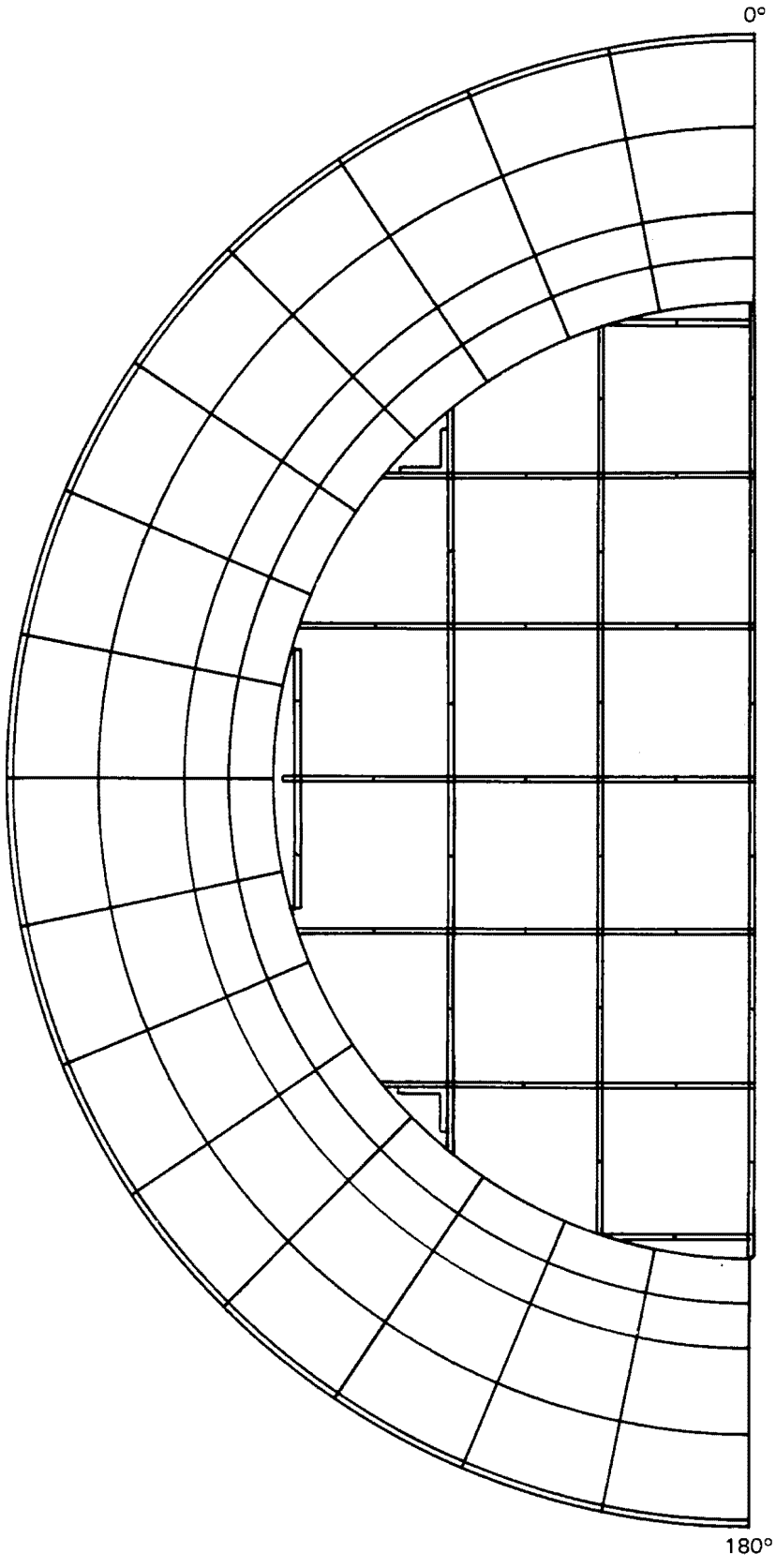

Figure 5-7. One-Half Transverse Section Computational Cask Model

Fluid-fluid conduction between neighboring subchannels was modeled using a transverse control volume defined by a gap width, a centroid-to-centroid length, and an axial length. Axial fluid-fluid conduction was neglected.

Conduction heat transfer in the walls was modeled in the radial, circumferential, and axial directions via an input specification of thermal resistances between neighboring nodes. Each thermal resistance can reflect any combination of parallel and/or series resistance paths. An example of such a composite resistance in the TN-24P analyses is the polyethylene resin and copper fins, which formed the side neutron shield. In this region a resistance was calculated that represented the two parallel paths through the shield.

For the pretest analysis, conduction in the aluminum basket was limited to the radial direction, assuming significant resistance between the stacked aluminum plates that form the basket. The dominating resistance in the radial conduction path resulted from the gap between the aluminum basket and the inner cask wall. This resistance was calculated through an iterative procedure in which 1) the average basket temperature was predicted, 2) the expansion of the basket was determined, and 3) the gap resistance was calculated. Iteration on this term was necessary, as the average basket temperature was directly related to the gap resistance.

The contribution of convection heat transfer within the cask is dependent on the predicted flow field. For the TN-24P simulations, the flow field was obtained iteratively by adjusting the total pressure drop until 1) the pressure drop across all subchannels was equal and 2) the total net flow rate was zero. Therefore, the basket and the fuel assembly flow resistances were important convection parameters. The surface friction for all of the subchannels was approximated using a friction factor of $f = 100/Re$, which was derived for a square rod array with pitch-to-diameter ratios typical of PWRs (25).

Convective heat transfer from the rod and wall surfaces to the fluid was prescribed using a film coefficient having the form $Nu = 3.66$ (26). This correlation is the analytical solution of the energy equation for a constant temperature and fully developed temperature and velocity profiles in a circular tube. Previous work (22) that investigated the effect of various values of Nusselt number on COBRA-SFS temperature predictions determined that a value of 3.66 gave the best overall results for the nitrogen and helium fill media.

Radiation heat transfer was treated on an assembly-by-assembly basis. In each basket fuel tube containing a PWR fuel assembly, rod-rod, rod-wall, and wall-wall radiative heat transfer were modeled by specification of gray body exchange factors. The exchange factors for the fuel rods and walls were calculated using one-quarter pin surface segments and the cross-string correlation method of Hottel (27) to define the radiation view factors. This is a more exact approach than the assumption of uniform radiosity around a rod surface. Radiation exchange in the empty basket enclosures, which consisted of either basket walls, or basket walls and the inner cask wall, was determined using wall-wall view factors input by the user. The COBRA-SFS code used these factors along with appropriate emissivities to calculate the gray body exchange factors.

Boundary Specifications

The TN-24P COBRA-SFS model comprised three axial regions: 1) the main region containing the fuel assemblies, fuel basket, and cask body; 2) the upper plenum region; and 3) the lower plenum region. For each axial region, the boundary conditions were specified via heat transfer coefficients representing the heat transfer from the cask surface to ambient air. In this section the boundary conditions used for each model are described.

The outside cask surface was a painted, smooth surface. The heat removal rate from the cask side surfaces by natural convection was calculated using a modified version of the Nusselt number expression for vertical cylinders in air at 1 atm (28). The referenced expression was multiplied by a factor of 1.4 after earlier cask analyses underpredicted the surface to ambient heat transfer (22). The 1.4 multiplier was a modification based on sets of parameter studies from the referenced COBRA-SFS analyses:

$$Nu = 0.13\ (GrPr)^{1/3} \text{ (Original expression)} \qquad (5\text{-}7)$$

$$Nu = 0.18\ (GrPr)^{1/3} \text{ (Modified version).} \qquad (5\text{-}8)$$

The cask lid heat transfer to ambient was modeled by a natural convection expression for Nusselt number for a horizontal plate in air at 1 atm (28). Again, this expression was modified to reflect earlier work:

$$Nu = 0.14\ (GrPr)^{1/3} \text{ (Original expression)} \qquad (5\text{-}9)$$

$$Nu = 0.20\ (GrPr)^{1/3} \text{ (Modified version).} \qquad (5\text{-}10)$$

In the vertical orientation cases, the cask was placed on a rail car. The cask bottom to ambient air boundary condition assumed no natural convection in the pretest simulations, only conductance through the rail car followed by heat transfer to ambient via a heat transfer coefficient of the form Nu = 1.0, or h = k/d, where d was half of the distance between the rail car to the ground and k was the conductivity of nitrogen.

The radiation heat transfer from the top and side outer surfaces to the surrounding environment was a function of surface emissivity and the ambient conditions. In the pretest simulations, the ambient air was assumed to be a black body at a temperature of 18.25°C (65°F). The formulation for radiation heat transfer from the cask outer surface to ambient was identical to the expression for parallel plates:

$$q''_{rad} = \frac{1}{\frac{1}{\varepsilon_1} + \frac{1}{\varepsilon_2} - 1} \sigma \left(T_1^4 - T_2^4\right) \qquad (5\text{-}11)$$

The surface to ambient heat transfer correlations used in the pretest analyses are summarized in Table 5-2.

Material Properties

The material properties used for the TN-24P model are presented in Table 5-3. All surface emissivities and the greater portion of the solid thermal conductivities were provided by Transnuclear, Inc. The thermal properties of the solids were assumed constant, and properties of the fill gas were specified as a function of temperature.

Table 5-2

BOUNDARY CONVECTION HEAT TRANSFER CORRELATIONS

Type	Region	Natural Convection Component
Axial	Upper plenum	$Nu = 0.20\ (GrPr)^{1/3}$
Radial	Upper plenum	$Nu = 0.18\ (GrPr)^{1/3}$
Radial	Cask side	$Nu = 0.18\ (GrPr)^{1/3}$
Radial	Lower plenum	$Nu = 0.18\ (GrPr)^{1/3}$
Axial	Lower plenum	$Nu = 1.0$

Table 5-3

MATERIAL PROPERTIES

Thermal Conductivities, watt/m°C (Btu/ft-h-°F)			Surface Emissivities	
Steel cask body	41.5	(24.0)	Fuel rods	0.8
Polyethylene resin	0.2	(0.1)	Fuel basket	0.8
Aluminum basket	206.0	(119.0)	Plated cask surfaces	0.9
Copper fins	377.3	(218.0)	Painted cask surfaces	0.9
Steel shell	41.5	(24.0)	Copper fin surface	0.5
Polypropylene	0.2	(0.1)		

Modeling Uncertainties

The COBRA-SFS TN-24P model contained a number of uncertainties in cask design information that limited its ability to accurately predict the thermal performance of the cask. Separate effects analyses have shown that uncertainties in the following parameters account for the greater portion of the total uncertainty:

- The aluminum basket was designed to allow for thermal expansion in the radial direction; no mechanical connections existed between the inside cask wall and the basket. To approximate the thermal resistance attributed to the gap existing between the basket and the inside cask wall, an average basket temperature was predicted, a radial expansion calculated, and a new value for the gap determined. This iterative procedure assumed that the basket was originally centered within the cask (for the vertical orientation) and that the basket expanded uniformly.

- Each fuel assembly was assumed to be centered (again, only for vertical orientation), within the basket fuel tube such that the basket-to-outer rod distance was identical on all four sides of the fuel assembly, at all axial locations. It is more likely that the assembly is positioned off-center with axially varying distances to the basket walls.

- The heat transfer from the outside cask surface to ambient air through natural convection is difficult to predict accurately. The correlation used is based on a smooth, vertical surface in a static environment. Modifications were made to reflect experience gained from previous cask simulations; however, sensitivity to changes in this correlation are cask-dependent.

- The connection between the cask bottom and ambient was modeled as the sum of two resistances: 1) heat transfer through a simplified version of the rail car and 2) conduction through stagnant ambient air. This was a simplified approach, because the rail car acted as a fin.

- The lower plenum was modeled as an empty space in which fill gas was assumed to mix and achieve a constant temperature regardless of radial location within the cask. In reality, the plenum contained the lower unheated portions of the fuel assemblies, and the temperature of the fill gas probably varied as a function of radial position.

- The axial decay heat profile used in the COBRA-SFS analyses was not an experimentally measured quantity. Deviations from the true profile result in substantial differences in the predicted temperature as demonstrated by past cask analyses (23).

- Some uncertainty exists in the convective heat transfer coefficient used in the TN-24P models.

COBRA-SFS SIMULATIONS COMPARED TO TEST DATA

The two COBRA-SFS geometric models were used to predict temperature and velocity distributions within the TN-24P spent fuel storage cask. The analyses were conducted in two steps. First, a set of predictions was made using the pretest model. It is important to note that each pretest simulation was completed and reported prior to the completion of the corresponding experimental test run. Second, following comparisons of pretest predictions with data, justifiable improvements were identified. These changes were incorporated into the two models, and a set of post-test simulations conducted. The predictive capability of the COBRA-SFS computer code is assessed for the pretest and post-test simulations in the following sections.

Pretest Predictions Compared to Test Data

Comparisons are presented in three parts: 1) a summary of peak guide tube temperature predictions is compared to data for all six test runs; 2) pretest axial and radial temperature profiles are compared to data for helium, nitrogen, and vacuum fill gases in the vertical orientation, and 3) pretest axial and radial temperature profiles are compared to data for all three fill gases in the horizontal orientation. All stated percentage temperature deviations are based on the ambient-to-peak guide tube temperature difference.

Pretest Peak Temperature Predictions Compared to Test Data. The COBRA-SFS pretest comparisons with experimental data are summarized for the six test runs in bar chart format in Figure 5-8. Peak-to-ambient temperature comparisons for all six test runs are illustrated. All test runs were conducted with the cask located inside the TAN warm shop with an ambient temperature of approximately 18°C (65°F). The peak guide

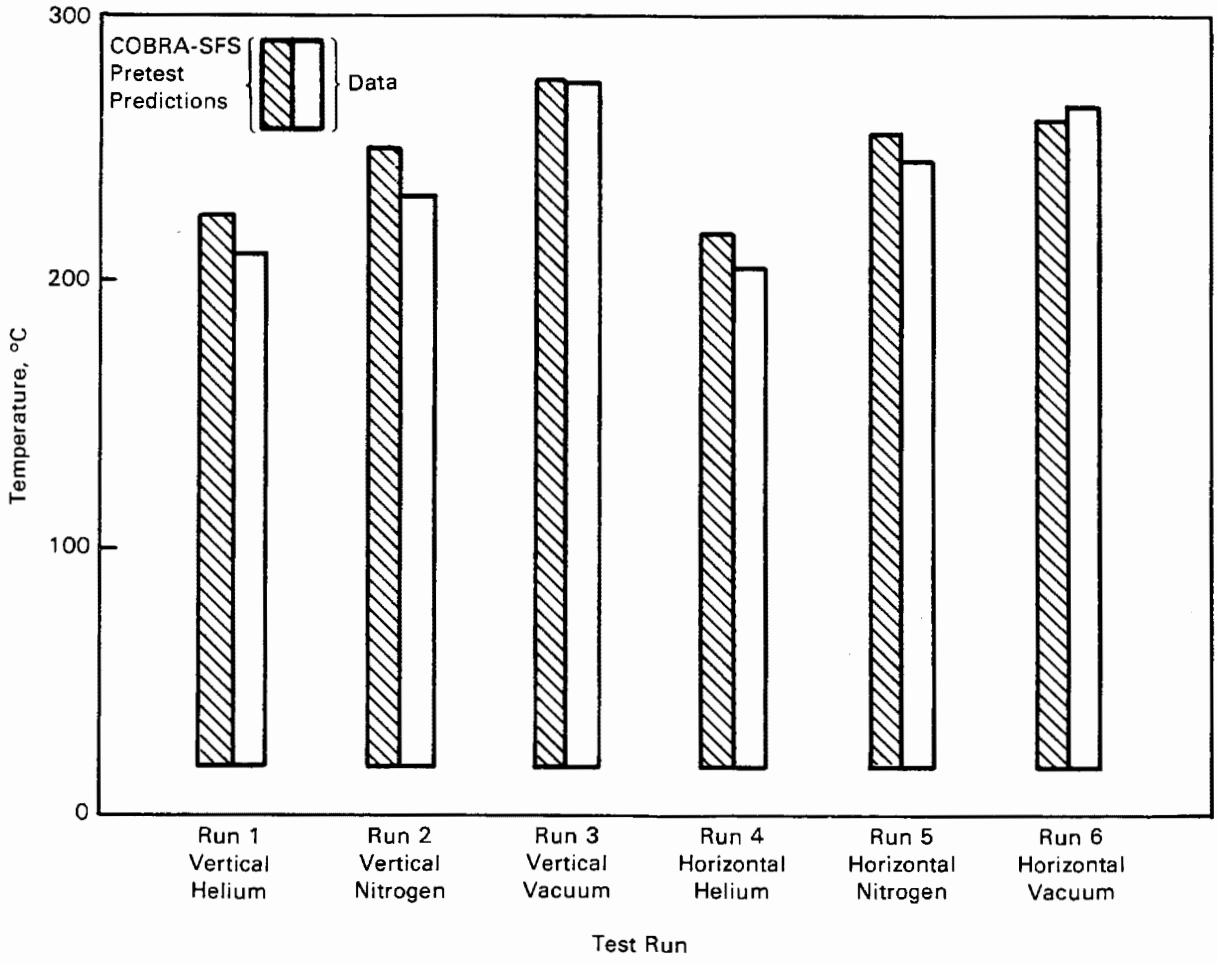

Figure 5-8. Pretest Peak Temperature Predictions Compared to Test Data

tube temperature for each case was located in the centermost assembly. The axial location of the peak temperature varied as a function of cask orientation and fill gas.

In general, the COBRA-SFS pretest predictions of peak guide tube temperatures agreed well with the experimental data. The largest variation occurred for the vertical nitrogen case, where a 9.1% (20°C) higher peak guide tube temperature was predicted. The mean difference between calculated and measured temperatures of the peak fuel tube for the six test runs was 4.3% (9°C), with a standard deviation of ±3.8% (±8.0°C). Only the horizontal vacuum simulation underpredicted (1.7%, 4°C) the peak fuel tube temperature. The test runs with the largest discrepancies between peak temperature predictions and data were the vertical helium and nitrogen fill gas cases. This finding is attributed to the insufficient axial heat-transfer to the

lower plenum and the absence of axial basket conduction in the pretest model. This will be described in more detail during the post-test discussions.

Pretest Vertical Predictions Compared to Test Data. The pretest axial temperature profile predictions for the vertical orientation with helium, nitrogen, and vacuum backfills are presented in Figures 5-9, 5-10, and 5-11. Predicted temperature profiles are given along with the discrete data measurements for the following locations: 1) the ambient temperature, 2) the outer cask surface at 0°, 3) a basket location, 4) guide tube location 4 in the fuel assembly in fuel tube D6, 5) guide tube location 6 in the fuel assembly in fuel tube D5, 6) guide tube location 4 in the fuel assembly in guide tube D4, and 7) guide tube location 5 in the fuel assembly in fuel tube D1 (see Figures 3-8 and 3-17). A detailed sketch of the locations for presented temperature profiles is shown on each figure.

The helium results given in Figure 5-9 clearly show overpredictions (30°C) by the pretest model; however, fairly good agreement between the radial temperature differences at the different axial locations is shown. The largest temperature deviations, which occur at the lower section of the cask, are the result of underestimated heat transfer to the plenum. The predicted peak temperature was 7.6% (15°C) higher than the data.

For the vertical nitrogen run, the effect of the insufficient heat transfer to the lower plenum from the TN-24P pretest model is apparent in Figure 5-10. The upward skew of the axial data indicates that significant convection occurred within the cask for a nitrogen fill gas. For this cask, the radial temperature difference comparisons are fairly good, but the model overpredicting the measured peak temperature by 9.1% (20°C).

Figure 5-11, the vertical vacuum test run comparison, shows good agreement (25°C) between the data and the COBRA-SFS pretest predictions. The lack of modeling axial conduction in the basket resulted in predicted temperature profiles that were less rounded near the end-points of the assembly active lengths. The temperature profiles in this nonconvection run directly reflect the assumed axial power profile. The peak temperature was overpredicted for the vertical vacuum test run by 0.4% (1.0°C) which indicates surface emissivities and thermal conductivities were satisfactorily selected.

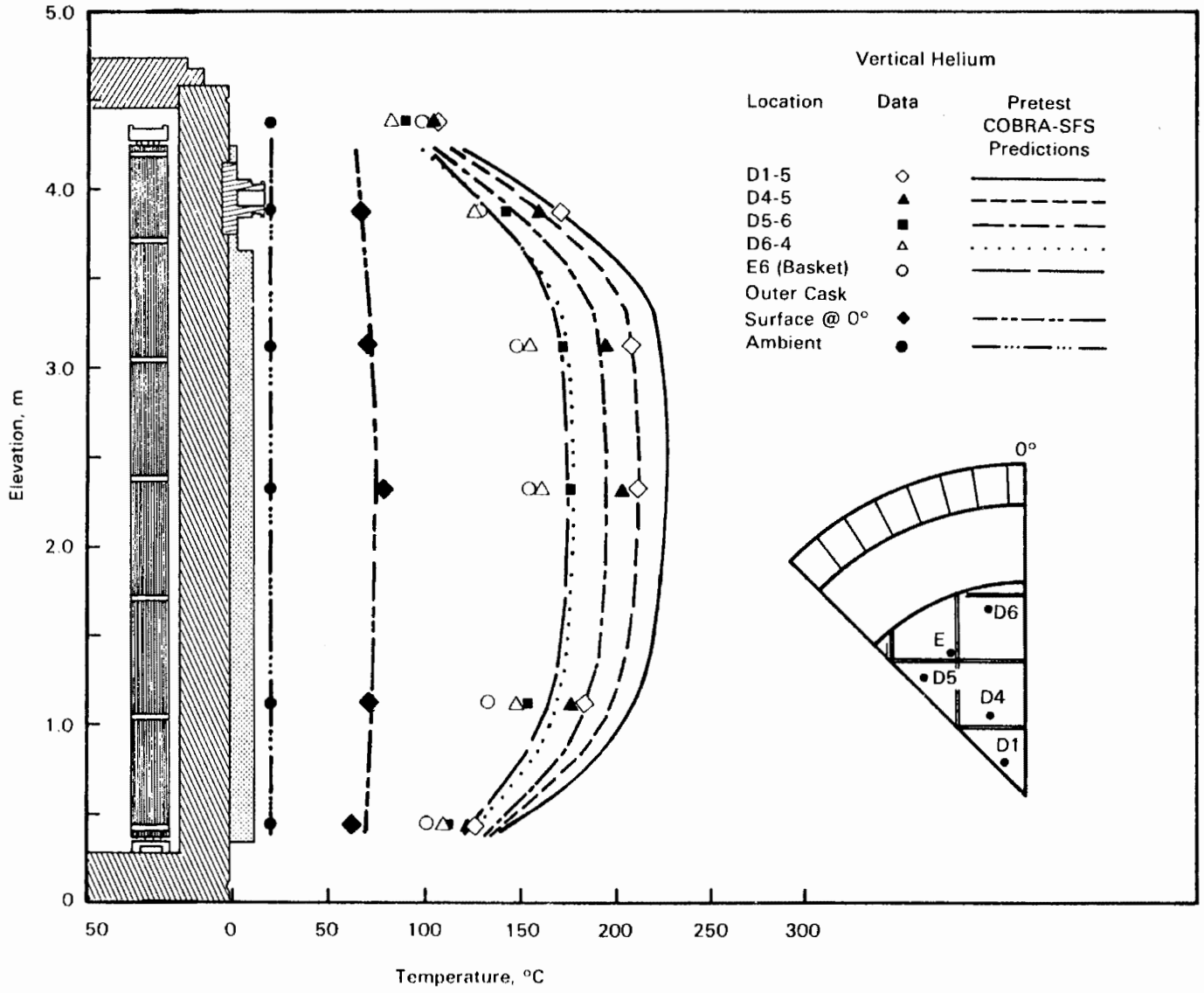

Figure 5-9. Pretest Vertical, Helium Axial Temperature Profile Predictions Compared to Test Data

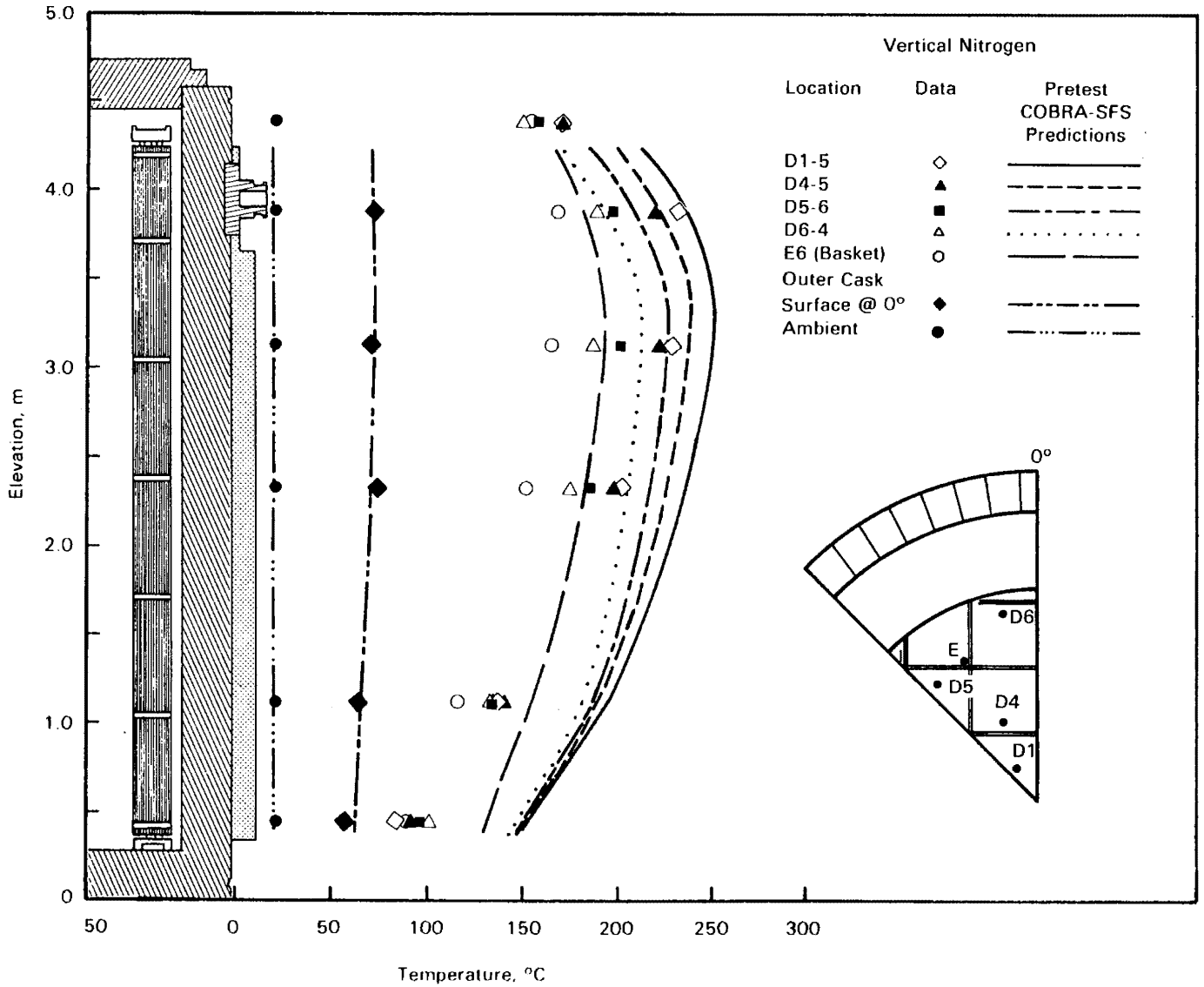

Figure 5-10. Pretest Vertical, Nitrogen Axial Temperature Profile Predictions Compared to Test Data

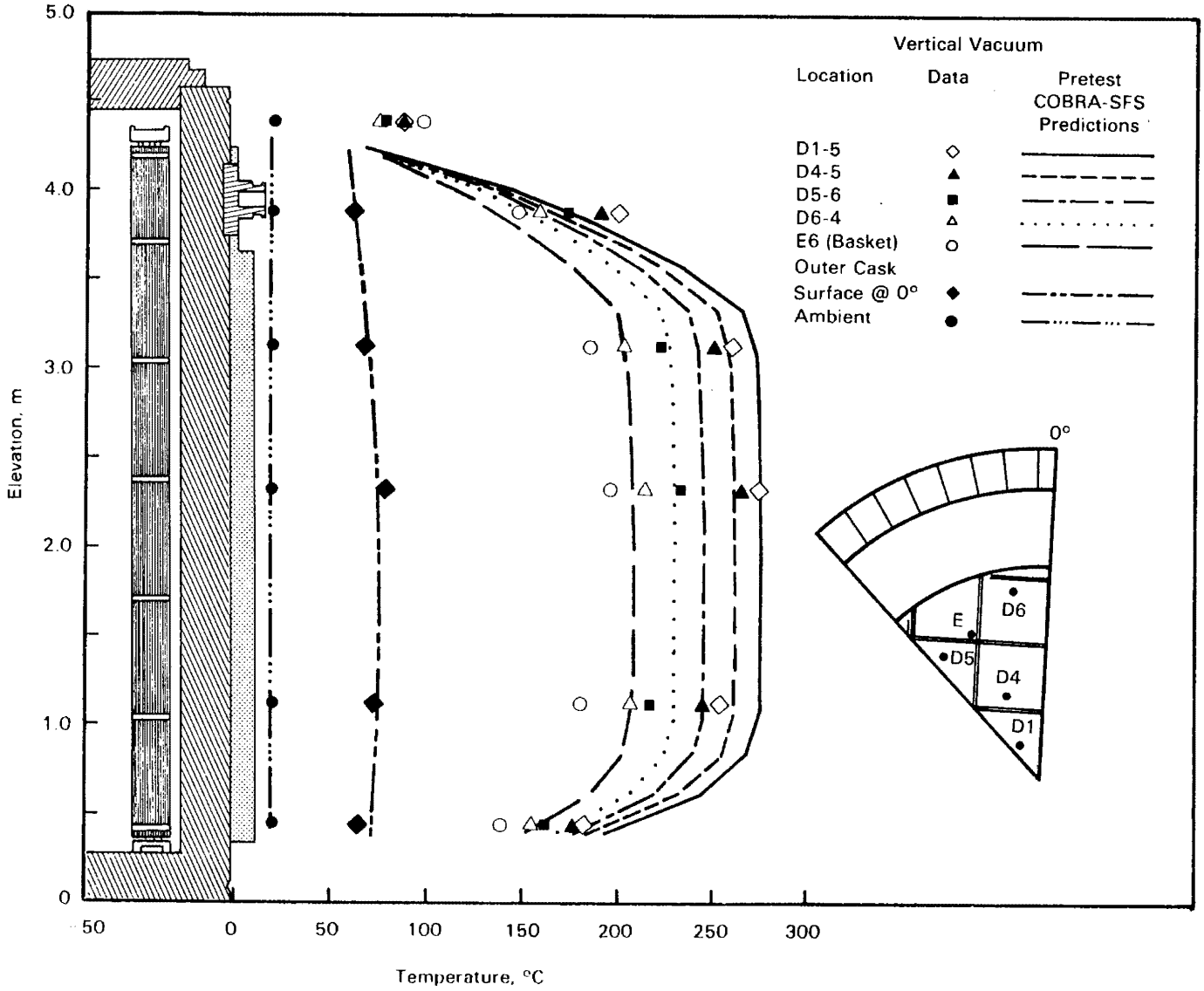

Figure 5-11. Pretest Vertical, Vacuum Axial Temperature Profile Predictions Compared to Test Data

The effect of fill gas on thermal performance is presented in Figure 5-12, which is a composite of the peak temperature profiles for each of the vertical orientation runs. A comparison of the vacuum and nitrogen test runs shows that convection within the cask is the sole reason for a 44°C lower peak temperature in the nitrogen fill case. Both cases used nitrogen properties in the conduction model; the only major difference was that the vacuum simulation had a negligible flow field. The presence of convection in the helium test run is indicated by the shape of the peak axial temperature profile which is skewed slightly towards the upper end of the basket.

Radial temperature profiles are presented in Figure 5-13, which clearly relates the distribution of thermal resistance through the cask for the vertical test runs. The radial profiles are given at the measured axial peak temperature location. The steepest temperature gradient within the cask occurred in the gap between the outer fuel assembly and the inside cask wall. This was particularly evident in the vacuum and nitrogen fill gas cases, where the gas conductivity is an order of magnitude less than that of helium. In the hottest case, the vacuum run, the predicted 84°C temperature drop across the gap represented 31% of the entire temperature drop through the cask. The copper fins embedded in the polyethylene resin neutron shield provided an excellent heat transfer path, with a maximum temperature drop of 18°C from the inside wall surface to the shell outer surface for the three vertical test runs. In all three test runs, the COBRA-SFS model showed good agreement (15°C) with measured guide tube temperatures in the radial direction. The greatest disagreement (23°C) occurred at the basket thermocouple location. Two possible reasons for the larger disagreement in basket temperature predictions are 1) the thermocouples may have been measuring a temperature between that of the basket and gas because of the attachment method and 2) the heat transfer between the basket and gas was lightly underpredicted.

Pretest Horizontal Predictions Compared to Test Data. Convection within the cask is assumed to be negligible in the horizontal orientation and is therefore not included in the COBRA-SFS model. However, two important effects that were accounted for are 1) shifting of the basket into contact with the inside cask wall at the lower side and 2) movement of fuel assemblies within each basket fuel tube to the lowest side. The axial temperature profiles shown in Figures 5-14, 5-15, and 5-16 for the horizontal orientation represent the same radial locations as in the vertical model.

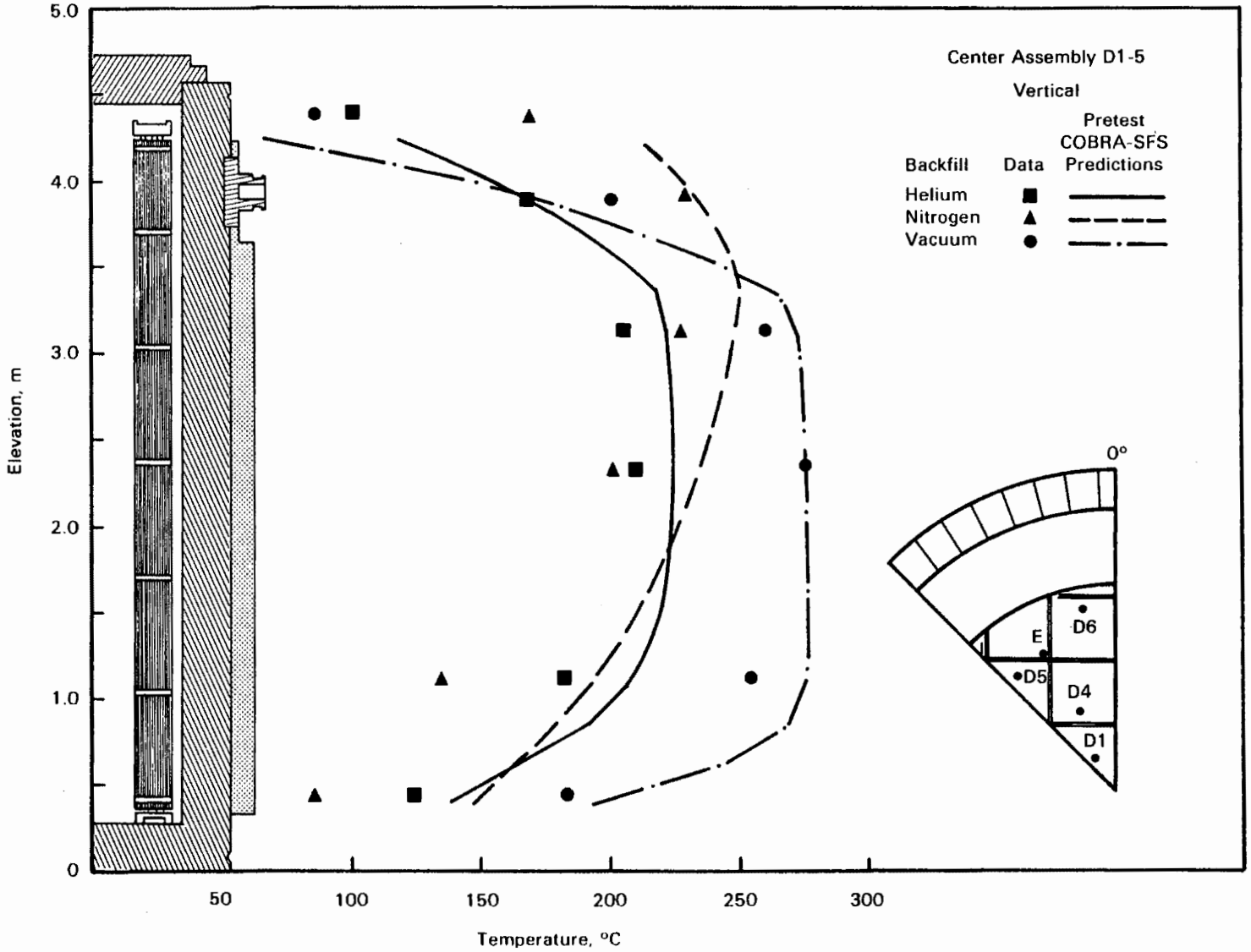

Figure 5-12. Pretest Vertical, Helium, Nitrogen, and Vacuum Axial Temperature Profile Predictions Compared to Measured Hot Assembly Data

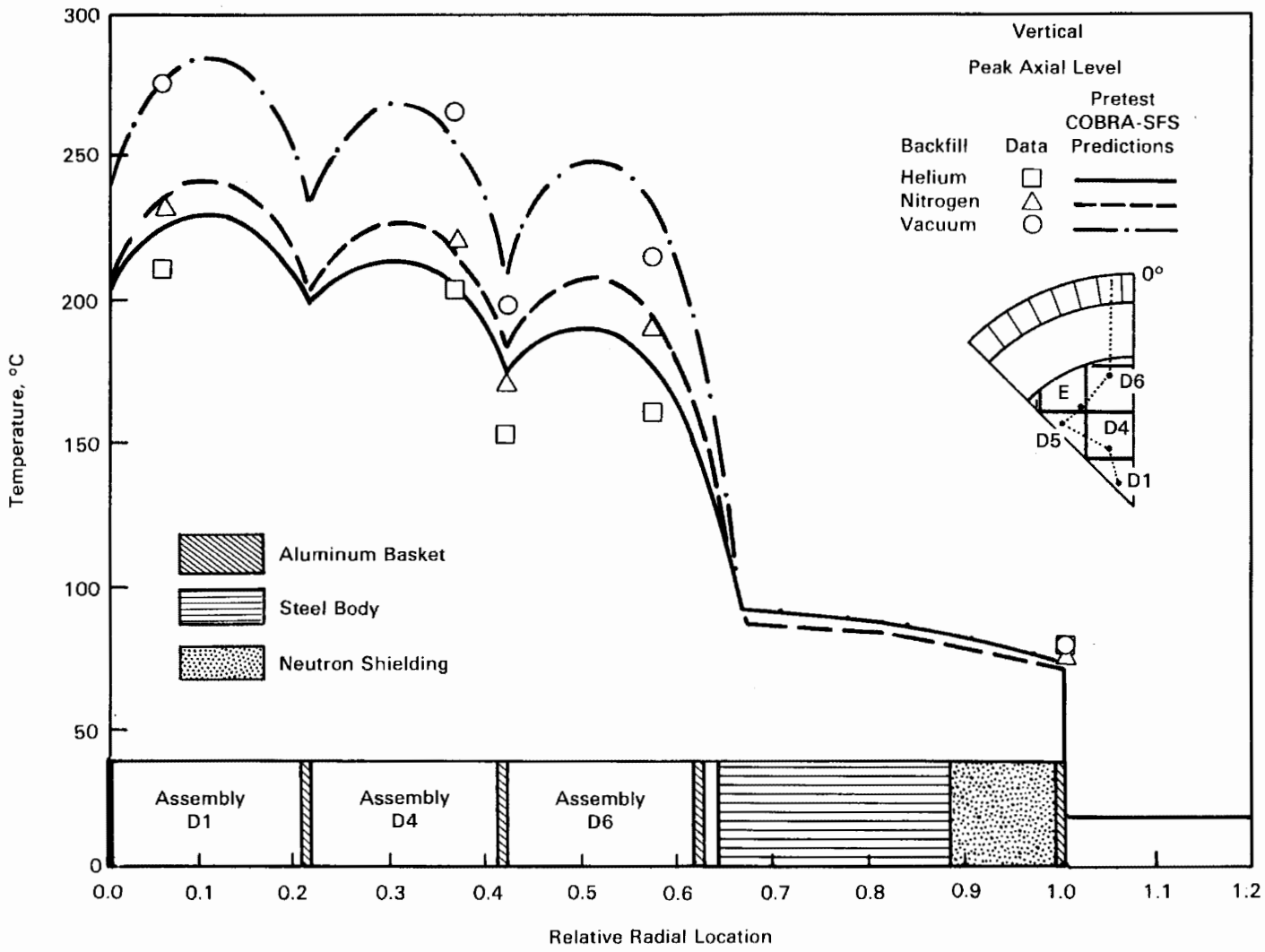

Figure 5-13. Pretest Vertical, Helium, Nitrogen, and Vacuum Radial Temperature Profile Predictions Compared to Test Data at Peak Temperature Axial Locations

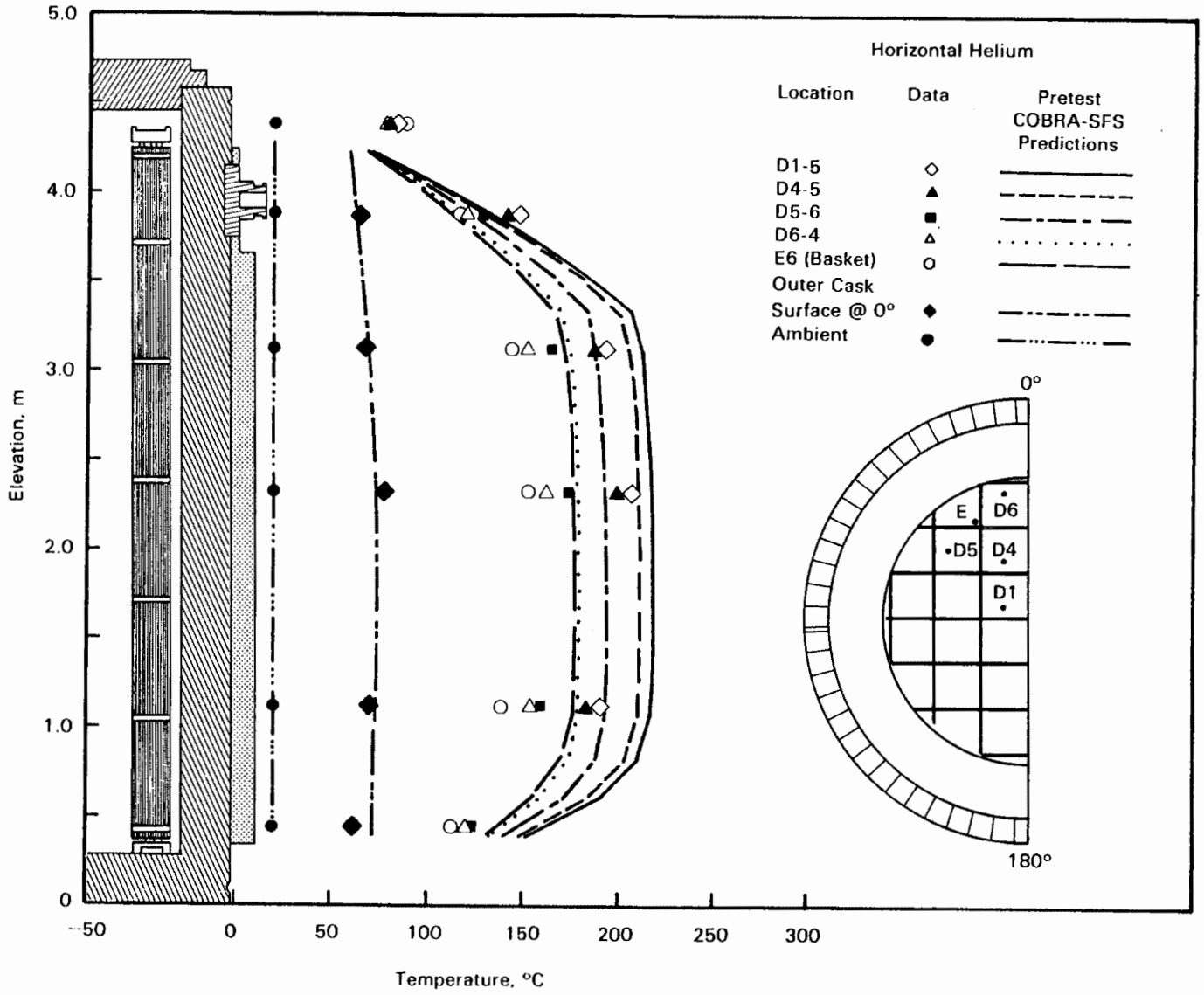

Figure 5-14. Pretest Horizontal, Helium Axial Temperature Profile Predictions Compared to Test Data

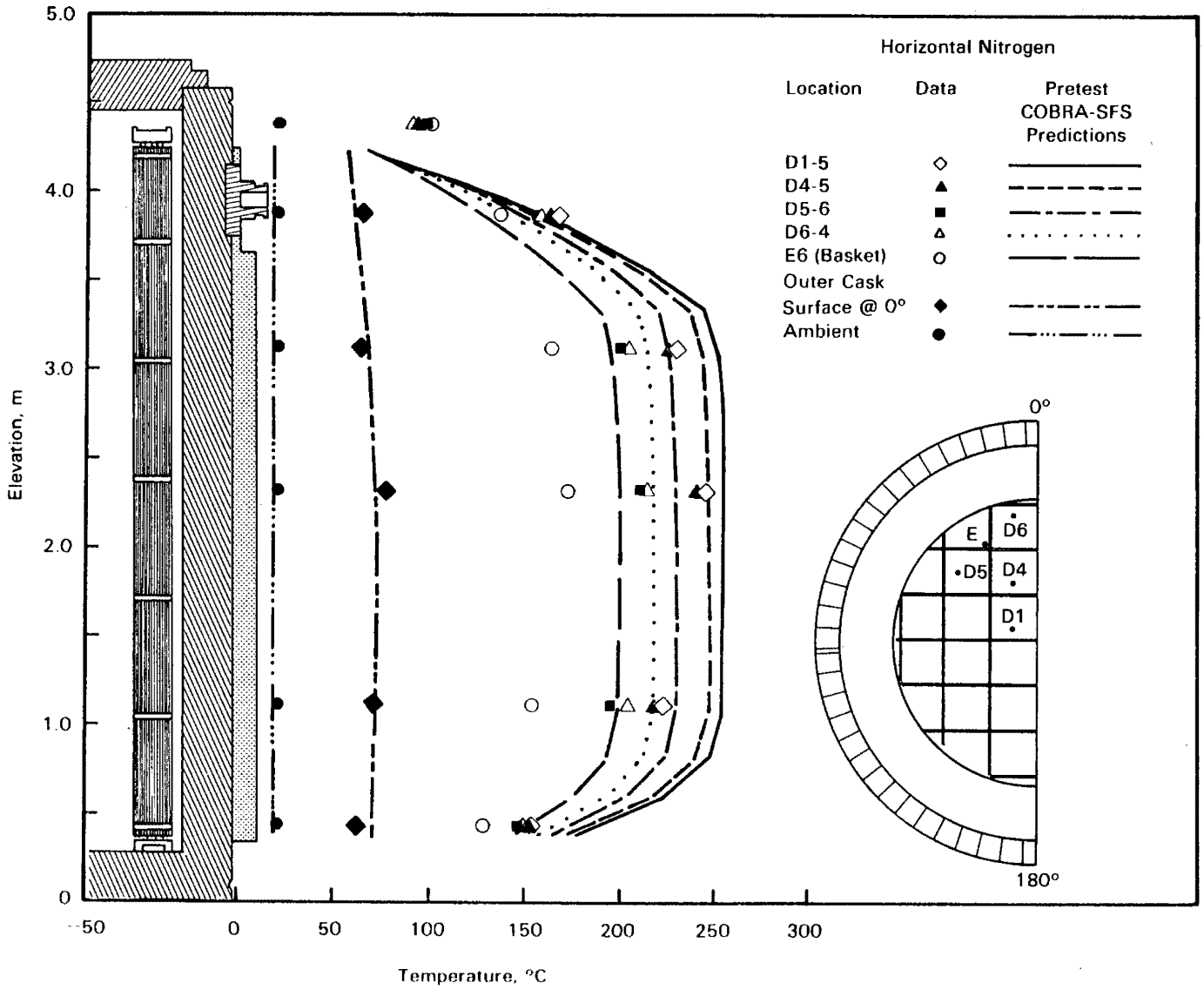

Figure 5-15. Pretest Horizontal, Nitrogen Axial Temperature Profile Predictions Compared to Test Data

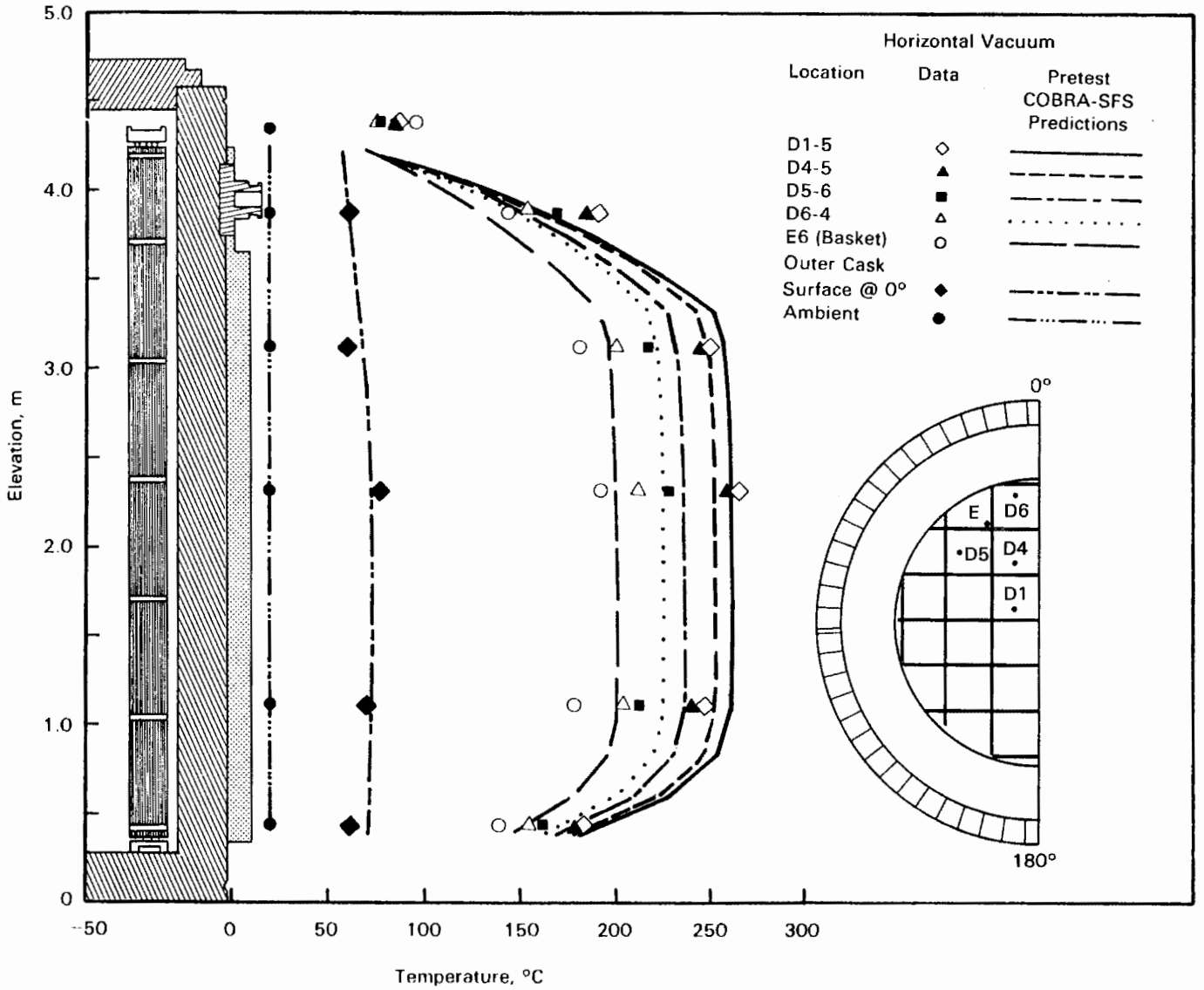

Figure 5-16. Pretest Horizontal, Vacuum Axial Temperature Profile Predictions Compared to Test Data

The axial profiles for the helium fill gas are presented in Figure 5-14. The peak temperature was overpredicted by 6.1% (11°C). As in the vertical orientation, the disagreement (38°C) with data found near the bottom of the cask is attributed to insufficient modeling of the heat transfer to the plenum. Neglecting axial conduction in the basket resulted in the overly flat axial profiles. An interesting result was that both the measured and calculated temperatures for the horizontal helium case are lower than those of the vertical helium case. This indicates that the decreased contribution of convection heat transfer in the horizontal orientation is more than compensated for by the increased heat transfer due to contact of the aluminum basket with the inside cask wall and shifting of fuel assemblies within basket fuel tubes.

The predicted nitrogen horizontal axial profiles displayed in Figure 5-15 show fairly good agreement with data, with the peak temperature being overpredicted by 4.3% (10°C). The COBRA-SFS model neglected convection in the horizontal orientation; therefore, it was not possible to model any convection influenced temperature effects for the horizontal nitrogen run. In this case alone, the outer assembly (D6) ran warmer experimentally than its nearest neighboring assembly (D5). This is probably the result of recirculating flow within the empty outer basket enclosure next to the assemblies in question (Figure 4-12). The measured and predicted peak temperatures for nitrogen in the horizontal orientation were higher than in the vertical run. Convection in nitrogen for the vertical orientation therefore contributed more to overall heat transfer than did the increased heat transfer due to the basket contact with the inside cask wall and assembly contact with fuel tube walls in the horizontal orientation.

Predicted axial profiles for the horizontal vacuum case displayed in Figure 5-16 show excellent agreement with data. The peak temperature was underpredicted by 1.7% (4°C), and the absence of modeling axial conduction is noticeable in profile comparisons. The major difference between the vertical and horizontal vacuum test runs was the shifting of the cask internals in the horizontal orientation. Both the predictions and the data show a lower peak temperature for the horizontal run, reflecting the increased heat transfer due to basket contact with the inner cask wall and assembly contact fuel tube walls.

The effect of fill gas on the horizontal orientation predictions is displayed in Figure 5-17, where the predicted peak temperature profiles for the three fill gases are presented along with the data. The profiles generally have the same shape

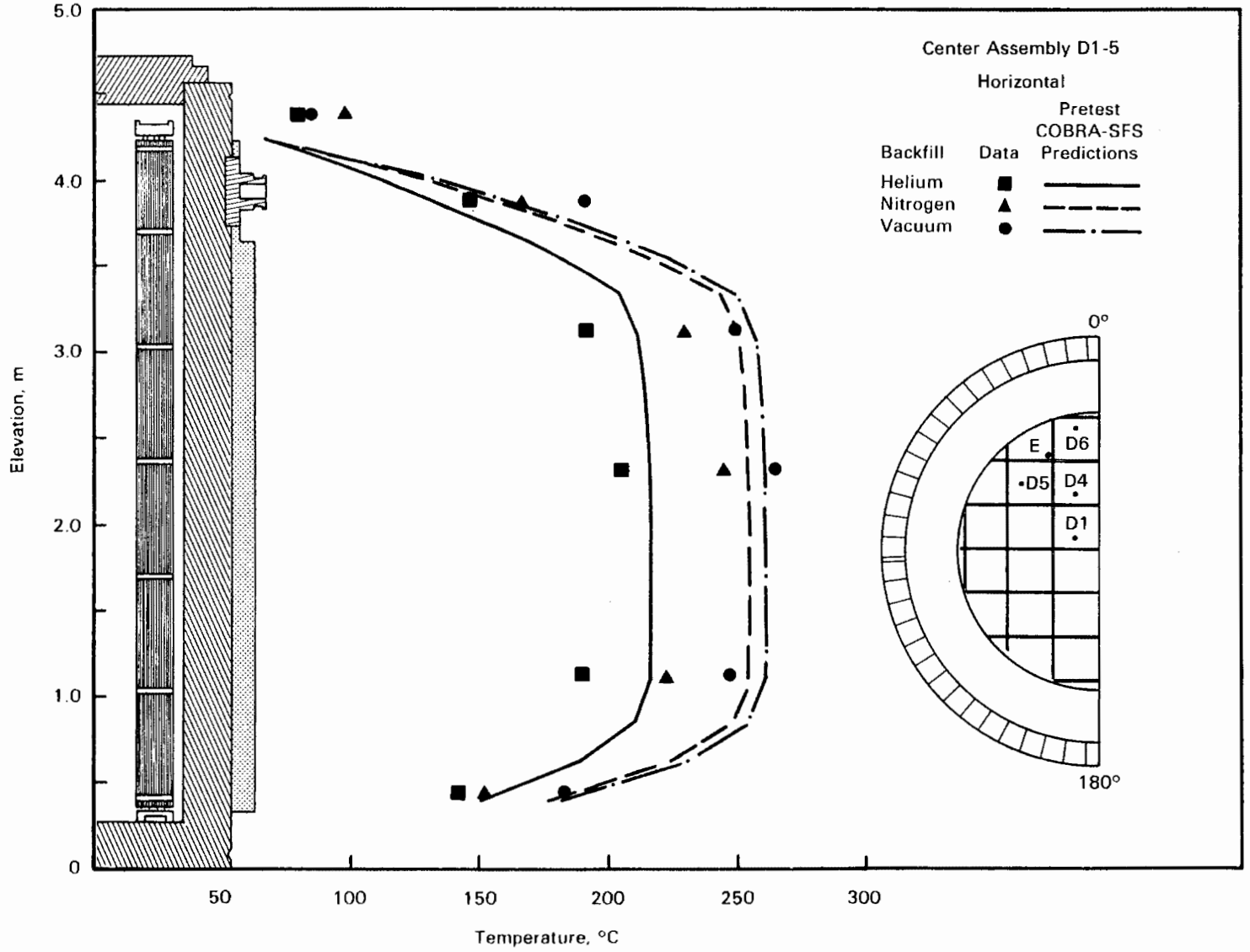

Figure 5-17. Pretest Horizontal, Helium, Nitrogen, and Vacuum Axial Temperature Profile Predictions Compared to Measured Hot Assembly Data

indicating the absence of convection; only the magnitudes differ as a result of different backfill thermal conductivities and radiation heat transfer contributions.

The diametrical profiles at the peak axial temperature location for each of the three fill gases are shown in Figure 5-18. The main point of interest is the observed skew in the radial profiles towards the upper (0°) surface of the cask. The predicted and measured data both show higher assembly temperatures in the upper portion of the cask, which is directly related to 1) the increased gaps between the basket and the inside cask wall at the upper basket locations (0°C) and 2) the decreased gaps between the basket and the inside cask wall near the bottom of the cask (180°). The guide tube temperatures were again predicted within 15°C while predicted basket temperatures agreed with test data within 25°C. The reasons for the less accurate basket temperature predictions are the same as those previously discussed for the vertical orientation.

Conclusions From Pretest Comparisons. Comparisons of pretest predictions with experimental data led to the following conclusions:

- The pretest peak temperature predictions were in exceptionally good agreement with data, the maximum disagreement being 9.1% (20°C) for the vertical nitrogen run.
- The predicted axial profiles were also in good agreement for all cases other than the nitrogen test run, which was not in satisfactory agreement.
- Guide tube temperatures were consistently predicted better (up to 15°C) than basket temperatures. Possible reasons for less accurately predicted basket temperatures are 1) the thermocouples may have been measuring temperatures between those of the basket and the gas because of the attachment method and 2) the heat transfer between the basket and gas was slightly underpredicted.
- A possible cause of the deviation of predicted temperatures from measured data is the correlation used to represent the heat transfer to and from the fluid to solid surfaces (Nu = 3.66). The better accuracy of the vacuum simulation compared to the helium and nitrogen backfill cases led to this conclusion.
- Deviations between predicted and measured temperature profiles in the lower regions of the cask were probably caused by an insufficient heat transfer model from cask-to-railcar-to-ambient.

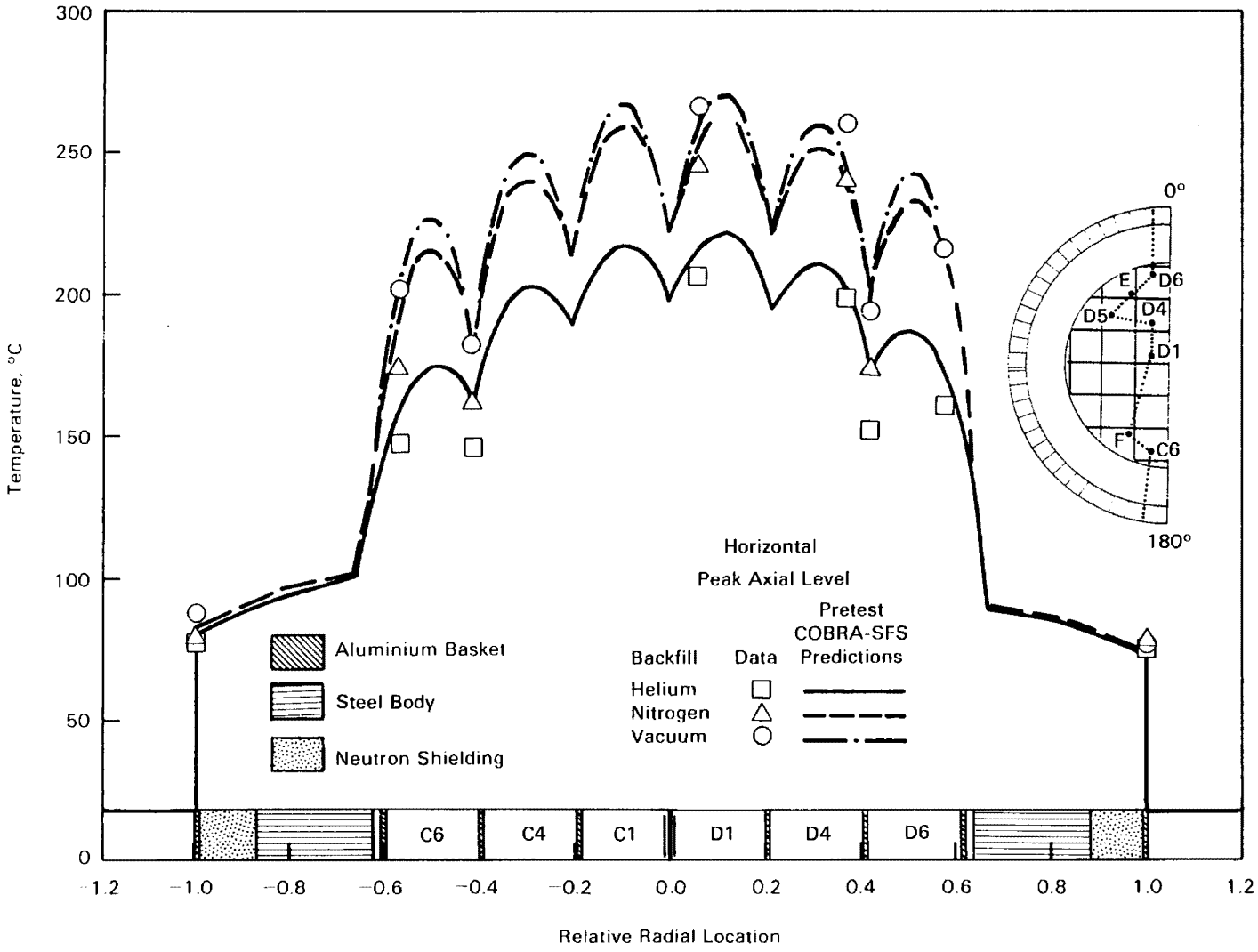

Figure 5-18. Pretest Horizontal, Helium, Nitrogen, and Vacuum Radial Temperature Profile Predictions Compared to Test Data at Peak Temperature Axial Locations

Post-Test Predictions Compared to Test Data

A discussion of the post-test model alterations precedes the presentation of the individual post-test predictions. The comparisons of post-test predictions with data are presented in the same fashion as were the pretest: 1) summaries of post- and pretest peak guide tube temperatures are compared with data for all six test runs; 2) post-test axial and radial temperature profiles are compared with data for helium, nitrogen, and vacuum fill gases, for the vertical orientation; and 3) post-test axial and radial temperature profiles are compared with data for the three fill gases in a horizontal position. Predicted mass flow rate distributions for the vertical orientation are also described.

Model Changes. A thorough comparison of the pretest predictions with data found the shape of the axial temperature profiles to be of concern. Consistent differences in all six simulations were noted, and investigation led to the following model changes for the post-test simulations:

- The assumption that axial conduction in the aluminum basket could be neglected because of potentially large contact resistances at the plate interfaces was invalid. This assumption resulted in overly "flat" axial profiles due to the isolation of the effect of the plenums to only the uppermost and lowermost portions of the basket. Axial conduction was included in the post-test analysis.

- In the vertical orientation, the heat transfer from the cask bottom to ambient through the rail car was underpredicted by the pretest model. The model had assumed only conduction, first through a steel plate followed by heat transfer to ambient via a heat transfer coefficient of $h = 0.01$ Btu/h-ft^2-°F. Upon closer inspection of the rail car, it was determined that it was appropriate to model the rail car as an external fin in the post-test analysis, which enhanced the heat transfer through the cask bottom by approximately two orders of magnitude.

- The pretest models assumed that the heat transfer from the bottom of the aluminum basket, through the plenum, to the cask bottom was negligible. This assumption led to underpredicted heat transfer from the basket to the cask bottom. For the post-test model, the basket walls were thermally connected to the cask bottom via an effective conductivity, which represented a thermal path through the basket and the plenum.

- The modified surface-to-ambient heat transfer correlation used in the pretest simulations (Equation 5.8) slightly overpredicted the heat transfer. The original correlation (Equation 5.7) was applied in the post-test simulations.

Post-Test Peak Temperature Predictions Compared to Test Data. Comparisons of the peak-to-ambient pretest and post-test predictions with data for the six test runs are shown in Figure 5-19. The post-test model changes did little to change the

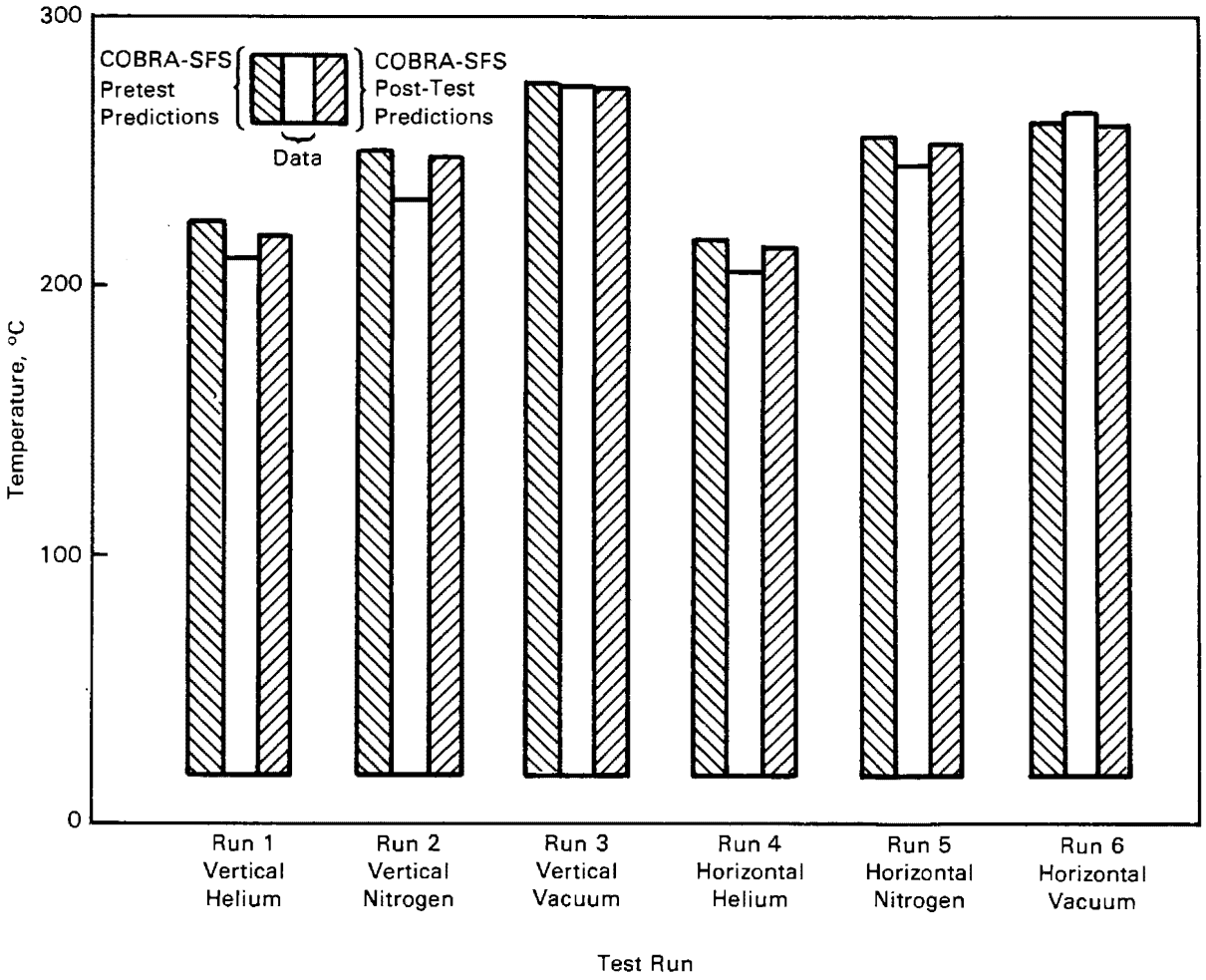

Figure 5-19. Post-Test Peak Temperature Predictions Compared to Pretest Predictions and Test Data

predicted peak guide tube temperatures, as the changes mainly influenced the shape of the axial temperature profiles. Again, as in the pretest predictions, the greatest discrepancy occurred for the vertical nitrogen case, where a 7.4% (16°C) overprediction existed. The mean temperature difference between the data and the post-test predictions for the six test runs was 2.9% (6°C), with a standard deviation of 3.4% (7°C). A summary of the pre- and post-test predictions compared to the experimental data for the six test runs is given in Table 5-4.

Post-Test Vertical Predictions Compared to Test Data. The post-test predictions of axial temperature profiles for the three fill gases in the vertical orientation are shown in Figures 5-20, 5-21, and 5-22. Figure 5-20, the helium fill gas case, displays the improvement in the profile shape expected from the inclusion of axial conduction in the basket. Also, the lower plenum heat transfer enhancements resulted

Table 5-4

PEAK TEMPERATURE COMPARISONS

Test Run	Backfill	Orientation	Pretest	Data	Post-Test
1	Helium	Vertical	225°C	211°C	220°C
2	Nitrogen	Vertical	251°C	232°C	247°C
3	Vacuum	Vertical	276°C	275°C	273°C
4	Helium	Horizontal	218°C	206°C	216°C
5	Nitrogen	Horizontal	255°C	246°C	253°C
6	Vacuum	Horizontal	262°C	266°C	260°C

in a better comparison in the lower portion of the cask. The peak measured temperature was overpredicted in this case by 4.8% (9°C). At other radial locations, predicted temperatures were as much as 20°C higher than measured values.

A clear improvement in the shape of the predicted axial profiles is shown for the nitrogen vertical test run in Figure 5-21. This run proved to be the most difficult to simulate accurately, reflecting the difficulty in modeling the effects of convective heat transfer. COBRA-SFS overpredicted the peak guide tube temperature in this case by 7.4% (15°C). However, predicted temperatures at other locations where as much as 30°C higher than measured temperatures.

The post-test vertical vacuum predictions presented in Figure 5-22 are in excellent agreement (20°C) with the experimental data. This result indicates that the radiation heat transfer model is accurate, as convection is negligible and conduction through the vacuum (low pressure nitrogen) is not significant. The simulation underpredicted the peak temperature data by 0.9% (2°C), with good agreement with axial temperature profiles.

Figure 5-23 is a composite of the predicted peak guide tube temperatures for each of the three vertical orientation runs, along with its respective measured temperature. Temperatures and axial temperature profiles were predicted much more accurately (10°C) for the helium and vacuum runs than the nitrogen run. Temperatures with significant nitrogen convection were less accurately predicted (30°C) by COBRA-SFS. A prediction accuracy of 30°C over the complete length of an assembly is believed to be exceptionally good considering the complexity of the simulation.

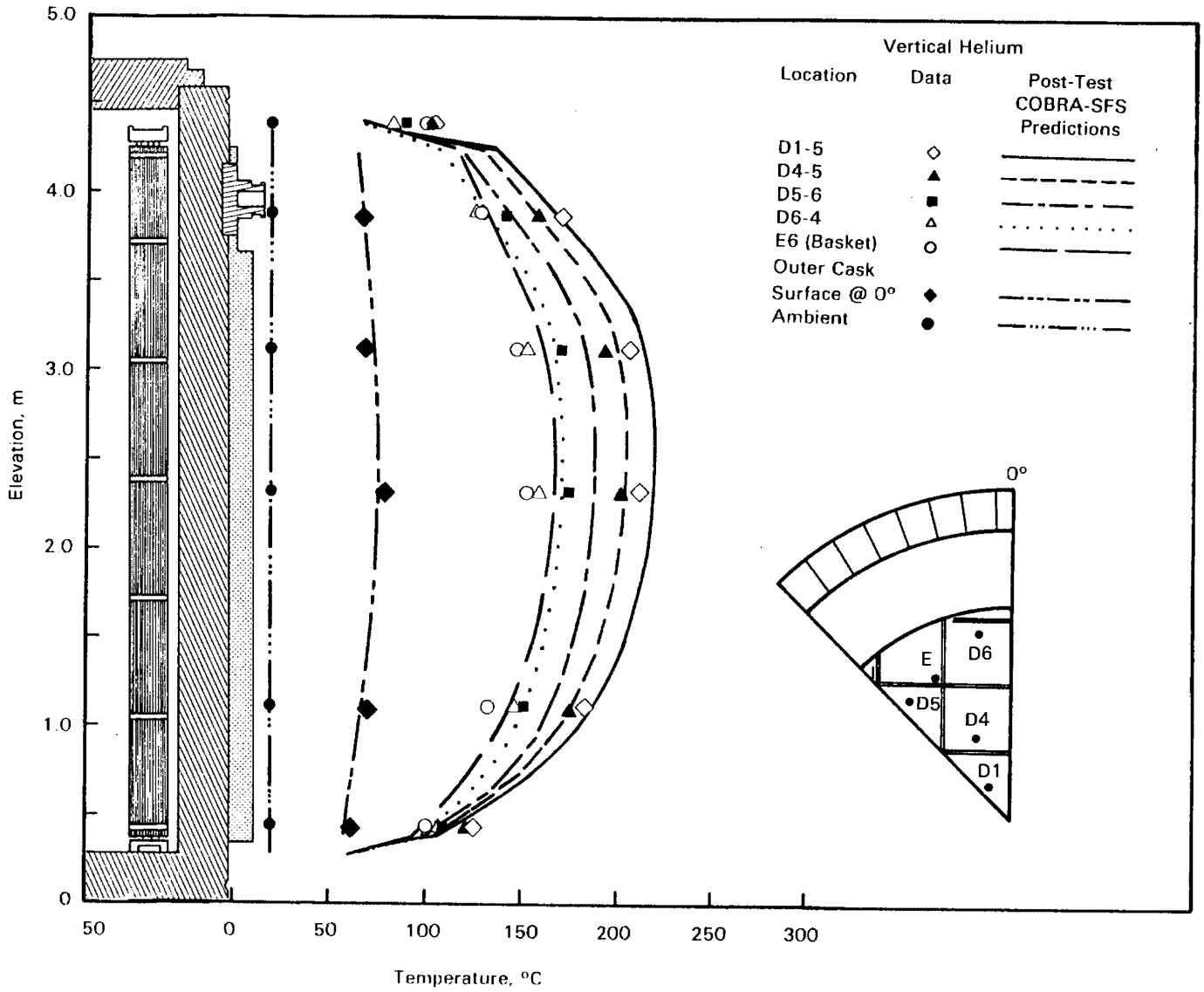

Figure 5-20. Post-Test Vertical, Helium Axial Temperature Profile Predictions Compared to Test Data

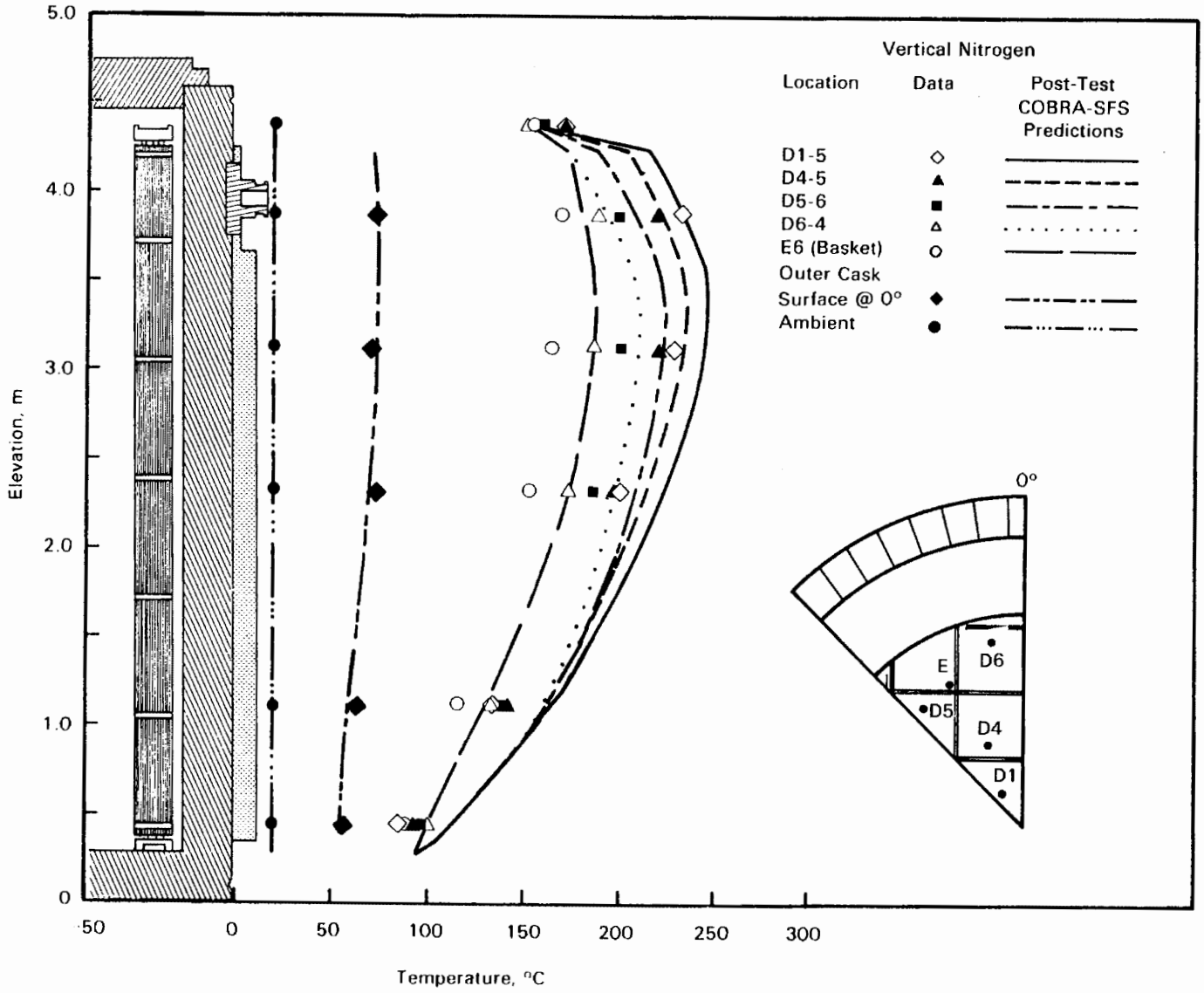

Figure 5-21. Post-Test Vertical, Nitrogen Axial Temperature Profile Predictions Compared to Test Data

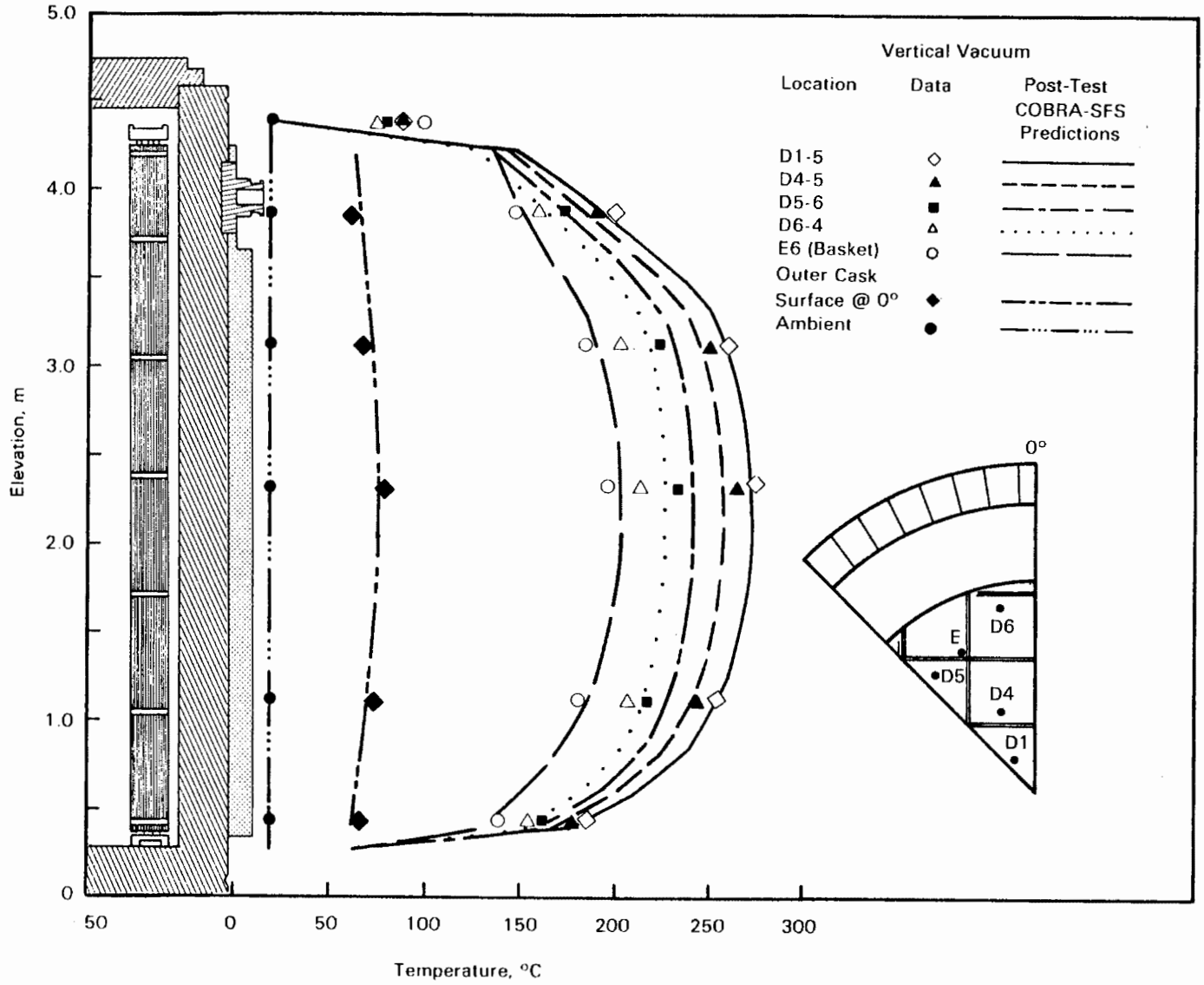

Figure 5-22. Post-Test Vertical, Vacuum Axial Temperature Profile Predictions Compared to Test Data

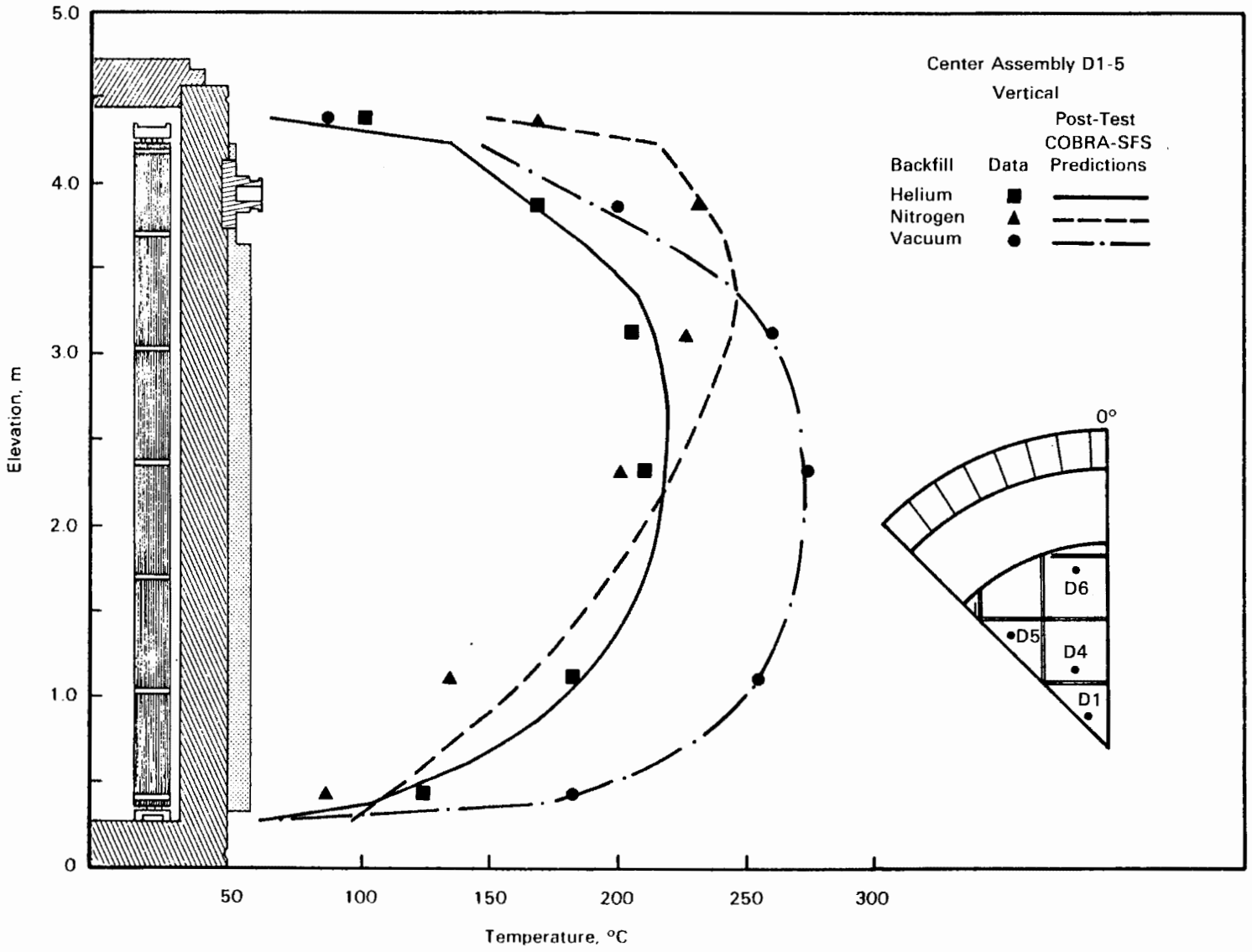

Figure 5-23. Post-Test Vertical, Helium, Nitrogen, and Vacuum Axial Temperature Profile Predictions Compared to Test Data

The post-test radial temperature profiles at peak axial temperature locations for each of the vertical test runs are presented in Figure 5-24. Only small differences from the pretest results are observed. However, it is noted that the measured basket temperature was consistently cooler (up to 25°C) than the predicted temperature.

Post-Test Horizontal Predictions Compared to Test Data. The post-test axial profiles for the horizontal orientation are displayed in Figures 5-25, 5-26, and 5-27. The modeling of the rail car as a fin was not included in the horizontal simulations. All other post-test changes used in the one-eighth section model were applied to the one-half section model.

The temperature predictions for the helium fill gas shown in Figure 5-25 are in good agreement (25°C) with data. The peak guide tube temperature was overpredicted by 5.0% (10°C). The most significant change in the predictions with the post-test model is that the shape of the profile more accurately follows the experimental data.

The predicted horizontal nitrogen axial temperature profiles presented in Figure 5-26 show a substantial improvement in shape. The peak guide tube temperature was overpredicted by 3.4% (7°C) with the greatest disagreement (25°C) occurring at the basket location. As in the pretest model, the COBRA-SFS post-test model did not include the convection effects necessary to predict that the outermost assembly (D6) would run warmer than its nearest inward neighbor (D5).

Excellent agreement (10°C) with experimental data is shown in Figure 5-27 for the horizontal vacuum test. Consistent with the other post-test simulations, the greatest improvement was in the shape of the temperature profiles. The peak guide tube temperature was underpredicted by 2.2% (6°C). Improvements in this case are attributed to the inclusion of axial conduction in the basket to the post-test model.

The effect of fill gas for the horizontal post-test runs is shown in Figure 5-28. The peak guide tube temperatures for all three cases have nearly the same profile but differ in magnitude. The vacuum data were slightly underpredicted (6°C) while the helium and nitrogen data were slightly overpredicted (10°C).

The post-test diametrical profiles at the peak axial temperature location for the three horizontal runs are shown in Figure 5-29. The post-test predicted temperature distribution through the cask differed by less than 5°C from the pretest predictions, as little effect from the post-test model changes was seen at the peak axial temperature level.

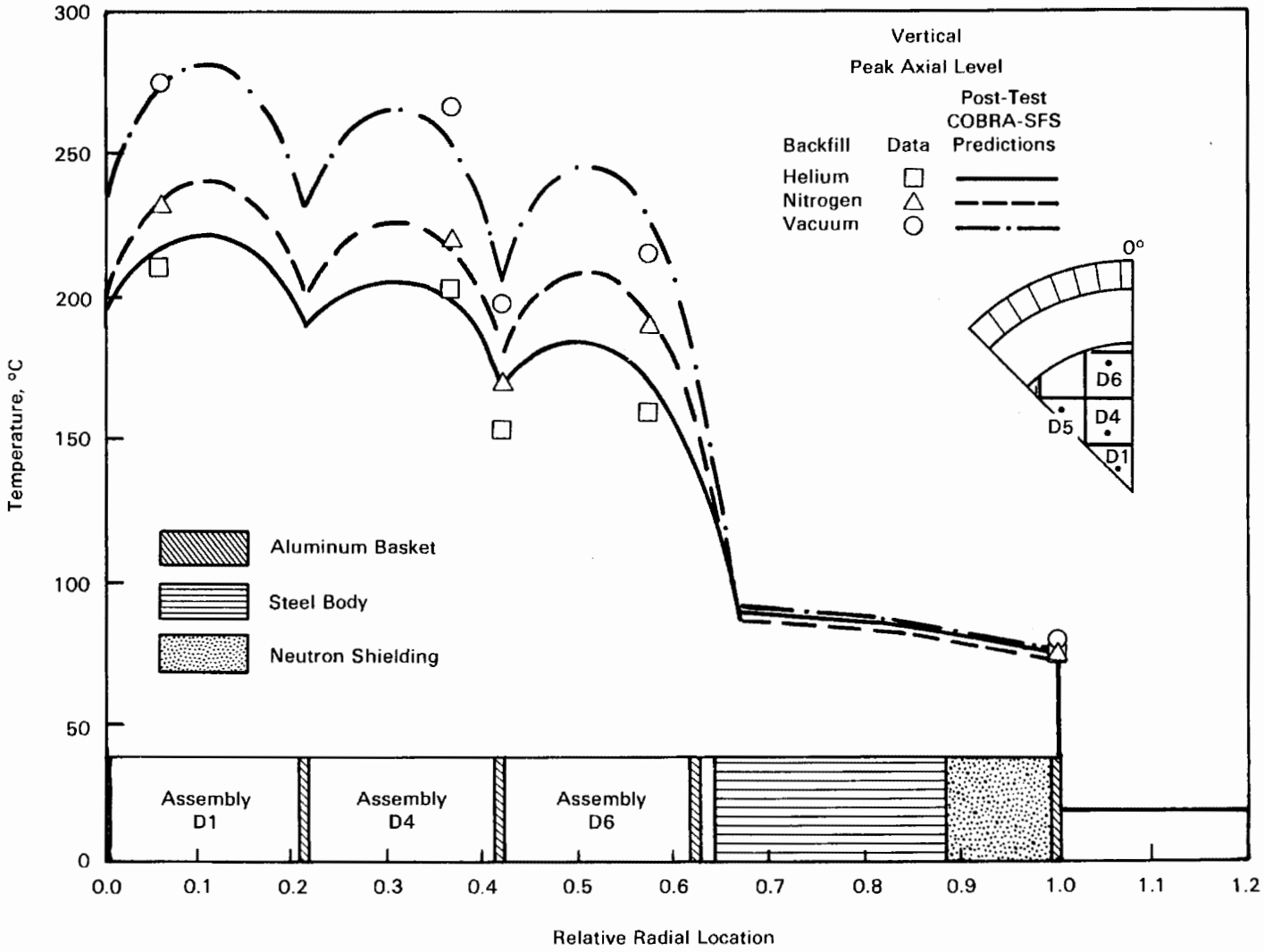

Figure 5-24. Post-Test Vertical, Helium, Nitrogen, and Vacuum Radial Temperature Profile Predictions Compared to Test Data at Peak Temperature Axial Locations

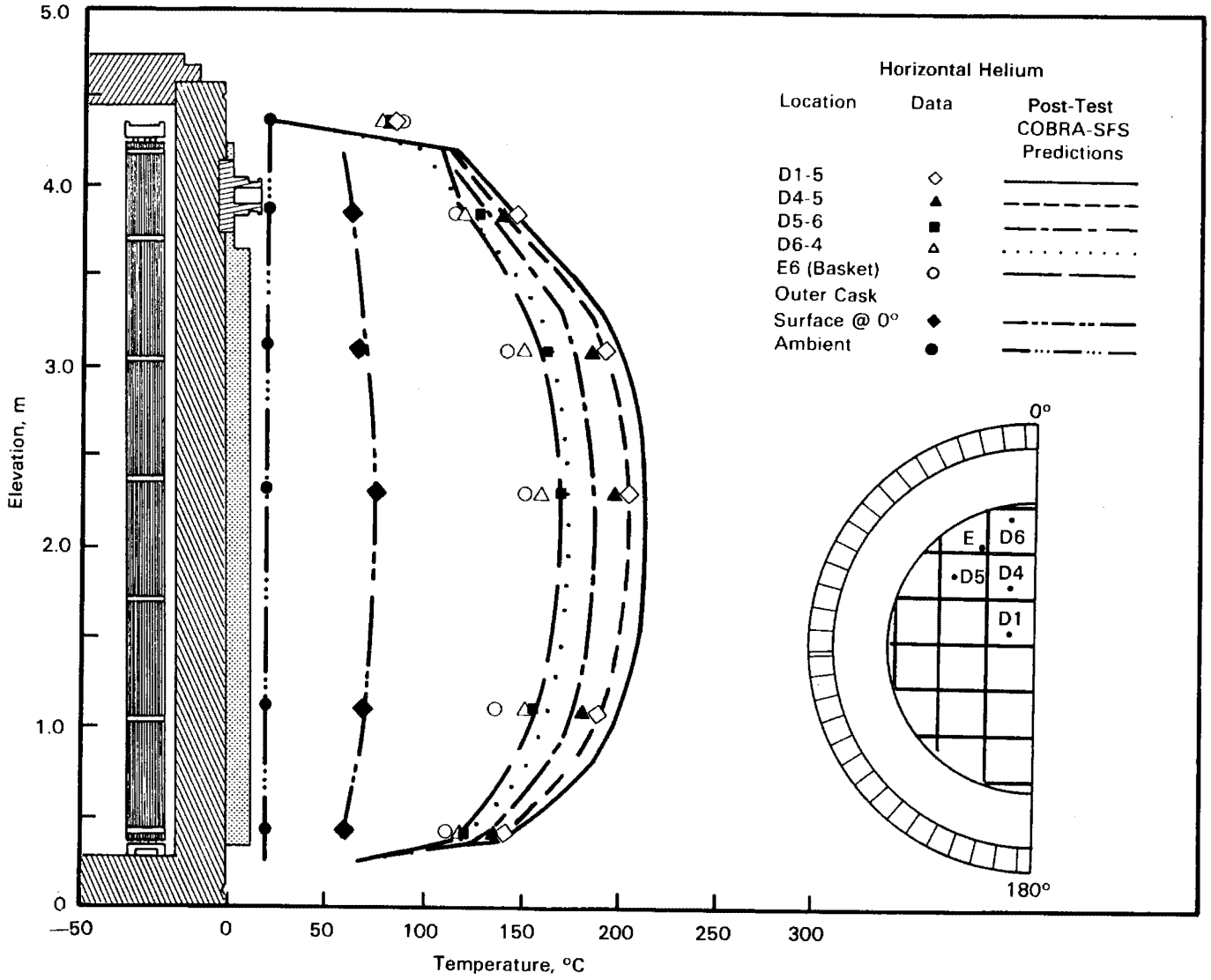

Figure 5-25. Post-Test Horizontal, Helium Axial Temperature Profile Predictions Compared to Test Data

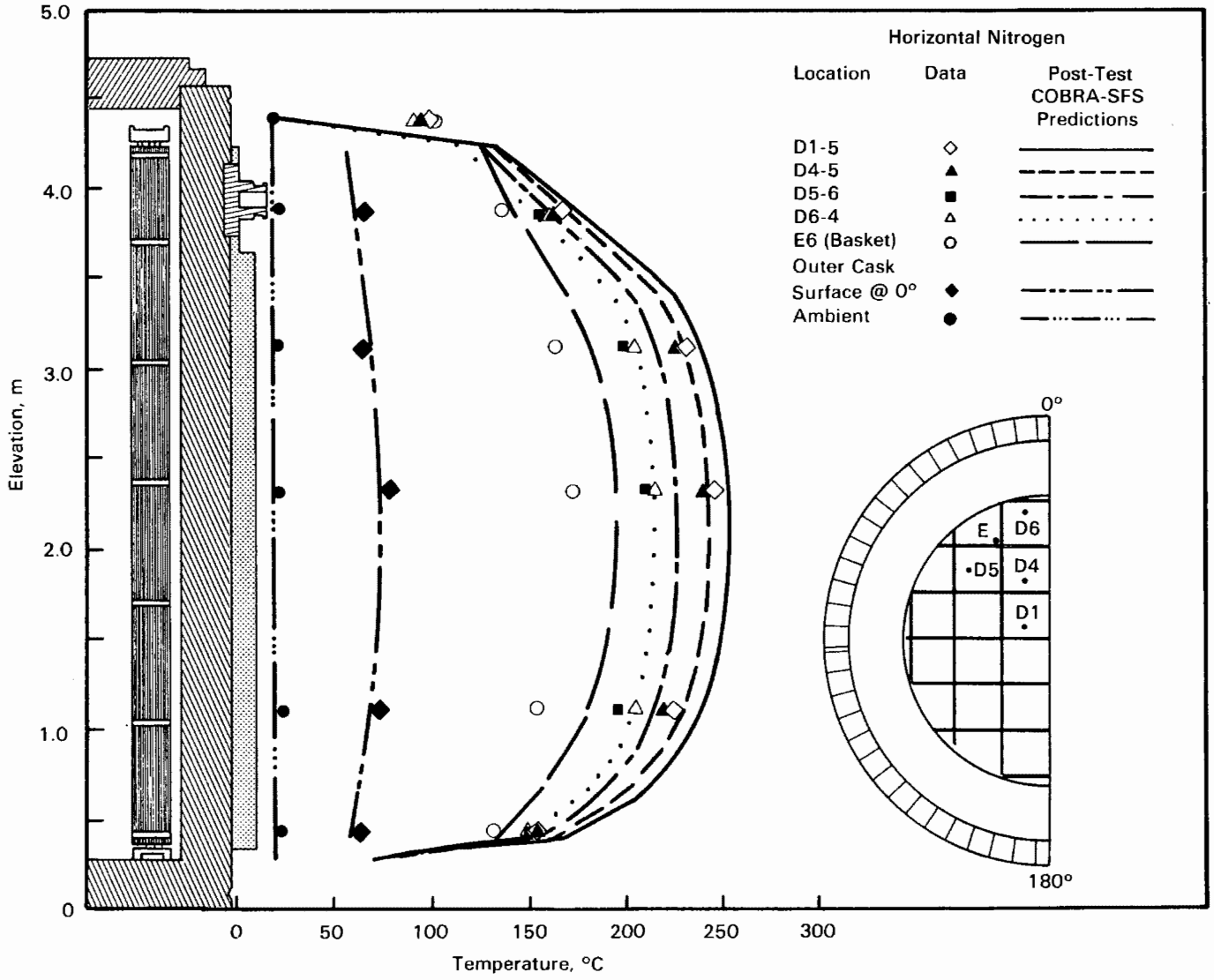

Figure 5-26. Post-Test Horizontal, Nitrogen Axial Temperature Profile Predictions Compared to Test Data

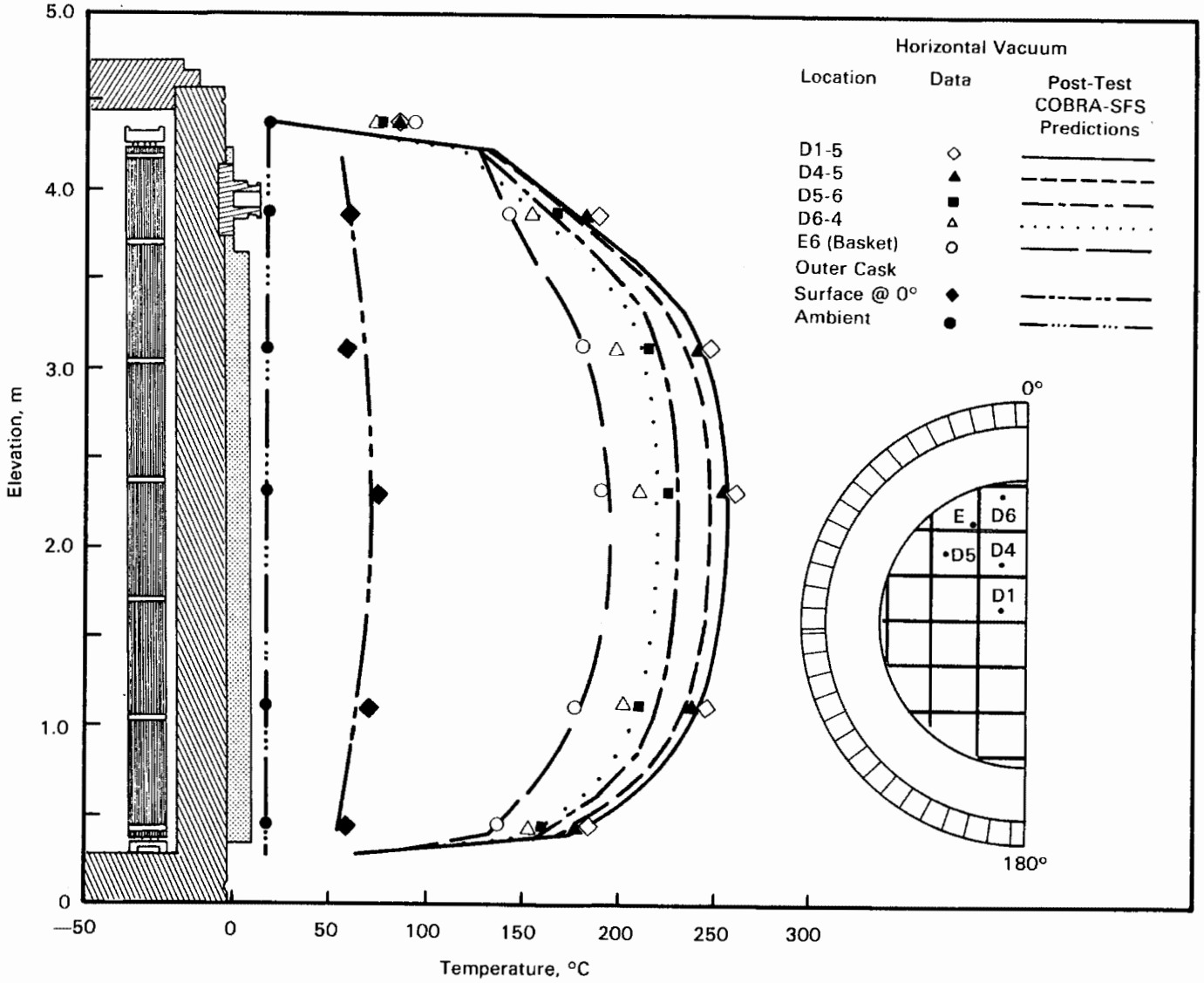

Figure 5-27. Post-Test Horizontal, Vacuum Axial Temperature Profile Predictions Compared to Test Data

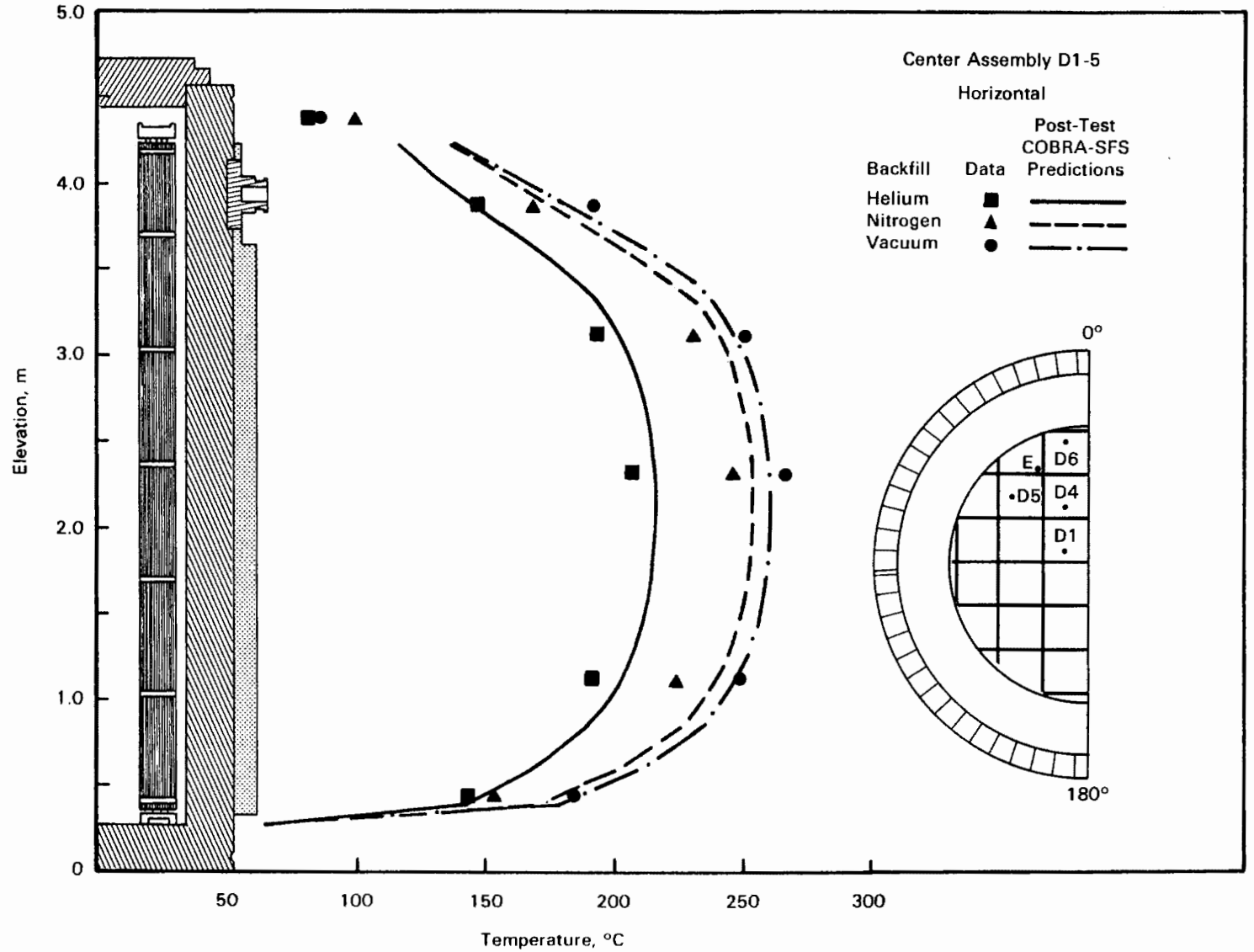

Figure 5-28. Post-Test Horizontal, Helium, Nitrogen, and Vacuum Axial Temperature Profile Predictions Compared to Test Data

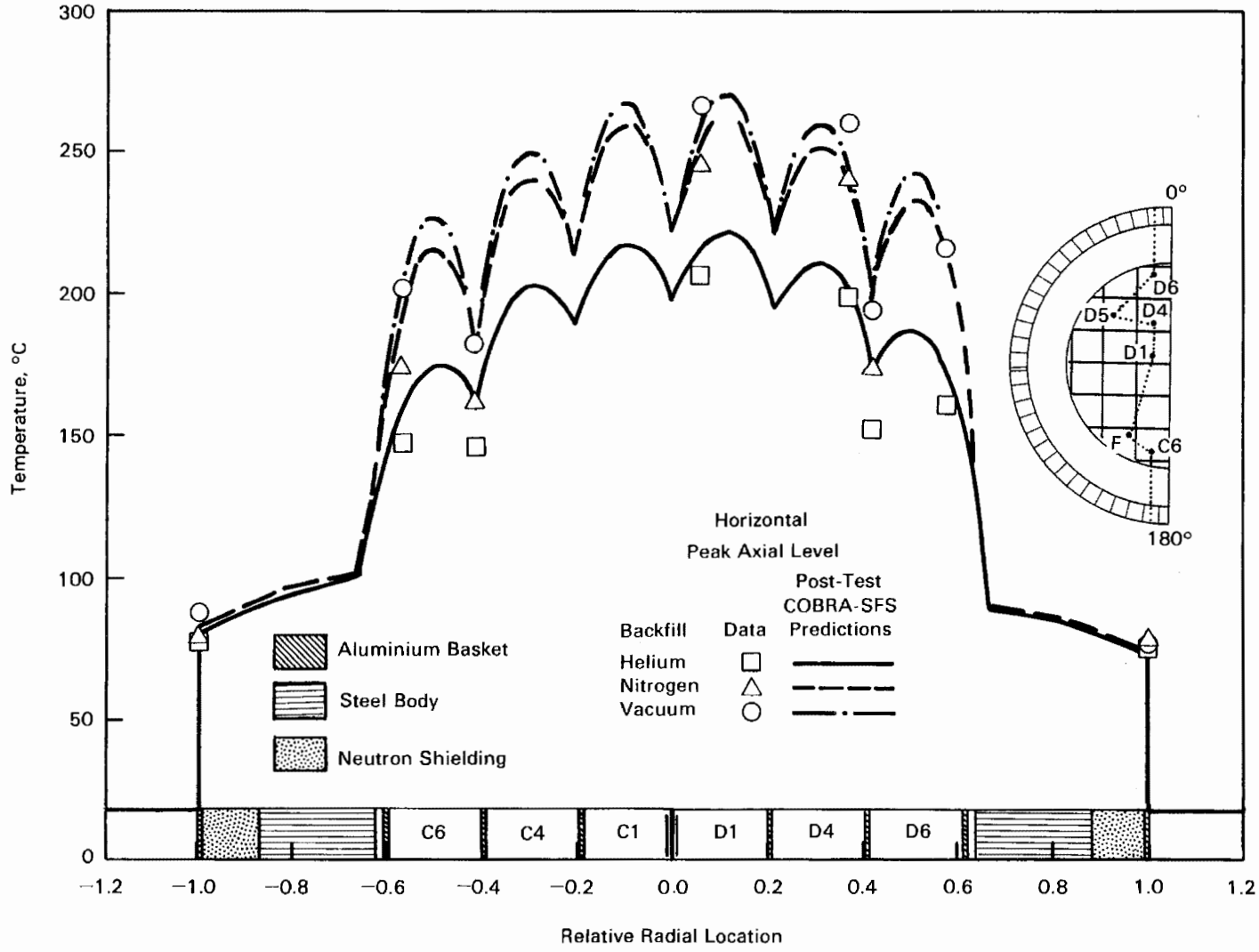

Figure 5-29. Post-Test Horizontal, Helium, Nitrogen, and Vacuum Radial Temperature Profile Predictions Compared to Test Data at Peak Temperature Axial Locations

Post-Test Velocity Distribution Predictions. The post-test vertical helium and nitrogen predicted bulk velocity distributions are shown in Figure 5-30. The average nitrogen upflow was approximately 3 times higher than the average helium upflow, which was reflected in the shape of the temperature profiles.

Conclusions From Post-Test Comparisons. Comparisons of post-test predictions with experimental data led to the following conclusions:

- The post-test peak temperature predictions were in excellent agreement with data, the maximum disagreement being 7.4% (15°C) for the vertical nitrogen runs.
- The predicted axial profiles were also in excellent agreement for all cases other than the nitrogen test run, which was in reasonably good agreement.
- Guide tube temperatures were again consistently predicted better (up to 15°C) than basket temperatures. Possible reasons for less accurately predicted basket temperatures remain to be 1) thermocouple may have been measuring temperatures between that of the basket and the gas because of the attachment method and 2) the heat transfer between the basket and gas was slightly underpredicted.

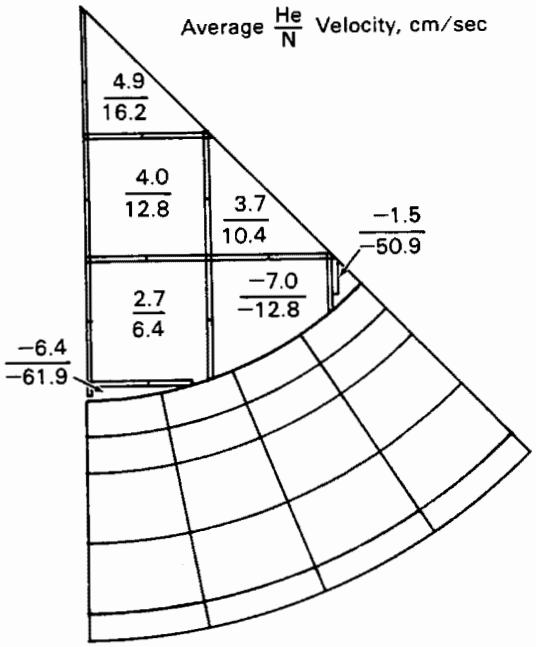

Figure 5-30. Post-Test Velocity Distribution Predictions for Vertical, Helium and Nitrogen Test Runs

- A possible cause of the deviation of predicted temperatures from measured data is the correlation used to represent the heat transfer to and from the fluid to solid surfaces (Nu = 3.66). The better accuracy of the vacuum simulation compared to the helium and nitrogen backfill cases led to this conclusion.

- Temperature predictions in the lower region of the cask were significantly improved with a more detailed cask-to-railcar-to-ambient heat transfer model.

MAXIMUM CASK HEAT LOAD PREDICTIONS

The maximum cask decay heat load under licensing conditions for helium and nitrogen backfills was investigated for a vertically oriented cask with the post-test input and computational model refinements. The maximum heat load in the cask is limited by four constraints on the fuel and cask component temperatures:

- 380°C maximum fuel temperature
- 250°C maximum aluminum temperature
- 150°C maximum side neutron shield (polyethylene resin) temperature
- 140°C maximum lid neutron shield (polypropylene granulars) temperature.

The fuel temperature limit is a constraint dictated by current information regarding fuel rod cladding integrity (3). The temperature limit for the aluminum basket reflects the maximum allowable temperature prior to possible creep as provided by Transnuclear, Inc. The maximum temperature for the polyethylene resin side neutron shield and the polypropylene granulars in the lid neutron shield were provided by Transnuclear, Inc.

The maximum heat rates were predicted for the helium and nitrogen fill gas cases under the following conditions:

- vertical orientation
- uniform assembly decay heat rates
- 54°C ambient temperature
- lid neutron shield in place
- stagnant ambient conditions.

In the helium case, the predicted aluminum basket temperature was the limiting factor. A uniform heat rate of 1.03 kW per assembly resulted in the basket temperature reaching its creep temperature at the cask center. The peak fuel cladding

temperature for this loading was 272°C, substantially under the limit of 380°C. This indicates that the thermal conduction through the cask with a helium backfill is exceptional. The predicted peak axial temperature profile is shown in Figure 5-31, along with the post-test prediction of the vertical helium peak axial temperature profile and corresponding test data. Note that the predicted temperature profile at the maximum heat dissipation rate was calculated using an ambient temperature of 54°C, while the post-test prediction used the actual TAN warm shop temperature of 18°C.

For the nitrogen case, the lid neutron shield was identified as the first temperature limit to be encountered. This limit was reached at a heat rate of 0.50 kW per assembly, which corresponded to a fuel cladding temperature of only 210°C. The nitrogen case resulted in a lower allowable heat rate because of the increased convection within the cask, which resulted in higher temperatures in the upper portion of the cask. If the lid neutron shield limit was neglected, a maximum heat rate of 0.8 kW per assembly was allowable before the aluminum basket temperature limit was reached. A comparison of the post-test predictions and test data with the 0.85 kW-per-assembly maximum heat load analysis is presented in Figure 5-32. The post-test analysis was based on an average loading of 0.870 kW per assembly. Therefore, the only significant differences were the ambient temperatures (18°C for the post-test analysis, 54°C for the maximum heat load analysis) and the additional thermal resistance of the lid neutron shield in the maximum heat load case.

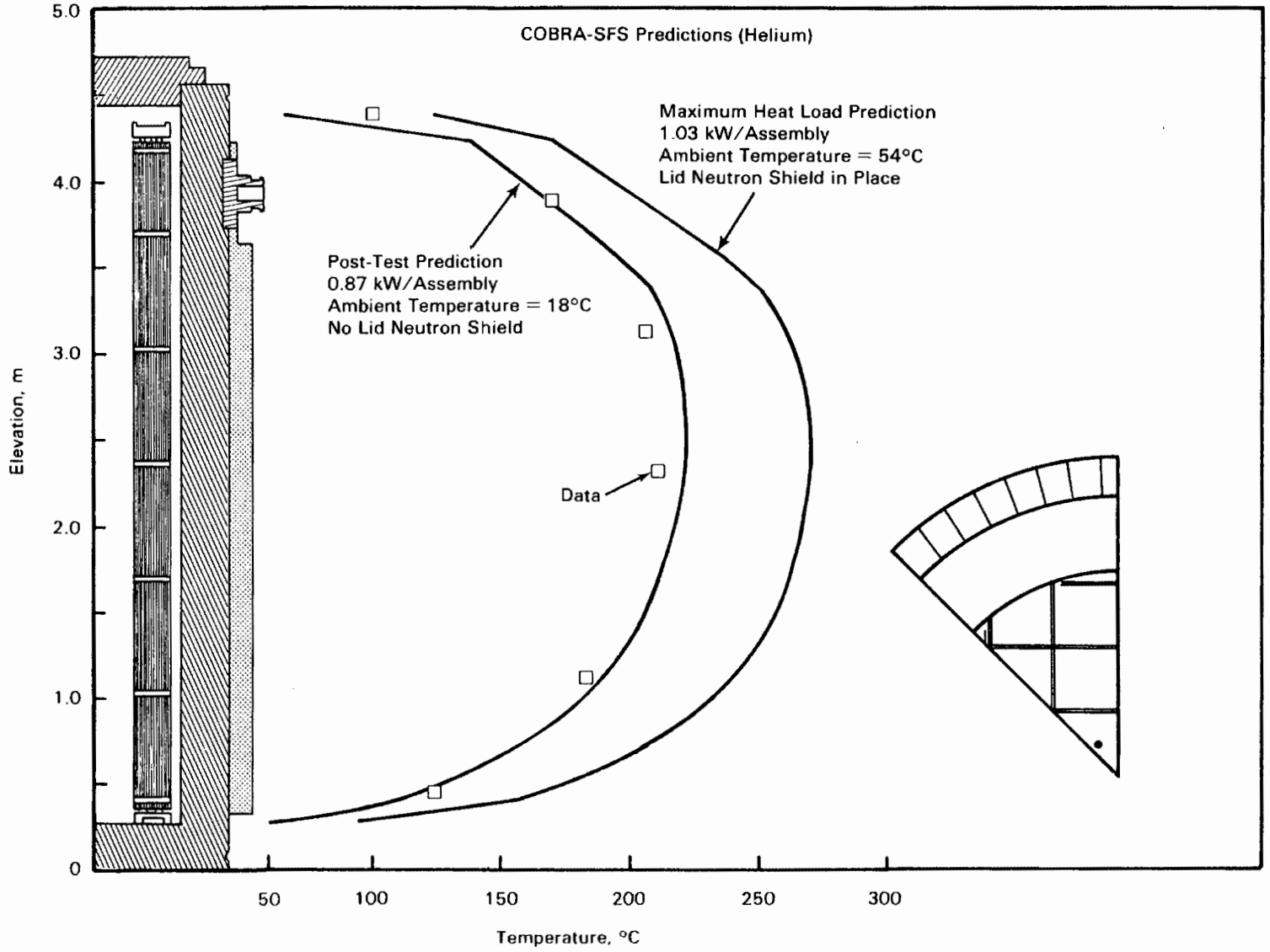

Figure 5-31. Predicted Maximum Cask Heat Load with Helium Backfill

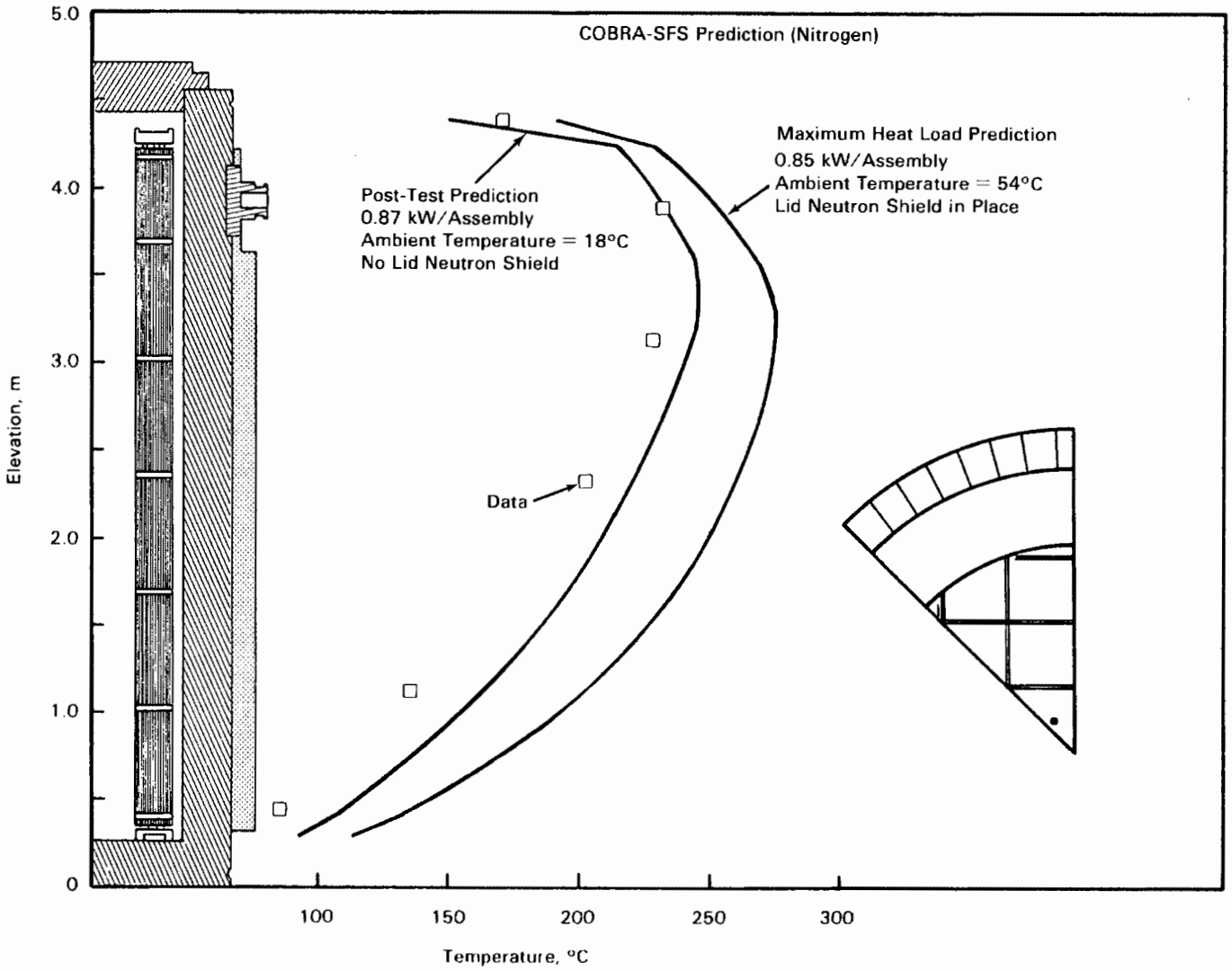

Figure 5-32. Predicted Maximum Cask Heat Load with Nitrogen Backfill

Section 6

REFERENCES

1. U.S. Department of Energy. Spent Fuel Storage Requirements. Richland, Washington: Richland Operations Office, 1985. DOE/RL-85-2.

2. J. M. Creer, R. A. McCann, M. A. McKinnon, J. E. Tanner, E. R. Gilbert, R. L. Goodman, D. H. Schoonen, M. Jensen, C. Mullen, D. Dziadosz, and E. V. Moore. CASTOR-V/21 PWR Spent Fuel Storage Cask Testing and Analyses. Richland, Washington: Pacific Northwest Laboratory, 1986. PNL-5917/NP-4887.

3. A. B. Johnson, Jr., and E. R. Gilbert. Technical Basis for Storage of Zircaloy Clad Fuel in Inert Gases. Richland, Washington: Pacific Northwest Laboratory, 1983. PNL-4835.

4. TN-24 Dry Storage Cask Topical Report. White Plains, New York: Transnuclear, Inc., 1985. E-7107.

5. TN-24P Cask Operations Manual. White Plains, New York: Transnuclear, Inc., 1985. E-7455, rev. 0.

6. M. A. McKinnon, J. W. Doman, J. E. Tanner, R. J. Guenther, J. M. Creer, and C. E. King. BWR Spent Fuel Storage Cask Performance Test: Volume I - Cask Handling Experience and Decay Heat, Heat Transfer, and Shielding Data. Richland, Washington: Pacific Northwest Laboratory, 1986. PNL-5777, vol. I.

7. F. M. Cummings. TACI-A Code for Interactive Analysis of Neutron Data Produced by a Tissue Equivalent Proportional Counter. Richland, Washington: Pacific Northwest Laboratory, 1984. PNL-5136.

8. A. G. Croff. ORIGEN-2--A Revised and Updated Version of the Oak Ridge Isotope Generation and Depletion Code. Oak Ridge, Tennessee: Oak Ridge National Laboratory, 1980. ORNL-5621.

9. W. D. Leggett III and L. D. Eisenhart. INCORE Code. Richmond, Virginia: Virginia Power Company, 1967. WCAP-7149.

10. T. K. Ross. NEWTOTE Code. Richmond, Virginia: Virginia Power Company, 1984. NFD-CCR-6, rev. 8.

11. R. B. Davis. Data Report for the Nondestructive Examination of Turkey Point Spent Fuel Assemblies B02, B03, B17, B41, and B43. Richland, Washington: Hanford Engineering Development Laboratory, 1980. HEDL-TME-79-68.

12. R. Gunnink and J. B. Niday. Computerized Quantitative Analysis of Gamma Ray Spectrometry. Livermore, California: University of California Research Laboratory, 1972. UCRL-51061.

13. Keithly DAS Series 500 Measurement and Control System. Solon, Ohio: Keithly DAC Division and Control, 1984. Document No. 500-904-01B.

14. E. R. Gilbert, C. A. Knox, and G. D. White. "Behavior of Spent LWR Fuel in Nitrogen and in Air." In Proceedings of the Third International Spent Fuel Storage Technology Symposium/Workshop, vol. I, 1986, pp. S263-S278.

15. D. S. Rowe. COBRA-IIIC: A Digital Computer Program for Steady-State and Transient Thermal-Hydraulic Analysis of Rod Bundle Nuclear Fuel Elements. Richland, Washington: Pacific Northwest Laboratory, 1973. BNWL-1695.

16. C. W. Stewart, C. L. Wheeler, R. J. Cena, C. A. McMonagle, J. M. Cuta, and D. S. Trent. COBRA-IV: The Model and the Method. Richland, Washington: Pacific Northwest Laboratory, 1977. BNWL-2214.

17. T. L. George, K. L. Basehore, C. H. Wheeler, W. A. Prather, and R. E. Masterson. COBRA-WC: A Version of COBRA for Single-Phase Multi-Assembly Thermal-Hydraulic Transient Analysis. Richland, Washington: Pacific Northwest Laboratory, 1980. PNL-3259.

18. E. U. Khan, W. A. Prather, T. L. George, and J. M. Bates. A Validation Study of the COBRA-WC Computer Program for LMFBR Thermal-Hydraulic Analysis. Richland, Washington: Pacific Northwest Laboratory, 1981. PNL-4128.

19. J. M. Cuta, D. R. Rector, and J. M. Creer. Thermal-Hydraulic Analysis of Consolidated Spent PWR Fuel Rods. Palo Alto, California: Electric Power Research Institute, 1984. NP-3764.

20. N. J. Lombardo, T. E. Michener, C. L. Wheeler, and D. R. Rector. COBRA-SFS Predictions of Single-Assembly Spent Fuel Heat Transfer Data. Richland, Washington: Pacific Northwest Laboratory, 1986. PNL-5781.

21. J. M. Cuta and J. M. Creer. Comparisons of COBRA-SFS Calculations with Data From Simulated Sections of Unconsolidated and Consolidated BWR Spent Fuel. Palo Alto, California: Electric Power Research Institute, 1986. NP-4593.

22. L. E. Wiles, N. J. Lombardo, C. M. Heeb, U. P. Jenquin, T. E. Michener, C. L. Wheeler, J. M. Creer, and R. A. McCann. BWR Spent Fuel Storage Cask Performance Test: Volume II - Pre- and Post-Test Decay Heat, Heat Transfer, and Shielding Analyses. Richland, Washington: Pacific Northwest Laboratory, 1986. PNL-5777, vol. II.

23. D. R. Rector, R. A. McCann, U. P. Jenquin, C. M. Heeb, J. M. Creer, and C. L. Wheeler. CASTOR-1C Spent Fuel Storage Cask Decay Heat, Heat Transfer, and Shielding Analyses. Richland, Washington: Pacific Northwest Laboratory, 1986. PNL-5974.

24. D. R. Rector, J. M. Cuta, and N. J. Lombardo. COBRA-SFS Thermal-Hydraulic Analysis of the CASTOR-1C and REA 2023 BWR Storage Casks Containing Consolidated Spent Fuel. Richland, Washington: Pacific Northwest Laboratory, 1986. PNL-5802.

25. E. M. Sparrow and A. L. Loeffler, Jr. "Longitudinal Laminar Flow Between Cylinders Arranged in Regular Array." AIChE Journal. 5(3):325-330, 1959.

26. W. M. Kays and M. E. Crawford. Convection Heat and Mass Transfer. New York: McGraw-Hill, Inc., 1980.

27. R. L. Cox. Radiation Heat Transfer in Arrays of Parallel Cylinders. Oak Ridge, Tennessee: Oak Ridge National Laboratory, 1977. ORNL-5239.

28. M. R. Lindeburge. Mechanical Engineering Review Manual, 6th ed. San Carlos, California: The Professional Engineering Program, 1981.

Appendix A

FUEL ASSEMBLY DATA

Table A-1

SURRY 2, CYCLE 4 REACTOR OPERATING HISTORY

Dates, mo/da/yr		Elapsed Time,	Reactor Power Level,
From	To	days	Fraction of 2441 MWth
10/09/77	10/11/77	3	0.019
10/12/77	10/12/77	1	0.539
10/13/77	10/13/77	1	0.868
10/14/77	11/17/77	35	0.990
11/18/77	11/18/77	1	0.109
11/19/77	11/26/77	8	0.0
11/27/77	11/28/77	2	0.565
11/29/77	03/19/78	111	0.987
03/20/78	04/07/78	19	0.0
04/03/78	04/08/78	1	0.185
04/09/78	05/23/78	45	1.000
05/24/78	05/24/78	1	0.613
05/25/78	05/29/78	5	0.0
05/30/78	05/30/78	1	0.884
05/31/78	07/06/78	37	0.989
07/07/78	07/07/78	1	0.039
07/08/78	07/31/78	24	0.0
08/01/78	08/02/78	2	0.482
08/03/78	09/29/78	58	0.997
09/30/78	10/04/78	5	0.846
10/05/78	10/05/78	1	0.145
10/06/78	10/14/78	9	0.0
10/15/78	10/15/78	1	0.633
10/16/78	12/02/78	48	0.994
12/03/78	12/03/78	1	0.035
12/04/78	02/02/79	61	0.992
02/03/79	02/03/79	1	0.789
02/04/79	02/04/79	1	0.036

Table A-2

SURRY 2, CYCLE 5 REACTOR OPERATING HISTORY

Dates, mo/da/yr		Elapsed Time,	Reactor Power Level,
From	To	days	Fraction of 2441 MWth
08/17/80	08/19/80	3	0.077
08/20/80	08/22/80	3	0.455
08/23/80	08/23/80	1	0.128
08/24/80	08/26/80	3	0.427
08/27/80	08/28/80	2	0.287
08/29/80	08/30/80	2	0.466
08/31/80	09/01/80	2	0.624
09/02/80	09/30/80	2	0.936
09/04/80	09/08/80	5	0.653
09/09/80	10/31/80	53	0.997
11/01/80	11/02/80	2	0.592
11/03/80	03/20/81	138	0.999
03/21/81	03/22/81	2	0.461
03/23/81	04/05/81	14	0.996
04/06/81	04/06/81	1	0.683
04/07/81	04/17/81	11	0.995
04/18/81	04/18/81	1	0.064
04/19/81	04/27/81	9	0.0
04/28/81	04/28/81	1	0.758
04/29/81	05/04/81	6	0.998
05/05/81	05/06/81	2	0.573
05/07/81	06/28/81	53	0.998
06/29/81	06/30/81	2	0.795
07/01/81	07/16/81	16	0.998
07/17/81	07/18/81	2	0.556
07/19/81	08/12/81	25	0.998
08/13/81	08/13/81	1	0.779
08/14/81	09/02/81	20	0.995
09/03/81	09/09/81	7	0.0
09/10/81	09/10/81	1	0.629
09/11/81	10/10/81	30	0.993
10/11/81	10/12/81	2	0.793
10/13/81	11/06/81	25	0.996

Table A-3

FUEL ASSEMBLY DATA

Fuel Assembly ID No.	V03	V10	V16	V18	V22	V26
Fuel Assembly ANSI No.	LM0427	LM042B	LM041C	LM0422	LM040Y	LM041H
Initial Enrichment, wt%	2.91	2.91	2.91	2.91	2.91	2.91
Active Fuel Length, in.	144	144	144	144	144	144
Burnup, GWd/MTU	30.557	30.557	30.557	31.511	31.511	30.557
Decay Heat, W (1/14/86)	869.7	869.7	869.7	919.2	919.2	869.7
Cooling Time, days	1530	1530	1530	1530	1530	1530
Cycles Irradiated	S2C4 S2C5	S2C4 S2C5	S2C4 S2C5	S2C4 S2C5	S2C4 S2C5	S2C4 S2C5

Fuel Assembly ID No.	W01	W02	W06	W10	W13	W16
Fuel Assembly ANSI No.	LM040R	LM040P	LM040K	LM0410	LM0409	LM0404
Initial Enrichment, wt%	3.20	3.20	3.20	3.20	3.20	3.20
Active Fuel Length, in.	144	144	144	144	144	144
Burnup, GWd/MTU	29.987	29.795	30.521	29.795	30.521	29.795
Decay Heat, W (1/14/86)	851.9	845.5	859.1	845.5	859.1	845.5
Cooling Time, days	1530	1530	1530	1530	1530	1530
Cycles Irradiated	S2C4 S2C5	S2C4 S2C5	S2C4 S2C5	S2C4 S2C5	S2C4 S2C5	S2C4 S2C5

Fuel Assembly ID No.	W17	W19	W23	W27	W28	W34
Fuel Assembly ANSI No.	LM040T	LM040V	LM040C	LM0411	LM0419	LM041B
Initial Enrichment, wt%	3.20	3.20	3.20	3.20	3.20	3.20
Active Fuel Length, in.	144	144	144	144	144	144
Burnup, GWd/MTU	29.987	29.795	29.795	30.521	29.987	30.521
Decay Heat, W (1/14/86)	851.9	845.5	845.5	859.1	851.9	859.1
Cooling Time, days	1530	1530	1530	1530	1530	1530
Cycles Irradiated	S2C4 S2C5	S2C4 S2C5	S2C4 S2C5	S2C4 S2C5	S2C4 S2C5	S2C4 S2C5

Fuel Assembly ID No.	W38	W44	W45	W46	W49	W52
Fuel Assembly ANSI No.	LM041Z	LM041X	LM041R	LM0415	LM0418	LM0426
Initial Enrichment, wt%	3.20	3.20	3.20	3.20	3.20	3.20
Active Fuel Length, in.	144	144	144	144	144	144
Burnup, GWd/MTU	29.987	29.987	29.795	29.987	29.795	29.987
Decay Heat, W (1/14/86)	851.9	851.9	845.5	851.9	845.5	851.9
Cooling Time, days	1530	1530	1530	1530	1530	1530
Cycles Irradiated	S2C4 S2C5	S2C4 S2C5	S2C4 S2C5	S2C4 S2C5	S2C4 S2C5	S2C4 S2C5

Appendix B

TEMPERATURE AND PRESSURE MEASUREMENT UNCERTAINTIES

Appendix B

TEMPERATURE AND PRESSURE MEASUREMENT UNCERTAINTIES

Temperature measurement uncertainty is produced by the thermocouples, extension wires, and data acquisition system. Each component in the temperature measurement chain adds to the overall uncertainty. The measurement chain is shown below.

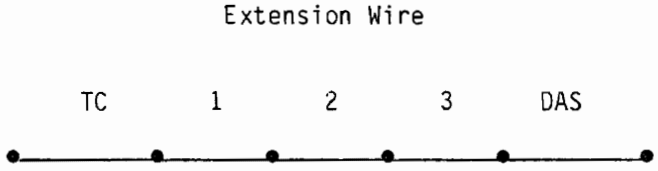

Following the derivation of Schenck (1), the overall uncertainty is equal to the square root of the sum of the squares of the individual temperature measurement uncertainties. The individual uncertainties are:

Lance Thermocouples

$T = 0.989*T_m - 1.8$, $\sigma = \pm 0.38°C$

Vendor Specification for External Thermocouples

σ equals the maximun of ±2.2°C or 0.75%. Because the maximum surface temperature was less than 100°C, $\sigma = \pm 2.2°C$.

Extension Wire - three segments were used for each thermocouple

σ equals the maximun of ±2.2°C or 0.75%. Because the extension wire was near 25°C, $\sigma = \pm 2.2°C$.

Data Acquisition System

σ was estimated to be less than ±1°C.

Taking the square root of the sum of the squares of the deviations led to the following estimates of uncertainty for temperature measurements:

For the lance thermocouples,

$\sigma = \pm 4°C$

For the surface thermocouples,

$\sigma = \pm 4.5°C$.

Pressure measurements were obtained from a Leybold Heraeus model MAC 2000 pressure transducer with a 4- to 20-milliampere output. The 4- to 20-milliampere signal was fed through a precision resistor to create the signal processed by the data acquisition system. The pressure transducer was calibrated prior to use and had a precision of ±0.0112 amperes. The dropping resistor was measured to be a 249.2-ohm resistor with a precision of ±0.25 ohms. The equation relating the pressure reading from the data acquisition system to the output of the pressure transducer is of the form

$$P = 0.5017(I*R) - 500$$

where P = pressure
I = milliampere output of pressure transducer
R = resistance of dropping resistor.

Using the method of Schenck (1), the uncertainty of the pressure measurements is

$$\sigma_p^2 = (0.5017 \cdot 249.2)^2 (0.0112)^2 + (0.5017 \cdot I)^2 (0.25)^2$$

$$\sigma_p^2 = 1.9537 + 0.0157 (I^2)$$

which gives an uncertainty of ±1.5 mbar for vacuum measurements (near 0 mbar) and ±6 mbar for pressure readings in the vicinity of 1500 mbar.

REFERENCE

1. H. Schenck, Jr. Theories of Engineering Experimentation. New York: McGraw-Hill, 1961, pp. 40-48

Appendix C

HEAT TRANSFER DATA

Table C-1

CORRECTED TEMPERATURE DATA FOR TN-24P CASK PERFORMANCE TEST[a]

RUN No.	1	2	3	4	5	6
DATE: mo/da/yr	01/14/86	01/17/86	01/20/86	01/27/86	01/31/86	02/06/86
TIME: hr/min/sec	60002	100002	120002	60002	100002	50002
Orientation	Vertical	Vertical	Vertical	Horizontal	Horizontal	Horizontal
Backfill	Helium	Nitrogen	Vacuum	Helium	Nitrogen	Vacuum
PRES. mbar	1506	1529.4	2.4	1525.1	1580.5	1.1

Thermocouple	Temperature, °C						Elevation[b] or Radius,[c] cm	Angle, degrees[d]	Location[e]
TC1	99.9	88.1	139.3	111.8	128.6	138.6	0.447		E
TC2	132.1	115.4	181.1	137.9	154.3	178.8	1.117		
TC3	152.9	151.2	196.7	151.9	173.1	193.4	2.317		
TC4	147.5	164.4	185.6	142.8	164.4	181.8	3.117		
TC5	127.2	168.6	147.8	115.3	137.5	143.5	3.867		
TC6	98.2	154.1	98.5	86.6	102.3	95.4	4.367		
TC7	124.4	86.3	182.9	142.2	152.3	183.3	0.447		D1-5
TC8	182.6	135.3	254.6	190.3	223.3	247.9	1.117		
TC9	210.6	201.8	275.3	206.2	245.6	265.8	2.317		
TC10	206.3	228.0	260.9	193.0	230.5	250.4	3.117		
TC11	169.8	231.6	201.1	147.2	167.7	192.3	3.867		
TC12	102.2	170.4	87.9	81.7	99.2	86.3	4.367		
TC13	121.5	91.2	177.8	138.5	153.2	179.5	0.447		D4-5
TC14	175.6	139.2	245.5	183.0	218.8	241.1	1.117		

[a]Calibration equation $T_{corr} = 0.989T_{meas} - 1.8$ was used to correct lance TC readings.

[b]From exterior bottom of cask.

[c]From cask centerline.

[d]From 0° orientation mark.

[e]See Figure 3.8 for TC lance locations.

Table C-1

(CONTD)[a]

RUN No.	1	2	3	4	5	6
DATE: mo/da/yr	01/14/86	01/17/86	01/20/86	01/27/86	01/31/86	02/06/86
TIME: hr/min/sec	60002	100002	120002	60002	100002	50002
Orientation	Vertical	Vertical	Vertical	Horizontal	Horizontal	Horizontal
Backfill	Helium	Nitrogen	Vacuum	Helium	Nitrogen	Vacuum
PRES. mbar	1506	1529.4	2.4	1525.1	1580.5	1.1

Thermocouple	Temperature, °C						Elevation[b] or Radius,[c] cm	Angle, degrees[d]	Location[e]
TC15	202.2	198.2	265.7	198.7	241.1	259.1	2.317		D4-5
TC16	193.0	221.5	251.4	186.9	227.0	244.6	3.117		
TC17	158.2	219.4	191.1	139.8	163.5	185.2	3.867		
TC18	103.1	171.8	87.4	78.6	96.6	85.0	4.367		
TC19	110.0	95.3	161.9	123.0	146.7	161.9	0.447		D5-6
TC20	152.7	136.0	217.7	158.7	195.8	213.5	1.117		
TC21	175.1	185.7	234.6	172.8	211.3	229.3	2.317		
TC22	171.1	201.3	223.6	164.2	200.7	218.5	3.117		
TC23	141.3	198.5	174.5	127.6	156.6	170.8	3.867		
TC24	89.5	158.1	78.7	78.9	98.7	77.6	4.367		
TC25	18.7	19.9	20.5	18.5	21.3	19.1			AMBIENT
TC26	16.1	18.2	18.1	15.9	19.6	17.6			AMBIENT
TC27	20.6	21.6	21.9	21.1	23.1	20.6			AMBIENT

[a]Calibration equation $T_{corr} = 0.989T_{meas} - 1.8$ was used to correct lance TC readings.

[b]From exterior bottom of cask.

[c]From cask centerline.

[d]From 0° orientation mark.

[e]See Figure 3.8 for TC lance locations.

Table C-1

(CONTD)[a]

RUN No.	1	2	3	4	5	6
DATE: mo/da/yr	01/14/86	01/17/86	01/20/86	01/27/86	01/31/86	02/06/86
TIME: hr/min/sec	60002	100002	120002	60002	100002	50002
Orientation	Vertical	Vertical	Vertical	Horizontal	Horizontal	Horizontal
Backfill	Helium	Nitrogen	Vacuum	Helium	Nitrogen	Vacuum
PRES. mbar	1506	1529.4	2.4	1525.1	1580.5	1.1

Thermocouple	Temperature, °C						Elevation[b] or Radius,[c] cm	Angle, degrees[d]	Location[e]
TC31	107.7	99.4	154.9	119.4	148.2	154.9	0.447		D6-4
TC32	146.5	133.8	206.9	153.5	205.1	204.6	1.117		
TC33	159.6	174.4	215.0	161.4	215.3	212.6	2.317		
TC34	153.1	186.8	204.0	151.7	205.4	201.4	3.117		
TC35	125.6	188.6	159.5	118.8	159.0	156.5	3.867		
TC36	81.4	150.4	75.3	77.1	91.5	75.3	4.367		
TC37	102.9	96.1	148.6	108.3	116.0	146.0	0.447		C6-5
TC38	141.2	130.0	200.2	138.9	161.8	189.3	1.117		
TC39	158.6	176.5	213.5	148.0	174.6	199.8	2.317		
TC40	152.7	185.0	202.4	138.5	162.1	188.6	3.117		
TC41	125.8	184.3	159.1	108.9	122.9	148.7	3.867		
TC42	86.8	152.7	78.1	68.5	85.3	76.9	4.367		

[a]Calibration equation $T_{corr} = 0.989T_{meas} - 1.8$ was used to correct lance TC readings.

[b]From exterior bottom of cask.

[c]From cask centerline.

[d]From 0° orientation mark.

[e]See Figure 3.8 for TC lance locations.

Table C-1

(CONTD)[a]

RUN No.	1	2	3	4	5	6
DATE: mo/da/yr	01/14/86	01/17/86	01/20/86	01/27/86	01/31/86	02/06/86
TIME: hr/min/sec	60002	100002	120002	60002	100002	50002
Orientation	Vertical	Vertical	Vertical	Horizontal	Horizontal	Horizontal
Backfill	Helium	Nitrogen	Vacuum	Helium	Nitrogen	Vacuum
PRES. mbar	1506	1529.4	2.4	1525.1	1580.5	1.1

Thermocouple	Temperature, °C						Elevation[b] or Radius,[c] cm	Angle, degrees[d]	Location[e]
TC43	102.4	92.0	136.4	111.0	122.5	133.6	0.447		F
TC44	133.8	118.4	179.3	137.6	152.0	170.3	1.117		
TC45	152.7	151.4	195.7	146.5	162.0	181.7	2.317		
TC46	148.3	165.8	185.0	136.7	153.0	170.0	3.117		
TC47	126.2	168.8	145.1	108.9	124.0	133.0	3.867		
TC48	99.4	154.8	94.5	81.6	92.2	88.9	4.367		
TC49	109.7	95.7	159.4	122.0	137.6	157.4	0.447		B5-7
TC50	153.8	135.5	217.3	158.3	185.5	209.2	1.117		
TC51	173.4	183.5	232.7	166.8	199.5	218.9	2.317		
TC52	167.8	199.3	219.7	156.2	188.0	206.2	3.117		
TC53	138.6	197.2	170.7	120.6	143.8	160.2	3.867		
TC54	84.8	158.5	76.7	75.6	90.2	75.5	4.367		
TC55	126.0	85.7	184.8	143.4	152.2	185.3	0.447		A1-5
TC56	182.5	134.6	254.6	191.8	224.9	248.5	1.117		

[a]Calibration equation $T_{corr} = 0.989T_{meas} - 1.8$ was used to correct lance TC readings.

[b]From exterior bottom of cask.

[c]From cask centerline.

[d]From 0° orientation mark.

[e]See Figure 3.8 for TC lance locations.

Table C-1

(CONTD)[a]

RUN No.	1	2	3	4	5	6
DATE: mo/da/yr	01/14/86	01/17/86	01/20/86	01/27/86	01/31/86	02/06/86
TIME: hr/min/sec	60002	100002	120002	60002	100002	50002
Orientation	Vertical	Vertical	Vertical	Horizontal	Horizontal	Horizontal
Backfill	Helium	Nitrogen	Vacuum	Helium	Nitrogen	Vacuum
PRES. mbar	1506	1529.4	2.4	1525.1	1580.5	1.1

Thermocouple	Temperature, °C						Elevation[b] or Radius,[c] cm	Angle, degrees[d]	Location[e]
TC57	213.9	201.8	278.4	208.0	247.5	267.9	2.317		A1-5
TC58	207.3	228.0	262.0	194.2	231.3	252.3	3.117		
TC59	170.2	231.8	202.1	148.1	168.7	194.2	3.867		
TC60	102.3	175.5	87.1	81.6	99.2	85.4	4.367		
TC61	63.2	57.9	68.2	64.5	66.8	64.9	0.140	0	SURFACE
TC62	60.8	55.5	64.5	60.0	61.7	60.2	0.447		
TC63	69.8	62.7	72.7	68.9	70.9	69.7	1.117		
TC64	77.9	72.4	78.8	75.9	78.1	76.9	2.317		
TC65	68.7	69.5	67.6	65.7	65.1	59.2	3.117		
TC66	65.5	71.4	62.2	62.6	66.0	61.0	3.700		
TC67			55.1	58.3	62.7	56.2	4.367		
TC68			53.3	56.1	60.3	54.1	4.533		
TC69	65.5	57.6	69.0	73.7	72.7	76.1	1.117	135	
TC70	74.2	68.8	75.7	81.0	80.5	84.4	2.317		

[a]Calibration equation $T_{corr} = 0.989T_{meas} - 1.8$ was used to correct lance TC readings.

[b]From exterior bottom of cask.

[c]From cask centerline.

[d]From 0° orientation mark.

[e]See Figure 3.8 for TC lance locations.

Table C-1

(CONTD)[a]

RUN No.	1	2	3	4	5	6
DATE: mo/da/yr	01/14/86	01/17/86	02/20/86	01/27/86	01/30/86	02/06/86
TIME: hr/min/sec	60002	100002	120002	60002	100002	50002
Orientation	Vertical	Vertical	Vertical	Horizontal	Horizontal	Horizontal
Backfill	Helium	Nitrogen	Vacuum	Helium	Nitrogen	Vacuum
PRES. mbar	1506	1529.4	2.4	1525.1	1580.5	1.1

Thermocouple	Temperature, °C						Elevation[b] or Radius,[c] cm	Angle, degrees[d]	Location[e]
TC71	66.3	72.7	62.9	67.9	69.0	72.1	3.700	135	SURFACE
TC72	61.6	75.9	55.1	61.4	64.3	63.3	4.367		
TC73	59.8	52.5	62.0	66.2	64.8	76.4	1.117	180	
TC74	73.2	68.2	74.7	83.1	82.7	87.4	2.317		
TC75	38.7	41.8	39.5	72.2	74.2	43.9	3.700		
TC76	63.5	78.8	57.1	64.1	66.9	66.3	4.367		
TC77	67.1	58.6	69.2	69.7	70.2	71.6	1.117	270	
TC78	74.3	68.9	75.6	75.2	77.0	78.9	2.317		
TC79	69.2	76.5	66.3	68.2	70.9	70.9	3.700		
TC80	68.5	61.6	71.9	69.1	70.9	70.0	1.117	315	
TC81	74.4	68.9	75.8	72.8	75.0	73.8	2.317		
TC82	65.0	71.6	62.0	60.8	64.2	61.4	3.700		
TC83	60.4	75.1	53.2	56.1	60.0	54.7	4.367		

[a]Calibration equation $T_{corr} = 0.989T_{meas} - 1.8$ was used to correct lance TC readings.

[b]From exterior bottom of cask.

[c]From cask centerline.

[d]From 0° orientation mark.

[e]See Figure 3.8 for TC lance locations.

Table C-1

(CONTD)[a]

RUN No.	1	2	3	4	5	6
DATE: mo/da/yr	01/14/86	01/17/86	01/20/86	01/27/86	01/31/86	02/06/86
TIME: hr/min/sec	60002	100002	120002	60002	100002	50002
Orientation	Vertical	Vertical	Vertical	Horizontal	Horizontal	Horizontal
Backfill	Helium	Nitrogen	Vacuum	Helium	Nitrogen	Vacuum
PRES. mbar	1506	1529.4	2.4	1525.1	1580.5	1.1

Thermocouple	Temperature, °C						Elevation[b] or Radius,[c] cm	Angle, degrees[d]	Location[e]
TC84	61.1	84.1	48.7	54.6	59.0	51.1	0.383	0	TOP
TC85	59.3	78.7	49.3	53.9	58.3	51.1	0.765	0	
TC86	58.7	78.3	49.0	55.1	58.7	54.6	0.765	180	
TC87	61.6	85.7	49.5	55.6	59.7	54.0	0.383	270	
TC88	59.7	79.7	50.1	55.1	59.0	53.6	0.765	270	
TC89	42.9	53.6	49.2	56.1	60.4	53.7	0.000	0	
TC90				66.4	69.3	66.2	0.499	0	BOTTOM
TC91				59.5	62.3	60.2	0.998	0	
TC92				64.2	64.5	65.9	0.998	180	
TC93				67.3	69.5	68.4	0.499	270	
TC94				61.9	64.0	63.5	0.998	270	
TC95				69.3	71.9	70.0	0.000	0	

[a] Calibration equation $T_{corr} = 0.989T_{meas} - 1.8$ was used to correct lance TC readings.

[b] From exterior bottom of cask.

[c] From cask centerline.

[d] From 0° orientation mark.

[e] See Figure 3.8 for TC lance locations.

Table C-1

(CONTD)[a]

RUN No.	1	2	3	4	5	6
DATE: mo/da/yr	01/14/86	01/17/86	01/20/86	01/27/86	01/31/86	02/06/86
TIME: hr/min/sec	60002	100002	120002	60002	100002	50002
Orientation	Vertical	Vertical	Vertical	Horizontal	Horizontal	Horizontal
Backfill	Helium	Nitrogen	Vacuum	Helium	Nitrogen	Vacuum
PRES. mbar	1506	1529.4	2.4	1525.1	1580.5	1.1

Thermocouple	Temperature, °C						Elevation[a] m	X[b] m	Y[b] m	R[b] m	Location
TC97	64.4	57.8	70.0	66.9	69.4	66.8	0.405	-0.639	0.347	0.727	BASKET
TC98	92.3	84.7	95.8	93.1	95.8	95.3	2.230	-0.639	0.347	0.727	
TC99	92.5	84.9	95.8	92.7	95.8	93.6	2.230	-0.718	0.116	0.727	
TC100	88.4	91.8	87.1	86.6	89.6	87.8	3.180	-0.639	0.347	0.727	
TC101	75.8	91.4	69.2	71.1	76.1	70.6	3.990	-0.639	0.347	0.727	
TC102	67.5	87.3	58.4	61.4	66.7	59.9	4.420	-0.639	0.347	0.727	
TC103	91.0	96.2	124.0	94.8	114.4	123.0	0.405	-0.578	0.347	0.674	
TC104	116.4	107.9	166.3	123.3	151.5	168.6	2.230	-0.462	0.347	0.578	
TC105	129.3	136.9	179.4	127.3	147.4	176.3	2.230	-0.462	0.347	0.578	
TC106	123.2	130.6	152.8	121.5	140.5	148.0	2.230	-0.578	0.231	0.622	
TC107	194.9	179.8	251.9	192.5	222.9	242.6	2.230	0.000	0.000	0.000	
TC108	149.2	152.5	193.9	147.9	177.5	193.6	2.230	-0.693	-0.116	0.703	
TC109	148.5	203.5	166.2	128.7	148.9	158.8	3.990	0.000	0.000	0.000	
TC110	119.7	176.7	112.5	97.1	109.4	106.6	4.420	0.000	0.000	0.000	

[a]From exterior bottom of cask.

[b]From cask centerline.

Appendix D

DOSE RATE DATA

Table D-1

DOSIMETER RADIATION MEASUREMENTS FROM TN-24P CASK PERFORMANCE TEST

Location		Exposure Time, h	TLD Dose Rate,[d] mR/h	TED Dose Rate,[e] mrem/h
Angle,[a] degrees	Elevation[b] or Radius,[c] mm			
SIDE				
45	140	89.42	6.0	15.3
	187	89.40	12.8	21.3
	234	89.40	23.7	28.0
	281	89.38	34.3	
	330	89.38	35.9	43.4
	980	89.47	9.6	1.3
	1630	89.38	10.3	1.9
	2280	89.40	10.3	3.1
	2930	89.38	9.8	2.7
	3580	89.45	8.6	1.7
	4235	89.33	9.7	7.8
	4282	89.35	28.4	22.3
	4329	89.35	23.3	16.7
	4376	89.33	17.0	14.6
	4423	89.33	12.1	
	4470	89.32	12.5	9.7
	4517	89.32	6.8	10.2
	4565	89.32	11.1	7.9
60	2280	88.60	12.6	2.8
75	2280	88.62	12.2	3.4
90	140	88.82	10.0	19.0
	187	88.80	21.9	23.3
	234	88.78	36.4	28.2
	281	88.78	54.3	32.4
	330	88.77	52.7	36.5
	980	88.78	11.7	2.7
	1630	88.77	12.8	4.0
	2280	88.78	13.1	2.1
	2930	88.78	12.6	2.4
	3580	88.77	10.3	2.3
	4235	88.75	22.2	13.6
	4282	88.75	32.9	20.7

[a]From 0° orientation mark.

[b]From exterior bottom of cask.

[c]From cask centerline.

[d]Gamma.

[e]Neutron.

Table D-1

(CONTD)

Location		Exposure Time, h	TLD Dose Rate,[d] mR/h	TED Dose Rate,[e] mrem/h
Angle,[a] degrees	Elevation[b] or Radius,[c] mm			
90	4329	88.72	24.4	18.5
	4376	88.70	16.5	15.8
	4423	88.70	11.3	14.3
	4470	88.70	11.5	9.3
	4517	88.68	6.7	13.8
	4565	88.70	15.0	7.8
105	2280	88.68	13.1	3.4
120	2280	88.68	12.6	2.8
TOP				
45	0	73.35	50.6	31.1
	140	73.22	57.7	33.2
	230	73.20	46.8	
	345	73.18	35.7	26.7
	460	73.17	30.8	27.9
	575	73.07	20.8	30.5
	705	73.03	11.3	15.4
90	0	73.00	45.5	27.5
	115	72.98	42.9	30.5
	230	72.97	36.9	27.3
	345	72.95	34.9	30.2
	460	72.95	28.3	28.9
	575	72.93	24.4	19.7
	690	72.93	16.8	17.1
	741	72.93	14.5	11.9
	792	72.92	65.3	13.5
	843	72.90	34.8	13.2
	894	72.90	297.2	18.7
	945	72.88	76.7	7.3
	998	72.83	31.5	7.3

[a]From 0° orientation mark.

[b]From exterior bottom of cask.

[c]From cask centerline.

[d]Gamma.

[e]Neutron.

Table D-1

(CONTD)

Location		Exposure Time, h	TLD Dose Rate,[d] mR/h	TED Dose Rate,[e] mrem/h
Angle,[a] degrees	Elevation[b] or Radius,[c] mm			
BOTTOM				
45	0	72.57	126.4	63.8
	115	72.57	135.0	63.8
	230	72.55	128.0	57.7
	345	72.55	125.8	55.9
	460	72.53	103.3	54.4
	575	72.53	69.8	59.3
	705	72.52	25.4	41.9
90	0	72.53	143.0	62.1
	115	72.52	136.6	63.4
	230	72.52	124.9	61.3
	345	72.50	115.1	55.8
	460	72.48	104.9	52.5
	575	72.48	91.0	44.6
	690	72.47	54.1	32.7
	741	72.47	33.8	29.7
	792	72.47	17.4	15.5
	843	72.45	8.5	20.2
	894	72.45	3.6	15.4
	945	72.47	1.7	9.3
	987	72.47	1.1	7.2
EXTRAS				
EDGE OF LID				
45	+30	71.63	80.9	11.0
	+80	71.62	173.6	9.6
	+120	71.60	267.9	13.4
	+50	71.57	47.9	11.5
	+150	71.55	103.6	9.4
90	hole	71.53	43.5	25.8

[a]From 0° orientation mark.

[b]From exterior bottom of cask.

[c]From cask centerline.

[d]Gamma.

[e]Neutron.

Table D-1

(CONTD)

Location		Exposure Time, h	TLD Dose Rate,[d] mR/h	TED Dose Rate,[e] mrem/h
Angle,[a] degrees	Elevation[b] or Radius,[c] mm			
HEATING FINS				
81	2270	71.30	12.6	3.4
82	2270	71.30	11.9	2.6
83	2270	71.30	12.7	3.4
84	2270	71.30	13.7	3.9
85	2270	71.30	14.2	2.7
86	2270	71.30	12.2	2.9
87	2270	71.30	12.5	4.4
88	2270	71.30	11.8	2.7
89	2270	71.30	13.4	3.1

[a]From 0° orientation mark.

[b]From exterior bottom of cask.

[c]From cask centerline.

[d]Gamma.

[e]Neutron.

Table D-2

RADIATION SURVEY INSTRUMENT MEASUREMENT
RESULTS FROM TN-24P CASK PERFORMANCE TEST

Location		Dose Rates, mrem/h			
		PNL		INEL	
Angle,[a] degrees	Elevation[b] or Radius,[c] mm	Gamma[d]	Neutron[e]	Gamma[f]	Neutron[g]
SIDE					
45	140	9.5	45	10	20
	187	15	45	20	20
	234	22	45	27	20
	281	26.5	45	35	20
	330		45	30	20
	980	11	2.5	10	3
	1630	11.5	2.5	11	2
	2280	11	2	11	2
	2930	11	1.3	13	2
	3580	9.5	1.1	11	1.5
	4235	10.5	5	10	3
	4282	25	5	32	20
	4329	23		27	20
	4376	18		23	20
	4423	14		18	20
	4470	11.5	2.5	15	20
	4517	10	2.5	12	20
	4565	13		20	20
65	2280	13	2.5	15	1
75	2280	13.5	2.5	16	1.5
90	140	14	28	12	35
	187	23		30	35
	234	33	40	40	35
	281	39		50	35

[a] From 0° orientation mark.

[b] From exterior bottom of cask.

[c] From cask centerline.

[d] With an Eberline RO-3B.

[e] With a SNOOPY.

[f] With an Eberline RO-3A.

[g] With an Eberline PNR-4.

Table D-2

(CONTD)

Location		Dose Rates, mrem/h			
		PNL		INEL	
Angle,[a] degrees	Elevation[b] or Radius,[c] mm	Gamma[d]	Neutron[e]	Gamma[f]	Neutron[g]
SIDE	330	33	30	40	25
90	980	12	9	14	5
	1630	13.5	3.5	16	3.5
	2280	13	2	18	1.5
	2930	13	2	15	2.5
	3580	10	4.5	12	3
	4235	21		25	20
	4282	27	16	32	20
	4329	23.5		30	20
	4376	18	16	25	20
	4423	14		18	20
	4470	11	16	15	20
	4517	9		10	10
	4565	13		20	20
105	2280	13	2.5	17	2
120	2280	12	2	16	2
TOP					
	center of cask	52	30 (at	70	37
45	140	57	lances)	70	37
	230	45.5		50	25
	345	39		43	25
	460	31	25	30	25
	575	23		23	25
	705	16.5	18	15	25

[a] From 0° orientation mark.

[b] From exterior bottom of cask.

[c] From cask centerline.

[d] With an Eberline RO-3B.

[e] With a SNOOPY.

[f] With an Eberline RO-3A.

[g] With an Eberline PNR-4.

Table D-2a

(CONTD)

Location		Dose Rates, mrem/h			
		PNL		INEL	
Angle,[a] degrees	Elevation[b] or Radius,[c] mm	Gamma[d]	Neutron[e]	Gamma[f]	Neutron[g]
TOP	115 mm down from 90 degrees center of cask	48	40	60	25
90	115 from center	46	32	50	32
	230 " "	43		47	30
	345 " "	38.5	30	42	30
	460 " "	32.5		34	30
	575 " "	25	25	30	30
	690 " "	17	30	22	20
	741 " "	20		30	20
	792 " "	42		50	20
	843 " "	42		50	20
	894 " "	145		160	20
	945 " "	135	17	150	20
	998 " "	105		110	20
BOTTOM					
	center of cask	145	90	170	100
45	115 from center	150		170	80
	230 " "	145		165	80
	345 " "	137	70	155	
	460 " "	115		135	70
	575 " "	75	60	75	
	705 " "	29	45	45	40

[a]From 0° orientation mark.

[b]From exterior bottom of cask.

[c]From cask centerline.

[d]With an Eberline RO-3B.

[e]With a SNOOPY.

[f]With an Eberline RO-3A.

[g]With an Eberline PNR-4.

Table D-2

(CONTD)

Location		Dose Rates, mrem/h			
		PNL		INEL	
Angle,[a] degrees	Elevation[b] or Radius,[c] mm	Gamma[d]	Neutron[e]	Gamma[f]	Neutrsn[g]
BOTTOM					
	115 mm down from 90 degrees center of cask	143	100	160	100
90	115 from center	142		160	100
	230 " "	135	75	150	100
	345 " "	128	70	140	100
	460 " "	115	60	125	50
	575 " "	95	55	110	50
	690 " "	62		60	25
	741 " "	36.5	40	50	25
	792 " "	24		27	25
	843 " "	14.5		16	25
	894 " "	8.5	25	10	25
	945 " "	5.5		6	25
	987 " "	3.3	14	5	25

[a]From 0° orientation mark.

[b]From exterior bottom of cask.

[c]From cask centerline.

[d]With an Eberline RO-3B.

[e]With a SNOOPY.

[f]With an Eberline RO-3A.

[g]With an Eberline PNR-4.

Table D-3

INEL RADIATION SURVEY INSTRUMENT MEASUREMENTS
AT THE TN-24P SURFACE AND 1 M AND 2 M FROM THE CASK

Location		Dose Rate, mrem/h					
		Surface		1 m		2 m	
Angle,[a] degrees	Elevation[b] or Radius,[c] mm	Gamma[d]	Neutron[e]	Gamma[d]	Neutron[e]	Gamma[d]	Neutron[e]
SIDE							
0	L/2[b]	17	2	7.5	1.5	3	1
45		13	2	7.5	1.5	4	1
90		17	3	8	1.5	4	1
180		15	2	9	1.5	4	1
225		16	2	10	1.5	4	1
270		17	2	10	1.5	6	1
LID							
--	R/2[c]	30[f]	38[f]	17	4.5	11	3
--	R	*[f]	*[f]	25	12	--	8
BOTTOM	R/2	*[f]	*[f]	20	--	--	--
	R	*[f]	*[f]	15	3.5	10	2.5

[a] From 0° orientation mark.

[b] L - TN-24P cask total length.

[c] R - TN-24P cask outer radius.

[d] With an Eberline RO-3A.

[e] With an Eberline PNR-4.

[f] See Table D-2.